

# UC Berkeley

## UC Berkeley Electronic Theses and Dissertations

### Title

Synthesis, Hydrogenation, and Hydrodeoxygenation of Biomass-Derived Furans for Diesel Fuel

### Permalink

<https://escholarship.org/uc/item/5wx0k5pg>

### Author

Louie, Ying Lin

### Publication Date

2017

Peer reviewed|Thesis/dissertation

# Synthesis, Hydrogenation, and Hydrodeoxygenation of Biomass-Derived Furans for Diesel Fuel

By

Ying Lin Louie

A dissertation submitted in partial satisfaction of the

requirements for the degree of

Doctor of Philosophy

in

Chemical Engineering

in the

Graduate Division

of the

University of California, Berkeley

Committee in charge:

Professor Alexis T. Bell, Chair

Professor Alexander Katz

Professor F. Dean Toste

Summer 2017

Synthesis, Hydrogenation, and Hydrodeoxygenation of Biomass-Derived Furans for Diesel Fuel

© 2017  
Ying Lin Louie  
All rights reserved

## Abstract

### Synthesis, Hydrogenation, and Hydrodeoxygenation of Biomass-Derived Furans for Diesel Fuel

by

Ying Lin Louie

Doctor of Philosophy in Chemical Engineering

University of California, Berkeley

Professor Alexis T. Bell, Chair

Hydrogenation and hydrodeoxygenation (HDO) processes are critical for the chemical conversion of lignocellulosic biomass into liquid transportation fuels such as gasoline, jet, and diesel. Hydro-treatment processes can remove undesired functionalities and reduce the oxygen content in biomass-derived oxygenates to produce candidates suitable for fuel blends. In this study, the liquid phase hydrogenation and hydrogenolysis of several model substrates including, 2,5-dimethylfuran (DMF), 5-methylfurfural (5-MF), bis(5-methylfuran-2-yl)methane (BMFM), and 5-(2-(5-methylfuran-2-yl)vinyl)furan-2-aldehyde (MFVFAL), were investigated over noble metal catalysts (Pd, Pt, Ru) at moderate conditions (353 – 473 K, 0.55 – 5.1 MPa). Understanding the mechanism and kinetics by which undesired functionalities found in these substrates, such as aromatic furans, unsaturated C=C bonds, and C=O bonds, are removed during hydrogenation will allow for the design of efficient catalysts and processes to improve the hydrougrading reactions of biomass-derived fuels.

Unlike DMF and 5-MF, complex substrates such as BMFM and MFVFAL are not available commercially. To this end, we investigated synthetic strategies to produce these C<sub>11</sub> – C<sub>12</sub> oxygenates. BMFM was synthesized by electrophilic aromatic substitution of 2-MF with formalin catalyzed by acidic protons at 333K. The use of 5-methylfurfuryl alcohol in place of formalin, and heterogeneous SO<sub>3</sub>H-SiO<sub>2</sub> improved the yield of BMFM from 70% (using homogeneous HCl) to 91%. MFVFAL was synthesized via base catalyzed nucleophilic self-condensation of 5-methylfurfural. We identified heterogeneous base K<sub>3</sub>PO<sub>4</sub> that catalyzed the reaction 10 times faster than homogeneous hydroxide and ethoxide bases at 338K in ethanol solution. Through solvent and isotopic exchange studies, we identified dissociated ethoxide species on the surface of K<sub>3</sub>PO<sub>4</sub> to be responsible for the initial proton abstraction, forming the reactive carbanion species involved in condensation reactions.

Our investigation in liquid phase hydrogenation of aromatic furans begins with a simple C<sub>6</sub> substituted furan, 2,5-dimethylfuran (DMF). The activity and selectivity of carbon-supported Pt, Pd, Rh, and Ru were compared under identical conditions (353 K, 0.55 MPa). Pt/C exhibited the highest activity and selectivity for C-O bond hydrogenolysis, producing 2-hexanone as the

major product, whereas all other catalysts exhibited a high selectivity for ring hydrogenation to form 2,5-dimethyltetrahydrofuran. The reaction kinetics were measured in detail over Pt/C, under conditions that excluded the effects of internal or external mass transfer (333K – 363K,  $p_{H_2} = 0.41 - 0.69$ MPa). A reaction mechanism is proposed to explain the parallel formation of 2,5-dimethyltetrahydrofuran, 2-hexanone, and 2-hexanol. The mechanism involves C-O hydrogenolysis of the aromatic ring to form an enol intermediate responsible for 2-hexanone and 2-hexanol products. 2,5-dimethyltetrahydrofuran was not an intermediate to ring-opened products under studied reaction conditions. The kinetics of DMF hydrogenation over Pt metals were described by a Langmuir-Hinshelwood model that assumed non-competitive adsorption of organic species and hydrogen atoms. The step involving C-O bond cleavage of the aromatic ring had the highest activation energy, 48.3 kJ/mol, and is favored over the steps involving C=C bond hydrogenation of the furan ring at elevated temperatures and low  $p_{H_2}$ .

We applied the findings from our model system, DMF, to understand the hydrogenation behavior of more complex furanyl substrates, such as BMFM over noble metal catalysts. BMFM contains two adjacent aromatic rings – a structure commonly found in products of hydroalkylation reactions using 2-methylfuran. Kinetics of liquid phase hydrogenation of BMFM over Pt/C and Pd/C at moderate conditions (430 K – 473 K, 2 MPa  $H_2$ ) were investigated. As found in our DMF system, ring opening and ring saturation of the aromatic rings of BMFM occurred in parallel, with the former preferred over Pt/C catalysts and at elevated temperatures. Contrary to the DMF system, hydrogenation of BMFM occurred an order of magnitude more rapidly on Pd/C than on Pt/C, with significant activity toward C-O hydrogenolysis (15-30% selectivity to single ring-opened species). Over Pt/C, products from C-O cleavage of one or multiple rings accounted for 80-90% selectivity of the products. Again, the formation of an enol intermediate following ring opening is evidenced by the parallel production of ketone and alcohol products. Alcohols were predominantly formed over ketones when Pd/C was employed due to the nature of Pd surfaces to readily saturate the C=C bonds of enol intermediates. Additional differences in the activity and selectivity between Pt and Pd catalysts were discussed within the context of the differences in BMFM adsorption energy and bonding configuration over the metal surfaces. The reaction kinetics revealed that BMFM could be selectively hydrogenated to cyclic ethers only over Pd/C at low temperatures conditions (373 K, 2.0 MPa  $H_2$ ).

Finally, we address the selective hydrodeoxygenation of 5-MF to DMF and MFVFAL into 1,2-bis(5-methyltetrahydrofuran-2-yl)ethane (BMTHFE), a saturated cyclic ether product, in ethanol over noble metals (Pt, Pd, Ru) and Pd bimetallic catalysts. During hydrogenation (453 K, 5.2 MPa  $H_2$ ) over such catalysts, the C=O aldehyde group of these substrates is first hydrogenated to C-OH and hydrodeoxygenated, forming a terminal methyl group and releasing water. Group VIII metals such as Pt, Pd, and Ni demonstrated activity for decarbonylation and ring hydrogenation/hydrogenolysis due to strong interactions between the C=O group and the furan ring, respectively, and the metal surface. These reactions, along with etherification reactions, reduce selectivity to the desired HDO product. The incorporation of 1wt% Cu to 1wt% Pd/C resulted in 15-30% higher selectivity to HDO products for 5-MF and MFVFAL than 1wt% Pd/C. Monometallic Cu catalysts were inactive toward hydrodeoxygenation and deactivated

during reaction. Although PdCu/C catalysts had high activity in converting the C=O aldehyde into  $-CH_3$ , weak interactions between the aromatic ring and metal surface prevented hydrogenation of the ring into cyclic ethers, which have been determined to be high cetane value diesel fuel candidates. After selective HDO over PdCu/C, a secondary hydrogenation step using 1wt% Pd/C at 373 K, 2.1 MPa  $H_2$  resulted in a 78% yield of BMTHFE.

To my siblings,

for treasuring my personal pursuits and ambitions as if they were their own.

## Table of contents

Abstract.....	1
Table of contents.....	ii
List of Figures.....	v
List of tables.....	vii
List of Abbreviations and Symbols.....	ix
Acknowledgments.....	xi
1 Introduction.....	1
2 Synthesis of Diesel Range Oxygenates from Biomass-Derived Furans.....	5
2.1 Introduction.....	5
2.2 Electrophilic Aromatic Substitution of 2-MF.....	6
2.2.1 Experimental.....	6
2.2.2 Results and Discussion.....	8
2.3 Nucleophilic Condensation of 5-MF.....	11
2.3.1 Experimental.....	11
2.3.3 Results and Discussion.....	13
2.4 Conclusions.....	23
2.5 Supplemental Information.....	25
2.5.1 CO <sub>2</sub> TPD profiles of base catalysts.....	25
2.5.2 Initial rates 5-MF conversion over K <sub>3</sub> PO <sub>4</sub> catalysts treated at 673 K -1073 K..	26
3 Kinetics of Hydrogenation and Hydrogenolysis of 2,5-Dimethylfuran over Noble Metals Catalysts under Mild Conditions.....	27
3.1 Introduction.....	27
3.2 Experimental.....	28
3.2.1 Materials.....	28
3.2.2 Catalyst synthesis.....	28
3.2.3 Catalyst characterization.....	29
3.2.4 Catalytic hydrogenation.....	29
3.2.5 Product analysis.....	30
3.3 Results.....	30
3.3.1 Hydrogenation of DMF over carbon-supported noble metals.....	30



3.3.2	Effect of reactant concentration on the kinetics of DMF hydrogenation .....	33
3.3.3	2-Hexanone hydrogenation over Pt/C .....	34
3.3.4	Effects of reaction temperature .....	34
3.3.5	Effects of catalyst support composition on the hydrogenation of DMF and 2-hexanone	37
3.4	Discussion .....	38
3.4.1	Mechanism of DMF hydrogenation .....	38
3.4.2	Kinetic modeling of the hydrogenation of DMF .....	40
3.5	Conclusions .....	49
3.6	Supplemental Information .....	50
3.6.1	Mass transfer effects in semi-batch hydrogenation system .....	50
3.6.2	Product selectivity as a function of DMF conversion .....	51
3.6.3	Calculation of dissolved H <sub>2</sub> in system .....	51
3.6.4	Derivation of rate expressions in kinetic model .....	52
3.6.5	Kinetic model of 2-hexanone hydrogenation .....	55
3.6.6	Results of parameter fitting to proposed kinetic model for DMF hydrogenation	58
4	Hydrogenation and Hydrogenolysis of BMFM over Noble Metal Catalysts .....	61
4.1	Introduction .....	61
4.2	Experimental .....	63
4.2.1	Materials .....	63
4.2.2	Catalyst characterization .....	63
4.2.3	Catalytic hydrogenation .....	64
4.2.4	Product analysis .....	64
4.3	Results .....	65
4.3.1	Hydrogenation of BMFM among various metals .....	65
4.3.2	Effects of reactant concentration on the kinetic network of Pd/C and Pt/C .....	69
4.3.3	Effects of temperature of the kinetics of BMFM hydrogenation .....	69
4.4	Discussion .....	70
4.4.1	Identification of the network for BMFM hydrogenation over Pd/C and Pt/C ..	70
4.4.2	Role of palladium hydride species .....	74
4.4.3	Development of a kinetic model for BMFM hydrogenation over Pd/C and Pt/C	75

4.5	Conclusions .....	81
4.6	Supplemental Information.....	82
4.6.1	Catalysts properties .....	82
4.6.2	Elimination of mass transfer effects in semi-batch hydrogenation system .....	82
4.6.3	Hydrogenation of BMFM over noble metals on carbon support .....	84
4.6.4	BMFM hydrogenation kinetics over Pd/C and Pt/C catalysts.....	86
4.6.5	Derivation of rate expressions in kinetic model.....	91
4.6.6	Results of kinetic model for BMFM hydrogenation Pd/C and Pt/C catalysts....	96
5	Selective Hydrogenation of Nucleophilic Condensation Products.....	100
5.1	Introduction.....	100
5.2	Experimental .....	101
5.2.1	Chemicals and catalysts.....	101
5.2.2	Synthesis of substrates via nucleophilic addition.....	101
5.2.3	Catalytic Hydrogenation.....	102
5.3	Results and Discussion.....	103
5.3.1	Characterization of catalysts.....	103
5.3.2	Selective HDO of 5-MF over noble metal catalysts.....	103
5.3.3	Selective HDO of MFVFAL over noble metal catalysts.....	106
5.4	Conclusions.....	112
	References.....	113
	Appendix A1 – Chemical Characterization .....	120
A1.1	NMR 5-MF Dimer (MFVFAL).....	120
A1.2	NMR Data 5-MF Trimer .....	122
A1.3	FT-IR spectra of C11 oxygenates.....	124

## List of Figures

Figure 2.1. Temporal profiles of the electrophilic aromatic substitution reaction between 2-MF and formalin.....	10
Figure 2.2. Temporal profiles of % yield of BMFM during reaction using HCl and SO <sub>3</sub> H-SiO <sub>2</sub> catalysts .....	11
Figure 2.3. Selectivity toward products 1a and 2a as a function of 5-MF for ethoxide catalysts. 16	
Figure 2.4. Time course of 5-MF Dimerization over K <sub>3</sub> PO <sub>4</sub> .....	17
Figure 2.5. Initial conversion of 5-MF with (•) and without (♦)solid K <sub>3</sub> PO <sub>4</sub> . .....	18
Figure 3.1 Concentration profile of reactor composition during the course of DMF hydrogenation over 5% Pt/C.....	32
Figure 3.2 Effect of temperature on the ratio of concentration of 2-hexanol to 2-hexanone (HXL:HEX) during the course of DMF conversion.....	33
Figure 3.3 Effect of initial DMF concentration on selectivity toward ring opening and on the initial rates of DMF hydrogenation over 5% Pt/C.....	35
Figure 3.4 Effect of p <sub>H2</sub> on the selectivity to ring opening and on initial rates of DMF hydrogenation over 5% Pt/C.....	35
Figure 3.5 Effect of initial 2-hexanone concentration and effect of p <sub>H2</sub> on the initial rate of hydrogenation of 2-hexanone to 2-hexanol using 5% Pt/C.....	36
Figure 3.6 Arrhenius plots of initial rates normalized by dependence on C <sub>H2</sub> <sup>n</sup> for reaction temperatures (343 – 373 K) using 5% Pt/C,.....	36
Figure 3.7 Comparison of experimental data (symbols) and concentration profiles fitted for the model (lines) during DMF hydrogenation over 5% Pt/C. ....	46
Figure 3.8 Comparison of experimental and fitted concentration profiles for 2-hexanone hydrogenation to 2-hexanol over 5% Pt/C 353K.....	46
Figure 3.9. Selectivity toward 2-hexanone as a function of DMF conversion and temperature. .	49
Figure 4.1. Evolution of products during BMFM hydrogenation.....	68
Figure 4.2. Selectivity to products described in Scheme 4.1 as a function of BMFM conversion. ....	70
Figure 4.3 Comparison of experimental and simulated concentration profiles reaction network of BMFM hydrogenation .....	79
Figure 5.1 Conversion and product distribution of hydrogenation of 5-MF over noble metal catalysts. ....	105
Figure 5.2. Production of selective HDO products over time during hydrogenation of MFVFAL over noble metal and Pd alloy catalysts.....	107
Figure 5.3. Product distribution as a function of time for MFVFAL hydrogenation over PdCu/C catalysts. ....	107
Scheme 2.1. Examples of acid and base catalyzed condensation chemistries for the formation of diesel range oxygenates discussed in Chapter 2.....	6
Scheme 2.2 Proposed mechanism for acid catalyzed, electrophilic aromatic substitution reaction between 2-MF and formaldehyde.....	9

Scheme 2.3 Hydrolysis of 2-MF to form 2-oxobutanal and resulting products from additional condensation reactions and ring hydrolysis.....	10
Scheme 2.4. C <sub>12</sub> and C <sub>18</sub> products from the self dimerization of 5-MF over base catalysts.....	14
Scheme 2.5 Proposed reaction mechanism for base-catalyzed self-dimerization of 5-MF into dimer and trimer products.....	15
Scheme 2.6 Examples of products and their masses resulting from isotopic exchange experiments using deuterated ethanol solvents. ....	20
Scheme 2.7 Proposed mechanism for 5-MF self-dimerization to form product 1b over K <sub>3</sub> PO <sub>4</sub> in ethanol-d solvent.....	21
Scheme 2.8 Mechanism for Tishchenko reaction between alkoxide species and aromatic aldehydes to form aromatic alcohols and esters. ....	22
Scheme 2.9 Cross condensation products between 5-MF and furfural or benzaldehyde over K <sub>3</sub> PO <sub>4</sub> in ethanol.....	22
Scheme 3.1 Proposed reaction network for the hydrogenation of DMF into ring saturated and ring opened products over Pt/C. ....	39
Scheme 3.2 Schematic of the elementary reactions involved in the overall reaction network shown in Scheme 1. ....	41
Scheme 4.1 Products of BMFM hydrogenation over noble metals. ....	66
Scheme 4.2. Reaction network of BMFM hydrogenation and hydrogenolysis over Pt and Ru based catalysts. ....	71
Scheme 4.3. Reaction network of BMFM hydrogenation and hydrogenolysis over Pd based catalysts. ....	72
Scheme 4.4. Cleavage of the internal vs. external aromatic C-O bond to form enol intermediates and ring opened species. ....	72
Scheme 5.1 Hydrogenation/hydrodeoxygenation network of 5-methylfurfural (5-MF) over noble metals.....	104
Scheme 5.2. Reaction network for MFVFAL Hydrogenation/hydrodeoxygenation in ethanol over noble metal catalysts.....	109
Scheme 5.3. Adsorption modes of furfural over hydrogenation metal surfaces as described by Sitthisa et al. ....	111
Scheme 5.4. Possible species on the surface of hydrogenation metal catalysts during conversion of furfuryl alcohol to 2-MF proposed by Sitthisa et al. [100] .....	111
Scheme 5.5. Two-step selective hydrodeoxygenation/hydrogenation over PdCu/C and Pd/C catalysts for the production of cyclic ethers. ....	112

## List of tables

Table 1.1 Predicted and experimentally measured derived cetane numbers (DCN) for furan condensation products following varying degrees of hydrogenation.....	4
Table 2.1. Electrophilic aromatic substitution reactions of 2-MF for the formation of BMFM over homogeneous and heterogeneous acid catalysts.....	8
Table 2.2 Initial rates of self-dimerization of 5-MF for homogeneous base catalysts and heterogeneous K <sub>3</sub> PO <sub>4</sub> (873 K) catalysts.....	14
Table 2.3 Screening of solid base catalysts for the nucleophilic self-condensation of 5-MF in ethanol. ....	16
Table 2.4 5-MF dimerization over K <sub>3</sub> PO <sub>4</sub> (873 K) in various solvents in q-tube reactors. ....	19
Table 2.5 Cross condensation of 5-MF and FUR over K <sub>3</sub> PO <sub>4</sub> (873 K) in q-tube reactors. ....	22
Table 2.6 Cross condensation of 5-MF and benzaldehyde over K <sub>3</sub> PO <sub>4</sub> (873 K) in q-tube reactors. ....	23
Table 3.1 Density of supported metal and average particle size for metal nanoparticles.....	31
Table 3.2 Turnover frequency (TOF) for DMF consumption and product selectivity for carbon-supported noble metals. ....	31
Table 3.3 TOFs obtained from initial rates for hydrogenation of DMF over 5% Pt/C.....	33
Table 3.4 Apparent rate parameters for the hydrogenation of 2,5-dimethylfuran and 2-hexanone on Pt.....	37
Table 3.5 Turnover frequencies (TOFs) for hydrogenation over supported Pt catalysts when DMF or 2-hexanone was used as the substrate.....	37
Table 3.6 Rate parameters obtained by non-linear, least squares fitting of experimental data to proposed kinetic model for the reaction network of DMF hydrogenation. ....	47
Table 3.7 Rate parameters involved in eq. 7 obtained by non-linear, least squares fitting of experimental data for the hydrogenation of 2-hexanone to 2-hexanol.....	47
Table 4.1 Predicted and experimentally determined derived cetane numbers (DCN) for furan condensation products at varying degrees of hydrogenation.....	62
Table 4.2. Comparison of turnover frequencies and catalyst properties of the 1wt% and 5wt% loading of Pd catalyst for the Madon-Boudart test.....	65
Table 4.3. Turnover frequency (TOF) for BMFM consumption and product selectivity for carbon-supported noble metals. ....	66
Table 4.4. Initial rate order dependence with respect to p <sub>H<sub>2</sub></sub> for the rate of ring saturation (r <sub>BMH<sub>4</sub></sub> ) and rate of ring opening (r <sub>R.O.</sub> ) for Pd/C and Pt/C catalysts. ....	69
Table 4.5. Apparent activation energies determined from Arrhenius plots of the initial rates of hydrogenation over Pt/C and Pd/C. ....	70
Table 4.6. Distribution of single ring opened products resulting from hydrogenolysis of interior vs. exterior C-O bond to form either ketones or alcohols obtained at 30% conversion of BMFM. ....	73
Table 4.7. TOFs for ring saturation to form product 1b (BMTHFM) at < 30% conversion and at over 90% conversion of BMFM where mainly BMH <sub>4</sub> remains.....	74

Table 4.8. Rate parameters obtained by non-linear, least squares fitting of experimental data to proposed kinetic model for the reaction network proposed in Scheme 4.3 for BMFM hydrogenation over Pd/C.....	80
Table 4.9. Rate parameters obtained by non-linear, least squares fitting of experimental data to proposed kinetic model for the reaction network proposed in Scheme 4.2 for BMFM hydrogenation over Pt/C.....	80
Table 5.1 CO chemisorption at 310 K to titrate and quantify metal sites.....	103
Table 5.2. Conversion of 5-MF and selectivity to DMF and to decarbonylation.....	105
Table 5.3. Hydrodeoxygenation of furfural and tetrahydrofurfuryl alcohol over PdCu/C catalysts.....	108

## List of Abbreviations and Symbols

*	vacant sites on the catalyst surface for adsorption of organic species
* <sub>H</sub>	vacant sites on the catalyst surface for adsorption of atomic hydrogen
2-MF	2-methylfuran
5-MF	5-methylfurfural
A	pre-exponential factor given in the Arrhenius equation, $k = A\exp(-E_A/(RT))$
BMFM	bis(5-methylfuran-2-yl)methane
BMH <sub>4</sub>	2-methyl-5-((5-methyltetrahydrofuran-2-yl)methyl)furan
BMTHFE	1,2-bis(5-methyltetrahydrofuran-2-yl)ethane
BMTHFM	bis(5-methyltetrahydrofuran-2-yl)methane
C <sub>i</sub>	concentration of species i
C <sub>n</sub>	a molecule containing n carbon atoms
DCN	derived cetane number
DFT	density functional theory
DMF	2,5-dimethylfuran
DMM	dimethoxymethane
DMTHF	2,5-dimethyltetrahydrofuran
D <sub>p</sub>	nanoparticle diameter
E <sub>A</sub>	apparent activation energy given in the Arrhenius equation, $k = A\exp(-E_A/(RT))$
E <sub>app</sub>	apparent activation energy
EtOH	ethanol
FTIR	fourier transform infrared spectroscopy
FUR	furfural
FVFAL	5-(2-(furan-2-yl)vinyl)furan-2-aldehyde
GC/MS	gas chromatography/mass spectrometry
HDO	hydrodeoxygenation
HEX	2-hexanone
H <sub>H2</sub>	Henry's constant for H <sub>2</sub> in the liquid phase
HMF	5-hydroxymethylfurfural
HXL	2-hexanol
ICP-OES	inductively-coupled plasma optical emission spectrometry elemental analysis
I <sub>ix</sub>	partially hydrogenated intermediates adsorbed on surface
IWI	incipient wetness impregnation
K <sub>3</sub> PO <sub>4</sub>	potassium phosphate
k <sub>i</sub>	rate constant for reaction i
K <sub>i</sub>	adsorption equilibrium constant for organic species i
MeOH	methanol
mequiv	molar equivalent
MFOL	5-methylfuran-2-yl alcohol
MFVFAL	5-(2-(5-methylfuran-2-yl)vinyl)furan-2-aldehyde
NbOPO <sub>4</sub>	niobium Phosphate
NMR	nuclear magnetic resonance spectroscopy
PdH <sub>x</sub>	palladium hydride

$p_{H_2}$	partial pressure of $H_2$
PWA	phosphotungstic acid
R	molar gas constant
$r_i$	reaction rate for reaction i
RO	ring Opening
RS	ring Saturation
$S_{ad}$	entropy of adsorption
SEA	strong electrostatic adsorption
SFAL	5-styrylfuran-2-aldehyde
SFG-VS	sum frequency generation vibration spectroscopy
T	reaction temperature
t	reaction time
THF	tetrahydrofuran
THFOL	tetrahydrofurfuryl alcohol
$TiO_2$	titanium dioxide
TMFM	tris(5-methylfuran-2-yl)methane
TOF	turnover frequency
TPD	temperature Programmed Desorption
TPR	temperature Programmed Reduction
V	solution volume in reactor
W	weight of catalyst loaded
$\gamma-Al_2O_3$	$\gamma$ -alumina
$\Delta G$	Gibbs free energy
$\Delta H_{ad}$	heat of adsorption



## Acknowledgments

It is a most humbling experience to reflect on all the people and events that have founded, shaped, and supported my graduate school journey. As difficult as it is to describe in words, I hope the extent of my gratitude is expressed in the space following. I am the person and the intellectual I am now because of all the support and help I received in the past 6 years.

I want to thank Professor Alex Bell for his patience and mentorship during my Ph.D. He provided the encouragement when I was in doubt and the guidance when I was lost. By having Alex as an adviser, I learned to ask the important questions, tell meaningful stories, and focus on the bigger picture. I am also lucky to be part of such an accomplished and established catalysis group that is full of brilliant minds. I want to thank the previous generation of Tan Hall members: Bean Getsoian, Sebastian Werner, David Hanna, Zheng Zhai, Greg, Johnson, Shannon Klaus, Amber Janda, Joe Gomes, and Jason Wu, that warmly welcomed me, entertained my questions, and provided the lab culture in which I grew into. I want to also thank the members at the Energy Bioscience Institute: Sean Dee, Eric Sacia, Kris Enslow, Kostas Goulas, and Balki Madhesan, for providing me with more biomass to biofuel literature than I could read, training me, and sitting through endless practice quals. I want to acknowledge Shylesh Pillai, Deepak Jadhav, Chris Ho and Neelay Phadke for their discussions on chemistry, catalysis, and synthesis. Lastly, I want to acknowledge a few colleagues that have put up with me and supported me on a daily basis. They are Alex Wang, who graciously adopted the organizational and safety responsibilities, Julie Rorrer, who can light up the entire hallway with her spirit and smile all the way from her desk at the back in the Toste lab, and Adam Grippo, who is still the nicest and most considerate person while facing me at my worse. Their support got me through the tougher times of science and they have made my time at EBI a wonderful experience.

Other parties instrumental to my scientific accomplishments include a group of dedicated visiting scholars and undergraduate students that I had the opportunity to mentor: Joseph Tang, ZhiChen Shi, and Alexander Hell. They worked alongside me to tackle some challenging problems and complicated setups. Much of the findings and conclusions presented here in my dissertation are fruits of their labor and perseverance. I also want to thank Professor Alex Katz for his mentorship when I was a GSI for CBE 142, his feedback, and his lab and instrumentation. The administrative assistants of the Chemical Engineering Department, Bell Group, and EBI have made my graduate research possible by handling department logistics, my tardy paperwork, and purchases with such efficiency so that I can focus on the science. Thank you to Carlet, Kristin, Joel, Katie, Mara, and Stefan.

My graduate school journey is described not only by my growth as a researcher and scientist, but also by my personal growth as a friend, a colleague, and an individual in various communities. I am proud to be part of the ChemE 2011 class - a community full of camaraderie, enthusiasm, passion, intelligence and great ideas. The support and love of celebration from this group fuel high quality of life. There are some individuals here whom I readily depend on for support, cheer, and commiseration throughout my PhD's summits and valleys. The first person I met during visit weekend was Rachel Licht. Ever since our failed boat race on top of the bar at Raleigh's, she has been a dear friend, a labmate, and a role model. Cynthia Chen is someone so

thoughtful and creative, from whom I draw a lot of enthusiasm and respect for life and its experiences. Edwin is a genuine confidant whom I can discuss all things of reason and unreason with. Eddie Buehler and David Liu have always been there for all of our last minute plans at Jupiter.

I am so incredibly lucky and grateful to have housemates who are also my personal crew of cheerleaders: Carly Anderson, Hilda Buss, and Nico Herman. Sometimes I feel so full of love and support that I might just spill over the sides like a glass of water poured past the brim. They have gone above and beyond for me and pushed me to be stronger, both mentally and physically. Joy is opening bottles of wine, cooking dinners, reenacting tricky bouldering problems, and sharing physical therapy exercises and gadgets with them. But there is no bigger cheerleader here than Jacob Thelen; he truly believes in me and holds me to such high esteem. He has kept me grounded during these years of my Ph.D., and because of him and his confidence in me, I am a stronger, better, and more independent and more emphatic person.

There are many others who have helped Bay Area capture my heart during these years by teaching me how to climb, driving to adventures in the mountains, and connecting with me through dance. I want to thank Nico Grosso for the belays and climbing trips, Phoebe, Velencia and Chae Young for fueling my dance addiction, and Fernando for his support and dances. The bay area climbing community and salsa dancing community have been so welcoming and friendly and I am happy to be part of it.

The foundation of my personal journey to, and through grad school has always been family – my parents for their dedication and sacrifices, and my siblings, Tracey, Anne, and Chris, and my adopted siblings, Matt and Jeremy. They make me feel as if I can take on the world because I know they unconditionally have my back. Leaving them and moving to California was a difficult decision that plagued my mind throughout my PhD, but I am so proud of how much they have grown through their own experiences and challenges. I was fortunate enough to have a bit of family in the Bay Area, Phoebe Lai. 14 years ago, she had said to me “mi casa es tu casa” and it is as true today as it was then. I greatly appreciate her making time for me at the drop of a hat, providing me a place to see as home, and enabling my city escapades.

Speaking of homes away from home, I want to acknowledge a few people that have always allowed me to find the comfort and ease of home, abroad – Marta, Kate, Lotte, Patrik, and Hedvig. My Fulbright year, before I joined UC Berkeley, was largely shaped by this crew and is a significant part of who I am now. Because of them, Sweden always feels like home. I am grateful for technology and WhatsApp that allows us to keep in touch over time zones and distances.

On a final note, I do understand how lucky I am to have so many people to be indebted to and to depend on. I am thankful for their influence and support during this chapter of my life and I look forward to their presence in the next.

## 1 Introduction

The transportation sector is the second largest contributor of greenhouse gas (GHG) emissions among the end-use sectors, accounting for 27% of all emissions in the U.S. and 30% world wide in 2015 [1]. Greenhouse gas emissions from this sector are a result of fossil fuels burned for road, rail, and air transportation. Since 95% of the world's transportation energy is currently derived from petroleum-based fuels, incorporation of alternative, renewable sources is an opportunity to mitigate GHG emissions [2]. Lignocellulosic biomass, the most abundant class of biomass, has the potential to be a carbon neutral energy source for the production of liquid fuels [3]. In fact, it is projected that by 2050, biofuels could provide between 15-30% of total transport fuel, particularly through the replacement of jet fuel, kerosene, and diesel [2].

Current strategies to convert lignocellulosic biomass into liquid fuels can be divided into two broad pathways, (1) thermochemical and (2) hydrolysis. Thermochemical processes involve treatment at high temperatures (750 to 1000 K), resulting in complete or extensive deconstruction of the organic structure. Examples include steam gasification to synthesis gas, a mixture of CO and H<sub>2</sub>, and anaerobic pyrolysis to oxygen-rich oils [4]. Synthesis gas can be converted to fuels by Fischer-Trosch synthesis [5], whereas pyrolysis oils can be hydro-treated and then refined together with petroleum [4,6].

Compared to thermochemical methods, hydrolysis of biomass occurs at milder conditions (350 to 400 K) and allows for more selective processing of the feedstock. During hydrolysis (acid or enzymatic), the cellulosic and hemicellulosic fractions (70-75%) of biomass are isolated and broken down into C<sub>6</sub> (glucose) and C<sub>5</sub> (xylose) sugars, respectively. These sugars can be utilized in enzymatic fermentation processes to produce biofuel alcohols, ethanol or butanol, or in catalytic processes to produce C<sub>6</sub> and C<sub>5</sub> furanic compounds, furfural (FUR) and 5-hydroxymethylfurfural (HMF), respectively. Bio-alcohols are not ideal candidates for diesel and jet fuel due to their higher volatility and oxygen content, and lower heating value and cetane number compared to conventional diesel fuel [7]. Furthermore, 33% of the carbon content of bio-derived sugars is lost as CO<sub>2</sub> during the fermentation process. In contrast, the FUR and HMF produced by catalytic dehydration of sugars retain all of the monosaccharide carbon, but contain ~ 50% less oxygen, and can be readily converted to jet and diesel fuel range oxygenates via aldol condensation [8,9], hydroalkylation [10–12], and etherification [13,14]. The oxygenate products from these C-C bond forming reactions are C<sub>9</sub>-C<sub>21</sub> furanics, which have cetane numbers (column 1, Table 1.1) below the minimum requirement, 40 and 50, for diesel fuel in the United States and European Union, respectively [15,16]. To obtain higher cetane numbers, furanic compounds must be hydrotreated in order to transform these oxygenated compounds into cyclic ethers by partial hydrogenation [17], or to hydrocarbons by hydrodeoxygenation [4,6,10] (Table 1.1).

Since hydrotreatment is the final, critical step in producing chemical species with suitable fuel properties, there is considerable interest in understanding the activity and selectivity of noble metal catalysts that can use for the hydrogenation and hydrodeoxygenation (HDO) of furan-containing compounds. The major objectives of the present study are to understand the mechanism and kinetics of hydrogenation and hydrogenolysis of various functional moieties commonly found in products from C-C coupling chemistries, such as furan rings, unsaturated C=C bonds, and C=O aldehydes, over noble metal catalysts.

The functional moiety of largest interest is the aromatic furan ring, which is ubiquitous in all of the condensation products derived from FUR and 5-HMF. Several pathways for scission of the C-O bond in the furan ring during hydrogenation have been discussed in literature. For example, C-O hydrogenolysis has been proposed to occur only after sequentially hydrogenating the C=C bonds of the aromatic ring into saturated tetrahydrofuran intermediates during hydrogenation of 2-methylfuran (2-MF), 2,5-dimethylfuran (DMF) and tris(5-methylfuran-2-yl)methane (TMFM, Table 1.1) over Pt and Pd catalysts [17–20]. On the other hand, ring hydrogenolysis has also been suggested to occur directly from alkylfurans (2-MF, DMF) over Pt and Pd catalysts based on observations of significantly lower activity to ring opening for tetrahydrofuran containing substrates versus aromatic furan containing substrates [21–23]. Lastly, it has been proposed that under HDO conditions (623 to 643 K, 1 – 6 MPa H<sub>2</sub>), hydrolysis of the furan ring into linear diketones, catalyzed by the high temperature water generated during HDO, is the initial step responsible for ring-opening of the furanyl condensates [24,25]. However, these linear di-ketones were not identified during such HDO reactions unless they were performed in aqueous systems [26,27].

In the present work, we have explored the mechanism and kinetics of hydrogenation and C-O hydrogenolysis for several model substrates: 2,5-dimethylfuran (DMF), bis(5-methylfuran-2-yl)methane (BMFM), 5-(2-(5-methylfuran-2-yl)vinyl)furan-2-aldehyde (MFVFAL), 5-(2-(furan-2-yl)vinyl)furan-2-aldehyde (FVFAL), and 5-styrylfuran-2-aldehyde (SFAL) over noble metal catalysts at moderate conditions (333K - 363K, 0.41-0.69 MPa H<sub>2</sub>). These substrates were chosen to because they are compounds produced by C-C coupling via aldol condensation and hydroalkylation. We note that while DMF is available commercially, the remaining, more complex, C<sub>11</sub>-C<sub>13</sub> substrates must be synthesized.

Chapter 2 discusses the synthetic strategies for the formation of the following substrates: BMFM, MFVFAL, FVFAL, and SFAL. BMFM is a C<sub>11</sub> oxygenate containing two adjacent furan rings and can be formed from Brønsted acid-catalyzed condensation of 2-methylfuran (2-MF) and formalin. Adjacent furanyl moieties such as the ones in BMFM, are common structures in the products of hydroalkylation involving the electrophilic aromatic substitution of 2-MF and other synthons [10,12]. MFVFAL, FVFAL and SFAL are compounds synthesized from base-catalyzed nucleophilic condensation of 5-methylfurfural with itself, furfural, or benzaldehyde, respectively. Conjugated systems such as the ones found in these substrates are common in base-catalyzed condensation of FUR or HMF with methylketones. Heterogeneous catalysts were identified for synthesizing each of the compounds discussed above.

In Chapter 3, we discuss the mechanism and kinetics for the hydrogenation of 2,5-dimethylfuran (DMF), the simplest substituted furan derived from biomass. Hydrogenation was carried out in a multi-phase batch reactor operated at temperatures of 333K - 363K and hydrogen pressures of 0.41-0.69 MPa. The hydrogenation activity of carbon-supported Pd, Pt, Rh, and Ru were compared on the basis of available metal surface area. Of the catalysts studied, Pt/C had the greatest activity for C-O hydrogenolysis to form 2-hexanone and 2-hexanol, whereas Pd/C was very selective for saturating the aromatic ring into 2,5-dimethyltetrahydrofuran. We proposed a reaction network in which ring opening and ring saturation of DMF compete and that an enol intermediate formed after C-O cleavage is the precursor to both 2-hexanone and 2-hexanol observed during hydrogenation of DMF over Pt. A microkinetic model derived from this

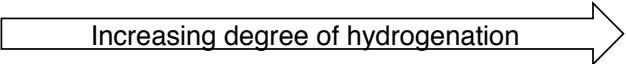
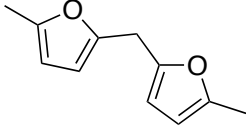
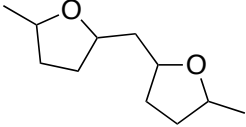

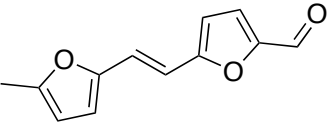
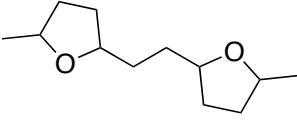

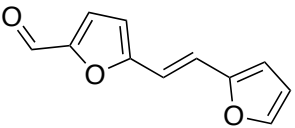
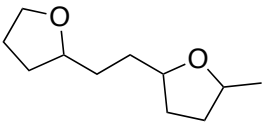
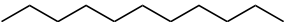
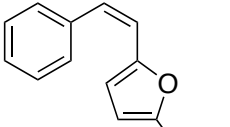
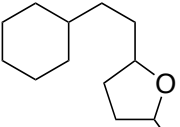
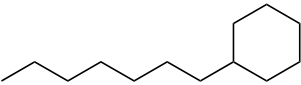
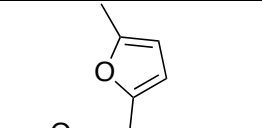
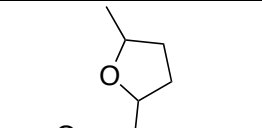

mechanism was found to give an accurate description of the experimentally observed reaction kinetics.

We next expanded our studies to address the hydrogenation of the more complex furanyl substrate, BMFM, which contains two furan moieties. In Chapter 4, we compare the activity of Pd/C and Pt/C for the hydrogenation of BMFM at moderate conditions (430K – 473K, 2 MPa H<sub>2</sub>). Unlike what was previously observed for hydrogenation of DMF, conversion of BMFM occurred an order of magnitude more rapidly on Pd/C than on Pt/C with significant selectivity for C-O hydrogenolysis – up to 30% yield of alcohols were achieved over Pd/C. The C-O hydrogenolysis observed during DMF hydrogenation studies was applicable to the studies of BMFM hydrogenation. Once again, ring opening occurred only at aromatic C-O bonds of furans, at elevated temperatures, and proceeded through an enol intermediate for the formation of ketones and alcohols.

Finally, in Chapter 5, we address the hydrogenation of a complex condensation product, MFVFAL, containing functional group moieties commonly found in aldol condensation reactions, namely, unsaturated C=C in conjugation with aromatic furans, and aldehyde groups. , Unlike BMFM, the two aromatic furan rings in MFVFAL are different, since one ring contains a C=O aldehyde substituent and the other contains a methyl substituent. Under hydrogenation conditions over noble metal catalysts (Pt, Pd, Ru), the aldehyde group can undergo selective HDO, resulting in a terminal methyl group and release of water. Selective HDO of FUR and HMF into 2-MF and DMF, respectively, has been achieved through the application of alloyed metals but this chemistry has not been applied to these diesel-range condensates. Pd based alloys were synthesized to improve selectively toward removal of the C=O group of MFVFAL and to saturate the furan moieties into desirable cyclic ethers.

The overall goal of this study is to provide an understanding of the complex network of hydrogenation and hydrogenolysis reactions required for the conversion of complex furanyl products derived from biomass to fuels. The understanding gained from these studies will enable the strategic choice of catalysts and reaction conditions required to convert biomass-derived compounds into hydrocarbons and cyclic ethers suitable for use as transportation fuels.

**Table 1.1** Predicted and experimentally measured derived cetane numbers (DCN) for furan condensation products following varying degrees of hydrogenation.

			
	Furan Condensation Products	Selective Hydrogenation Products	Hydrodeoxygenation Products
<b>Compounds explored in current study</b>	 $C_{11}H_{12}O_2$ 12.5 <sup>a</sup> BMFM	 $C_{11}H_{20}O_2$ 60.3 <sup>a</sup>	 $C_{11}$ $C_{11}H_{24}$ 83 <sup>b</sup>
	 $C_{12}H_{10}O_3$ 22.7 <sup>a</sup> MFVFAL	 $C_{12}H_{22}O_2$ 89.3 <sup>a</sup>	 $C_{12}$ $C_{12}H_{26}$ 88 <sup>b</sup>
	 $C_{11}H_8O_3$ 24.07 <sup>a</sup> FVFAL	 $C_{11}H_{20}O_2$ 83.5 <sup>a</sup>	 $C_{11}$ $C_{11}H_{24}$ 83 <sup>b</sup>
	 $C_{13}H_{10}O_2$ 13.9 <sup>a</sup> SFAL	 $C_{13}H_{24}O$ 73.7 <sup>a</sup>	 $C_{13}H_{26}$ 79 <sup>c</sup>
<b>Compound explored in previous studies [10–12]</b>	 $C_{16}H_{18}O_3$ 22.3 <sup>d</sup> TMFM	 $C_{16}H_{28}O_3$ 59.8 <sup>d</sup>	 $C_{16}$ $C_{32}H_{34}$ 45 <sup>b</sup>

<sup>a</sup> DCN values predicted by Mack and co-workers using artificial neural network [28]

<sup>b</sup> Value determined from Compendium of Experimental Cetane Numbers [29]

<sup>c</sup> Reported cetane number of n-heptylcyclohexane [30]

<sup>d</sup> DCN values determined experimentally [17]

## 2 Synthesis of Diesel Range Oxygenates from Biomass-Derived Furans

### 2.1 Introduction

Cellulose and hemicellulose constitute a significant fraction (70-75%) of lignocellulosic biomass and are attractive starting materials for the production of renewable diesel and jet fuel [4,31]. Hydrolysis of these polysaccharides produces C<sub>5</sub> and C<sub>6</sub> sugars, xylose and glucose, respectively. Transformation of these sugars into chemical compounds suitable for combustion in current diesel and jet engines requires decreasing the C/O ratio and increasing the carbon chain to 8-16 (jet fuel) or 9-21 (diesel fuel) carbon atoms [31,32]. Acid catalyzed dehydration of xylose and glucose removes approximately 50% of the oxygen without loss of carbon to produce furfural (FUR) and 5-hydroxymethylfurfural (HMF), respectively. These furanic species can be produced with high selectivity and yields (>90%), especially in biphasic systems where an organic phase facilitates the extraction of furanic products from an aqueous solution, reducing the formation of undesired humins [33]. FUR and HMF are valuable platform compounds that can be used as primary synthons or converted to secondary synthons. Examples of the latter include levulinic acid and  $\gamma$ -valerolactone through hydrolysis/hydrogenation reactions [32], 2-methylfuran, 2,5-dimethylfuran, and 5-methylfurfural via selective hydrodeoxygenation reactions over copper, chromium, or noble metal alloyed catalysts [34–36]. C<sub>5</sub>-C<sub>6</sub> methylketones can be sourced from 2-methylfuran and 2,5-dimethylfuran, respectively, by ring opening hydrogenolysis [37].

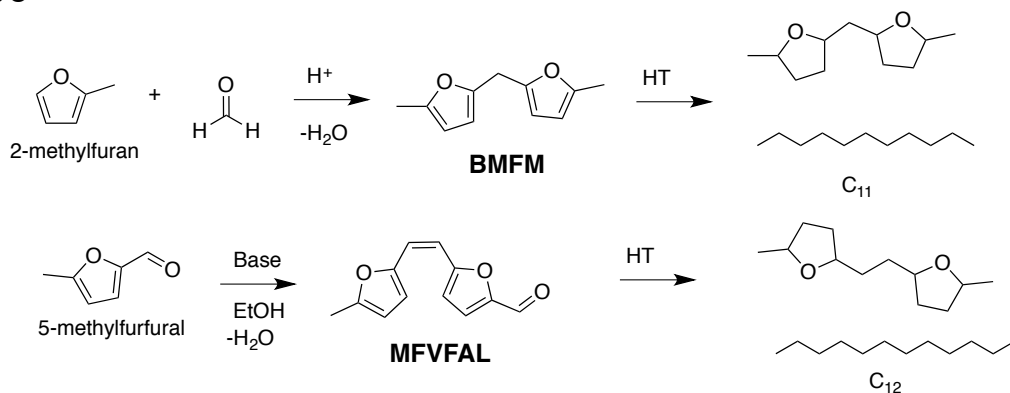
The primary and secondary synthons derived from xylose and glucose can be converted to diesel range products by C-C bond forming reactions. Common chemistries include pinacol coupling of FUR and aromatic aldehydes using a reducing metal in basic media [38], dehydrogenative cross-coupling of FUR with primary alcohols [39], base-catalyzed aldol condensation of furanyl aldehyde functionalities with ketones such as acetone or methylisobutylketone [8,9], and acid-catalyzed hydroalkylation reactions of aldehydes with 2-methylfuran [10–12].

Products from such condensation reactions have carbon numbers within the range required for diesel (C<sub>9</sub> – C<sub>21</sub>) and jet (C<sub>8</sub> – C<sub>16</sub>) [40]. However, these compounds are typically highly oxygenated and contain various functional groups, e.g., C=C, C=O, and furan rings, that results in poor combustion properties and prevents the direct use of these products as fuels or fuel blending agents. Therefore, hydrotreatment is required in order to remove these functional groups. Hydrotreatment of furanic compounds involve the addition of H<sub>2</sub> to saturate C=C and C=O bonds, cleave C-O bonds, and remove oxygen in the form of water. The products of hydrotreatment are either cyclic ethers or alkanes in the jet and diesel range (Scheme 2.1).

The aim of our work is to investigate the mechanism and kinetics of hydrogenation of complex furans compounds over noble metal catalysts. Simple, substituted, aromatic furans such as 2,5-dimethylfuran (DMF) are commercially available. But the investigation of complex, higher-molecular weight furanic compounds requires that these compounds be synthesized. In this chapter, we discuss synthetic strategies for producing the following C<sub>11</sub>-C<sub>13</sub> substrates: bis(5-methylfuran-2-yl)methane (BMFM), 5-(2-(5-methylfuran-2-yl)vinyl)furan-2-aldehyde (MFVFAL), 5-(2-(furan-2-yl)vinyl)furan-2-aldehyde (FVFAL), and 5-styrylfuran-2-aldehyde (SFAL).

In the first half of this chapter, we discuss the synthesis of BMFM, a C<sub>11</sub> oxygenate containing two adjacent furan rings, using 2-methylfuran (2-MF) and formalin in a Brønsted acid-catalyzed condensation. The dual, adjacent furanyl moieties present in BMFM are commonly formed during hydroalkylation reactions involving the electrophilic aromatic substitution of 2-MF with other synthons containing aldehyde or ketone functionalities such as cyclopentanone [41], angelica lactone [42], mesityl oxide [43], butraldehyde [44] and furfural [10–12]. Typical catalysts for these reactions are strong mineral acids such as HCl, H<sub>2</sub>SO<sub>4</sub> or H<sub>3</sub>PO<sub>4</sub>. Since product separation is difficult using liquid acids, we have explored the use of heterogeneous catalysts for preparing BMFM.

The second half of this chapter discusses the base-catalyzed nucleophilic condensation of 5-methylfurfural with itself, furfural, or benzaldehyde to produce MFVFAL, FVFAL and SFAL, respectively. These C<sub>12</sub>-C<sub>13</sub> oxygenates contain aromatic rings, conjugated C=C, and aldehyde functionalities commonly found in products of base-catalyzed aldol condensation between FUR or HMF and methylketones. Similar to aldol condensation, nucleophilic condensation involves base-catalyzed H abstraction to generate nucleophiles that target electrophilic aldehyde groups. Unlike aldol condensation where the reactive nucleophile is an enolate ion, the reactive nucleophile in our chemistry is the carbanion formed at the methyl group of 5-MF, which attacks the aldehyde group of another molecule of 5-MF in self-condensation reactions, or the aldehyde group of other substrates, such as FUR or benzaldehyde, in cross-condensation reactions. This chemistry has previously been used to synthesize conjugated polymers from 5-MF using strong homogeneous bases such as NaOH and t-buOK [45–47]. In our study, we report the use of a recyclable heterogeneous base, K<sub>3</sub>PO<sub>4</sub>, which exhibits an order of magnitude greater activity than homogeneous hydroxide and ethoxide bases for the condensation of 5-MF to C<sub>12</sub>-C<sub>13</sub> oxygenates.



**Scheme 2.1.** Examples of acid and base catalyzed condensation chemistries for the formation of diesel range oxygenates discussed in Chapter 2.

## 2.2 Electrophilic Aromatic Substitution of 2-MF

### 2.2.1 Experimental

#### Chemicals

Formalin (36 wt% in H<sub>2</sub>O, 10-15 wt% MeOH), 2-methylfuran, dimethoxymethane, and dodecane were purchased from Sigma-Aldrich. Pellets of Amberlyst-15® (hydrogen form) and Nafion SAC-13 ® were also purchased from Sigma Aldrich. Prior to use, these catalysts were



ground into fine powder (<45 $\mu$ m) and dried overnight at 383 K. P-toluenesulfonic acid monohydrate (p-TSA) was obtained from Spectrum Chemicals and hydrochloric acid, from Fisher Scientific. 30wt% phosphotungstic acid on SiO<sub>2</sub> (PWA-SiO<sub>2</sub>) catalyst was prepared by incipient wetness impregnation of phosphotungstic acid (Sigma-Aldrich) on silica gel support (Sigma-Aldrich). Silica sulfuric acid (SO<sub>3</sub>H-SiO<sub>2</sub>) was prepared by reaction of silica gel with chlorosulfonic acid, washed with ethanol, and then dried at 373 K for 12h [12]. Anhydrous inorganic solids (NaHCO<sub>3</sub> and NaBH<sub>4</sub>) were purchased from Sigma-Aldrich.

#### *Acid Catalyzed Condensation of 2-Methylfuran*

A mixture of 2-methylfuran (10 mmol) and formalin (5mmol) was added with the homogeneous or heterogeneous acid catalyst (5 mol% with respect to formalin) to a 5 mL V-vial equipped with a PTFE spinning vane. Vials were crimped sealed by a Teflon-faced silicone septum and placed into a preheated silicone oil bath (333 K) set on an IKA stir plate equipped with an ETS-D5 thermocontroller and contents of the vials were stirred at 600 rpm for 4 h. After reaction, the reaction mixture was diluted with 1M NaHCO<sub>3</sub> solution (4mL) to neutralize the acid and extracted with toluene (3 X 5 mL). The combined organic layers were dried over anhydrous Na<sub>2</sub>SO<sub>4</sub>. In the case of reaction catalyzed by a heterogeneous acid catalyst, the product solution was filtered through a SiO<sub>2</sub> column to remove solid particles. Dodecane (150mg) was added as an internal standard to the organic solution and the products in the solution were identified and quantified using gas chromatography/mass spectrometry.

For time course studies, a mixture of 2-MF (50 mmol), formalin (25 mmol), dodecane (600mg) and 5 mol% of H<sup>+</sup> catalysts (HCl or SO<sub>3</sub>H-SiO<sub>2</sub>) relative to formalin was added to a 20mL headspace vial. The vial was crimp sealed and stirred in an oil bath held at 333 K. A small aliquot (~0.1mL) of the reaction mixture was removed at various intervals using a needle and syringe. These samples were neutralized with solid NaHCO<sub>3</sub> and diluted with toluene for GC analysis.

#### *Synthesis of 5-methylfuranyl alcohol*

5-methylfuranyl alcohol (MFOL) was prepared from 5-MF using sodium borohydride (NaBH<sub>4</sub>) as a reducing agent. Reaction between 5-MF and NaBH<sub>4</sub> forms BH<sub>3</sub> and Na<sup>+</sup> coordinated alkoxide species. The addition of saturated NaCl solution to the mixture converts the alkoxide species to primary alcohols, forming MFOL in solution. Ethyl acetate was added to aid the phase separation and transfer of MFOL into the organic phase. The product solution was then extracted twice with a saturated NaCl solution and dried over anhydrous solid Na<sub>2</sub>SO<sub>4</sub>. Excess solvent was removed by rotary evaporation prior to purification by vacuum distillation.

#### *Product Analysis*

Quantitative analysis of products was performed using a Varian CP-3800 gas chromatograph (GC) equipped with a flame ionization detector (FID) coupled to a Varian 320-MS mass spectrometer. Product compounds were separated using a FactorFour capillary column (VF-5 ms, 30 m length, 0.25 mm diameter) coated with a 0.25 mm thick stationary phase (5% phenyl and 95% dimethylpolysiloxane) with hydrogen as a carrier gas. Dodecane was present in all samples as an internal standard to normalize variability in sample size delivery and detector signal strength. The characteristic retention times and the FID response factors using dodecane as internal standard for individual compounds were determined by calibration using pure compounds.

The conversion of 2-MF, yield and selectivity of BMFM were calculated according to equations below, considering that only 0.5 mole of BMFM can be formed per mole of 2-MF substrate.

$$\text{Conversion of 2-MF (mol \%)} = \frac{\text{mols of 2-MF reacted}}{\text{initial moles of 2-MF}} \times 100\%$$

$$\text{Yield of BMFM (mol \%)} = \frac{\text{mols of BMFM}}{0.5 \times \text{initial moles of 2-MF}} \times 100\%$$

$$\text{Selectivity}_{\text{BMFM}} \text{ (mol\%)} = \frac{\% \text{ Yield}_{\text{BMFM}}}{\% \text{ Conv.}_{\text{2-MF}}} \times 100\%$$

## 2.2.2 Results and Discussion

### Catalyst Selection

A series of homogeneous and heterogeneous Brønsted acid catalysts were screened for the condensation of 2-MF and formalin. Homogeneous acids, such as HCl and p-toluenesulfonic acid (p-TSA) were dissolved in the aqueous or organic phase of the reaction solution. Commercial acidic, ion-exchange polymer resins such as Amberlyst-15® and Nafion SAC-13 were considered because they are commonly used for acid-catalyzed condensation reactions [10–12]. Amberlyst-15® contains relatively large pores sizes (30nm in diameter) and a high density of sulfonic acid groups (4.7 meq/g) on a polystyrene backbone. Nafion SAC-13 is a nanocomposite resin material, containing 10–20% Nafion-H perfluorosulfonic acid resin, on amorphous silica (SiO<sub>2</sub>), also containing large pores (10nm in diameter). These catalysts particles were grounded to eliminate possible mass transfer effects and dried at 383 K overnight prior to use. Lastly, we screened SiO<sub>2</sub> (pore diameter = 2.73 nm) onto the surface of which acidic functional groups, such as phosphotungstic acid (PWA) and sulfonic acid (SO<sub>3</sub>H). SO<sub>3</sub>H-SiO<sub>2</sub> were grafted. These materials were expected to behave similarly to the sulfonic-based homogenous catalyst, p-TSA and the commercial resin, Amberlyst-15®. The results of the catalyst screenings for the condensation of 2-MF and formalin at 333K is presented in Table 2.1.

**Table 2.1. Electrophilic aromatic substitution reactions of 2-MF for the formation of BMFM over homogeneous and heterogeneous acid catalysts.**

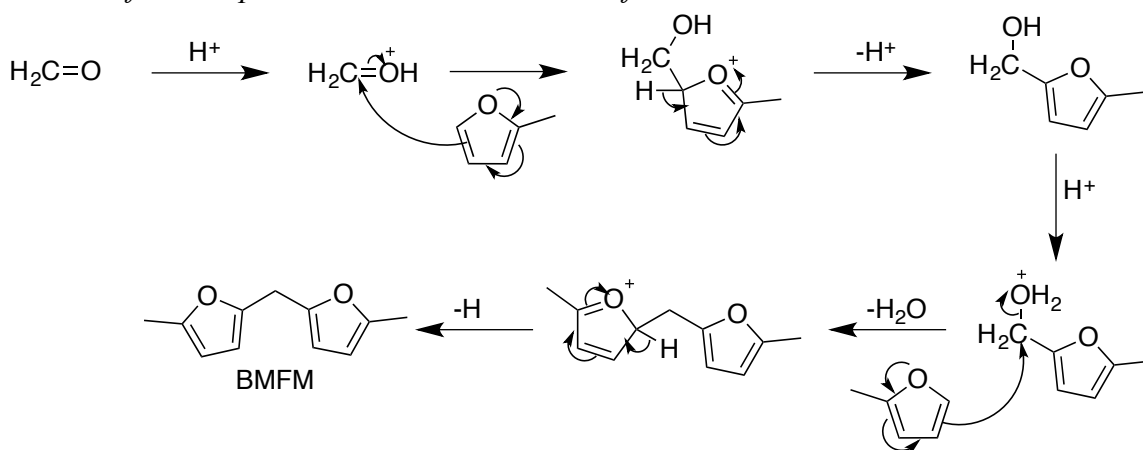
5mmol formalin/DMM, 10 mmol 2-MF, 0.25 mmol H<sup>+</sup> catalyst, 333 K, 4h, 600rpm.

Entry	Acid catalysts	Substrate	% Conversion MF	% Yield BMFM
1	HCl	formalin	95.2	78
2	p-TSA	formalin	95.9	66.8
3		Dimethoxymethane	66.2	23.1
4	Amberlyst-15 ®	formalin	92	64.7
5		Dimethoxymethane	68.1	43.5
6	Nafion SAC-13®	formalin	95.9	53.4
7	PWA-SiO <sub>2</sub>	formalin	79.2	50.5
8	SO <sub>3</sub> H-SiO <sub>2</sub>	formalin	90	70.7
9		Dimethoxymethane	68.6	50.7

Dimethoxymethane (DMM) was used as an alternative to formalin to avoid the use of a biphasic system since dimethoxymethane is miscible with 2-MF and releases 2 moles of methanol instead of water per mole of BMFM formed. Reactions were carried in the absence of water in order to reduce the hydrolysis of aromatic furans and water. However, the use of (DMM) resulted in slower reaction rates and lower selectivity for all catalysts tested when compared to the use of formalin (Table 2.1). The central carbon of DMM is less electrophilic than the carbon of formaldehyde, resulting in slower reaction rates with 2-MF.

For reactions performed using formalin, the selectivity to BMFM ranged from 55% to 80%; the highest selectivity was achieved using either aqueous HCl or  $\text{SO}_3\text{H-SiO}_2$ . Organic homogeneous acids such as p-TSA gave a 10% lower selectivity to BMFM compared to HCl. Products from etherification, hydrolysis, and polymerization are responsible for the lower selectivity to BMFM.

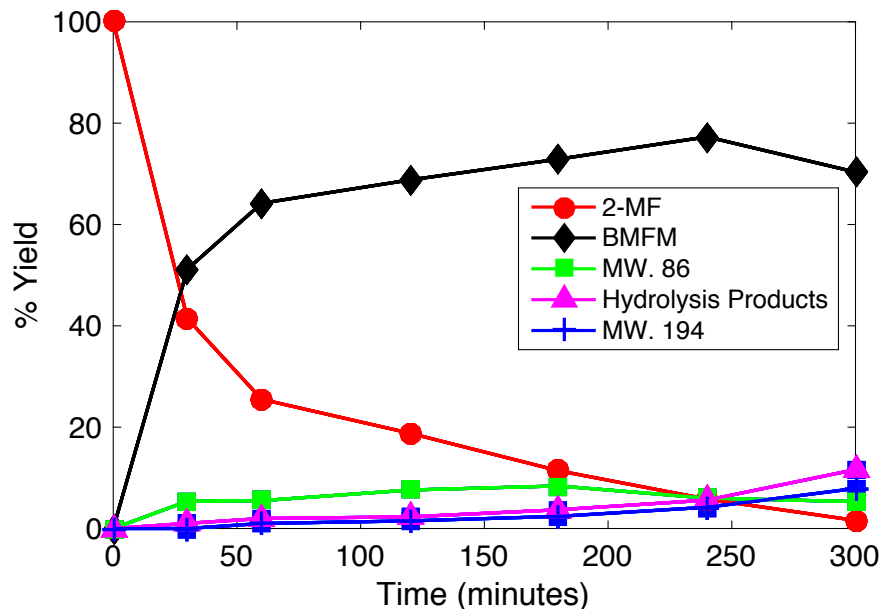
*Mechanism of Electrophilic Aromatic Substitution of 2-MF*



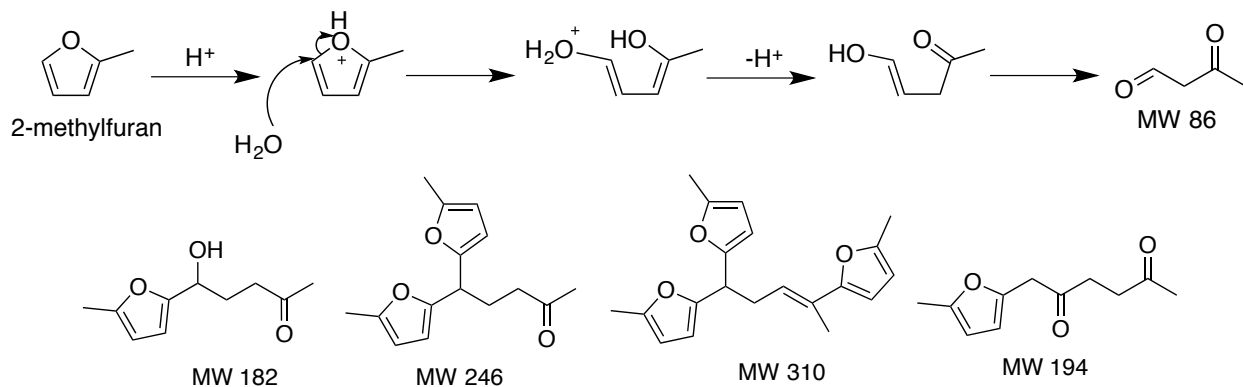
**Scheme 2.2 Proposed mechanism for acid catalyzed, electrophilic aromatic substitution reaction between 2-MF and formaldehyde**

The proposed mechanism for the condensation of 2-MF with formaldehyde is shown Scheme 2.2. The electron rich ring of 2-MF can undergo selective electrophilic aromatic substitution at the 5-position of the ring with the electrophilic C=O group of formaldehyde, forming 5-methylfurfuryl alcohol (MFOL) as an intermediate. After protonation of the hydroxyl group of MFOL, the carbon of C-OH<sub>2</sub><sup>+</sup> serves as suitable electrophile for an attack by additional 2-MF. Bis(5-methylfuran-2-yl)methane, BMFM, is formed after rearrangement and loss of a proton.

The reaction of 2-MF and formalin in a biphasic solution containing 5 mol% HCl to formalin was monitored over time. BMFM as well as hydrolysis products were observed during the course of reaction (Figure 2.1). In the presence of acidic catalysts and heat, 2-methylfuran can be hydrolyzed by H<sub>2</sub>O to form 2-oxobutanal (MW = 86) as shown in Scheme 2.3. 2-oxobutanal also contains two electrophilic groups where up to 3 additions of 2-MF can occur (MW = 182, 246, 310). These products are accounted for under ‘hydrolysis products’ in Figure 2.1. All furan containing products, including BMFM, is susceptible to ring hydrolysis. At extended reaction times, we observed products with MW = 194 resulting from hydrolysis of BMFM.

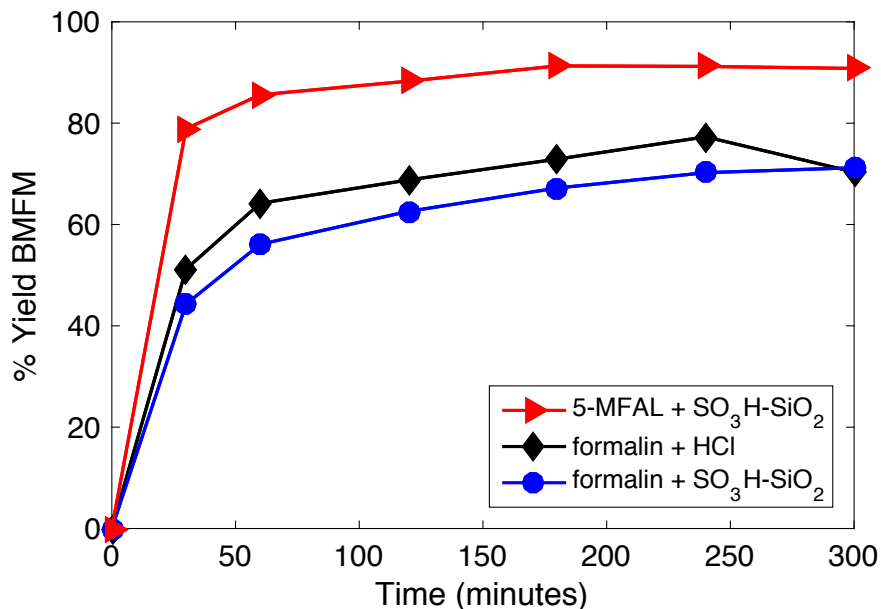


**Figure 2.1. Temporal profiles of the electrophilic aromatic substitution reaction between 2-MF and formalin.** Reaction conditions: 25 mmol formalin, 50 mmol 2-MF, 1.25 mmol HCl, 333 K, 5h, 600rpm.



**Scheme 2.3** Hydrolysis of 2-MF to form 2-oxobutanal and resulting products from additional condensation reactions and ring hydrolysis

We propose that, as shown in Scheme 2.2, 5-methylfurfuryl alcohol, is an intermediate produced after the addition of 2-MF to formaldehyde. We observed very little MFOL during reaction between formaldehyde and 2-MF, which suggests that MFOL is highly active under our reaction conditions. We suspect that BMFM yields can be improved by using MFOL instead of formaldehyde for electrophilic aromatic substitution with 2-MF. To this end, MFOL was synthesized by reduction of 5-methylfurfural using sodium borohydride in the procedure described earlier. Reaction between 2-MF and 5-MFOL (1:1 molar equiv.) was performed in neat conditions at 333 K over  $SO_3H-SiO_2$  catalysts. Over 91% yield of BMFM was achieved over  $SO_3H-SiO_2$  using MFOL compared to 64% yield achieved using formaldehyde (Figure 2.2).



**Figure 2.2. Temporal profiles of % yield of BMFM during reaction using HCl and SO<sub>3</sub>H-SiO<sub>2</sub> catalysts**  
 Reaction conditions: 25 mmol formalin or 50 mmol 5-MFOL, 50 mmol 2-MF, 1.25 mmol HCl or SO<sub>3</sub>H-SiO<sub>2</sub> catalysts, 333 K, 5h, 600rpm.

Although the yield of BMFM formed by reacting 2-MF and formaldehyde over HCl is 7-8% higher than that formed over heterogeneous SO<sub>3</sub>H-SiO<sub>2</sub> (Figure 2.2), we considered the use of SO<sub>3</sub>H-SiO<sub>2</sub> to be more practical than the use of homogeneous HCl solutions. The need to neutralize HCl after reaction was avoided by used of SO<sub>3</sub>H-SiO<sub>2</sub> as the catalyst. The combination of SO<sub>3</sub>H-SiO<sub>2</sub> and MFOL allows us to avoid the use of biphasic, homogeneous reaction system while providing high yield of BMFM (91%).

## 2.3 Nucleophilic Condensation of 5-MF

### 2.3.1 Experimental

#### Chemicals

5-methylfurfural (5-MF), furfural (FUR), benzaldehyde, 2-hexanone, cyclohexanone, and 4-heptanone, were purchased from Sigma-Aldrich. Ethanol solvent (200 proof) was purchased from Koptec and deuterated ethanol solvents, ethanol -1,1,2,2,2-d<sub>5</sub>, (99.5% atom) and ethanol-OD (99.5% atom), used for isotopic exchange studies were purchased from Sigma-Aldrich. Additional solvents such as THF, 1-propanol, 1-pentanol, 1-undecanol, toluene, cyclohexane were purchased from Sigma-Aldrich. Molecular sieves (Grade 564, Type 3A) were obtained from Fisher Chemicals. Solid bases such as sodium ethoxide, lithium ethoxide, potassium ethoxide, sodium phenoxide, calcium phosphate, synthetic hydrotalcite, zirconium carbonate, magnesium oxide, calcium oxide, hydroxyapatite, sodium phosphate and Ambersep® 900 OH (Rohm and Haas) were purchased from Sigma-Aldrich; potassium phosphate (K<sub>3</sub>PO<sub>4</sub>) was purchased from Arcos Chemicals and sodium hydroxide was purchased from Fisher Scientific. Concentrated sodium hydroxide solution in ethanol was prepared in a 50mL volumetric flask and diluted accordingly to prepare reaction solution.

A series of potassium phosphate ( $K_3PO_4$ ) catalysts, purchased from Arcos Chemicals, was prepared by calcining the oxide material at different temperatures (673 K – 1073 K) in static air in a muffle furnace. The furnace was heated to the desired temperature at a ramp rate of 2 K/min, held for 2 h, and then cooled to 423 K before catalysts were removed from the oven and stored. All other base oxide catalysts were pretreated similarly at 873K. Ambersep® 900 OH resin catalyst was less thermally stable compared to basic oxides and was used as received from Sigma-Aldrich.

#### *Characterization of basic sites*

The concentration and relative strength of basic sites on oxide catalysts were determined by  $CO_2$  temperature programmed desorption (TPD) experiments using a Micromeritics AutoChem II 2920 instrument. Approximately 250 mg of catalyst was added to a quartz U-bend sample tube and loaded into the unit. The sample was heated to its pretreatment temperature at 10 K/min under flowing He (Praxair, 50 ml/min) to remove any  $CO_2$  or water adsorbed during exposure to atmosphere or storage. Sample was cooled to 318 K and exposed to flowing  $CO_2$  (100% Praxair, 50ml/min) for 30 minutes to titrate all available basic sites. He (50ml/min) was purged through sample for 1 h to remove excess and physisorbed  $CO_2$ . Under He flow, the sample was ramped from 318 K to 973K at 5 K/min to desorb  $CO_2$  from catalyst. The relative base strength was determined from the catalyst's peak desorption temperature. The number of available base sites was quantified by integrating the area of the desorption peak. The intensity of the TCD signal intensity was calibrated against known concentration of  $CO_2$  in stream of He (50 mL/min).

#### 2.3.2 Nucleophilic condensation reactions with 5-MF

In a typical base-catalyzed experiment, 5-150 mg of oxide catalyst (1.8  $\mu$ mol of base sites), 40 mg of grounded molecular sieves, 115 mg of 5-MF, 30mg dodecane as internal standard, and 1 mL of ethanol or other solvent were added to a 12mL Q-tube reactor, supplied by Q Labtech, containing a teflon-coated magnetic stir bar. In cross-condensation reactions, 1-10 equivalents of the carbonyl compounds with respect to loading of 5-MF were added to the reactor and the volume of ethanol was reduced accordingly in order to maintain the same initial concentration of 5-MF (1M) across all reactions. The reactor was sealed using a PTFE seal and placed into a preheated silicone oil bath (338 K) on an IKA stir plate equipped with an ETS-D5 temperature controller and the contents of the reactor were stirred at 650 rpm for 5-6 h. After reaction, the reactor was removed from the oil bath and cooled in an ice bath. The reaction mixture was diluted using ethyl acetate and the solid particles of catalyst were removed from solution by centrifugation. The products in solution were identified and quantified using gas chromatography/mass spectrometry.

Initial rate and time course studies were performed in a 50mL, three neck, round bottom flask containing a Teflon coated magnetic stir bar. 580mg of grounded molecular sieves, and 0.16 mol% – 5 mol% of base catalyst with respect to 5-MF, 450mg of dodecane, and 15 mL of ethanol (or other solvent) were added to the flask. The solution and headspace were purged with  $N_2$  gas for 60 s before connecting the flask to a reflux condenser, fitting a thermometer into the solution mixture, and sealing the system using a septum stopper. The solution was stirred and heated to reaction temperature in a silicone oil bath on an IKA stir plate equipped with an ETS-D5 temperature controller. When the solution reached the desired temperature, 1.7g of 5-methylfurfural was injected into the flask through the septum using a needle and syringe to avoid possible exposure to the atmosphere. During the course of reaction, under  $N_2$  atmosphere, small

aliquots (~0.1mL) of reaction mixture were removed via syringe and collected within a 1mL solution of ethyl acetate containing 0.03M acetic acid for neutralization. Solids from product mixture were removed by centrifugation and products in remaining solution were identified and quantified using gas chromatography/mass spectrometry.

### *Product Analysis*

Quantitative analysis of products was performed using a Varian CP-3800 gas chromatograph (GC) equipped with a flame ionization detector (FID) coupled to a Varian 320-MS mass spectrometer. Products were separated using a FactorFour capillary column (VF-5 ms, 30 m length, 0.25 mm diameter) coated with a 0.25 mm thick stationary phase (5% phenyl and 95% dimethylpolysiloxane) with hydrogen as a carrier gas. Dodecane was present in all samples as an internal standard to normalize variability in sample size delivery and detector signal strength. The characteristic retention times and the FID response factors were determined by calibration using pure compounds.

Initial rates of reactions were determined from the slope of the linear portion of the conversion vs. time profile of 5-MF (conversions < 20%). For reactions with an observed induction period, initial rates were determined based on when reaction commenced. The yield of dimer and trimer products were calculated according to the equations below, considering that for each dimer or trimer product,  $\delta = 2$  and  $\delta = 3$  moles of 5-MF were consumed, respectively.

$$\text{Conversion of 5-MF (mol \%)} = \frac{\text{mols of 5-MF reacted}}{\text{initial moles of 5-MF}} \times 100\%$$

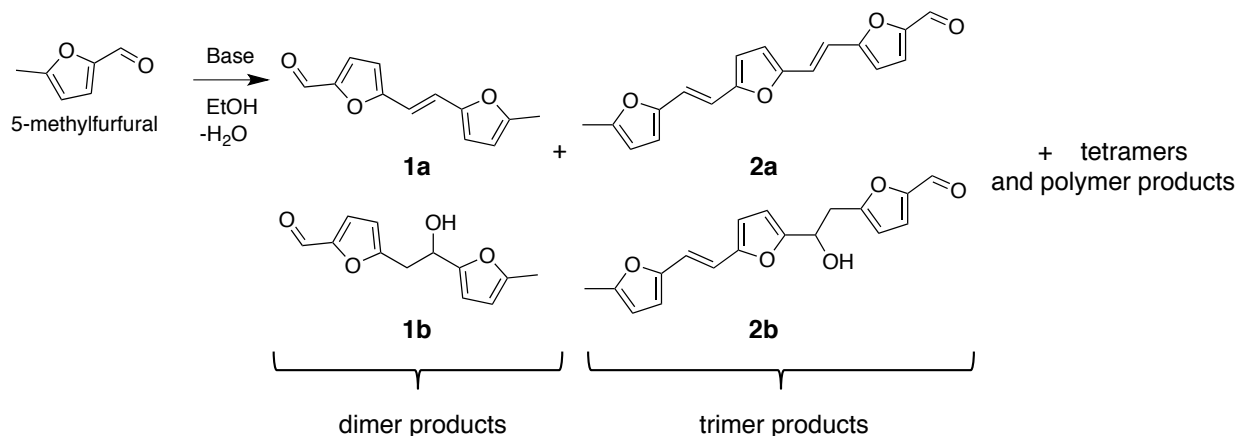
$$\text{Yield of product (mol \%)} = \delta \times \frac{\text{mols of dimer(or trimer)}}{\text{initial moles of 5-MF}} \times 100\%$$

$$\text{Selectivity}_{\text{dimer}} \text{ (mol\%)} = \frac{\% \text{ Yield}_{\text{dimer}}}{\% \text{ Conv.}_{5\text{-MF}}} \times 100\%$$

### *2.3.3 Results and Discussion*

#### *Catalyst Selection*

The activity of various homogeneous base catalysts were evaluated for the self-condensation of 5-MF in ethanol solution into C<sub>12</sub> dimer (**1a**, **1b**) and C<sub>18</sub> trimer products (**2a**, **2b**) as shown in Scheme 2.4. These products and small quantities of 5-methylfurfuryl alcohol (<5%) were the only products detected in GC analysis. It is possible that tetramer and heavier oligomers were formed but did not elute from the GC column at the temperature settings used for analysis. Comparison of initial activities of these bases is shown in Table 2.2. In this table, the pKa values of the conjugate acid (evaluated in H<sub>2</sub>O solutions at 298 K) are shown to provide a scale of base strength of the organic and inorganic bases. CH<sub>3</sub>CH<sub>2</sub>O<sup>-</sup> and OH<sup>-</sup> are similar in base strength and have similar rates of conversion of 5-MF. In comparison to CH<sub>3</sub>CH<sub>2</sub>O<sup>-</sup> and OH<sup>-</sup>, a weaker base such as C<sub>6</sub>H<sub>5</sub>O<sup>-</sup> is 10<sup>2</sup> times slower. In the case of C<sub>6</sub>H<sub>5</sub>O<sup>-</sup>, the reaction is limited to the first step, proton abstraction from 5-MF, and the major product is **1b**. The conversion of **1b** to **1a** requires a second base-catalyzed proton abstraction from **1b** followed by dehydration.



Scheme 2.4. C<sub>12</sub> and C<sub>18</sub> products from the self dimerization of 5-MF over base catalysts

Table 2.2 Initial rates of self-dimerization of 5-MF for homogeneous base catalysts and heterogeneous K<sub>3</sub>PO<sub>4</sub> (873 K) catalysts.

Reaction conditions: 15.9 mmol 5-MF, 2.65 mmol dodecane, 0.8 mmol homogeneous base or 400mg K<sub>3</sub>PO<sub>4</sub> catalyst, 15 mL EtOH, 338 K, reflux in N<sub>2</sub>.

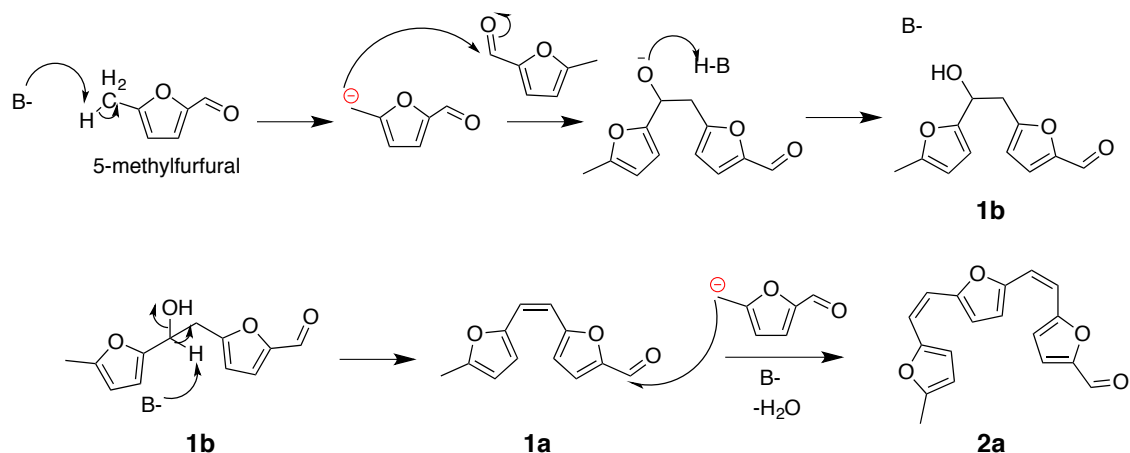
Catalyst	Solvent	Initial rate (TOF s <sup>-1</sup> )	pKa of conjugate acid <sup>a</sup>
NaOPh	EtOH	0.002	9.98
NaOH	EtOH	0.39	15.7
NaOEt	EtOH	0.47	16
LiOEt	EtOH	0.18	16
KOEt	EtOH	0.502	16
K <sub>3</sub> PO <sub>4</sub>	EtOH	1.28	12.3 <sup>b</sup>
K <sub>3</sub> PO <sub>4</sub>	1-undecanol	3.04	12.3 <sup>b</sup>

<sup>a</sup> pKa of functional group containing conjugate acid determined in H<sub>2</sub>O solution at 298 K [48,49]

<sup>b</sup> pKa of conjugate acid of HPO<sub>4</sub><sup>2-</sup> in H<sub>2</sub>O at 298 K [50]

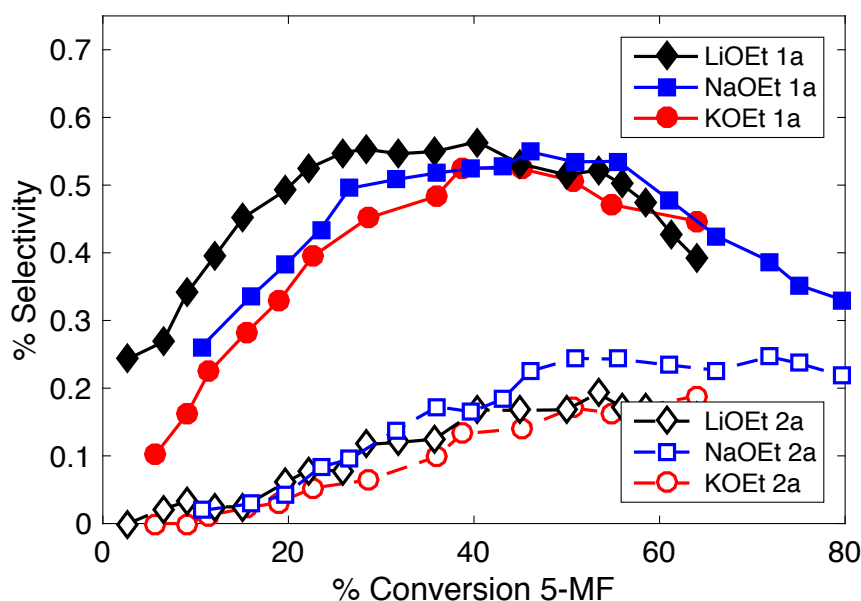
The proposed reaction mechanism for 5-MF condensation is illustrated in Scheme 2.5. A strong base catalyst, such as CH<sub>3</sub>CH<sub>2</sub>O<sup>-</sup> and OH<sup>-</sup>, first abstracts a proton from the methyl group of 5-MF to form a reactive carbanion (CH<sub>2</sub><sup>-</sup> group). This reactive nucleophile adds to the electrophilic C=O of another molecule of 5-MF, forming **1b** and regenerating the base catalyst. Subsequently, a base-catalyzed dehydration reaction occurs to remove the -OH group in the form of water thereby converting **1b** to **1a**. The C=O group of **1a** is also susceptible to nucleophilic attack by the carbanion, resulting in trimer products **2a** and **2b**. The production of trimers occurs especially at high conversions of 5-MF once the dimer concentration has risen. It is important to mention that the electron-withdrawing aldehyde group of 5-MF is necessary for reaction since less acidic protons of 2-methylfuran and 2,5-dimethylfuran were not abstracted even in the presence of a strong base catalysts, such as CH<sub>3</sub>CH<sub>2</sub>O<sup>-</sup> and OH<sup>-</sup>. Also, carbanion formation from **1a** is unlikely to occur since the electron-withdrawing (-CHO) group is too removed from the methyl group to influence the acidity of the methyl group hydrogen atoms in **1a**.





**Scheme 2.5** Proposed reaction mechanism for base-catalyzed self-dimerization of 5-MF into dimer and trimer products.

We also considered the role of the counter ion during reaction by comparing the initial rates of the series of homogeneous, organic bases, LiOEt, NaOEt, and KOEt. The participating base in all reactions was the ethoxide anion; however, the rate increased in the order  $\text{Li}^+ < \text{Na}^+ \sim \text{K}^+$  (Table 2.2). This trend is a consequence of ion-pairing between the metal ion and the nucleophile generated after the first proton abstraction. The step involving proton abstraction by  $\text{CH}_3\text{CH}_2\text{O}^-$  occurs readily and equilibrated; leaving the rate-limiting step to be the condensation of the 5-MF nucleophile with another molecule of 5-MF. Compared to  $\text{Na}^+$  and  $\text{K}^+$ , a smaller  $\text{Li}^+$  cation is capable of forming a tighter ion pair with the nucleophile, increasing stability and lowering the reactivity of the nucleophile. The counterion effect of increasing cation size was also observed in increased rates of nucleophilic condensation reactions of acetic acid and Wittig reagents [51,52]. However, as shown in Figure 2.3, no significant influence of these three positive counter ions was observed on the product selectivity of 5-MF condensation reaction. The maximum selectivity toward product **1a** occurred at 40% - 45% conversion of 2-MF, after which **1a** significantly competes with the remaining 5-MF in solution for condensation reactions with the nucleophile. To maximize production of **1a**, operation in semi batch mode is suggested in order to maintain a high concentration of 5-MF and promote formation of dimers instead of trimers and higher oligomers.



**Figure 2.3. Selectivity toward products 1a and 2a as a function of 5-MF for ethoxide catalysts.**

Reaction conditions: 15.9 mmol 5-MF, 2.65 mmol dodecane, 0.8 mmol ethoxide, 15 mL EtOH, 338 K, reflux in N<sub>2</sub>.

Since strong bases such as NaOEt and NaOH are highly corrosive and difficult to separate from reaction solution, we evaluated several heterogeneous bases for the nucleophilic self-condensation of 5-MF. The conversion and product selectivity obtained after 5 h reactions at 338 – 488 K are shown in Table 2.3. Strongly basic CaO ( $T_{CO_2} = 827$  K) achieved only 28% conversion after 5 h at 488 K. Of the heterogeneous basic oxides screened, only moderately basic tripotassium phosphate (K<sub>3</sub>PO<sub>4</sub>) exhibited high 5-MF dimer yields. When normalized by the number of basic sites available, calculated from CO<sub>2</sub> TPD, K<sub>3</sub>PO<sub>4</sub> is an order of magnitude more active than the homogeneous base catalysts, -OEt and -OH (Table 2.2). Further kinetic and mechanistic studies of 5-MF self-condensation were performed over K<sub>3</sub>PO<sub>4</sub> to explain its unique activity of this catalyst.

**Table 2.3 Screening of solid base catalysts for the nucleophilic self-condensation of 5-MF in ethanol.**

All base oxides were characterized and density of basic sites quantified by CO<sub>2</sub> TPD titration experiments. The mass loading of base catalyst was based on achieving a total of 0.023 mmol of base sites. Reaction conditions: 1 mmol 5-MF, 0.18 mmol dodecane, 5 – 150 mg base oxide catalyst, 1 mL EtOH, 338 K – 488 K, 5h.

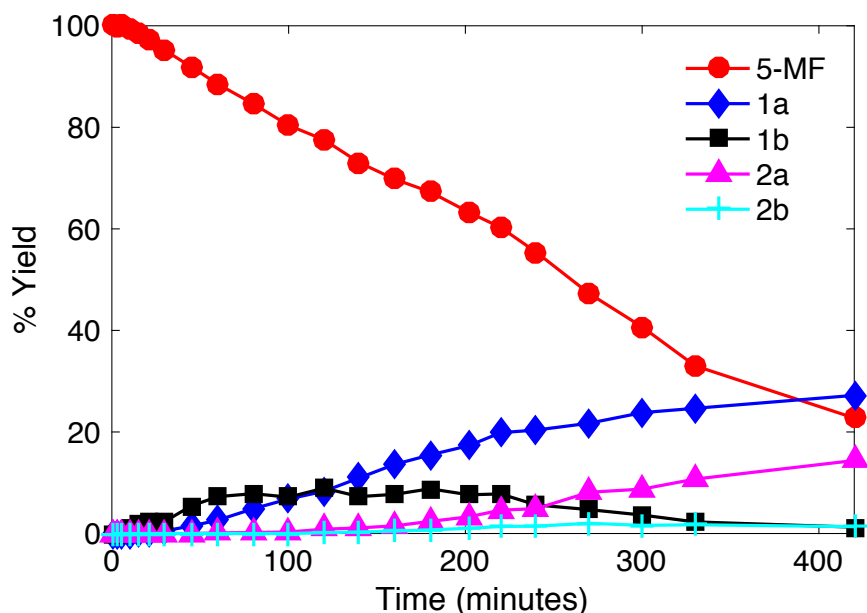
Catalyst	CO <sub>2</sub> TPD	Temp. (K)	% Conv.	%Y.			
	Peak Temp. (K)			1a	1b	2a	2b
K <sub>3</sub> PO <sub>4</sub>	487	338	59	24	3.7	8.9	1.6
Na <sub>3</sub> PO <sub>4</sub>	428	338	3.8	1	2.8	0	0
Ambersep® 900 OH	-- <sup>a</sup>	338	19	12	3.2	2.1	0.8
CaO	827	488	28	15	0.5	5	0.2
Mg-Al-O (HT)	360	488	15	11	1.5	0	1
HAP	361	488	26	17	0.3	5	0.5
ZrCO <sub>3</sub>	387	488	3	2	0.5	0	0

<sup>a</sup> Ambersep® 900 OH is a resin material with low thermal stability, therefore CO<sub>2</sub> temperature programmed desorption experiments were not performed on this material.

### Nucleophilic Self Condensation over $K_3PO_4$

Tripotassium phosphate,  $K_3PO_4$ , is a moderate-strength inorganic base that is non-toxic, inexpensive, and insoluble in most organic solvents, allowing for facile recycle. While monitoring the conversion of 5-MF over  $K_3PO_4$ , an induction period (<10 min.) was observed to precede the reaction (Figure 2.4). A similar induction period was observed for  $K_3PO_4$  used for phase-transfer hydrogenation and was attributed to adsorption of  $O_2$  or  $CO_2$  onto the surface of  $K_3PO_4$  [55]. For such reactions, operation under  $N_2$  atmosphere and the use of freshly distilled reactants reduced the length of induction period to 30 min and could not be resolved entirely. For our system, purging solution with  $N_2$  for 1 - 30 min prior to reaction did not shorten the observed induction period or improve the reaction rate. Therefore, all initial rate measurements of  $K_3PO_4$  were determined after the induction phase (~10 min).

The product formed initially is the dimer, **1b**, the condensation product between two molecules of 5-MF. The hydroxyl group of this product is removed in the form of water via base-catalyzed dehydration on  $K_3PO_4$  to form **1a**. The selectivity to **1a** increases until approximately 50% conversion of 5-MF, at which point the product **1a** competes with the substrate, 5-MF, in condensation reactions. The addition of 5-MF to the aldehyde group of **1a** results in the trimer products **2b** and **2a** (upon dehydration of **2b**). These products are also susceptible to 5-MF nucleophilic attack, leading to tetramers and heavier oligomerized species that are visible in the reaction solution as viscous, dark red solids, and not detected by GC analysis.

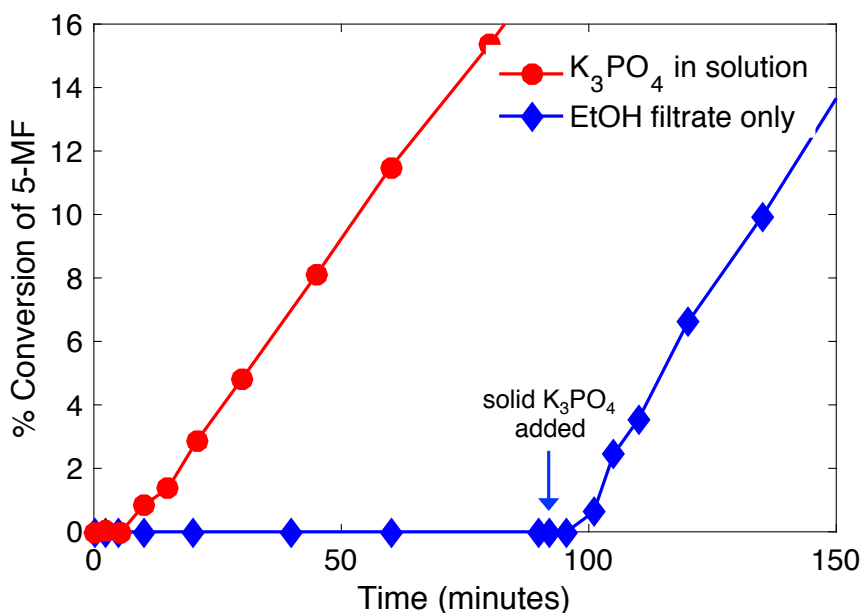


**Figure 2.4. Time course of 5-MF Dimerization over  $K_3PO_4$ .**

Reaction conditions: 15.9 mmol 5-MF, 2.65 mmol dodecane, 400 mg  $K_3PO_4$  (873 K) 15 mL EtOH, 338 K, reflux in  $N_2$ .

During our initial rates studies, we have observed that potassium ethoxide, soluble in ethanol, can readily catalyze 5-MF condensation reactions.  $K_3PO_4$  is insoluble in alcohols; however, there is a possibility that small amounts of ethoxide species are formed by reacting  $K_3PO_4$  with ethanol. To ensure that the reaction is occurring on the heterogeneous surface of  $K_3PO_4$  and not catalyzed by ethoxide anions in solution,  $K_3PO_4$  (calcined at 873 K), was refluxed

with ethanol for 3 h at 338 K. Solid  $K_3PO_4$  was removed by hot filtration and the solvent filtrate containing potentially dissolved ethoxide species was used as the reaction solution. 5-MF was added to the solution at 338 K but no reaction was observed for 1.5 h, indicating that potassium ethoxide species were not generated from  $K_3PO_4$  and EtOH at our reaction conditions. However, when solid  $K_3PO_4$  was added to the reaction mixture, conversion of 5-MF and formation of dimer species commenced after the expected induction period of  $\sim 10$  min (Figure 2.5). Similar studies confirming the absence of alkoxide species formed by  $K_3PO_4$  in isopropanol or methanol for phase transfer hydrogenation or transesterification reactions, respectively, have also been conducted [55,56]. Thus, our study confirms that reaction is occurring at sites on the surface of  $K_3PO_4$ . When normalized by the quantity of basic sites (0.065 mmol/g), as determined by  $CO_2$  TPD, the activity of  $K_3PO_4$  is an order of magnitude greater than strong, homogeneous bases, such as  $CH_3CH_2O^-$  and  $OH^-$  (Table 2.2). We pursued additional studies to understand the unique activity of  $K_3PO_4$ , a moderately basic, heterogeneous oxide, for the nucleophilic condensation of 5-MF.

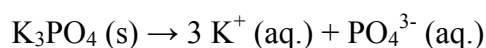


**Figure 2.5. Initial conversion of 5-MF with (•) and without (♦) solid  $K_3PO_4$ .**

Solution containing 5-MF and ethanol filtrate after refluxing with  $K_3PO_4$  for 3h at reaction conditions.  $K_3PO_4$  added to solution at 90min. Reaction conditions: 5-MF (15.9 mmol), dodecane (2.65 mmol), 400 mg of  $K_3PO_4$  (873 K), EtOH (15 mL), 338 K, reflux in  $N_2$ .

### Solvent studies

We also studied the influence of solvent environment on the nucleophilic condensation of 5-MF over  $K_3PO_4$ .  $K_3PO_4$  is soluble in aqueous systems, and insoluble in alcohol and organic solvents. In aqueous systems,  $K_3PO_4$  completely dissociates into potassium and phosphate ions according to the following reaction,



In aqueous solutions,  $PO_4^{3-}$  ions results in  $<10\%$  conversion of 5-MF after 6 h of reaction and the major product observed is **1b** (Table 2.4).  $K_3PO_4$  was inactive in nonpolar, aprotic solvents such as toluene and cyclohexane and in polar, aprotic solvents such as THF and furfural.

The activity of  $K_3PO_4$  for condensation of 5-MF was observed in polar, protic solvents, such as alcohols and the reaction proceeded more rapidly in the order of ethanol < 1-propanol < 1-pentanol < 1-undecanol (Table 2.4). The dielectric constant of alcohols is a relevant metric for describing these rates of dimerization observed. The dielectric constant of a solvent is a reflection of its polarity and its ability to insulate charges. Since the desired reaction is between a carbanion and the electrophilic C=O group, a more polar solvent such as ethanol, has a high dielectric constant and can better stabilize the negatively charged nucleophile, decreasing its nucleophilicity compared to less polar solvents. This order of decreasing dielectric constant mirrors the increased conversion of 5-MF observed for ethanol < 1-propanol < 1-pentanol < 1-undecanol). 5-MF condensation in 1-undecanol occurred ~2.4 times faster than in ethanol (See Table 2.2). The observed influence of solvent polarity is consistent with the influence of the counterion of organic bases discussed earlier in homogeneous base studies.

Based on the above solvation arguments and the influence of dielectric constants, we should expect the nucleophilicity of 5-MF<sup>-</sup> to be highest in aprotic, nonpolar solvents with low dielectric constants such as toluene and THF (Table 2.4). The lack of reactivity by  $K_3PO_4$  in aprotic solvents suggests a relationship between the catalytic surface and the -OH group of protic solvents.

**Table 2.4 5-MF dimerization over  $K_3PO_4$  (873 K) in various solvents in q-tube reactors.**

Reaction conditions: 1mmol 5-MF, 0.18mmol dodecane, 27mg  $K_3PO_4$  (873 K), 1mL solvent, 338 K .

Solvent	Dielectric Constant <sup>a</sup>	Time (h)	% Conv.	% Yield Dimer 1	% Yield Trimer 2
<b>H<sub>2</sub>O</b>	80.1	6	10	7.5	0
<b>cyclohexane</b>	2.02	6	0	--	--
<b>toluene</b>	2.4	6	0	--	--
<b>tetrahydrofuran</b>	7.58	6	0	--	--
<b>furfural</b>	42	6	3	2.5	0
<b>ethanol</b>	24.5	6	70	32.5	17.5
<b>ethanol</b>	24.5	1.5	20	17.5	1.5
<b>1-propanol</b>	20	1.5	22	18.7	1.8
<b>1-pentanol</b>	13.9	1.5	30	23.5	3
<b>1-undecanol</b>	6	1.5	40	30	5

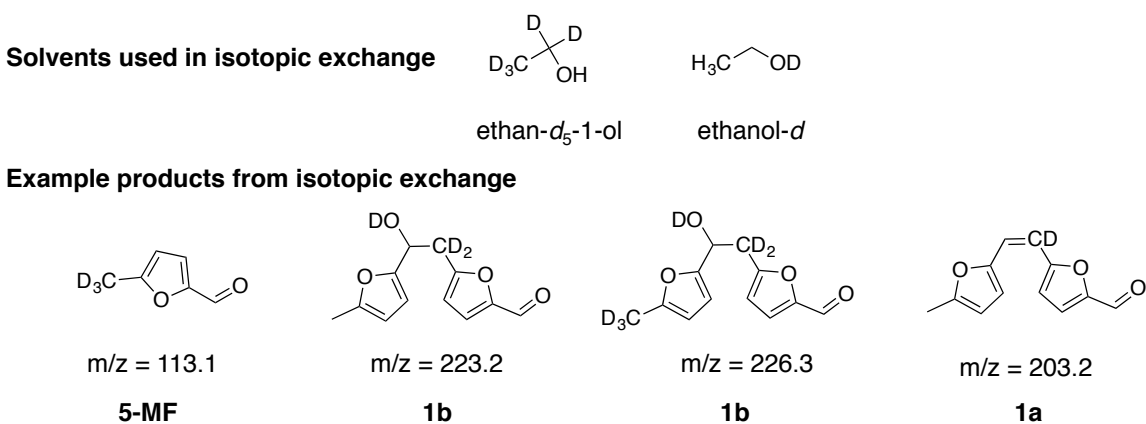
<sup>a</sup> Dielectric constants of solvents at 293 K [57]

#### *Reaction mechanism over $K_3PO_4$*

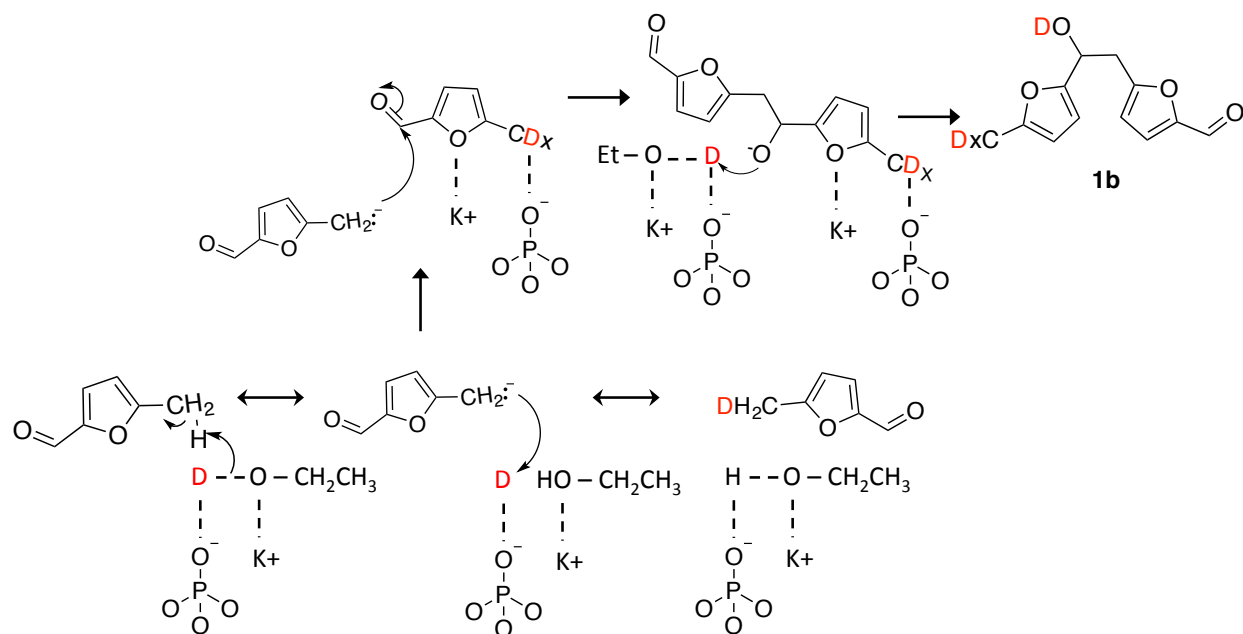
Since the condensation of 5-MF over  $K_3PO_4$  occurred in polar alcohols, we further investigated whether solvent protons are incorporated into the products during reaction (Scheme 2.5). In this context, we performed the condensation reactions of 5-MF over  $K_3PO_4$  in two different deuterated ethanol solvents, ethanol-1,1,2,2,2-d<sub>5</sub> (99.5%) and ethanol-OD, 99.5%. No deuterium incorporation was observed using ethanol-1,1,2,2,2-d<sub>5</sub> and products were equivalent to those when the reaction was performed in ethanol. However, dimerization performed in ethanol-OD revealed products of varying degree of H-D exchange (Scheme 1.6). Instead of m/z = 202 for **1a**, we observed m/z = 202 – 206 and instead of m/z = 220 for **1b**, we observed m/z = 220 – 226. The incorporation of up to 6 deuterium atoms in product compounds suggests that deuterium exchange with the 5-MF occurs rapidly before dimerization. In fact, the molecular ion peak of unreacted 5-MF in solution was no longer m/z = 110.1 but m/z = 111 – 113.1. This indicates that the solvent deuterium atoms are dissociated on the surface sites of  $K_3PO_4$  and that the first proton

abstraction from 5-MF and H-D exchange between 5-MF and the surface deuterium atoms occurs rapidly and is equilibrated.

Our isotopic exchange studies confirm that the rate-determining step in this reaction is the dimerization of the nucleophilic 5-MF<sup>-</sup> carbanion and another molecule of 5-MF. The isotopic exchange studies also indicate that surface alkoxide species are generated at K<sub>3</sub>PO<sub>4</sub> surface sites, and since K<sub>3</sub>PO<sub>4</sub> is inactive in aprotic solvents and alkoxides are stronger bases than phosphate groups, it is likely that these alkoxide species are responsible for the initial proton abstraction as well as the proton abstraction from product **1b** in dehydration reactions to form dimer **1a**. The formation of surface alkoxide species on K<sub>3</sub>PO<sub>4</sub> involves the adsorption of the –OH groups of the solvent to the exposed oxygen atoms of the phosphate groups and potassium atoms on K<sub>3</sub>PO<sub>4</sub> surface [58]. The configuration of adsorbed alcohol species on K<sub>3</sub>PO<sub>4</sub> for phase transfer hydrogenations had been proposed to involve oxygen bound to the potassium cation and hydrogen interacting with the exposed oxygen ion in the phosphate group [55]. We propose that this is the initial configuration that allows for dissociation of deuterium species and alkoxides on K<sub>3</sub>PO<sub>4</sub> surface. The proposed reaction mechanism occurring on the surface of K<sub>3</sub>PO<sub>4</sub> and in the presence of ethanol-OD is shown in Scheme 2.7.



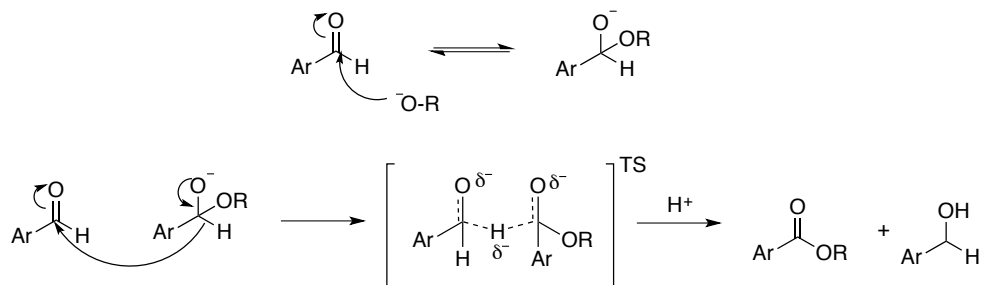
**Scheme 2.6** Examples of products and their masses resulting from isotopic exchange experiments using deuterated ethanol solvents.



**Scheme 2.7 Proposed mechanism for 5-MF self-dimerization to form product 1b over  $K_3PO_4$  in ethanol- $d$  solvent.**

The basicity of  $K_3PO_4$  can be modified with pretreatment temperatures (673 K – 1073K) and the concentration of basic sites present on its surface quantified by  $CO_2$  temperature-programmed desorption. Higher basicity results in a higher peak desorption temperature. Initial rates of 5-MF conversion for  $K_3PO_4$  catalysts calcined at temperatures 673 K – 1073K and the  $CO_2$  peak desorption temperatures of these catalysts are shown in (Figure S. 2.1). The initial rate of the least basic form of  $K_3PO_4$  (1073 K) was only 27% lower than that of the most basic form of  $K_3PO_4$  (873 K) (Figure S. 2.3). Overall, the relative basicity of  $K_3PO_4$  did not demonstrate a strong influence on the initial rates of dimerization, in contrast to what has been reported for phase transfer hydrogenation for which an order of magnitude difference in rates were achieved over  $K_3PO_4$  treated at temperatures from 573 K to 873 K [59]. The lack of influence by pretreatment temperature on dimerization rates is in line with our proposed mechanism in Scheme 2.5 where the catalytic active species are surface ethoxides, not basic sites of  $K_3PO_4$ , and the rate-limiting step is the condensation step of 5-MF.

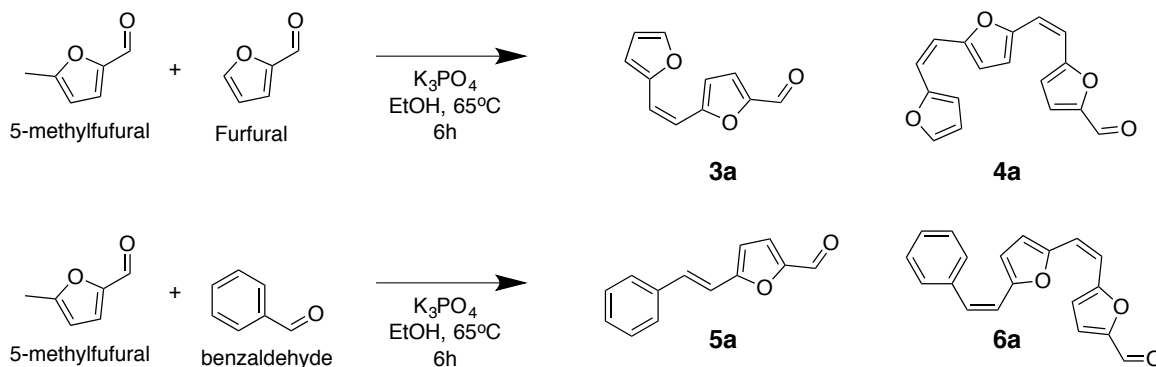
Although surface alkoxides were generated at  $K_3PO_4$  sites, Tishchenko reaction between the alkoxide and the  $C=O$  of 5-MF was not a significant side reaction. Evidence of Tishchenko reactions would have been the formation of esters, such as ethyl-5-methylfuran-2-carboxylate, and 5-methylfurfuryl alcohol. Although 5-methylfurfuryl alcohol (<2% yield) was detected at ~40% conversion (after 200 min), this product likely results from phase transfer hydrogenation/reduction of the  $C=O$  by ethanol [55,59], a reaction that occurs significantly more slowly than 5-MF self-dimerization. As the dielectric constant of the solvent was lowered (ethanol to 1-undecanol), a greater degree of ester product formation (<10% yield), resulting from Tishchenko reaction, was observed. This is also a result of the reduced solvation of the bulky anion intermediate formed between the alkoxide species to the  $C=O$  group of 5-MF (Scheme 2.8).



**Scheme 2.8 Mechanism for Tishchenko reaction between alkoxide species and aromatic aldehydes to form aromatic alcohols and esters.**

### *Nucleophilic cross-condensations with 5-MF*

After establishing the self-condensation of 5-MF over  $K_3PO_4$ , we explored the scope of possible substrates for cross condensation with 5-MF. To enable selective cross condensation between 5-MF and other electrophilic substrates, attention was restricted to substrates that do not contain an acidic  $\alpha$ -H, such as furfural and benzaldehyde (Scheme 2.9).



**Scheme 2.9** Cross condensation products between 5-MF and furfural or benzaldehyde over  $K_3PO_4$  in ethanol.

**Table 2.5 Cross condensation of 5-MF and FUR over  $K_3PO_4$  (873 K) in q-tube reactors.**

Reaction conditions: 1mmol 5-MF, 1-11.5 molar equivalent of furfural, EtOH added as a solvent for a total volume of 1mL, 0.18mmol dodecane, 27mg  $K_3PO_4$  (873 K), 338 K.

Entry	FUR : 5-MF (mequiv.)	Time (h)	% Conv. 5-MF	%S 3	%S 1	%S 4	%S 2
1	1 : 1	6	83	42	18	16	4.5
2	2.5 : 1	6	78	71	9.3	13	0.9
3	3.5 : 1	6	76	76	7.4	9.4	0.6
4	5 : 1	6	72	83	4.4	7.1	0.2
5	8 : 1	6	21	91	5.3	0.4	0.0
6	11.5 : 1 (neat)	6	3.0	100	0.0	0.0	0.0
7	5 : 1	8	79	90	2.9	4.3	0.0
8	8 : 1	24	61	90	2.9	2.2	0.0

Excess furfural was used in order to improve selectivity toward dimer (**3**). With increased concentrations of furfural relative to 5-MF, the selectivity to cross dimer product (**3**) increased from 42.3% (Table 2.5, Entry 1) to 91% (Table 2.5, Entry 1) and the selectivity to self-dimer (**1**) and to all trimer species (**2**, **4**) decreased. As discussed earlier, the cross condensation between 5-



MF and furfural does not occur under neat conditions (Table 2.5, Entry 6) because  $K_3PO_4$  is not basic enough to abstract a proton from 5-MF. The need for surface alkoxide species is demonstrated in the case of FUR: 5-MF (8:1 mequiv.) (Table 1.5, entry 5), where the conversion after 6 h was only 22%. The low conversion for this reaction compared to Entries 1-4 is a result of the lower concentration of ethanol (0.35mM) when 8:1 mequiv. FUR : 5-MF was used. However, when the reaction time was extended to 24 h (Table 1.5, entry 8), we were able to achieve 63% conversion and maintain a high selectivity (>90%) to the cross dimer product (**3a**). Cross condensation of 5-MF and benzaldehyde was also achieved over  $K_3PO_4$  in ethanol solution (Table 2.6).

The extent of conversion of 5-MF was not quantified due to overlapping GC retention times of the substrates. The total yields of condensation products were lower than those achieved in cross condensation with furfural. This is possibly due to the competing Tishchenko reaction with surface ethoxides to form benzyl alcohol and ethyl benzoate (6-10% yield with respect to 5-MF). The Tishchenko reaction was observed in the cross condensation of furfural or benzaldehyde and ethoxides but was absent for 5-MF self-condensation. 5-MF has a lower reactivity in Tishchenko reactions compared to FUR and benzaldehyde due to its electro-donating methyl group substituent. The presence of the  $-CH_3$  group of 5-MF makes the reversible formation of a hemiketal anion, an intermediate in the Tischenko reaction (See Scheme 2.8), less favorable.

**Table 2.6 Cross condensation of 5-MF and benzaldehyde over  $K_3PO_4$  (873 K) in q-tube reactors.**

Reaction conditions: 1mmol 5-MF, 3-8 molar equivalent of benzaldehyde, EtOH added as a solvent for a total volume of 1mL, 0.18mmol dodecane, 27mg  $K_3PO_4$  (873 K), 338 K.

MF : BEN (mequiv.)	Time (h)	% Conv. 5-MF <sup>a</sup>	%S 5	%S 1	% S 6	%S 2
1 : 3	6	-	27.1	12.3	8.6	3.3
1 : 5	6	-	36.3	9.3	5.7	1.6
1 : 5	8	-	38.9	10	9	1.7
1 : 8	24	-	16.8	1.9	0	0

<sup>a</sup> Benzaldehyde retention time coincided with that of 5-MF during GC analysis and accurate quantification of conversion was unable to be determined.

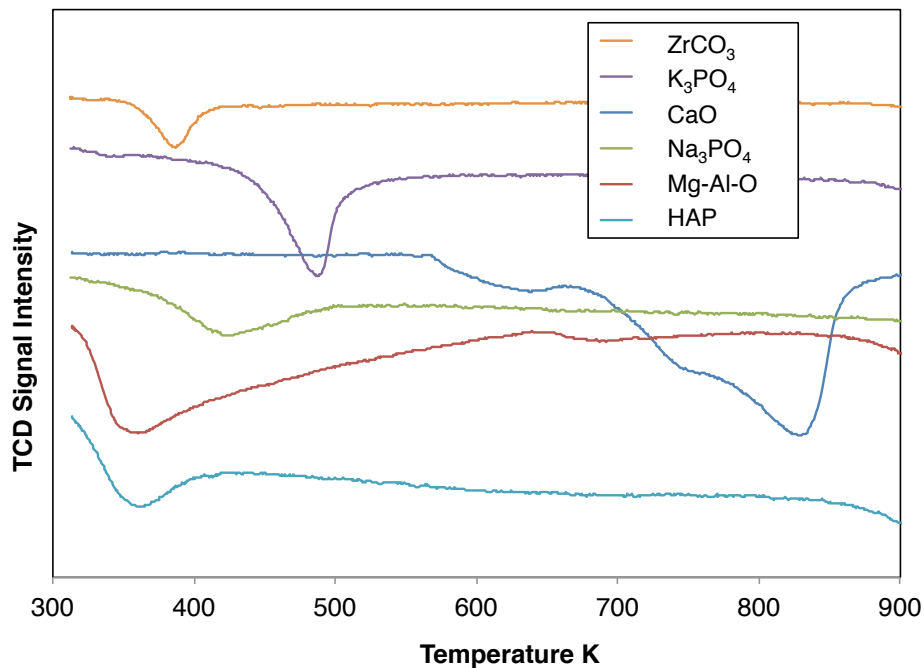
## 2.4 Conclusions

Bis(5-methylfuran-2-yl)methane ( $C_{11}$ , BMFM), can be synthesized in up to 70% yields using 2-MF and formaldehyde over silica-supported sulfonic acid. The use of 5-methylfurfuryl alcohol instead of formaldehyde resulted in yields up to 91% BMFM due to reduced hydrolysis of furanic compounds.  $C_{11}$  and  $C_{12}$  furanyl oxygenates can also be derived from base catalyzed condensation by cross-coupling 5-MF with furfural or self-coupling 5-MF with itself. This chemistry readily occurs at 338 K over heterogeneous  $K_3PO_4$  in protic solvents such as alcohols. Compared to other base catalysts used for aldol condensation,  $K_3PO_4$  has the unique ability to dissociate protic solvents and generate surface alkoxide species that are capable of abstracting an acidic proton from 5-methylfurfural, generating the nucleophilic species required to promote condensation reactions. The rate limiting step in aldol condensation is found to be C-C bond formation between the carbanion and the electrophilic C=O group. Consequently, the composition of the solvent and the identity of cations present in solution significantly affect rates

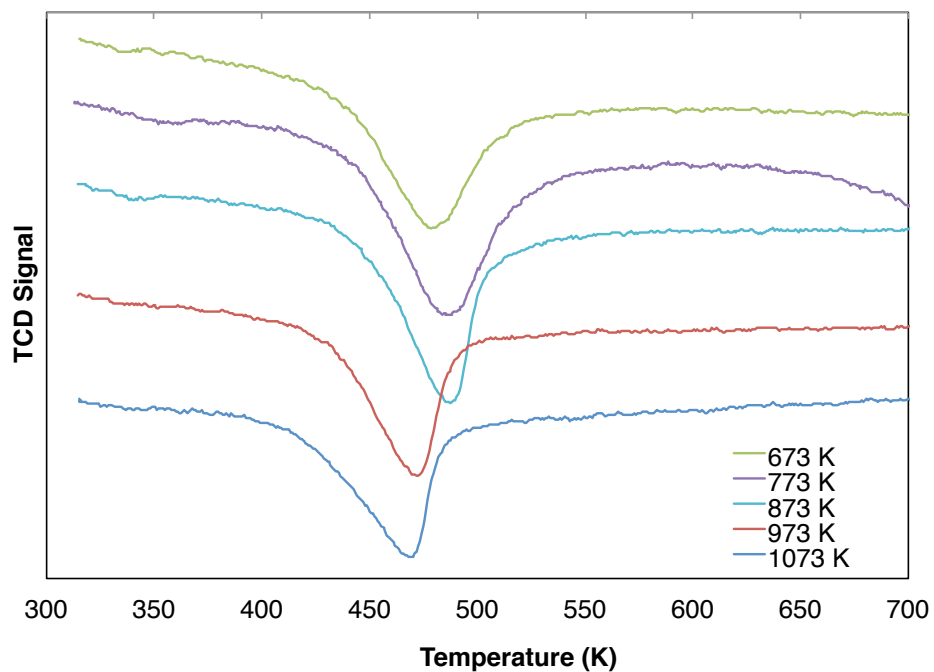
of 5-MF condensation. Increasing the concentration of electrophilic substrates such as FUR or benzaldehyde increases the selectivity to cross-condensation dimer products (>90%).

## 2.5 Supplemental Information

### 2.5.1 CO<sub>2</sub> TPD profiles of base catalysts

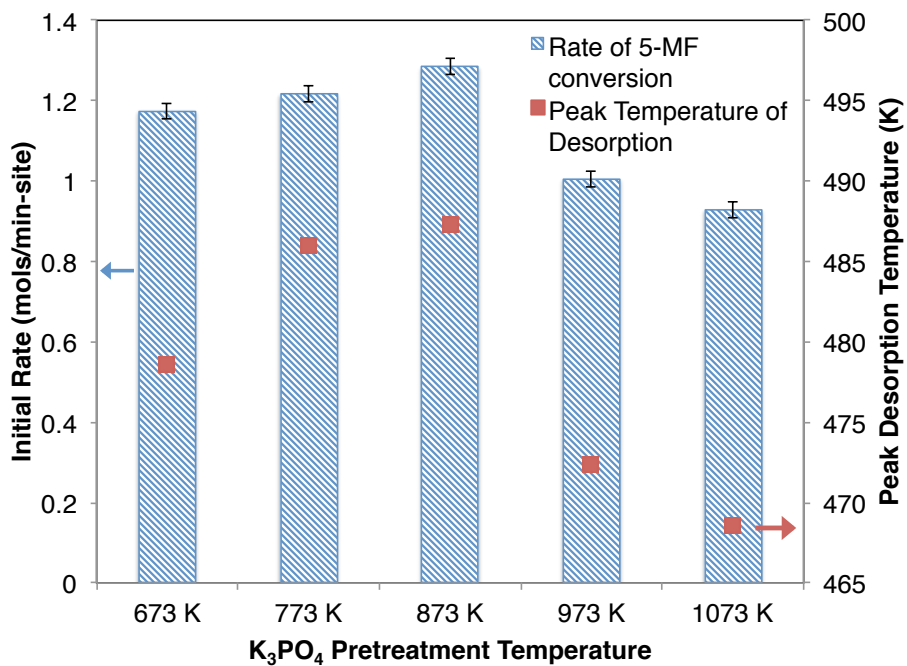


**Figure S. 2.1.** CO<sub>2</sub> TPD profiles of basic oxide catalysts pretreated at 873 K



**Figure S. 2.2.** CO<sub>2</sub> TPD profiles of K<sub>3</sub>PO<sub>4</sub> catalysts pretreated at 673 K – 1073 K in static air

2.5.2 Initial rates 5-MF conversion over  $K_3PO_4$  catalysts treated at 673 K -1073 K



**Figure S. 2.3. Initial rate of 5-MF condensation over  $K_3PO_4$  catalysts pretreated at 673 K – 1073 K in static air.**

Reaction conditions: 15.9 mmol 5-MF, 2.65 mmol dodecane, 400 mg  $K_3PO_4$  (873 K) 15 mL EtOH, 338 K, reflux in  $N_2$ .

## 3 Kinetics of Hydrogenation and Hydrogenolysis of 2,5-Dimethylfuran over Noble Metals Catalysts under Mild Conditions

### 3.1 Introduction

One of the strategies for transforming the hemicellulosic and cellulosic fractions of biomass into valued chemical products and fuel additives is hydrolysis of these polysaccharides to their respective sugar monomers, primarily xylose and glucose, followed by dehydration to produce furfural and 5-hydroxymethylfurfural, respectively [33]. Furanic compounds derived in this manner retain all of the monosaccharide carbon and contain roughly half as much oxygen, and can be converted to jet, diesel, and lubricants via aldol condensation [8,9], oligomerization [32,60], and hydroalkylation [10,12,61]. The resulting products are C<sub>9</sub>-C<sub>21</sub> furanics, which can, in turn, be converted to ketones or alcohols by partial hydrogenation, or to hydrocarbons by hydrodeoxygenation. Aldehydes and ketones sourced in this manner readily undergo C-C coupling via aldol condensation [8,9] or self-trimerization to produce diesel and jet fuel [62]. For these reasons, there is considerable interest in understanding the activity and selectivity of catalysts that can be used for the hydrogenation of furanic compounds, and in particular, what factors govern the selectivity for furan ring saturation versus furan ring hydrogenolysis to produce ketones, aldehydes, and alcohols.

Vapor-phase hydrogenation of low molecular weight furanics, such as 2-methylfuran (2-MF), 2,5-dimethylfuran (DMF), and furfural (FUR), has been investigated over Pd, Pt, Ni, Cu, and Co catalysts at moderate conditions (363K – 473K, 0.1 MPa) [10,12,18,61,63–65]. The products observed include partially or fully saturated derivatives of tetrahydrofuran and ring-opened products, such as alcohols, ketones, and aldehydes. Higher selectivity toward ring-opened products has been observed over Pt, whereas higher selectivity to tetrahydrofuran products has been reported over Pd [20–22,66]. Several studies have also observed a greater degree of ring opening, cracking, and decarbonylation when hydrogenation was performed at temperatures above 493 K [18,21,65,66]. Finally, application of harsher conditions (573K – 673K, 7-20MPa H<sub>2</sub>) during hydrogenation over noble metals resulted in complete oxygen removal and the production of hydrocarbons [4,6,10].

Relatively little is known about the reaction network by which the hydrogenation of furanic compounds occurs and in particular, the mechanism responsible for the formation of ring-opened products, i.e., ketones and alcohols. Kliewer et al. [18] and Runnebaum et al. [19] have proposed that over Pt, the formation of butanal and butanol results from hydrogenolysis of tetrahydrofuran formed by ring hydrogenation of furan. Similarly, Kang et al. have suggested, based upon isotopic-labeling studies, that C-O bond hydrogenolysis occurs at the etheric C-O bonds and not at the aromatic C-O bonds of the furan ring during vapor-phase hydrogenation of DMF and MF over Pt and Pd catalysts [20]. On the other hand, studies of liquid-phase hydrogenation of alkylfurans (2-MF, DMF) suggest that ring hydrogenolysis occurs directly from the alkylfuran substrates based on the observation of significantly lower activity toward ring opening in tetrahydrofuran derivatives versus alkylfurans [21–23]. The 2-methylfuran intermediate formed during hydrodeoxygenation of furfural over Pt/C has been reported to

produce 2-methyltetrahydrofuran and 2-pentanol in parallel, but intrinsic rate data could not be obtained due to the occurrence of mass transfer effects in the liquid phase flow system used for the study [37].

Although direct ring scission of the aromatic furan has been suggested by the aforementioned studies, few have addressed the mechanism and kinetics involved. In a recent study by Vlachos and coworkers, isotopic labeling and density functional calculations were used to show that certain metals, such as Ru, activate the furan ring, resulting in scission of the C-O bond in 2-methylfuran [67]. Although the proposed mechanism supports ring opening of the furan moiety at the metal site, this reaction was only found to occur at unsubstituted  $\alpha$  carbon positions; consequently, the mechanism by which ring opening occurs for highly substituted compounds such as DMF remains uncertain. In addition, the pathways responsible for preferential formation of ketones versus alcohols following C-O hydrogenolysis of substituted furans have not been clearly defined. Corma et al. have reported 100% yield of 2-hexanone upon gas-phase hydrogenation of DMF over Pt/C at 623K [10]. By contrast, Smith and Fuzek have reported exclusive production of butanol and 2-hexanol during liquid-phase hydrogenation of furan and DMF, respectively, over platinum oxide in acetic acid at 308K, 0.14 – 0.41MPa [23], and Aliaga et al. have observed the formation of C<sub>5</sub> and C<sub>6</sub> alcohols but no ketones during gas phase hydrogenation of MF and DMF, respectively, over supported Pt nanoparticles [65]. Therefore, the mechanism by which furanic compounds are hydrogenated appear to be strongly influenced by the reaction conditions employed as well as the catalyst composition [21].

Given the current level of knowledge, systematic studies that consider the kinetics of all reactions involved in the hydrogenation of furanic compounds (ring opening, ring saturation, C=O hydrogenation) are needed in order to obtain a fundamental understanding of the molecular relationships between catalyst properties and their activity and selectivity. The aim of this study was to elucidate the reaction mechanism and kinetics for the hydrogenation of 2,5-dimethylfuran (DMF) over noble metals. DMF was chosen as a model for furanic compounds derived from biomass. To this end, we investigated the influence of catalyst composition and reaction conditions on the product selectivity and the rate parameters for both ring hydrogenolysis and ring saturation.

## 3.2 Experimental

### 3.2.1 Materials

2,5-Dimethylfuran, 2,5-dimethyltetrahydrofuran, 2-hexanone, 2-hexanol, and nonane were purchased from Sigma-Aldrich. Hydrogenation catalysts, including Pd/carbon (10 wt%), Pt/carbon (5 wt%), Ru/carbon (5 wt%) and Rh/carbon (5 wt%), were used as received from Sigma-Aldrich, USA after drying overnight at 383 K to remove residual moisture. All oxide supports,  $\gamma$ -Al<sub>2</sub>O<sub>3</sub>, TiO<sub>2</sub> (anatase), and NbOPO<sub>4</sub> (niobium phosphate, CBMM) were calcined at 573 K for 3 h prior to dispersion of Pt.

### 3.2.2 Catalyst synthesis

To investigate the effects of support composition of the catalyst on the rates of DMF and 2-hexanone hydrogenation, Pt was dispersed onto oxide supports either by strong electrostatic adsorption (SEA) or incipient wetness impregnation (IWI) methods. SEA allows for the

preparation of highly dispersed metal nanoparticles with particle size controlled by varying the calcination temperature post adsorption [68]. Supports with a low PZC, such as NbOPO<sub>4</sub>, were slurried in 80mL H<sub>2</sub>O and the pH was increased to 9.5 by addition of ammonia hydroxide. A predetermined loading of tetraamineplatinum(II) nitrate (Pt(NH<sub>3</sub>)<sub>4</sub>(NO<sub>3</sub>)<sub>2</sub>), was dissolved in 10mL of H<sub>2</sub>O and added to the slurry. For supports with higher PZC such as  $\gamma$ -Al<sub>2</sub>O<sub>3</sub>, the pH of the slurry was adjusted to 4.4 using HCl and chloroplatinic acid (H<sub>2</sub>PtCl<sub>6</sub>) was used as the anionic precursor. After stirring for 1 h, the impregnated solid was washed, filtered and dried overnight at 373 K under flowing air. All filtrate was collected and analyzed via ICP-MS to determine the final loading of Pt on supports. All SEA preparation procedures resulted in <4% of metal precursor remaining in the filtrate, which indicated virtually all metal had been adsorbed on to support.

The SEA method applied to TiO<sub>2</sub> support did not result in high adsorption of the Pt precursor on TiO<sub>2</sub>. Therefore, Pt/TiO<sub>2</sub> was prepared using chloroplatinic acid by the incipient wetness method. A calculated volume of aqueous solution containing the Pt precursor was added dropwise to TiO<sub>2</sub> to saturate the pore volume of the catalyst, which was subsequently dried at 383K overnight. The IWI and SEA catalysts were calcined in flowing air at temperatures from 573 K to 773 K at 1K/min to the final temperature and held for 3h. Following calcination, all catalysts were reduced under flowing H<sub>2</sub> (Praxair, 99.999%) at 523 K at 5 K/min and holding for 2h.

### 3.2.3 Catalyst characterization

Metal dispersion and active site density were measured by CO chemisorption at 313K on a Micrometrics AutoChem 2920 Pulse Chemisorption System, assuming CO atom to surface metal atom stoichiometry of 1.0 for Pt and 2.0 for Pd based catalysts. Prior to CO exposure, the catalyst was pretreated in flowing H<sub>2</sub> (10% in He) at 50mL/min for 1h at 523K. An average particle diameter was determined for all supported metals based on the measured dispersion of the metal.

### 3.2.4 Catalytic hydrogenation

Batch hydrogenation of DMF and 2-hexanone was conducted in a HEL ChemScan high-pressure parallel reaction system equipped with eight 16mL, independently controlled Hastelloy autoclave reactors. Reactors were loaded with a solution containing solid catalyst, substrate, nonane solvent, and dodecane as an internal standard. The reactors were operated at a pressures of 0.41 MPa to 0.69 MPa H<sub>2</sub> and temperatures ranging from 333 K to 393 K. Standard reaction conditions were 0.55 MPa H<sub>2</sub>, 353 K, 1.12 M of substrate in nonane, metal catalyst (0.2 mol% of substrate loaded, ~40 mg) for a total volume of 4.66 mL. Prior to the addition of hydrogen, the reactors were purged with N<sub>2</sub> three times and heated to reaction temperature. No conversion of the substrate was observed until the introduction of the reactive gas, H<sub>2</sub>. Experimental data for initial rate studies and for time course studies were obtained by running individual reactors for a desired reaction time. After each reaction, the reactor was immersed in an ice bath and quickly cooled to room temperature, after which the reactor was vented and purged with inert gas. The catalyst was then separated from the reaction mixture by centrifugation and filtration, and the

filtered liquid was then diluted with acetone to reach a concentration suitable for quantification by GC/MS. Carbon balances for all experimental measurements were greater than 96%.

### 3.2.5 Product analysis

Quantitative analysis of products was performed using a Varian CP-3800 gas chromatograph (GC) equipped with a flame ionization detector (FID) coupled to a Varian 320-MS mass spectrometer. Product compounds were separated using a FactorFour capillary column (VF-5 ms, 30 m length, 0.25 mm diameter) coated with a 0.25 mm thick stationary phase (5% phenyl and 95% dimethylpolysiloxane) with hydrogen as a carrier gas. Dodecane was present in all samples as an internal standard to normalize variability in sample size delivery and detector signal strength. Initial rates of DMF and 2-hexanone disappearance were evaluated using the slope of the linear portion of the conversion profile, for conversions < 25%. Reactant conversion and product selectivity were defined as follows:

$$\text{Conversion (mol\%)} = \frac{\text{moles of DMF or 2-hexanone reacted}}{\text{moles of initial substrate}} \times 100\%$$

$$\text{Selectivity}_{\text{species } i} \text{ (mol\%)} = \frac{\text{moles of species } i}{\sum \text{moles of product}} \times 100\%$$

Since the number of active metal centers per mass loading of all catalysts was determined by CO chemisorption, the turnover frequency (TOF) was calculated as:

$$\text{TOF} = \frac{\text{Moles of substrate reacted}}{(\text{Moles of active centers})(\text{seconds})}$$

## 3.3 Results

### 3.3.1 Hydrogenation of DMF over carbon-supported noble metals

Prior to measuring the initial rates of DMF hydrogenation in the liquid phase, a number of systematic studies were performed to verify that neither external nor internal mass transfer affected the measured rates of reaction (see SI 3.6.1). After verification, all subsequent experiments were carried out using the appropriate stirring speed and catalyst particle size required to avoid effects of mass transfer.

The products of DMF hydrogenation over the supported noble metals reported in Table 3.1 include 2,5-dimethyltetrahydrofuran (DMTHF), 2-hexanone, 2-hexanol, and trace amounts of *n*-hexane. The turnover frequency (TOF) for each catalyst in Table 3.2 was determined on the basis of the initial rate of DMF consumption normalized by the number of active centers on the supported metal catalysts (quantified by CO chemisorption). The initial rate of DMF consumption measured at 353K and 0.55MPa of H<sub>2</sub>, decreased in the order Pt/C > Rh/C > Pd/C > Ru/C. Of these transition metals, only Pt/C exhibited high selectivity to products obtained by C-O bond hydrogenolysis (principally 2-hexanone and 2-hexanol), whereas all of the other catalysts exhibited lower activity and high selectivity for ring saturation to form DMTHF. The difference in activity and selectivity among the noble metals is due to the nature of the metal



since all catalysts had comparable metal particle size (Table 3.1). Under the mild reaction conditions (353 K and 0.55 MPa of H<sub>2</sub>) employed during liquid-phase hydrogenation, the main products observed for Pt and Pd catalysts are similar to those reported for gas-phase hydrogenation discussed earlier [10,12,61].

**Table 3.1 Density of supported metal and average particle size for metal nanoparticles.**

Average particle size determined by CO chemisorption. Commercial catalysts (carbon supports) were used as received. Other catalysts were either prepared by strong electrostatic adsorption (SEA) or by incipient witness impregnation (IWI) methods.

	Method of Preparation	M/Support Density (mg M/m <sup>2</sup> support)	D <sub>p</sub> , Particle Size (nm)
5% Pt/C	As received	0.074	4.6
10% Pd/C	As received	0.148	5.4
5% Rh/C	As received	0.074	4.5
5% Ru/C	As received	0.074	5.3
1.1% Pt/NBP	SEA	0.074	4.0
1.4% Pt/Al <sub>2</sub> O <sub>3</sub>	SEA	0.074	4.7
1.4% Pt/TiO <sub>2</sub>	IWI	0.074	15.5

**Table 3.2 Turnover frequency (TOF) for DMF consumption and product selectivity for carbon-supported noble metals.**

TOFs normalized by the total number of surface metal atoms. 0.2 mol% metal loading, T = 353 K, p<sub>H2</sub> = 0.55MPa, 1.12 M DMF in nonane, 750 rpm.

Hydrogenation Catalyst	TOF (s <sup>-1</sup> )	% Selectivity <sup>a</sup>			Total R.O. products
		DMTHF (% cis)	2-hexanone	2-hexanol	
5% Pt/C	1.77	6.0 (95)	85	9.1	93.6
5% Rh/C	0.62	95 (91)	4.6	0.0	4.6
10% Pd/C	0.25	100 (86)	0.0	0.0	0.0
5% Ru/C <sup>b</sup>	0.00	--	--	--	--
5% Ru/C <sup>c</sup>	0.27	69 (90)	27	3.1	25

<sup>a</sup> Selectivity of the products observed at 10% conversion of DMF

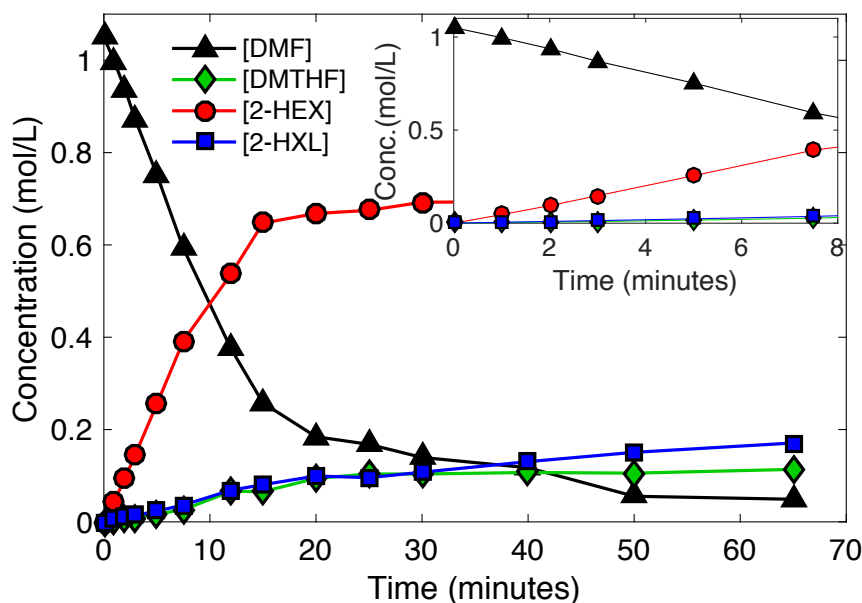
<sup>b</sup> Ru/C unreactive at 353K

<sup>c</sup> Performed at T = 43 3K since reactions below 433 K exhibited a significant induction phase

Since 2-hexanone and 2-hexanol are useful starting materials for C-C coupling chemistry [62], further experiments were undertaken with Pt/C in order to gain insight into the pathways for the formation of all products. Figure 3.1 shows that for reaction times below 12 min., the concentrations of DMTHF, 2-hexanone, and 2-hexanol all increase linearly. For longer reaction times, the concentrations of these products increase with time in a sub-linear manner, coincident with a decrease in the rate of DMF consumption. These patterns suggest that the hydrogenation of DMF to DMTHF and the formation of 2-hexanone and 2-hexanol occur via parallel and independent pathways, and that the conversion of DMTHF to 2-hexanol is not a prominent pathway. This conclusion is verified by our experiments in which DMTHF was reacted over Pt/C under conditions identical to those used for hydrogenation of DMF. Only trace amounts of ring-

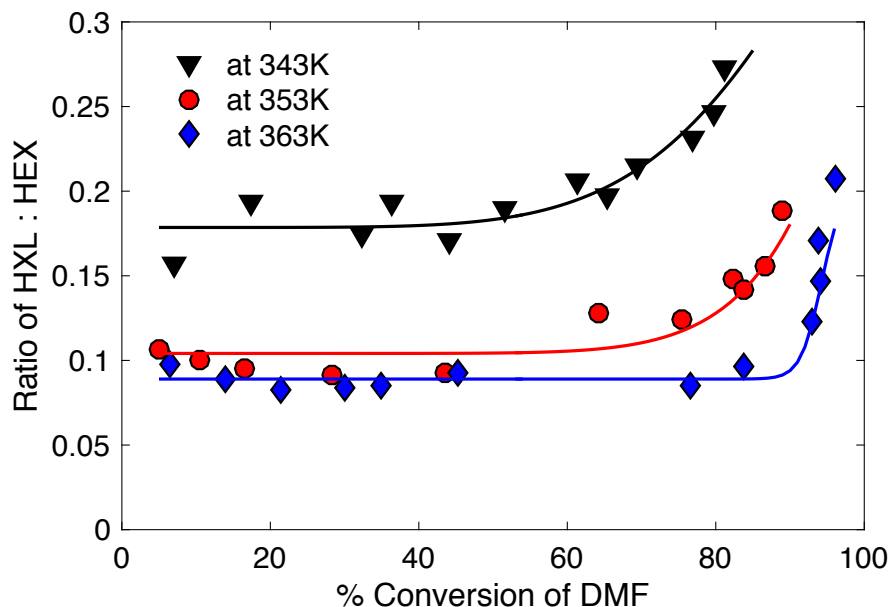
opened products, 2-hexanone and 2-hexanol (<5% yield), were observed even after extended reaction times (2h). Therefore, despite previous studies proposing the contrary [18,20], we conclude that DMTHF is not an intermediate to C-O hydrogenolysis products under the conditions of the present study.

Another feature of DMF hydrogenation is the relationship of the concentrations of 2-hexanol (HXL) to 2-hexanone (HEX) and 2-hexanol to DMTHF. Figure 3.2 illustrates the variation in the concentrations of 2-hexanol to 2-hexanone as a function of the consumption of DMF. Below a DMF conversion of ~ 50%, the ratio of 2-hexanol to 2-hexanone is constant and increases only for DMF conversions above 50%. The constancy of the ratio of HXL/HEX concentrations at low DMF conversions suggests that these species originate from a common intermediate, and not through secondary hydrogenation of 2-hexanone as suggested previously [20,69]. However, the increase in the ratio of HXL/HEX concentrations at higher conversions of DMF can be attributed to progressive hydrogenation of 2-hexanone, since 2-hexanone is now available in the system at significant concentrations. It is also evident from Figure 3.1 that the ratio of concentrations of 2-hexanol to DMTHF is close to unity throughout the reaction. This behavior suggests the production of 2-hexanol occurs at a rate comparable to that for the production of DMTHF. Parallel formation of the three products, DMTHF, 2-hexanone, and 2-hexanol is also observed in Figure 3.2, in which their selectivity remains constant during DMF conversions below 40%.



**Figure 3.1** Concentration profile of reactor composition during the course of DMF hydrogenation over 5% Pt/C.

Conditions: 0.2 mol% Pt/C, T = 353 K,  $p_{H_2}$  = 0.55 MPa, 1.04 M DMF in nonane, 750rpm.



**Figure 3.2** Effect of temperature on the ratio of concentration of 2-hexanol to 2-hexanone (HXL:HEX) during the course of DMF conversion.

Conditions: 0.2 mol% loading Pt/C,  $p_{H_2} = 0.55$  MPa, 1.12 M DMF in nonane, 750 rpm,  $T = 343$  K, 353 K, 363 K.

Table 3.3 compares the measured initial rates of DMF consumption ( $r_{DMF}$ ), ring opening ( $r_{RO}$ ) and ring saturation ( $r_{RS}$ ) over Pt/C at 0.55MPa  $H_2$ , 353K. Also listed is the rate of 2-hexanol production ( $r_{HXL}$ ) from DMF and the rate of C=O hydrogenation when 2-hexanone is reacted as the substrate ( $r_{HEX}$ ). It is noted that  $r_{RO}$  is significantly larger than all other rates in the network, suggesting that cleavage of the aromatic C-O bond of DMF to form ring opened products occurs more rapidly than both the hydrogenation of aromatic C=C bonds to form DMTHF and the hydrogenation of the C=O bond of 2-hexanone to form 2-hexanol.

**Table 3.3** TOFs obtained from initial rates for hydrogenation of DMF over 5% Pt/C.

0.2 mol% Pt/C,  $T = 353$  K,  $p_{H_2} = 0.55$  MPa, 1.12 M DMF in nonane, 750 rpm.  $r_{HEX}$ , was determined using 2-hexanone as the reactant.

	TOF ( $s^{-1}$ )
$r_{DMF}$	1.75
$r_{RO}$	1.63
$r_{RS}$	0.12
$r_{HXL}$	0.15
$r_{HEX}$	0.67

### 3.3.2 Effect of reactant concentration on the kinetics of DMF hydrogenation

Experiments were conducted with initial DMF concentrations ranging from 0.66 M to 1.23 M at 353 K, 0.55 MPa (Figure 3.3). The initial loading of DMF had minimal effect on both the rate of DMF consumption and the product selectivities. A similar dependence on substrate concentration has also been reported previously for the liquid-phase hydrogenation of DMF and 2-methylfuran over platinum oxide [23].

Experiments to determine the effect of hydrogen partial pressure on the kinetics of DMF hydrogenation were conducted by measuring initial rates of  $r_{DMF}$ ,  $r_{RO}$ , and  $r_{RS}$  for  $H_2$  pressures between 0.41 MPa and 0.69 MPa. The rates of ring saturation and ring opening of DMF increased with increasing  $H_2$  partial pressure. The empirical rate orders on  $H_2$  partial pressure were determined from the slopes when reaction rates vs.  $p_{H_2}$  are plotted on a natural log plot, as presented in Figure 3.4. The slopes are  $\sim 2$  for ring saturation and  $\sim 0.6$  for ring opening, suggesting separate reaction mechanisms and rate-limiting steps for the two pathways – the addition of the fourth hydrogen atom for the path leading to ring saturation and the addition of the first hydrogen atom for the path leading to ring opening [70]. The lower order dependence on  $p_{H_2}$  in  $r_{RO}$  is reflected in the higher selectivity for 2-hexanone and 2-hexanol products obtained at lower  $p_{H_2}$ .

### 3.3.3 2-Hexanone hydrogenation over Pt/C

2-hexanone formed by ring-opening hydrogenation of DMF can undergo further hydrogenation to produce 2-hexanol. The kinetics of this process were investigated by carrying out the hydrogenation of 2-hexanone over 5% Pt/C under conditions identical to those used for hydrogenation of DMF. The only product observed was 2-hexanol. The rate of 2-hexanone hydrogenation was similarly zero order in 2-hexanone and  $\sim 1.2$  order in the partial pressure of  $H_2$  (Figure 3.5). A similar dependence on the partial pressure of  $H_2$  has been reported by Sen and Vannice for the hydrogenation of acetone over various oxide-supported Pt catalysts resulting from the 2<sup>nd</sup> addition of H atom being the rate determining step [71].

### 3.3.4 Effects of reaction temperature

Initial rates of all reaction pathways and selectivity were investigated for a temperature range of 343 K – 373 K. In general, an increase in temperature favors ring cleavage over ring saturation of DMF and increases the selectivity toward 2-hexanone over 2-hexanol, which is also shown in Figure 3.2. The apparent activation energies,  $E_{app}$ , for all pathways were determined from Arrhenius plots of the initial rates of formation of DMTHF and initial rates of formation of ring-opened products, 2-hexanone and 2-hexanol, during hydrogenation of DMF (Figure 3.6). These values, along with the rate order dependence on reactants for each pathway, are listed in Table 3.4. The apparent activation energy for ring saturation of DMF to form DMTHF is 10.2 kJ/mol. By contrast, the apparent activation for ring-opening of DMF to form 2-hexanone and 2-hexanol is 45.3 kJ/mol. An Arrhenius plot for the hydrogenation of 2-hexanone to 2-hexanol is also shown in Figure 3.6. The apparent activation energy for this process is 27.6 kJ/mol.

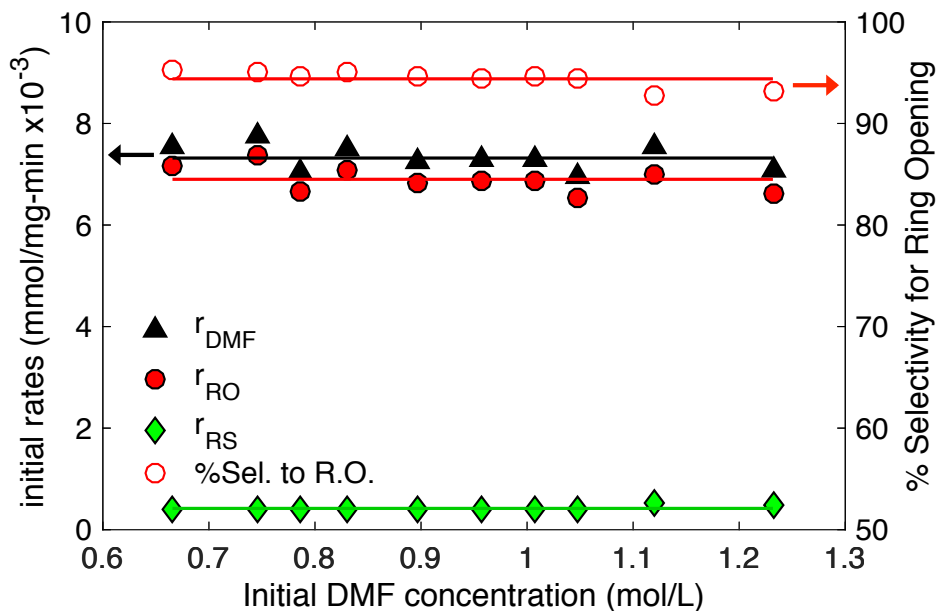


Figure 3.3 Effect of initial DMF concentration on selectivity toward ring opening and on the initial rates of DMF hydrogenation over 5% Pt/C.

Conditions: 0.2 mol% Pt/C, T = 353 K, p<sub>H2</sub> = 0.55 MPa, 0.66M-1.23 M DMF in nonane, 750rpm.

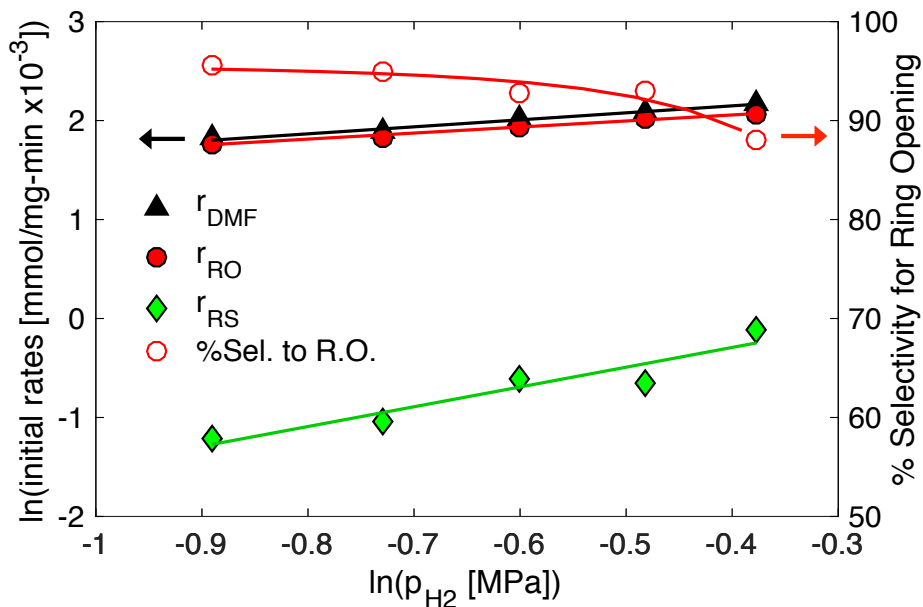


Figure 3.4 Effect of p<sub>H2</sub> on the selectivity to ring opening and on initial rates of DMF hydrogenation over 5% Pt/C.

Conditions: 0.2 mol% loading Pt/C, T = 353 K, p<sub>H2</sub> = 0.41-0.69 MPa, 1.12 M DMF in nonane, 750 rpm.

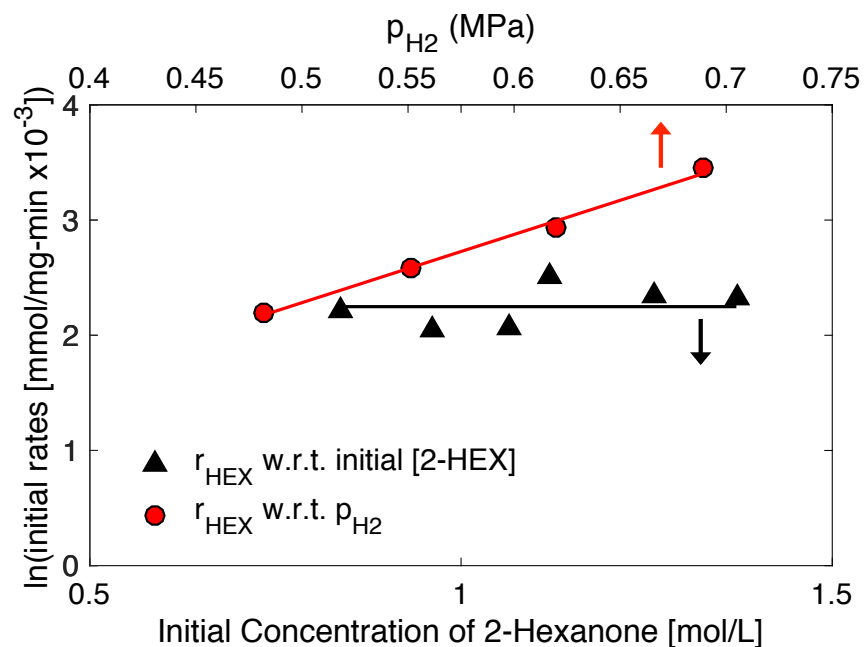


Figure 3.5 Effect of initial 2-hexanone concentration and effect of  $p_{H_2}$  on the initial rate of hydrogenation of 2-hexanone to 2-hexanol using 5% Pt/C

Conditions: 0.2 mol% Pt/C,  $T = 353$  K,  $p_{H_2} = 0.48$ - $0.69$  MPa,  $0.85$ - $1.41$  M DMF in nonane, 750 rpm.

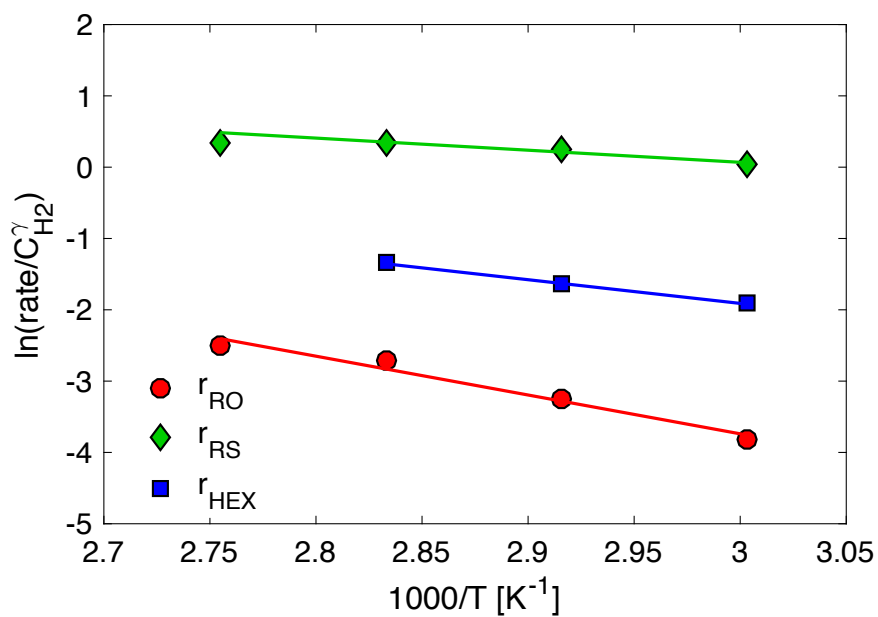


Figure 3.6 Arrhenius plots of initial rates normalized by dependence on  $C_{H_2}^2$  for reaction temperatures (343 – 373 K) using 5% Pt/C,

Conditions: 0.2 mol% loading Pt/C,  $T = 343$ - $373$  K,  $p_{H_2} = 0.55$  MPa, 1.12 M DMF in nonane, 750 rpm.  $r_{HEX}$  was determined using 2-hexanone as the reactant.

**Table 3.4 Apparent rate parameters for the hydrogenation of 2,5-dimethylfuran and 2-hexanone on Pt.**  $\beta$  and  $\gamma$  are values of rate-order dependence on the initial concentration of DMF and  $p_{H_2}$ , respectively.  $E_{app}$  calculated over the temperature range of 333 – 363K and for a  $H_2$  partial pressure of 0.55 MPa based on the Arrhenius relation:  $rate \propto exp\left(-\frac{E_{app}}{RT}\right) C_{DMF}^\beta C_{H_2}^\gamma$ . The concentration of  $H_2$  in the system was calculated from the  $p_{H_2}$  and the Henry's coefficient at the reaction conditions (see SI 3.6.3).

Rates of Reaction Network	$\beta$	$\gamma$	$E_{app}$ (kJ/mol)
Ring opening: $r_{RO}$	$\sim 0$	0.6	45.3
Ring saturation: $r_{RS}$	$\sim 0$	2	10.2
2-Hexanone hydrogenation: $r_{HEX}$	$\sim 0$	1.2	27.6

### 3.3.5 Effects of catalyst support composition on the hydrogenation of DMF and 2-hexanone

The effects of support composition on the hydrogenation of DMF and of 2-hexanone were investigated and the results are presented in Table 3.5. To isolate the effects of support composition, the Pt loading and particle size were kept constant, with the exception of Pt/TiO<sub>2</sub> for which the particle size was could not be controlled via the IWI method of Pt dispersion (Table 3.1).

The initial rates of DMF conversion and product distribution observed at 10% DMF conversion remained unchanged independent of support composition (see Table 3.5.). For all catalysts, the combined selectivity to 2-hexanone and 2-hexanol remained in the range of 90-95%, and only trace amounts of hexane were observed due to the presence of acidic sites on the supports. Although support effects were not observed for DMF hydrogenation, they were observed for 2-hexanone hydrogenation to 2-hexanol. For all oxide-supported Pt catalysts, the rates of ketone hydrogenation are 2- to 5-fold higher than that for Pt/C. The enhancement in C=O hydrogenation by oxide-supported Pt has been observed previously and is attributed to the Lewis acidity of the supports [72,73]. The free electrons of the oxygen atom in the carbonyl group of the ketone can coordinate to Lewis sites on the oxide support [72]. For the supports studied, the strength of the Lewis acid centers increases in the order of Al<sub>2</sub>O<sub>3</sub> < TiO<sub>2</sub> < NbOPO<sub>4</sub>. This trend is also reflected in the TOFs for the rate of 2-hexanone hydrogenation (Table 3.5.).

**Table 3.5 Turnover frequencies (TOFs) for hydrogenation over supported Pt catalysts when DMF or 2-hexanone was used as the substrate.**

TOFs normalized by the total number of surface metal atoms. 0.2 mol% metal loading, T = 353 K,  $p_{H_2}$  = 0.55MPa, 1.12 M substrate in nonane, 750 rpm.

Supported Pt Catalyst	TOF (s <sup>-1</sup> )		% Selectivity <sup>a</sup>			
	$r_{DMF}$	$r_{HEX}$	DMTHF	2-hexanone	2-hexanol	n-hexane
5% Pt/C	1.8	0.7	6.0	85.0	9.1	0.0
1.1% Pt/NBP	2.0	3.2	8.0	81.8	8.8	1.3
1.4% Pt/Al <sub>2</sub> O <sub>3</sub>	2.0	1.8	7.1	82.8	9.4	0.7
1.4% Pt/TiO <sub>2</sub>	1.7	2.3	10.2	74.2	11.2	4.5

<sup>a</sup> Selectivity of the products observed at 10% conversion of DMF

## 3.4 Discussion

### 3.4.1 Mechanism of DMF hydrogenation

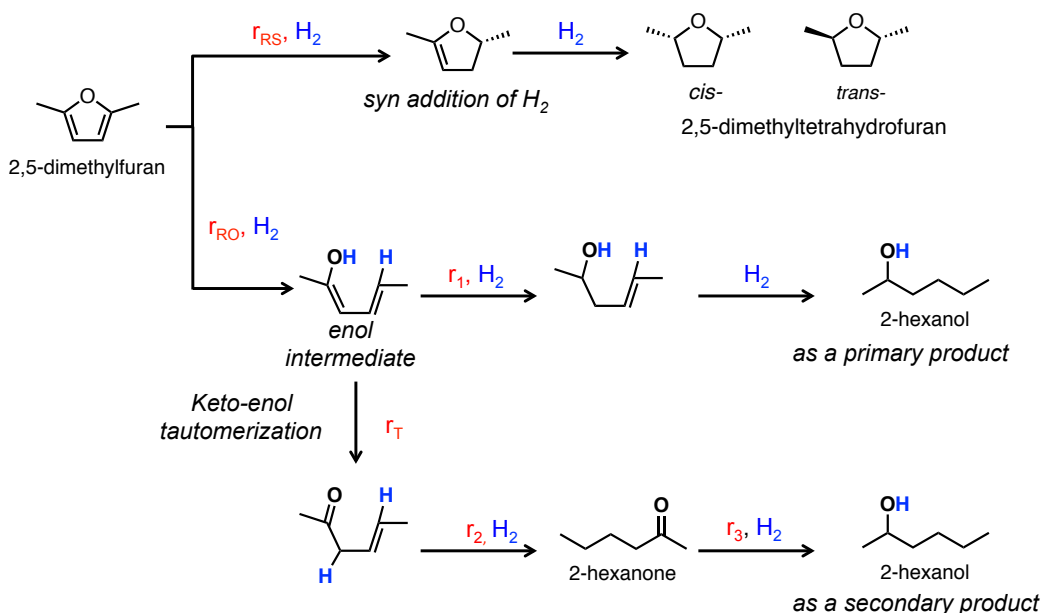
The results of this study suggest that during hydrogenation of DMF, ring saturation to form DMTHF and ring opening to form 2-hexanone and 2-hexanol occur as parallel pathways rather than in series, as proposed previously [18,20]. The argument for sequential hydrogenation of the aromatic furan ring and subsequent ring opening of the tetrahydrofuran derivative is based on the weaker strength (by  $\sim 28$  kJ/mol) of the C-O bond in DMTHF than in DMF [74]. Our studies, however, demonstrate that C-O bond cleavage occurs directly from the aromatic furan ring and does not occur with the saturated tetrahydrofuran ring. This behavior was also observed for hydrogenation of 2-methylfuran versus 2-methyltetrahydrofuran over Pt/C in liquid phase flow systems [37]. This behavior suggests that the interaction between the aromatic ring and the metal surface plays a crucial role in weakening the aromatic C-O bond, thereby enabling its cleavage. Several pieces of evidence support this view. For example, DFT studies find the binding strength of tetrahydrofuran with Pd surfaces to be weaker than that of furan [75]. Sum frequency generation vibration spectroscopy (SFG-VS) studies have shown that DMF adsorbs parallel to the surface of Pt via interaction with the  $\pi$  orbitals of the aromatic ring, whereas DMTHF adsorbs upright via the O atom [65]. This configuration of DMF is further supported by theoretical studies, which demonstrate that DMF adsorption parallel, rather than perpendicular, to the surface of Pt provides higher stability [76].

The selectivity to ring opening versus ring saturation during DMF hydrogenation depends on the identity of the noble metal, as seen in Table 3.2. The degree of ring opening of furfural over Pd, Cu and Ni catalysts has been attributed to differences in the strength of interaction between the ring and the metal surface and the type of surface intermediate each metal is able to stabilize [64]. Further insights come from DFT calculations, which reveal that the orbitals of DMF involved in the adsorption of this molecule depend on the metal [76]. DMF is found to bind parallel to noble metal surfaces either through a single,  $\pi$  C=C bond or through two s bonds with the two carbon atoms of the C=C bond. The latter form of bonding is preferred for Pt, whereas the  $\pi$ -bonded configuration is more favorable over Pd, Ru, and Rh. Of the noble metals investigated in our study, only Pt was highly selective for direct ring opening of the furan whereas Pd, Ru, and Rh were selective for saturation of the furan ring. This observation suggests that p-bonding is conducive to ring saturation and that s-bonding is conducive to ring opening, since s-bonding would disrupt the aromaticity of the furan ring by forming an oxametallacycle species. The presence of possible oxametallacycle intermediates on the surface of Pt during furan hydrogenation has been proposed based on SFG-VS studies [18]. The configuration of DMF adsorbed on metal sites can also be influenced by the degree of hydrogen coverage [76], which can lead to significant effects on the selectivity between ring opening and furan hydrogenation due to energetic differences [75]. However, in our liquid-phase reaction system, the concentration of hydrogen is limited by its low solubility in nonane. For the narrow range of  $p_{\text{H}_2}$  studied ( $p_{\text{H}_2} = 0.41$  MPa - 0.69 MPa), the coverage of H is expected to be in the Henry's law regime, and consequently the effects H coverage on adsorption of DMF and other organic species is expected to be negligible.

Our results suggest that the formation of 2-hexanone and 2-hexanol from DMF occur in parallel through a common intermediate formed after ring cleavage, since 2-hexanol was



detected immediately despite the low concentrations of 2-hexanone present at initial conversions of DMF and the selectivity for the two products in the reactor remains constant until ~40% conversion of DMF (Figure S. 3.2). For extended reaction times for which the concentration of 2-hexanone becomes significant and the concentration of DMF is low, additional 2-hexanol is produced via secondary hydrogenation of 2-hexanone. Scheme 3.1 captures these possibilities.



**Scheme 3.1** Proposed reaction network for the hydrogenation of DMF into ring saturated and ring opened products over Pt/C.

The formation of DMTHF is envisioned to begin with the syn-addition of hydrogen across the C=C bond of DMF adsorbed parallel to the Pt surface to form a dihydro intermediate. These intermediates are unlikely to be involved in ring opening and instead have been observed to contribute exclusively to the formation tetrahydrofuran species during hydrogenation over Pt (> 90% selectivity) [21,22]. Moreover, DFT calculations by Wang et al. of furan hydrogenation over Pd show that dihydro or trihydro intermediates are unlikely to undergo ring-opening due to the high energy barriers associated with these processes [75]. We note that dihydro and trihydro intermediates were not detected in the course of the present study, suggesting that further hydrogenation of these intermediates to DMTHF is rapid.

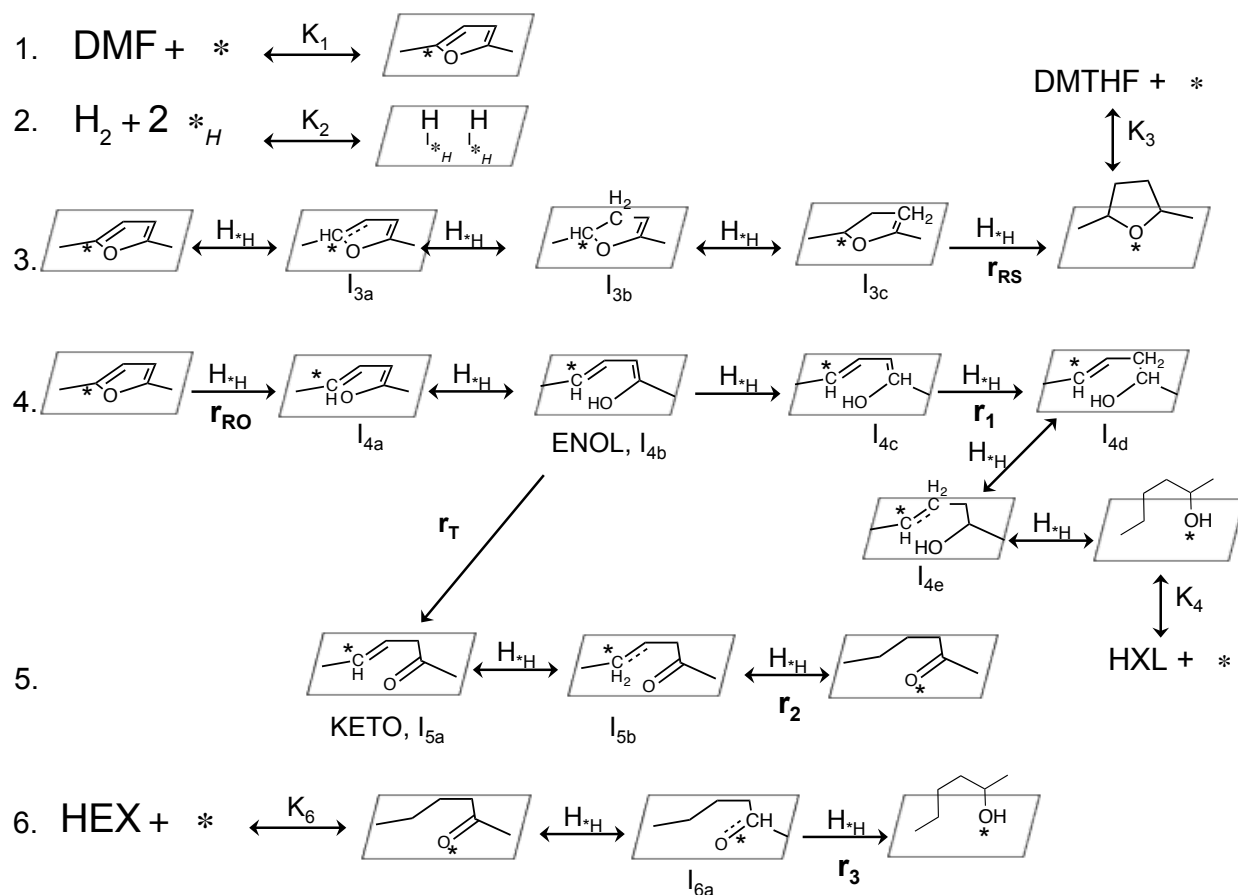
Since our method of identification and quantification (GC/MS) allowed us to distinguish between *cis* and *trans* isomers of DMTHF via characteristic retention times, it is interesting to observe that the production of the *cis* isomers is heavily favored over the production of the *trans* isomers, and that greater than 90% of DMTHF exists as the *cis* isomer at 10% conversion of DMF (Table 3.2). The preference for the *cis* isomer can be rationalized by the hypothesis that immediately after the first addition of  $H_2$ , the second C=C bond is hydrogenated in a similar manner before the dihydrofuran species can desorb, flip over, and re-adsorb to produce the *trans* isomer through another syn-addition of  $H_2$  across the remaining C=C bond. This hypothesis is supported by observations that the selectivity to *cis*-DMTHF increases up to > 99% at 10% DMF conversion, under higher  $H_2$  partial pressures (0.61 MPa) or under higher reaction temperatures

(363K). Under these reaction conditions, the rate at which hydrogenation of the second C=C bond occurs is very high, making it more difficult for desorption and re-adsorption of 2,5-dimethyldihydrofuran to occur rapidly enough to enable the formation of *trans*-DMTHF.

We propose that the first step in the ring-opening of DMF involves reductive cleavage of the aromatic C-O bond to form an enol intermediate. This species is postulated to be the precursor to both 2-hexanol and 2-hexanone. The Gibbs free energy difference at 353 K between the gas phase enol and its keto analog, 2-hex-4-enone, was calculated using DFT to be -33 kJ/mol. The enol intermediate is therefore likely to rapidly convert at reaction conditions to its thermodynamically favored keto tautomer, which can then undergo additional hydrogenation at the remaining C=C bond to form 2-hexanone. We also note that the double bond at the  $\alpha$  carbon of the enol can undergo hydrogenation before tautomerization to the keto form, resulting in the formation of 2-hexanol as a primary product, rather than as a secondary product of 2-hexanone hydrogenation. The proposed mechanism is supported by the observation that the initial ratio of 2-hexanol to 2-hexanone concentrations at low DMF conversions decreases with increasing temperature (Figure 3.2) because the keto tautomer is favored at increasing temperatures over the enol form. The preference for forming 2-hexanone versus 2-hexanol after ring-opening of DMF is governed by the relative rates of tautomerization of the enol ( $r_T$ ) and hydrogenation of the enol ( $r_I$ ). The existence of a primary pathway for forming 2-hexanol directly from DMF is supported by the results shown in Table 3.5 for DMF and 2-hexanone hydrogenation over Pt supported on different oxides. We note that the selectivity for 2-hexanol at 10% DMF conversion is the same regardless of the support used because the production of 2-hexanol in this regime results directly from ring opening of DMF. At DMF conversion above 40%, additional 2-hexanol is formed by secondary hydrogenation of 2-hexanone, a process that is enhanced by the Lewis acidity of the support.

#### 3.4.2 Kinetic modeling of the hydrogenation of DMF

To develop a model for the kinetics of DMF hydrogenation, the reaction network proposed in Scheme 3.1 is represented as the sequence of elementary reactions shown in Scheme 3.2. Scheme 3.2 is based on a Langmuir-Hinshelwood model with all surface reactions occurring stepwise between an adsorbed organic species and a dissociated hydrogen atom. The symbols \* and  $*_H$  represent vacant sites on the catalyst surface that can accommodate organic species and atomic hydrogen, respectively.  $K_i$  is the adsorption equilibrium constant for organic species  $i$ . Partially hydrogenated intermediates adsorbed on the surface are depicted as  $I_{ix}$ . However, none of these intermediates nor any unsaturated species were detected as stable products and, hence, the steps involving these species were treated as quasi-equilibrated or the species were treated as reactive intermediates in the pseudo steady-state approximation in the derivation of rate expressions (see SI 3.6.4).



**Scheme 3.2 Schematic of the elementary reactions involved in the overall reaction network shown in Scheme 1.**

The elementary reactions are grouped into six categories of reactions in Scheme 3.2. Reactions 1 and 2 represent the adsorption of DMF and dissociative adsorption of  $\text{H}_2$ , respectively. Reaction 3 depicts the formation of the ring-saturated product, DMTHF, after four step-wise additions of hydrogen atoms ( $\text{H}^*_{\text{H}}$ ). As the ring becomes more distorted with each addition of hydrogen, the intermediates lift up from the surface until DMTHF, which is bound perpendicular to the surface through its oxygen atom [75], is formed. Reaction 4 involves the ring opening of adsorbed DMF during the addition of the first hydrogen atom, and sequential hydrogenations to form 2-hexanol (HXL) as a primary product. Reaction 5 leads to the formation of 2-hexanone (HEX) after tautomerization of the enol species ( $\text{I}_{4\text{b}}^*$ ) to the keto species ( $\text{I}_{5\text{a}}^*$ ), in which the rate is given by  $r_{\text{T}}$ . Finally, Reaction 6 accounts for the hydrogenation of the carbonyl group of HEX to form HXL as a secondary product. The intermediates portrayed in the scheme were not detected during product analyses but are proposed on the basis of intermediates suggested by DFT calculations for furan hydrogenation over Pd [75].

An important feature of the proposed mechanism is that the adsorption of organic species and  $\text{H}_2$  occur non-competitively, and therefore adsorption sites for organic species and for atomic hydrogen are treated separately. This choice was motivated by the observation that mechanisms involving competitive adsorption of DMF and  $\text{H}_2$  on a single site did not lead to rate expressions consistent with the observed dependencies on  $\text{H}_2$  partial pressure for ring opening and ring saturation,  $\sim 0.61$  and  $\sim 2.0$ , respectively, and with the observed zero order dependence on DMF

concentration for all reactions. Specifically, if the adsorption of reactants were truly competitive, we would observe a decrease in the rate of hydrogenation with increased loading of DMF due to increasing competition with hydrogen for surface coverage. Non-competitive adsorption between the substrates and H<sub>2</sub> can occur if the catalyst surface is saturated with organic species but interstitial sites between the adsorbed species are likely to remain accessible for the much smaller hydrogen atoms. The observed zero order dependence with respect to DMF or HEX loading indicates saturation of surface sites by substrate. This non-competitive behavior in kinetic models is supported by experimental data for several hydrogenation reactions of aromatic hydrocarbons for which the reaction order in benzene partial pressure was observed to be zero [70].

The mechanism proposed in Scheme 3.2 was used to derive rate expressions for the rates of ring saturation and ring opening as a function of the concentrations of DMF (C<sub>DMF</sub>) and 2-hexanone (C<sub>HEX</sub>), and the partial pressure of H<sub>2</sub> (p<sub>H2</sub>) (see SI 3.6.4 for details). Ring saturation of DMF to produce DMTHF occurs via a sequence of steps in which one H atom is added at each step (Reaction 3). In order to capture the roughly second order (2) dependence of the rate of formation of DMTHF on H<sub>2</sub> partial pressure, we assume that the first three additions of H atoms are quasi-equilibrated and that the fourth and final addition of hydrogen is rate-limiting. Under these constraints, the rate of ring-saturation is given by the following expression:

$$r_{RS} = \frac{k_{RS}K_1C_{DMF}(\sqrt{K_2H_{H_2}p_{H_2}})^4}{(1+K_1C_{DMF}+K_6C_{HEX})(1+\sqrt{K_2H_{H_2}p_{H_2}})} \quad (1)$$

In this expression,  $k_{RS}$  is the reaction rate constant for ring saturation,  $K_1$  and  $K_6$  are adsorption equilibrium constants for DMF and HEX, respectively,  $K_2$  is the equilibrium constant for dissociative adsorption of H<sub>2</sub>, and  $H_{H_2}$  is the Henry's constant relating the concentration of dissolved H<sub>2</sub> in the liquid phase to the partial pressure of H<sub>2</sub>, p<sub>H2</sub>. Determination of  $H_{H_2}$  for our reaction system can be found in SI 3.6.3.

Both HEX and HXL are produced after ring cleavage of DMF. To capture the experimentally observed ~0.6 rate order dependence in  $r_{RO}$  with respect to H<sub>2</sub> partial pressure, we propose that the rate-limiting step for ring opening is the irreversible addition of the first H atom to adsorbed DMF (Reaction 4). Under this assumption, the rate of ring opening is then given by the following expression:

$$r_{RO} = \frac{k_{RO}K_1C_{DMF}\sqrt{K_2H_{H_2}p_{H_2}}}{(1+K_1C_{DMF}+K_6C_{HEX})(1+\sqrt{K_2H_{H_2}p_{H_2}})} \quad (2)$$

where  $k_{RO}$  is the reaction rate constant associated with ring opening.

The set of differential equations describing the temporal evolution in the concentrations of ring-opened (HEX + HXL), C<sub>RO</sub>, and ring-saturated (DMTHF), C<sub>RS</sub>, products formed during DMF hydrogenation in a well stirred, batch reactor can be written as

$$\frac{V}{W} \frac{dC_{DMF}}{dt} = -r_{RO} - r_{RS} \quad (3)$$

$$\frac{V}{W} \frac{dC_{RS}}{dt} = r_{RS} \quad (4)$$

$$\frac{V}{W} \frac{dC_{RO}}{dt} = r_{RO} \quad (5)$$

with the following initial conditions:

$$t = 0; \quad C_{DMF} = C_{DMF}^0 \quad C_{RO} = 0 \quad C_{RS} = 0 \quad (6)$$

In eqns. 3 – 5, V is the solution volume in the reactor and W is the weight of catalyst.

Values for the rate and equilibrium constants appearing in eqns. 1 and 2 were evaluated by solving the system of differential equations for an initial set of these parameters to determine concentrations of DMF, DMTHF, and HEX+HXL as functions of time and then comparing these values to those obtained experimentally. The objective function in a nonlinear, least-squares regression was then minimized by varying the rate and equilibrium constants in order to obtain the best-fit values of these constants. The ordinary differential equation solver, ODE15s, and the nonlinear optimization solver for the residual sum of squares, fmincon, provided in Matlab were used for parameter estimation. The parameters evaluated at different temperatures (343 – 363K) were correlated using the Arrhenius equation to obtain respective activation energies and pre-exponential factors. The kinetic parameters of eqns. 1 and 2 obtained in this manner are summarized in Table 3.6. Fig. 7a illustrates the extent to which the model of DMF hydrogenation kinetics capture the competitive ring opening vs. ring saturation behavior at 353 K.

The equilibrium constant for the adsorption of HEX,  $K_6$ , was determined by fitting a model of the rate of HEX hydrogenation to HXL over Pt/C (see SI 3.6.5). The sequence of elementary steps in this study is described by Reaction 6 in Scheme 3.2. For the reaction conditions studied (0.55 Mpa, 333 K – 353 K), HXL was the only product observed and no evidence for the dehydrogenation of HXL to HEX was observed. The rate expression developed to describe the conversion of HEX to HXL when 2-hexanone is used as the substrate is as follows:

$$r_3 = \frac{k_3 K_6 C_{HEX} (\sqrt{K_2 H_{H_2} P_{H_2}})^2}{(1 + K_6 C_{HEX} + K_4 C_{HXL}) (1 + \sqrt{K_2 H_{H_2} P_{H_2}})} \quad (7)$$

Values of the rate and equilibrium constants associated with HEX hydrogenation, eq. 7, were obtained by the parameter estimation procedure described earlier. Values of these constants at 353 K and their associated parameters are presented in Table 3.7. Comparison between the experimental data and the fitted model is shown in Figure 3.8 for HEX hydrogenation at 353 K.

Fits to experimental data obtained at other temperatures and plots of the rate and equilibrium constants appearing in eqn. 7 can be found in

**Figure S. 3.3** and **Figure S. 3.4**. The calculated activation energy (23.7 kJ/mol) is consistent with the apparent activation energy determined from initial rate studies of HEX hydrogenation over Pt/C (Table 3.4).

The model of the reaction kinetics developed above was expanded to distinguish between production of HEX and HXL after C-O hydrogenolysis. As discussed earlier, HXL can be produced as both a secondary product by hydrogenation of HEX ( $r_3$ ), and a primary product by hydrogenation of the enol intermediate ( $r_I$ ) before tautomerization to the keto ( $r_T$ ). The enol ( $I_{4b}$ )

is treated as a reactive intermediate formed by ring-opening ( $r_{RO}$ ) of DMF and is consumed by competing reactions ( $r_I$  and  $r_T$ ). The species  $I_{4a}$  and  $I_{4c}$  were also treated as reactive species in the stepwise addition of H atoms to form HXL as a primary product. Because the initial ratio of HXL to HEX was found to depend on  $p_{H_2}$ , we assumed that the tautomerization step is not in equilibrium in our reaction system. We also note that 10% of ring-opened products appear as HXL during initial conversion of DMF despite the keto form being thermodynamically preferred over the enol form ( $\Delta G = -33$  kJ/mol), which suggests that  $r_I$  occurs fast enough to compete with  $r_T$ . It is assumed that tautomerization is irreversible and once the keto tautomer is formed, it goes exclusively to form HEX after hydrogenation of the unsaturated C=C bond,  $r_2$ . Therefore, the rate of HEX produced from DMF is governed by the rate of tautomerization,  $r_T$ .

The rate of production of HEX ( $r_T$ ) and the rate of production of HXL ( $r_I$ ) after ring opening of DMF are dependent on the coverage of the reactive intermediate, enol species ( $I_{4b}$ ), given by

$$\theta_{I_{4b}} = \frac{k_T k_{RO} K_1 C_{DMF} (\sqrt{K_2 H_{H_2} p_{H_2}})}{(1 + K_1 C_{DMF} + K_6 C_{HEX})(1 + \sqrt{K_2 H_{H_2} p_{H_2}})} \quad (8)$$

$$k_1 \left( \frac{\sqrt{K_2 H_{H_2} p_{H_2}}}{1 + \sqrt{K_2 H_{H_2} p_{H_2}}} \right) + k_T$$

To describe the main reactions occurring after cleavage of the aromatic ring in DMF, the following additional rate expressions are developed based on experimental observations, assuming the rate-limiting step for hydrogenation of C=O bonds involves the addition of a second hydrogen atom.

$$r_T = \frac{k_T k_{RO} K_1 C_{DMF} (\sqrt{K_2 H_{H_2} p_{H_2}})}{(1 + K_1 C_{DMF} + K_6 C_{HEX})(1 + \sqrt{K_2 H_{H_2} p_{H_2}})} \quad (9)$$

$$k_1 \left( \frac{\sqrt{K_2 H_{H_2} p_{H_2}}}{1 + \sqrt{K_2 H_{H_2} p_{H_2}}} \right) + k_T$$

$$r_1 = \frac{k_1 k_{RO} K_1 C_{DMF} (\sqrt{K_2 H_{H_2} p_{H_2}})^2}{(1 + K_1 C_{DMF} + K_6 C_{HEX})(1 + \sqrt{K_2 H_{H_2} p_{H_2}})^2} \quad (10)$$

$$k_1 \left( \frac{\sqrt{K_2 H_{H_2} p_{H_2}}}{1 + \sqrt{K_2 H_{H_2} p_{H_2}}} \right) + k_T$$

$$r_3 = \frac{k_3 K_6 C_{HEX} (\sqrt{K_2 H_{H_2} p_{H_2}})^2}{(1 + K_1 C_{DMF} + K_6 C_{HEX} + K_3 C_{DMTHF} + K_4 C_{HXL})(1 + \sqrt{K_2 H_{H_2} p_{H_2}})} \quad (11)$$

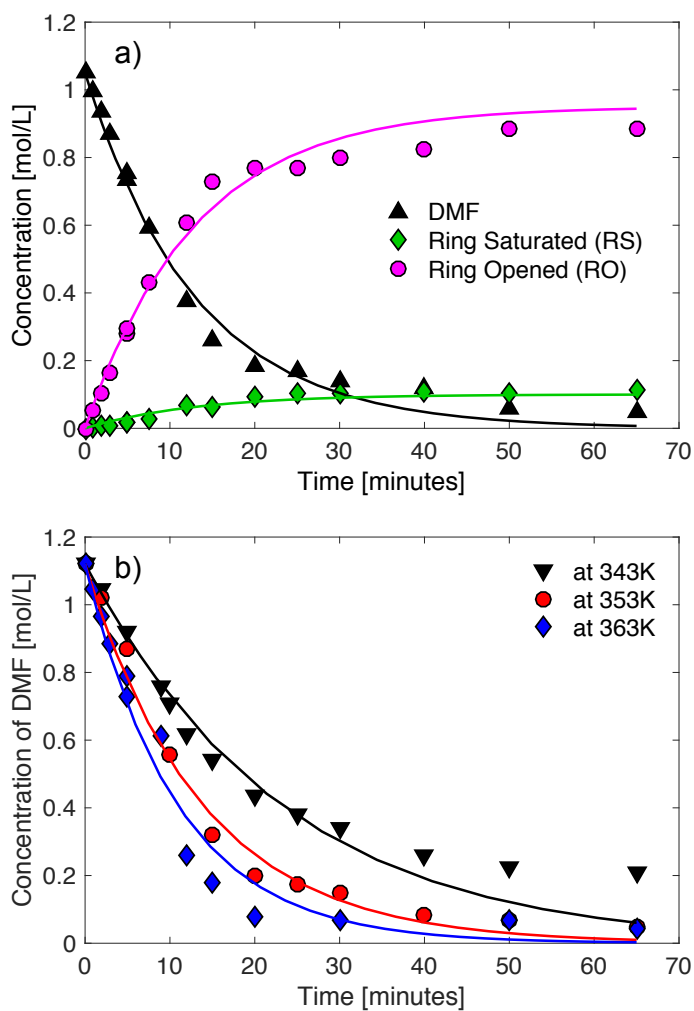
where  $k_T$ ,  $k_1$ , and  $k_3$  are the reaction rate constants associated with the rate of tautomerization of enol, hydrogenation of the unsaturated bond of enol, and hydrogenation of C=O of HEX, respectively.  $K_3$  is the equilibrium constant for adsorption of DMTHF. The value of  $K_3$  appears in the equation for  $r_3$ , since product inhibition was observed when DMTHF (0.2 M) was added with 2-hexanone as a substrate during initial rate experiments. The initial rate of HEX hydrogenation was ~10% slower with the presence of additional DMTHF. This inhibition was not observed when DMTHF (0.2 M) was added during the initial-rate experiments for DMF hydrogenation over Pt/C. But overall, the inhibition by DMTHF on  $r_3$  is expected to be minimal since the maximum concentration of this product reached is 0.1 M for DMF conversions >80%.

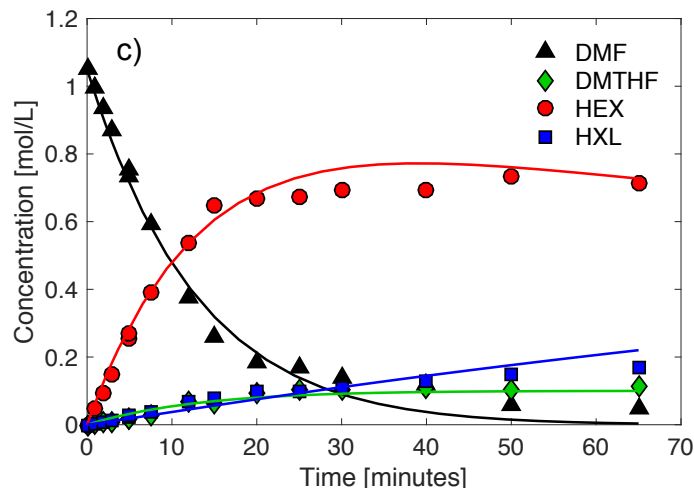
The differential equation describing the concentration of ring-opened products,  $C_{RO}$ , can be replaced by the following two differential expressions to describe the concentrations of 2-hexanone and 2-hexanol,  $C_{HEX}$  and  $C_{HXL}$ .

$$\frac{V}{W} \frac{dC_{HEX}}{dt} = r_T - r_3 \quad (12)$$

$$\frac{V}{W} \frac{dC_{HXL}}{dt} = r_1 + r_3 \quad (13)$$

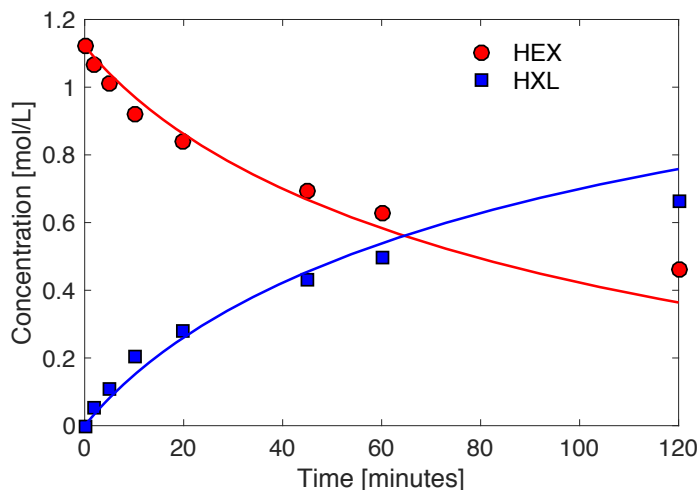
Estimates of the rate parameters involved in  $r_T$ ,  $r_1$  and  $r_3$  were obtained by the same procedure described earlier. Arrhenius plots of the estimated values of rate constants and equilibrium constants for the kinetic model obtained for temperatures 343 K – 363 K are shown in Figure S. 3.6. Values of these constants at 353 K and their associated activation barriers and pre-exponential factors are summarized in Table 3.6.





**Figure 3.7 Comparison of experimental data (symbols) and concentration profiles fitted for the model (lines) during DMF hydrogenation over 5% Pt/C.**

a) the parallel pathways of ring opening (HEX, HXL) and ring saturation (DMTHF) at  $T = 353\text{K}$ ,  $0.2 \text{ mol}\% \text{ Pt/C}$ ,  $p_{\text{H}_2} = 0.55 \text{ MPa}$ ,  $1.04 \text{ M DMF}$  in nonane,  $750 \text{ rpm}$ . b) DMF in the system at temperatures ( $343 \text{ K}$ - $363 \text{ K}$ ). c) all observed products of DMF at conditions in a).



**Figure 3.8 Comparison of experimental and fitted concentration profiles for 2-hexanone hydrogenation to 2-hexanol over 5% Pt/C 353K.**

Reactions performed using  $0.2 \text{ mol}\% \text{ Pt/C}$ ,  $p_{\text{H}_2} = 0.55 \text{ MPa}$ ,  $1.12 \text{ M 2-hexanone}$  in nonane,  $750 \text{ rpm}$ . Model fit: solid lines. Measurement: symbols.

Figure 3.7(a) compares the concentration profiles for DMF, DMTHF, and HEX+HXL as functions of time predicted by the model and those observed experimentally and Figure 3.7b) presents a similar comparison for the effects of reaction temperature on the variation in the concentration of DMF as a function of time. Additional temporal plots comparing the experimental data to the kinetic model at additional temperatures are found in Figure S. 3.5. In all instances, the quality of the agreement between the predictions by the model and the experimental data is good. The model captures the steady, linear conversion of DMF for short



reaction times and the competitive nature between ring opening and ring saturation for the substrate.

In addition, the model describes the parallel formation of all three products as observed experimentally (Figure 3.7(c)) during initial conversion of DMF ( $t < 15$  min) – 1. ring saturation to produce DMTHF ( $r_{RS}$ ), 2). tautomerization of enol intermediate ( $r_T$ ) after ring opening to produce HEX, and 3. hydrogenation of enol intermediate ( $r_1$ ) after ring opening to produce HXL. For extended reaction times and higher conversions of DMF ( $>75\%$ ), the major pathway to HXL is no longer via hydrogenation of the enol ( $r_1$ ) but instead, secondary hydrogenation of HEX present in the system ( $r_3$ ).

**Table 3.6 Rate parameters obtained by non-linear, least squares fitting of experimental data to proposed kinetic model for the reaction network of DMF hydrogenation.**

Rate or Equilibrium Constant	Parameters at 353K		$E_a$ or $\Delta H_{ad}$		$\ln(A)$ or $S_{ad}$
$k_{RS}$	5.7	mol/g-min	10.1	kJ/mol	5.2
$k_{RO}$	0.09	mol/g-min	45.4	kJ/mol	12.9
$k_T$	8.74	mol/g-min	9.6	kJ/mol	5.4
$k_1$	7.69	mol/g-min	4.8	kJ/mol	3.6
$k_3$	0.06	mol/g-min	11.2	kJ/mol	1.0
$K_1$	13	L/mol	-12.3	kJ/mol	-1.6
$K_2$	0.56	L/mol	-3.8	kJ/mol	-1.9
$K_3$	12	L/mol	-7.8	kJ/mol	-0.18

**Table 3.7 Rate parameters involved in eq. 7 obtained by non-linear, least squares fitting of experimental data for the hydrogenation of 2-hexanone to 2-hexanol.**

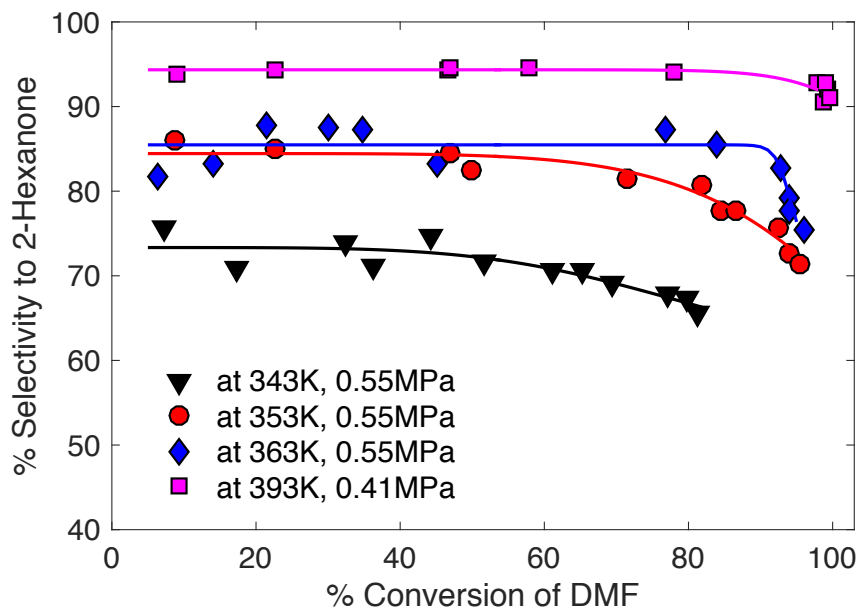
Rate or Equilibrium Constant	Parameters at 353K		$E_a$ or $\Delta H_{ad}$		$\ln(A)$ or $S_{ad}$
$k_3$	0.15	mol/g-min	23.7	kJ/mol	6.2
$K_2$	0.58	L/mol	-4.8	kJ/mol	-2.2
$K_6$	15	L/mol	-16.1	kJ/mol	-2.8
$K_4$	25	L/mol	-12.0	kJ/mol	-0.9

The predicted rate constant associated with the secondary hydrogenation of HEX to HXL,  $k_3$ , obtained from our investigation of HEX hydrogenation is 2.5x larger (Table 3.7) than the value of  $k_3$  predicted from the simulation DMF hydrogenation (Table 3.6). However, this larger value of  $k_3$  appearing in  $r_3$  is still insufficient to account for all HXL observed during the initial conversion of DMF. If we first assume that HXL is produced exclusively through secondary hydrogenation ( $r_3$ ) and use the value of  $k_3 = 0.15$  mol/g-min as determined from our study of HEX hydrogenation, we are still unable to capture the immediate production of HXL during initial conversion of DMF. As seen in Figure S. 3.7(a), assumption of secondary hydrogenation alone inevitably under predicts the amount of HXL present at the beginning of the reaction since  $r_3$  is dependent on the quantity of HEX available. Alternatively, if we neglect the secondary hydrogenation and assume HXL is solely produced through the hydrogenation of the enol intermediate,  $r_1$ , we are unable to capture the continuous production of HXL after DMF has been consumed (in Figure S. 3.7(b)). The fitted rate constant associated with the primary formation

of HXL,  $k_1$ , is predicted to be several times larger than that associated with the secondary formation of HXL,  $k_3$  (Table 3.6-3.7). But both rates are dependent on other intermediates present in the reactor, resulting in  $r_1$  to produce HXL during the initial phase of DMF hydrogenation when the concentration of HEX is too low for  $r_3$  to be a significant and  $r_3$  to produce HXL via hydrogenation of HEX after DMF is depleted.

The activation energies predicted for the three reaction pathways – ring opening, ring saturation, 2-hexanone hydrogenation follows the order of  $E_{RS} < E_{HEX} < E_{RO}$ , consistent with the trend in apparent activation energies determined empirically from initial rate experiments (Table 3.4). The calculated activation energies for ring opening and ring saturation are 45.4 kJ/mol and 10.1 kJ/mol, respectively, and are consistent with the observed apparent activation energies,  $E_{app}$ , obtained from an analysis of the initial rates during DMF hydrogenation (Table 3.4). Our results also agree with the limited information in the literature concerning the kinetics of ring-opening of alkylfurans during liquid-phase hydrogenation. In these studies the step with highest activation energy is typically associated with breaking the aromatic C-O bond of the furanic species [77].

The selectivity between ring saturation and ring opening is dependent on the relative magnitudes of  $r_{RS}$  and  $r_{RO}$ . While the activation energy for the former process is lower, it has a higher order dependence on the concentration of  $H_2$  available. Since the concentration of  $H_2$  in liquid phase is low under the reaction conditions employed, the overall rate of formation of DMTHF occurs more slowly than the rate of formation of ring opened products through C-O bond hydrogenolysis (Table 3.3). A similar argument can be made for the selectivity between formation of 2-hexanone and 2-hexanol following ring opening of DMF. Since these products are produced by competing reactions involving the enol intermediate, the formation of 2-hexanol over 2-hexanone is again governed by the relative rates of hydrogenation of the C=C bond ( $r_I$ ) and the tautomerization of the enol ( $r_T$ ). The rate constants for tautomerization and enol hydrogenation are comparable at 353 K (see Table 3.6). The activation barrier for tautomerization step is higher and the rate is independent of the  $p_{H_2}$ , whereas the hydrogenation of the C=C bond has a lower activation barrier and a  $\sim 1.0$  order dependence on  $p_{H_2}$ . Under the reaction conditions employed, the magnitude of  $r_T$  is greater than the magnitude of  $r_I$ , resulting in 2-hexanone as the major product during DMF hydrogenation over Pt/C. An understanding of the influence of reaction conditions on the kinetics of DMF hydrogenation can be used to help tune the process to produce 2-hexanone selectively during DMF hydrogenation. Operation at low  $p_{H_2}$  and elevated temperatures will favor ring opening over ring saturation, favor tautomerization over enol hydrogenation, and minimize C=O hydrogenation to improve selectivity toward 2-hexanone. Indeed we were able to achieve 92% selectivity of 2-hexanone at 100% conversion of DMF by applying appropriate reaction conditions (0.41MPa, 393K) (Figure 3.9). This is the highest selectivity to 2-hexanone achieved in liquid-phase hydrogenation under mild conditions.



**Figure 3.9. Selectivity toward 2-hexanone as a function of DMF conversion and temperature.** All hydrogenations performed at 0.2 mol% active 5% Pt/C,  $T = 353\text{ K}$ ,  $p_{\text{H}_2} = 0.55\text{ MPa}$ , 1.12 M DMF in nonane, 750 rpm, except for the optimized reaction ( $T = 493\text{ K}$ ,  $0.42\text{ MPa}$ ) to improve selectivity toward 2-hexanone. Solid lines are present to guide the eye.

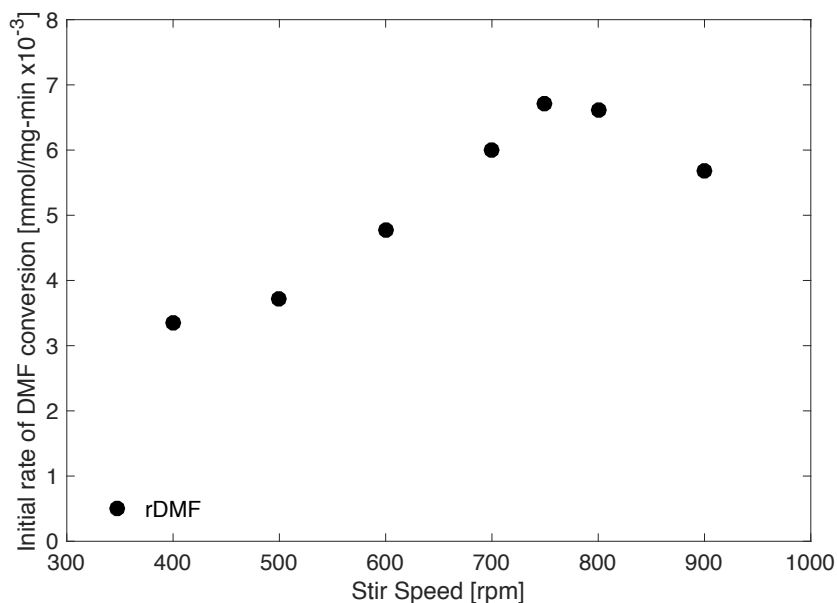
### 3.5 Conclusions

The liquid-phase hydrogenation of DMF was investigated over carbon-supported Pt, Pd, Rh, and Ru with the aim of identifying catalysts that exhibit selectivity for ring opening as opposed to ring saturation. High selectivity toward ring-opening products, 2-hexanone and 2-hexanol, were observed only for Pt/C, whereas Pd/C, Rh/C, and Ru/C produced 2,5-dimethyltetrahydrofuran preferentially via ring saturation. The kinetics of DMF hydrogenation over Pt/C in the liquid phase were found to be zero order in DMF and positive order in the partial pressure of  $\text{H}_2$ . Time-course studies demonstrated that 2-hexanone and 2-hexanol are produced in parallel, and further hydrogenation of 2-hexanone to 2-hexanol is slow. Our proposed mechanism for DMF hydrogenation explains the experimental behaviors observed. The key element of the mechanism is the formation of an enol intermediate that rapidly isomerizes to the thermodynamically preferred keto form. The reason why this reaction pathway occurs preferentially on Pt is attributed to the specifics of how DMF bind to this metal. A microkinetic model was developed on the basis of the proposed mechanism and successfully describes the observed kinetics very well. The microkinetic model was used to show that both primary and secondary production of 2-hexanol from DMF and from 2-hexanone, respectively, are needed in order to obtain temporal profiles of  $C_{\text{HXL}}$  that agreed with experimental observations for the duration of DMF hydrogenation. The activation barrier for ring opening of DMF was found to have a higher activation energy and a lower dependence on  $p_{\text{H}_2}$  than ring saturation. This finding shows that ring opening is favored by operating at elevated temperatures and low  $p_{\text{H}_2}$ . Using this strategy, we were able to achieve 92% selectivity to 2-hexanone at full conversion of DMF.

### 3.6 Supplemental Information

#### 3.6.1 Mass transfer effects in semi-batch hydrogenation system

A number of checks were made to assess whether or not mass-transfer from of  $H_2$  from the gas phase to the liquid or from the liquid to the catalyst affected the measure rates of reaction. The extent of external diffusion limitation of transporting dissolved reactants to the catalyst surface was determined by varying the reactor stir speed from 400 rpm to 900 rpm. The initial rate of conversion of DMF increased with increasing stir speed but reached a plateau region above 700 rpm. Reaction rates dropped at high stir speeds of 900rpm due to entrainment of catalyst particles on reactor walls (Figure S. 3.1). Therefore, all experiments were performed using a stirring speed of 750 rpm to avoid external mass transfer resistance as well as loss of catalyst mass to entrainment. To establish the absence of internal mass transfer effects, commercial 5% Pt/C was sieved and separated into four ranges of particle size ( $< 35$ , 35-53, 53-75, and  $> 75\mu\text{m}$ ). No effect of particle size on the initial rates of DMF conversion was observed for particles smaller than  $75\mu\text{m}$  (Table S. 3.1). For all subsequent kinetic experiments, particles sizes of  $< 45\mu\text{m}$  were used.



**Figure S. 3.1 Rate of conversion of DMF in system as a function of stir speed.**  
Reaction conditions: 0.2 mol% Pt/C,  $T = 353\text{ K}$ ,  $p_{H_2} = 0.55\text{ MPa}$ , 1.12M DMF in nonane.

**Table S. 3.1 Rate of conversion of DMF as a function of 5% Pt/C particle size from <35um to >75um.**

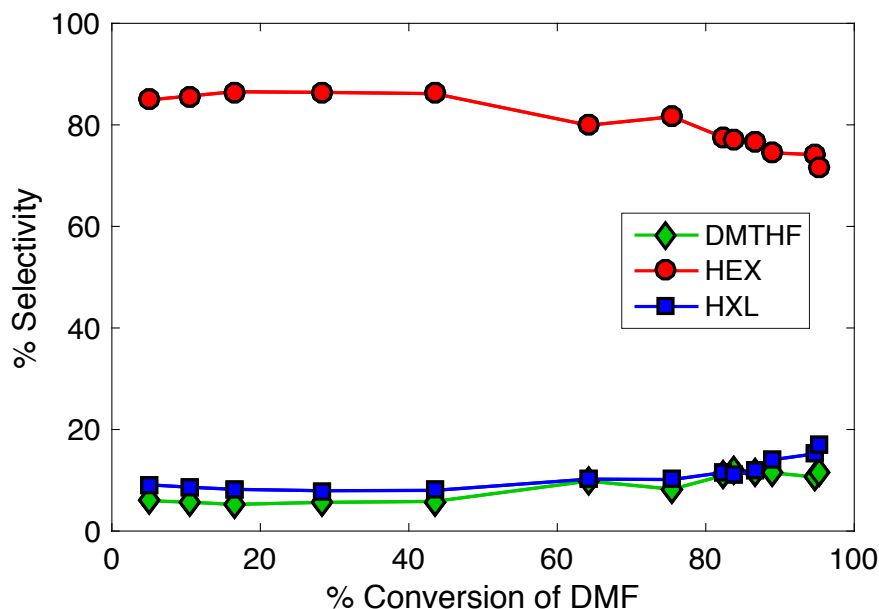
The rate is independent of particle size for particle sizes <75um, confirming absence of internal mass transfer limitations. Reaction conditions: 0.048 mol% Pt/C, T = 353 K,  $p_{H_2} = 0.55$  MPa, 1.12M DMF in nonane, 750 rpm.

5% Pt/C Particle Size (mm)	rDMF (mmols /site-min)
<35	105
35-53	106
53-75	102
>75	82
<b>Mixture as received</b>	107

**Rate of conversion of DMF as a function of 5% Pt/C particle size from <35um to >75um.**

The rate is independent of particle size for particle sizes <75um, confirming absence of internal mass transfer limitations. Reaction conditions: 0.048 mol% Pt/C, T = 353 K,  $p_{H_2} = 0.55$  MPa, 1.12M DMF in nonane, 750 rpm.

### 3.6.2 Product selectivity as a function of DMF conversion



**Figure S. 3.2 Product selectivity as a function of DMF conversion.**

Reactions performed using 0.2 mol% Pt/C,  $p_{H_2} = 0.55$  MPa, 1.04 M DMF in nonane, 353 K, 750 rpm

### 3.6.3 Calculation of dissolved $H_2$ in system

The concentration of dissolved hydrogen,  $C_{H_2}$ , in the system is a function of the hydrogen partial pressure, temperature and solvent.  $H_2$  is sufficiently dilute in the liquid system and Henry's law was determined valid at the range of reaction conditions studied (333K-363K, 0.41-0.69 MPa). In accordance to Henry's Law, the concentration of dissolved  $H_2$  in the solution is proportional to the partial pressure of hydrogen above the liquid by the proportionality constant,  $H_{H_2}$ , which is the Henry's constant for a particular temperature and solvent solubility. Predicted values for  $K_H$  in nonane solvent and at temperatures 333K - 363K were determined from the studies by E. Brunner et al [78]. The concentration of  $H_2$  in nonane at 353K was determined to be 0.023M.

### 3.6.4 Derivation of rate expressions in kinetic model

Reactions 1 – 6 in the hydrogenation network in Scheme 3.2 of text.

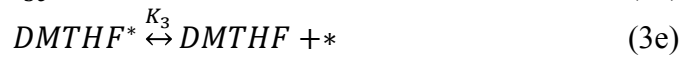
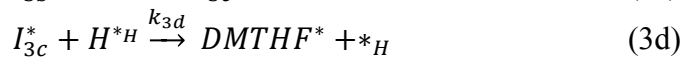
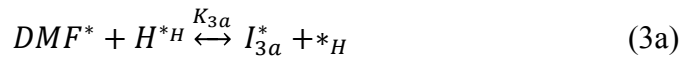
Reaction 1:



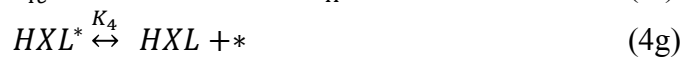
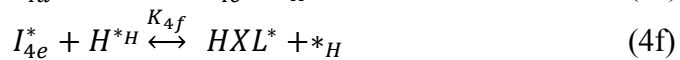
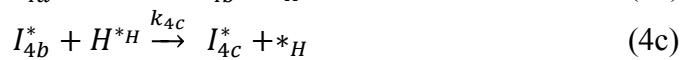
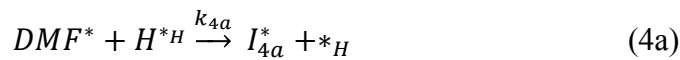
Reaction 2:



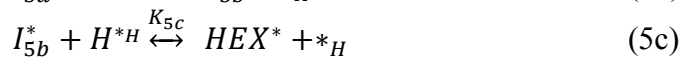
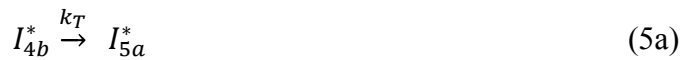
Reaction 3:



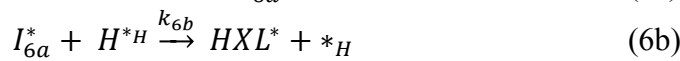
Reaction 4:



Reaction 5:



Reaction 6:



The rates for ring opening ( $r_{RO}$ ), ring saturation ( $r_{RS}$ ), hydrogenation of enol ( $r_1$ ), tautomerization of enol ( $r_T$ ), and hydrogenation of 2-hexanone ( $r_3$ ) as functions of concentration of DMF ( $C_{DMF}$ ), concentration of 2-hexanone ( $C_{HEX}$ ) and partial pressure of  $H_2$  ( $p_{H_2}$ ) are derived as follows:

*Surface coverage:*

$$\begin{aligned}\theta_{DMF} &= K_1 C_{DMF} \theta^* \\ \theta_{HEX} &= K_6 C_{HEX} \theta^* \\ \theta_H &= \sqrt{K_2 H_{H_2} P_{H_2}} \theta_H^*\end{aligned}$$

*Site balance for  $\theta^*$  and  $\theta_H^*$ :*

$$\begin{aligned}\theta_{DMF} + \theta_{HEX} + \theta^* &= 1 \\ \theta_H + \theta_H^* &= 1 \\ \theta^* &= \frac{1}{1 + K_1 C_{DMF} + K_6 C_{HEX}} \\ \theta_H^* &= \frac{1}{1 + \sqrt{K_2 H_{H_2} P_{H_2}}}\end{aligned}$$

*Rate of ring opening:*

$$\begin{aligned}r_{RO} &= k_{4a} \theta_{DMF} \theta_H \\ k_{RO} &= k_{4a} \\ r_{RO} &= \frac{k_{RO} K_1 C_{DMF} \sqrt{K_2 H_{H_2} P_{H_2}}}{(1 + K_1 C_{DMF} + K_6 C_{HEX})(1 + \sqrt{K_2 H_{H_2} P_{H_2}})}\end{aligned}$$

*Rate of ring saturation:*

$$\begin{aligned}r_{RS} &= k_{3d} \theta_{I3c} \theta_H \\ \theta_{I3c} &= \frac{K_{3a} K_{3b} K_{3c} \theta_{DMF} \theta_H^3}{\theta_H^{*3}} \\ k_{RS} &= k_{3d} K_{3a} K_{3b} K_{3c} \theta_{DMF} \\ r_{RS} &= \frac{k_{RS} K_1 C_{DMF} (\sqrt{K_2 H_{H_2} P_{H_2}})^4}{(1 + K_1 C_{DMF} + K_6 C_{HEX})(1 + \sqrt{K_2 H_{H_2} P_{H_2}})}\end{aligned}$$

*After ring opening, tautomerization ( $r_T$ ) and hydrogenation ( $r_1$ ) of the enol species ( $I_{4b}^*$ )*

$$\begin{aligned}r_T &= k_T \theta_{I4b} \\ r_1 = r_{4d} &= k_{4d} \theta_{I4c} \theta_H\end{aligned}$$

Applying PSSH on the following species adsorbed on the surface:  $I_{4a}^*$ ,  $I_{4b}^*$ ,  $I_{4c}^*$ ,

$$\frac{d(\theta_{I4c})}{dt} = 0 = r_{4c} - r_{4d}$$

$$\begin{aligned}
r_{4c} &= k_{4c}\theta_{I4b}\theta_H \\
\theta_{I4c} &= \frac{k_{4c}}{k_{4d}}\theta_{I4b} \\
r_1 = r_{4d} &= k_{4c}\theta_{I4b}\theta_H \\
k_1 &= k_{4c}
\end{aligned}$$

$$\begin{aligned}
\frac{d(\theta_{I4a})}{dt} &= 0 = r_{RO} - r_{4b} \\
r_{4b} = r_{RO} &= k_{RO}\theta_{DMF}\theta_H
\end{aligned}$$

$$\begin{aligned}
\frac{d(\theta_{I4b})}{dt} &= 0 = r_{4b} - r_{4c} - r_T \\
0 &= k_{RO}\theta_{DMF}\theta_H - k_{4c}\theta_{I4b}\theta_H - k_T\theta_{I4b}
\end{aligned}$$

$$\begin{aligned}
\theta_{I4b} &= \frac{k_{RO}\theta_{DMF}\theta_H}{k_{4c}\theta_H + k_T} \\
\theta_{I4b} &= \frac{k_{RO}\theta_{DMF}\theta_H}{k_1\theta_H + k_T}
\end{aligned}$$

$$r_1 = k_1 \frac{k_{RO}\theta_{DMF}\theta_H^2}{k_1\theta_H + k_T} = \frac{k_1 k_{RO} K_1 C_{DMF} (\sqrt{K_2 H_{H2} p_{H2}})^2}{(1 + K_1 C_{DMF} + K_6 C_{HEX})(1 + \sqrt{K_2 H_{H2} p_{H2}})^2} \frac{1}{k_1 \left( \frac{\sqrt{K_2 H_{H2} p_{H2}}}{1 + \sqrt{K_2 H_{H2} p_{H2}}} \right) + k_T}$$

$$r_T = k_T \frac{k_{RO}\theta_{DMF}\theta_H}{k_1\theta_H + k_T} = \frac{k_T k_{RO} K_1 C_{DMF} (\sqrt{K_2 H_{H2} p_{H2}})}{(1 + K_1 C_{DMF} + K_6 C_{HEX})(1 + \sqrt{K_2 H_{H2} p_{H2}})} \frac{1}{k_1 \left( \frac{\sqrt{K_2 H_{H2} p_{H2}}}{1 + \sqrt{K_2 H_{H2} p_{H2}}} \right) + k_T}$$

Hydrogenation of 2-hexanone ( $r_3$ ) in the DMF system:

$$\begin{aligned}
r_3 = r_{6b} &= k_{6b}\theta_{I6a}\theta_H \\
\theta_{I6a} &= \frac{K_{6a}\theta_{HEX}\theta_H}{\theta_H^*} \\
r_3 &= \frac{k_{6b}K_{6a}\theta_{HEX}\theta_H^2}{\theta_H^*} \\
k_3 &= k_{6b}K_{6a} \\
r_3 &= \frac{k_3 K_6 C_{HEX} (\sqrt{K_2 H_{H2} p_{H2}})^2}{(1 + K_1 C_{DMF} + K_6 C_{HEX} + K_3 C_{DMTHF} + K_7 C_{HXL})(1 + \sqrt{K_2 H_{H2} p_{H2}})}
\end{aligned}$$



### 3.6.5 Kinetic model of 2-hexanone hydrogenation

The hydrogenation of 2-hexanone to form 2-hexanol was studied separately under the same reaction conditions used for the hydrogenation of DMF (0.55MPa H<sub>2</sub>, 1.12M, 40mg Pt/C) for temperatures 333K – 353K for up to 2h. Under these reaction conditions, the Gibbs free energy for the formation of 2-hexanol is favorable by ~9 kcal/mol. At higher temperatures, the formation of alcohol becomes less favorable until 2-hexanone becomes the thermodynamically preferred product (~450K). Therefore, 2-hexanol fed into a reactor under certain reaction conditions, can completely dehydrogenated to 2-hexanone in the presence of H<sub>2</sub> over Pt nanoparticles at (623K, 1 atm p<sub>H2</sub>) [10]. However for the conditions of this study, when 2-hexanol was used as the substrate under hydrogenation conditions, the yield of 2-hexanone was less than < 0.3% yield after 2 h of reaction. Therefore, for our system, the reverse reaction of dehydrogenation of 2-hexanol to 2-hexanone is minimal and 2-hexanone hydrogenation can be considered as irreversible.

To account for the observed zero<sup>th</sup> order and ~1.2 order dependence of the initial rate of 2-hexanone hydrogenation on the 2-hexanone concentration and hydrogen partial pressure, respectively, the second addition of hydrogen was assumed to be the rate-limiting step and the organic species and hydrogen to be adsorbed noncompetitively on the catalyst surface. The following rate expression was developed to describe the conversion of 2-hexanone to 2-hexanol:

$$r_3 = \frac{k_3 K_6 C_{HEX} (\sqrt{K_2 H_{H_2} p_{H_2}})^2}{(1 + K_6 C_{HEX} + K_7 C_{HXL})(1 + \sqrt{K_2 H_{H_2} p_{H_2}})}$$

In this expression, k<sub>3</sub> is the reaction rate constant associated with the hydrogenation of C=O, K<sub>6</sub> and K<sub>7</sub> are adsorption equilibrium constants for 2-hexanone and 2-hexanol, respectively, K<sub>2</sub> is the equilibrium constant for dissociative adsorption of H<sub>2</sub>, and H<sub>H2</sub> is the Henry's constant relating the concentration of dissolved H<sub>2</sub> in the liquid phase to the partial pressure of H<sub>2</sub>, p<sub>H2</sub>. Although the initial rate of 2-hexanone hydrogenation is high, it slows down as the reaction proceeds due to product inhibition by 2-hexanol.

The differential equations describing the concentrations of 2-hexanone and 2-hexanol, C<sub>HEX</sub> and C<sub>HXL</sub>, in the reactor are

$$\frac{V}{W} \frac{dC_{HEX}}{dt} = -r_3$$

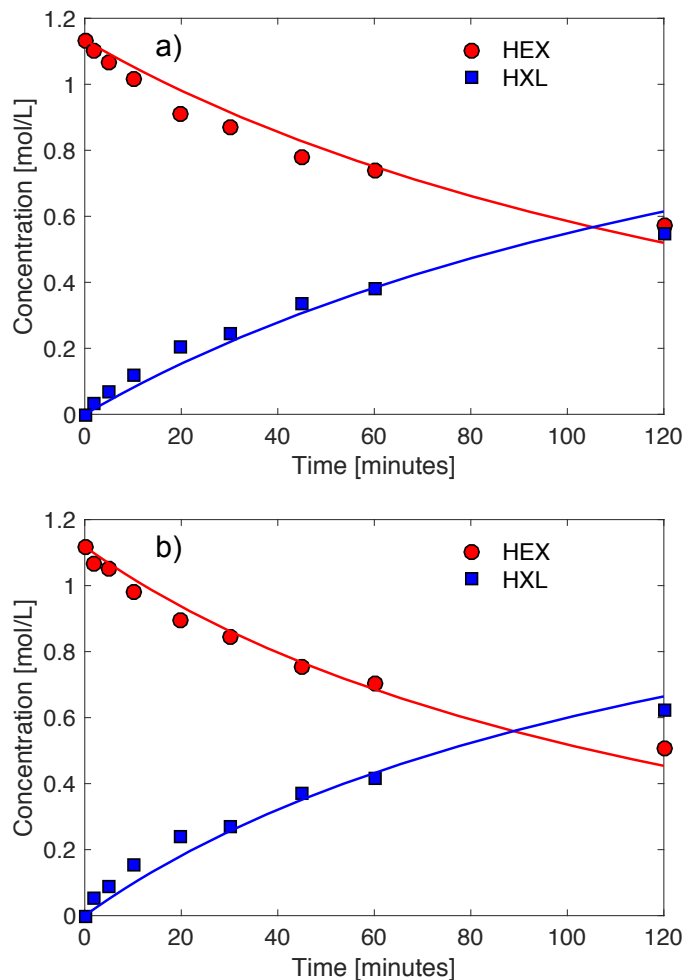
$$\frac{V}{W} \frac{dC_{HXL}}{dt} = r_3$$

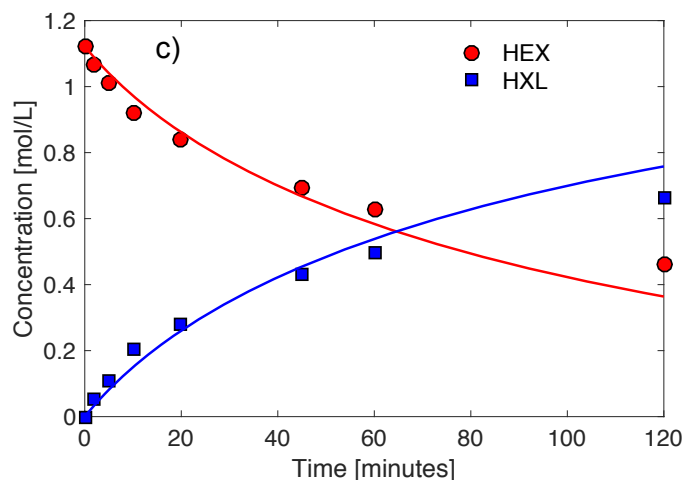
with the following initial conditions:

$$t = 0; \quad C_{HEX} = 1.12M, C_{HXL} = 0$$

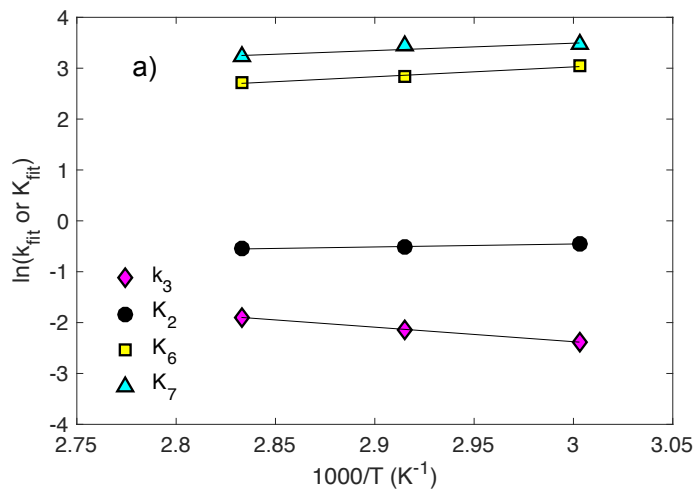
In the equations above, V is the solution volume in the reactor and W is the weight of catalyst.

Values for the rate and equilibrium constants appearing in the expression for,  $r_3$ , above were determined by solving the differential equation and fitting parameters contained in them to a set of time course data obtained for a particular reaction temperature. Details of the parameter estimation method are described in the main text. The parameters evaluated at different temperatures (333 K – 353 K) were plotted versus  $1/T$  and these plots were then used to obtain activation (or adsorption) energies and pre-exponential factors. These plots are shown in Figure S. 3.4 and the parameters determined from them are summarized in Table 3.7 of the main text.



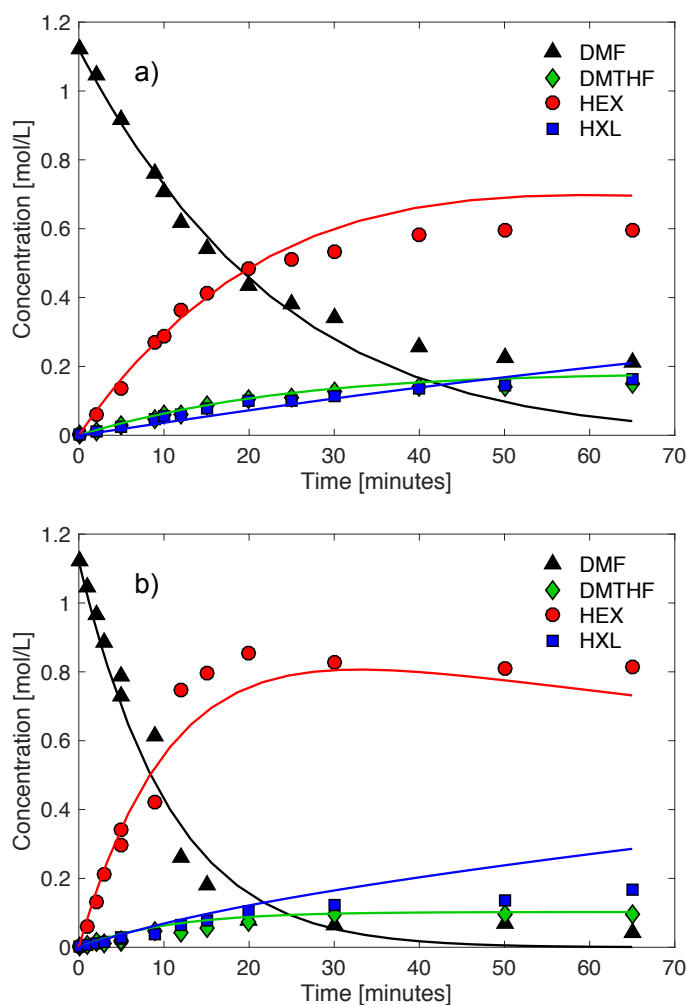


**Figure S. 3.3** Comparison of experimental and fitted concentration profiles for 2-hexanone hydrogenation to 2-hexanol over 5% Pt/C at temperatures a) 333K, b) 343K, and c) 353K. Reactions performed using 0.2 mol% Pt/C,  $p_{H_2} = 0.55$  MPa, 1.12 M 2-hexanone in nonane, 750 rpm. Model fit: solid lines. Measurement: symbols.

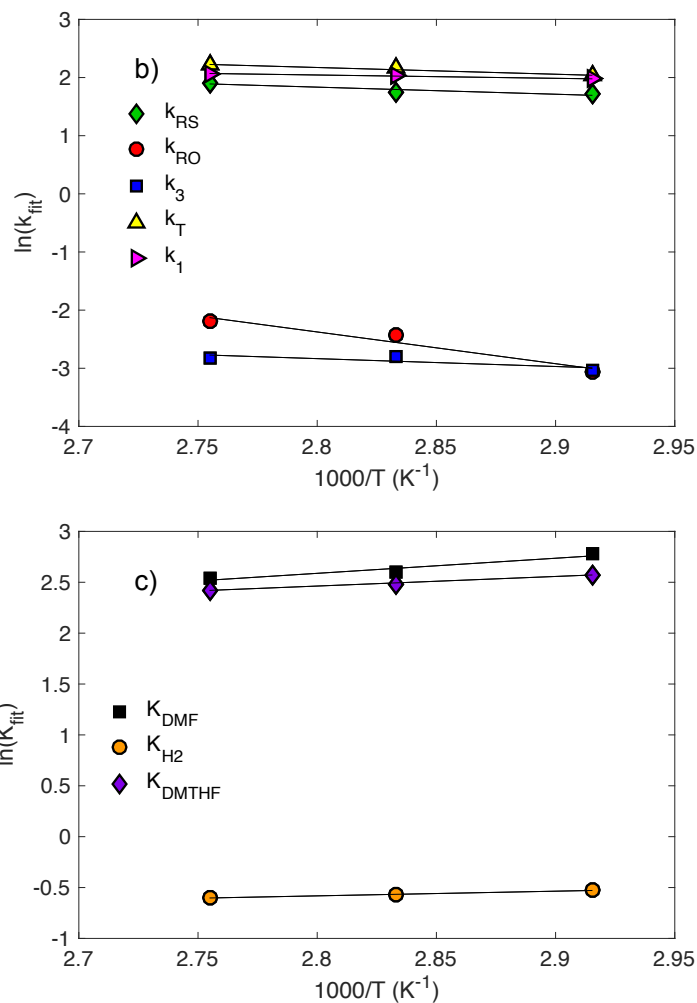


**Figure S. 3.4** Arrhenius plot of the estimated rate parameters fitted through the proposed kinetic model for 2-hexanone hydrogenation to form 2-hexanol at temperatures (333K – 353K).

### 3.6.6 Results of parameter fitting to proposed kinetic model for DMF hydrogenation

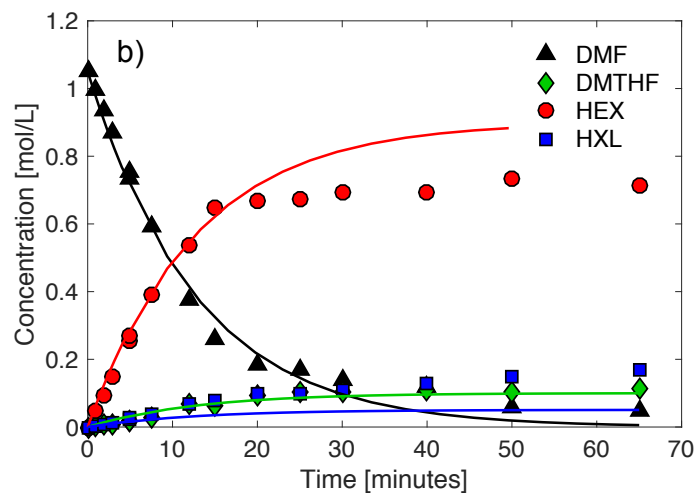
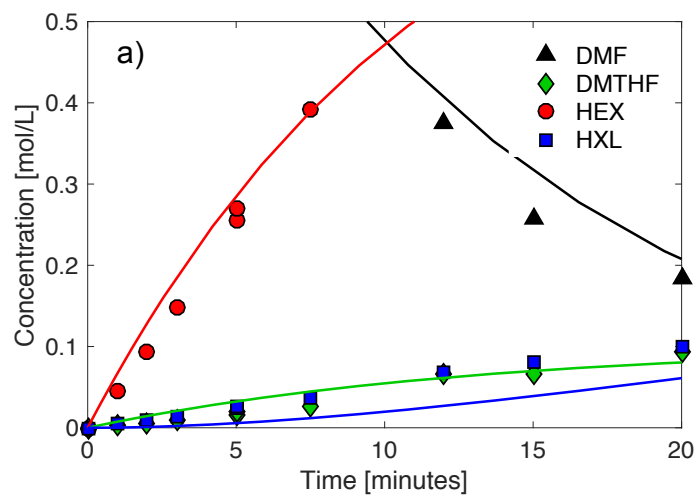


**Figure S. 3.5 Comparison of experimental and fitted concentration profiles for all observed products of DMF hydrogenation over 5% Pt/C at temperatures a) 343K and b) 363K.** Reactions performed using 0.2 mol% Pt/C,  $p_{H_2} = 0.55$  MPa, 1.04 M DMF in nonane, 750 rpm. Model fit: solid lines. Measurement: symbols.



**Figure S. 3.6 Arrhenius plots of estimated rate parameters fitted through the proposed kinetic model at temperatures (343K – 363K) with temperature.**

a) Rate coefficients of all kinetically relevant reactions in the network. b) Equilibrium constants for the adsorption of DMF, HEX, and dissociative adsorption of H<sub>2</sub>.



**Figure S. 3.7 Modeling the DMF hydrogenation network assuming production of 2-hexanol (HXL) occurs exclusively via a) secondary hydrogenation of 2-hexanone (HEX) and b) hydrogenation of the enol intermediate.**

## 4 Hydrogenation and Hydrogenolysis of BMFM over Noble Metal Catalysts

### 4.1 Introduction

Strategies for converting the lignocellulosic biomass to transportation fuels continue to be a subject of considerable interest. One of the approaches examined begins with the hydrolysis of the cellulosic and hemicellulosic portions of biomass to release the constituent sugars, principally glucose and xylose, followed by the dehydration of these six and five carbon sugars to produce 5-hydroxymethylfurfural (HMF) and furfural (FUR) [79]. These furanic products can be converted to a variety of higher carbon value compounds (C8-C16) containing aromatic furan rings through acid catalyzed hydroalkylation [10–12], or base catalyzed condensation [8,9]. The resulting products have the appropriate carbon numbers for jet (C8 – C16) and diesel (C9 – C21) [40], but cannot be used directly without hydrogenation and hydrodeoxygenation. To be suitable for jet fuel, all oxygen functionality must be removed from the final products in order to raise the energy density, and to be suitable for diesel fuel, the cetane number of the final products must be increased to at least 40 in the US and 50 in Europe [15–17].

Table 4.1 illustrates for compounds of interest in this study how hydrotreatment to remove oxygen and unsaturation affect the cetane number of the final product [17].

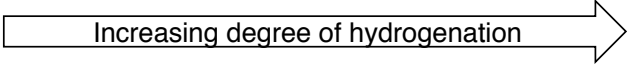
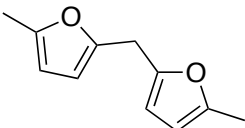
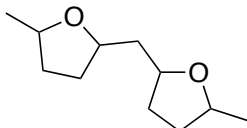
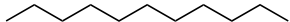
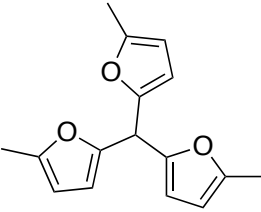
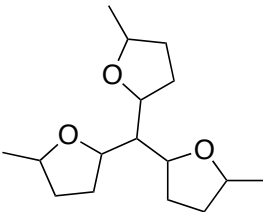
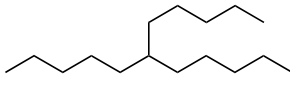
A number of liquid-phase studies of the hydrogenation and hydrodeoxygenation (HDO) of compounds containing furan rings have been reported. Many of these investigations have applied harsh reaction conditions (573 K – 673 K, 7-20 MPa H<sub>2</sub>) and employed noble metal catalysts sometimes supported on acidic oxide [4,6,10,24] in order to drive reaction towards complete deoxygenation and the production of hydrocarbons. However, because of the high temperatures used, this end is accompanied by noticeable production of low molecular weight products due to cracking and hydrogenolysis, independent of the choice of metal. Moreover, studies conducted under these harsh conditions do not allow the influence of the metal used on the reaction network to be clearly defined. Ring opening and hydrodeoxygenation of the furan moieties during hydrotreatment of a C<sub>16</sub> hydroalkylation product, formed by reaction of 2-MF and 5-methylfurfural (Table 4.1) has been proposed to proceed over Pt and Pd at 623-673 K through tetrahydrofuran containing intermediates [10,11]. Partial hydrogenation of the starting C<sub>16</sub> compound under milder conditions, 373 K – 413 K, 1.4 - 2.1 MPa H<sub>2</sub> over carbon-supported Pt, Pd, Ru, and Rh resulted in varying degrees of ring saturation and C-O cleavage [17]. It was proposed that the alcohol functional groups were formed after prolonged retention of the tetrahydrofuran moieties on the catalyst surface. Finally, it has been speculated that under HDO conditions (623 K – 643 K, 1 – 6 MPa H<sub>2</sub>), transformation of furanyl condensates into linear di-ketones occurs via hydrolysis of the furan ring by the water generated during HDO [24,25]. However, linear di-ketones were not observed during such HDO reactions unless they were performed in aqueous systems [26,27].

Recent studies of 2,5-dimethylfuran (DMF) hydrogenation have shown that cleavage of C-O bonds can be avoided by using milder reactions conditions, but in this case the extent to which DMF undergoes ring saturation versus ring opening depends on the choice of metal used to promote the reactions [20–22,66]. We have shown that the hydrogenation and hydrogenolysis of DMF under mild conditions (363 K, 0.69 MPa H<sub>2</sub>) results in ring saturation exclusively over Pd/C and in a high fraction of ring-opened products (86%) when the reaction is carried out over

Pt/C [80]. The mechanism by ring opening and ring saturation of the furan occurs involves a highly active enol intermediate that can lead to either a ketone via tautomerization or an alcohol production via hydrogenation of the C=C bond. Enol intermediates have also been proposed to explain the formation of diols observed after ring opening of 4-(2-furyl)-3-buten-2-one over various supported Pt catalysts at 473 K, 5 MPa H<sub>2</sub> [81]. While the authors propose a detailed reaction scheme to explain the formation of various ring-opened, partially-hydrogenated, oxygenated intermediate that lead to linear alcohols and octane, they did not attempt to describe the observed reaction kinetics based on this scheme.

The present study was undertaken with the aim of understanding how and why the choice of carbon-supported metal affects the rate and distribution of products formed upon hydrogenation of a C<sub>11</sub> compound containing two adjacent furan rings, bis(5-methylfuran-2-yl)methane, BMFM (Table 4.1). This compound, as well as a three ring analog, C<sub>16</sub>, described earlier can be derived from acid catalyzed condensation of 2-MF at high yields (80-97%) and are interesting intermediates for the production of biomass-derived components for diesel [17,82]. Our studies show that as in the case of DMF hydrogenation, the nature of the metal used for the strongly catalyst dictates its activity and product selectivity. Direct C-O hydrogenolysis is observed for all catalysts tested - Pd/C, Ru/C, and Pt/C. Based on the products formed during the course of the reaction over each of these catalysts, it was possible to identify major routes by which BMFM reacts. These schemes include a complex network of competitive and non-competitive pathways resulting in products of varying degree of hydrogenations. In this study, we address the influence of the noble metal identity, reaction temperature, and hydrogen partial pressure on the kinetics and the distribution of products formed. The results of this investigation provide useful insights for achieving selectivity to furan ring saturation relative to furan ring hydrogenolysis and suggest means for carrying out HDO at mild temperatures and H<sub>2</sub> pressures.

**Table 4.1** Predicted and experimentally determined derived cetane numbers (DCN) for furan condensation products at varying degrees of hydrogenation.

			
	Furan Condensation Product	Selective Hydrogenation	Full Hydrodeoxygenation
<b>Compound discussed in this study</b>			 C <sub>11</sub>
DCN	12.5 <sup>a</sup>	60.3 <sup>a</sup>	83 <sup>b</sup>
<b>Compound explored in previous studies [10-12]</b>			 C <sub>16</sub>
DCN	22.3 <sup>c</sup>	59.8 <sup>c</sup>	45 <sup>b</sup>

<sup>a</sup> DCN values predicted by Mack and co-workers using artificial neural network [28]

<sup>b</sup> Value determined from Compendium of Experimental Cetane Numbers [29]



<sup>c</sup> DCN values determined experimentally [17]

## 4.2 Experimental

### 4.2.1 Materials

Pd/Carbon (1wt%, 5wt%), Pt/Carbon (5wt%), Ru/Carbon (5wt%), and Ru/Carbon (5wt%) were purchased from Sigma-Aldrich. All catalysts were sieved to < 25  $\mu\text{m}$  and then reduced in flowing  $\text{H}_2$  (100  $\text{cm}^3/\text{min}$ ) at 473K for 0.5 h prior to reaction in order to remove residual moisture and fully reduce the metal.

2-undecanone and 2,5-dimethylfuran were purchased from Sigma-Aldrich. Bis(5-methylfuran-2-yl)methane (BMFM), **1**, was synthesized using a procedure adapted from the literature [12,82]. A mixture of 2-methylfuran (Sigma-Aldrich) and dimethoxymethane (Sigma Aldrich) in (5:1 molar ratio) and 2.5mol% (relative to loading of dimethoxymethane) of Amberlyst-15 (Sigma-Aldrich) were added to a 1L Parr reactor. The reactor was purged with  $\text{N}_2$  (Praxair 99.999%) 3x prior to reaction, heated to 338 K, and then held at 338 K for 3.5 h after which the contents were quickly cooled to room temperature by placing a cooling coil into the reactor contents. The spent catalyst was filtered from the reaction mixture and washed with ethyl acetate. The filtrate was passed through a column filter containing layered beds of silica and sodium bicarbonate ( $\text{NaHCO}_3$ ) to remove solid particles and to neutralize any acid remaining. Additional ethyl acetate was added to aid in phase separation and transfer of the product. The product solution was further washed with a solution of 10 mol%  $\text{NaHCO}_3$  and then extracted 2x with a saturated  $\text{NaCl}$  solution. The final solution was dried over anhydrous solid  $\text{Na}_2\text{SO}_4$  before excess solvents and light starting materials were removed by rotary evaporation. The resulting material was purified by vacuum distillation at 370-375 K and a pressure of 2-3 torr to form a light-yellow liquid at room temperature, and was stored at 273K prior to use.

The fully saturated analog of BMFM, bis(5-methyltetrahydrofuran-2-yl)methane (BMTHFM), **1b**, was obtained by hydrogenation of BMFM at conditions 363 K and 2 MPa for 3 h over 5% Pd/C. At the end of reaction, no BMFM was observed and only trace amounts of ring-opened products were present (<2%). Solid catalyst particles were removed by filtration and the mixture of isomers of **1b** was purified by vacuum distillation at 363 K and 2-3 torr. Saturated, single ring-opened species, **1c**, was obtained by hydrogenation of **1**, BMFM at optimized conditions (473K, 1.1 MPa) in 3h over 5% Pd/C. Solid catalyst particles were removed by filtration and the product solution was concentrated to a mixture of products **1b** and **1c** via rotary evaporation. **1c**, 6-(5-methyltetrahydrofuran-2-yl)hexan-2-ol, was isolated from the mixture by  $\text{SiO}_2$  column chromatography, using 1:3 ethyl acetate:hexane solution. Purified **1**, **1b**, and **1c** were characterized by NMR spectroscopy, FTIR spectroscopy, and mass spectrometry (See 0 Appendix). These compounds were used to generate response factors for product quantification by gas chromatography (see below).

### 4.2.2 Catalyst characterization

Metal dispersion was measured by CO chemisorption at 313 K using a Micromeritics AutoChem 2920 Pulse Chemisorption System, assuming CO atom to surface metal atom stoichiometry of 1.0 for Pt and 2.0 for Pd based catalysts [68,83]. Prior to CO exposure, the catalyst was pretreated in flowing  $\text{H}_2$  (10% in He) at 50 mL/min for 1h at 523K. An average

particle diameter was determined for all supported metals based on the measured dispersion of the metal.

Temperature-programmed reduction of the supported metal catalyst was also performed to determine the presence of hydride species in the catalyst. TPR studies used ~30-150 mg of material (depending on metal loading) after flushing the sample in Ar at room temperature for 10 min, 10% H<sub>2</sub>/Ar was passed over the sample while ramping the sample temperature 5 K/min from 313K – 873 K.

#### 4.2.3 Catalytic hydrogenation

Semi-batch hydrogenations of BMFM and other substrates were conducted in a 100 mL Parr Series 4590 Bench Top Micro Reactor equipped with a sampling dip tube, thermocouple, and an external gas burette containing H<sub>2</sub> (99.99% Praxair). A regulator located at the base of the gas burette maintained the pressure within the reactor at the desired level. For each reaction, the reactor was loaded initially with a solution containing solid catalyst, substrate, octane (solvent), and dodecane as an internal standard. Reactions were operated at pressures of 1.0 MPa to 2.0 MPa H<sub>2</sub> and temperatures ranging from 393 K to 453 K. Standard reaction conditions were 1.1 MPa H<sub>2</sub>, 433 K, 2.8 mmol of substrate and 1 mmol dodecane (as an internal standard) in octane, metal catalyst (0.2 – 0.6 mol% of substrate loaded) for a total volume of 43 mL.

Prior to the addition of H<sub>2</sub>, the reactor was tested for leaks, purged with N<sub>2</sub> three times, and heated to reaction temperature. H<sub>2</sub> was introduced directly into the reacting solution via the dip-tube. Analysis of the reactor contents showed that no substrate conversion occurred prior to the addition of H<sub>2</sub>. On-line sampling of the reacting solution was achieved through the dip-tube, driven by the pressure difference between the reactor contents and atmosphere. Each sample passed through a condenser and was collected in an Eppendorf tube (0.4mL). The catalyst contained in the sample was separated from the reaction mixture by centrifugation, and the residual liquid was diluted with ethyl acetate to reach a concentration suitable for quantification by GC/MS. Carbon balances for all experimental measurements were within 93-99%.

#### 4.2.4 Product analysis

Quantitative analysis of products was performed using a Varian CP-3800 gas chromatograph (GC) equipped with a flame ionization detector (FID) coupled to a Varian 320-MS mass spectrometer. Product compounds were separated using a FactorFour capillary column (VF-5 ms, 30 m length, 0.25 mm diameter) coated with a 0.25 mm thick stationary phase (5% phenyl and 95% dimethylpolysiloxane) with hydrogen as a carrier gas. Dodecane was present in all samples as an internal standard to normalize variability in sample size delivery and detector signal strength. The characteristic retention times and the FID response factors using dodecane as internal standard for individual compounds were determined by calibration using pure compounds.

Initial rates of BMFM conversion were determined using the slope of the linear portion of the conversion profile, for conversions < 30%. Reactant conversion and product selectivity were defined as follows:

$$\text{Conversion (mol\%)} = \frac{\text{moles of BMFM reacted}}{\text{moles of initial substrate}} \times 100\%$$

$$\text{Selectivity}_{\text{species } i} \text{ (mol\%)} = \frac{\text{moles of species } i}{\text{moles of BMFM reacted}} \times 100\%$$

The number of active metal centers per catalyst mass determined by CO chemisorption was taken to be a measure of the number of catalytically active site, and accordingly, the turnover frequency (TOF) was calculated as:

$$\text{TOF} = \frac{\text{Moles of BMFM reacted}}{(\text{Moles of active centers})(\text{second})}$$

## 4.3 Results

### 4.3.1 Hydrogenation of BMFM among various metals

Substrate loading, catalyst loading, and reaction conditions were chosen to avoid transport limitations during the liquid phase hydrogenation of BMFM. Systematic studies were performed to verify that the measured rate of BMFM hydrogenation was not affected by the effects of external or internal mass transfer (See SI 4.6.2). Most importantly, the Madon-Boudart test [84] was applied to verify the absence of intraparticle heat and mass transfer effects during the hydrogenation of BMFM over Pd/C. Turnover frequencies were compared for Pd/C with Pd loadings of 1 wt% and 5 wt% but similar metal dispersions (Pd dispersion 47-50%). As seen in Table 4.2 and Figure S. 4.2, nearly identical TOFs were observed for the two loadings of Pd, indicating that transport effects do not affect the measured rates. Since other hydrogenation catalysts were significantly less active than Pd/C, we can safely conclude that neither external or internal mass transfer affected the measured rates of reaction over this catalyst.

**Table 4.2. Comparison of turnover frequencies and catalyst properties of the 1wt% and 5wt% loading of Pd catalyst for the Madon-Boudart test.**

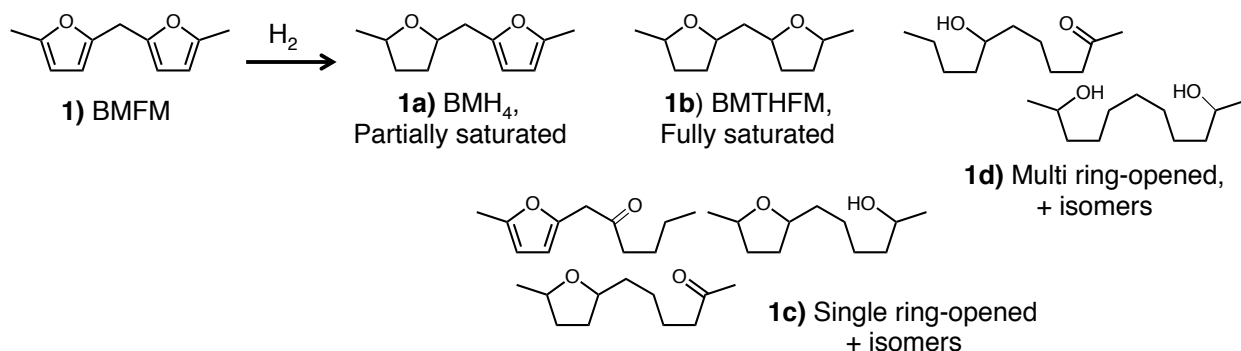
Reactions using 0.2mol% Pd/C at 433K, 1.1 MPa H<sub>2</sub>, 2.8mmol in octane

	1wt% Pd/C	5wt% Pd/C
<b>Dp (nm)</b>	2.2	2.4
<b>% Metal Dispersion</b>	47	50
<b>mmol Pd/g<sup>1</sup></b>	0.05	0.22
<b>BMFM TOF (s<sup>-1</sup>)</b>	467	461

<sup>1</sup> active sites per mass of catalyst quantified by CO Chemisorption based on metal dispersion.

The products observed during the course of BMFM hydrogenation are grouped into the following categories based on the degree of ring saturation and ring opening (**1a** – **1d**) described in Scheme 4.1. Comparison of the activity of Pd/C, Pt/C, and Ru/C for the hydrogenation of BMFM and the distribution of product observed at 30% conversion are shown in Table 4.3. Pd/C is an order of magnitude more active than Pt/C and Ru/C and hydrogenates the aromatic rings of BMFM preferentially to products **1a** and **1b**. In order to monitor the course of reaction at similar time scales to those used for Pd/C, larger amounts of Pt/C and Ru/C per unit volume of solvent

were used (0.6mol% to BMFM). Temporal profiles of reactant and product concentration for reactions over Pd/C, Pt/C, and Ru/C are shown in Figure 4.1. Identification of all product species (18+) formed over time can be found in SI 4.6.3.



**Scheme 4.1** Products of BMFM hydrogenation over noble metals.

**Table 4.3. Turnover frequency (TOF) for BMFM consumption and product selectivity for carbon-supported noble metals.**

TOFs normalized by the total number of surface metal atoms. 0.2 – 0.6 mol% metal loading, 433 K, 1.1 MPa H<sub>2</sub>, 2.8mmol in octane

Hydrogenation Catalyst	TOF (s <sup>-1</sup> )	% Selectivity <sup>a</sup>				
		BMH <sub>4</sub> (1a)	BMTHFM (1b)	Single R.O. (1c)	Multi R.O. (1c)	Others <sup>b</sup>
Pd/C	7.8	75.3	21.0	8.6	0.0	0.2
Pt/C <sup>c</sup>	0.3	32.0	7.0	45.0	15.6	0.4
Ru/C <sup>c</sup>	0.6	68.4	10.1	15.2	1.09	5.1

<sup>a</sup> Selectivity of the products observed at 30% conversion of BMFM

<sup>b</sup> Heavy oligomer products that eluted in GC at column temperatures above 573 K

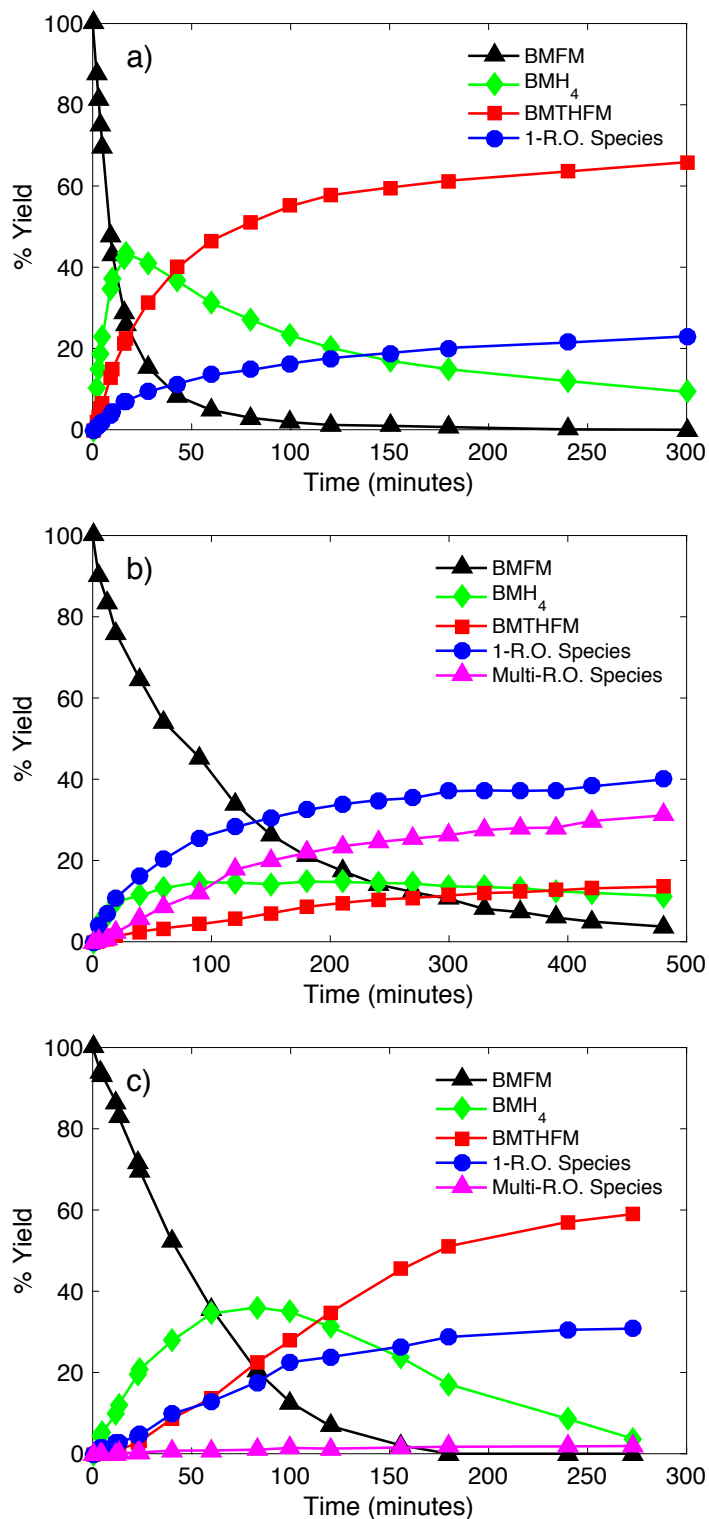
<sup>c</sup> 0.6mol% metal loading used since the reaction rates were significantly slower than Pd/C

Partially saturated intermediate, **1a**, BMH<sub>4</sub> was the major product observed during the initial conversion of BMFM over each catalyst. The slower hydrogenation of this species compared to BMFM can be attributed in part to the fact that the planar and highly aromatic BMFM adsorbs more strongly than BMH<sub>4</sub>, which cannot adsorb parallel to surface, but instead adsorbs upright via the oxygen atom [65,76]. From Figure 4.1(a), we see that three products, **1a**, **1b**, and **1c**, are produced in parallel during initial conversion of BMFM over Pd/C. Although the fully saturated product, **1b**, can be formed after additional hydrogenation of **1a**, we propose that there is an additional direct hydrogenation pathway to form BMTHFM from BMFM involving palladium hydride species (R<sub>RS1b</sub>). This pathway does not appear to be present for Pt and Ru catalysts, which do not form hydrides. Ringing opening of BMFM to form **1c** occurs more slowly than the ring saturation reactions that occur in parallel.

By contrast, direct ring opening of BMFM over Pt/C occurs more rapidly than the competing reaction to form BMH<sub>4</sub>, resulting in single- (**1c**) and multi-ring opened species (**1d**) as the major product (> 60% selectivity at 30% conversion) over the fully saturated **1b** (Table 4.3). The relatively slow rate of ring saturation relative to ring opening allows for the formation of **1d**. Product **1d** result from C-O bond cleavage of the remaining aromatic ring in **1c**. Product **1b** is

only formed from additional ring saturation reaction of BMH<sub>4</sub>, which exists in the reaction solution in moderate proportions (< 15% yield).

In order to confirm that C-O hydrogenolysis to form products **1c** and **1d** occurs directly from aromatic furan species, we isolated and purified the product, **1b**, BMTHFM, and used it as a substrate for hydrogenation studies over both Pt/C and Pd/C under the same reaction conditions used for BMFM hydrogenation (T = 433 K, P<sub>H<sub>2</sub></sub> = 1.1 MPa). Only trace amounts of ring-opened products were observed (< 0.5% yield) after 5 h of reaction clearly indicating that in contrast to what has been assumed previously [17,18,20], all C-O bond hydrogenolysis of furanyl compounds over both Pt/C and Pd/C occurs directly from the aromatic furan ring. The lack of reactivity of **1b** compared to BMFM is attributed to the lack of  $\pi$  orbitals in **1b**, which results in weaker binding of tetrahydrofuran than furan to the metal surface [75] and a different adsorption geometries between tetrahydrofuran and furan on Pd and Pt surfaces[65].



**Figure 4.1.** Evolution of products during BFM hydrogenation a) Pd/C, b) Pt/C, c) Ru/C catalysts at 0.2 – 0.6 mol% metal loading, 433 K, 1.1 MPa H<sub>2</sub>, 2.8mmol in octane.

#### 4.3.2 Effects of reactant concentration on the kinetic network of Pd/C and Pt/C

Reaction orders in BMFM and hydrogen for the primary reaction pathways over Pd and Pt catalysts were determined from initial rate studies. The reaction pathways considered are the formation of BMH<sub>4</sub> through ring saturation of BMFM, R<sub>RS1</sub>, the formation of BMTHFM through direct hydrogenation of BMFM, R<sub>RS1b</sub>, and the formation of products **1c** and **1d** through ring opening of BMFM (R<sub>RO1</sub>). Since Pt does not form a hydride, R<sub>RS1b</sub> is not relevant for this catalyst. The kinetics of BMFM hydrogenation were determined at 433 K for substrate concentrations ranging from 47 mM to 82 mM and H<sub>2</sub> pressures ranging from 1.0 MPa to 1.4 MPa. As observed previously for DMF hydrogenation [80] and observed by other groups [70], the rate of BMFM hydrogenation was zero order with respect to substrate concentration (see Figure S. 4.4).

The initial rates of BMFM hydrogenation and the initial rates of formation of all products increased with increasing H<sub>2</sub> concentration in the liquid (1.0-1.4MPa H<sub>2</sub>). For hydrogenation over Pd, a first order dependence on H<sub>2</sub> partial pressure for all reactions was determined from plots of the natural log of reaction rate vs. p<sub>H2</sub> (see Figure S. 4.5), which suggests that addition of the second H atom may be the rate-limiting step for all hydrogenation processes involving BMFM (Table 4.4). Initial-rate studies over Pt/C revealed an approximate first-order dependence on p<sub>H2</sub> for the rate of production of **1a**, R<sub>RS1</sub>, and a 0.65 order dependence on p<sub>H2</sub> for the rate of ring-opening, R<sub>RO1</sub>, to products **1c** and **1d** (See Figure S. 4.5). The difference in dependence on p<sub>H2</sub> between the two competing reactions is reflected in the higher selectivity to C-O bond cleaved products at lower p<sub>H2</sub>.

**Table 4.4.** Initial rate order dependence with respect to p<sub>H2</sub> for the rate of ring saturation (r<sub>BMH4</sub>) and rate of ring opening (r<sub>R.O.</sub>) for Pd/C and Pt/C catalysts.

Reaction at 433 K, 1.0-1.4 MPa H<sub>2</sub>, 2.8mmol in octane

	Over Pd/C	Over Pt/C
R <sub>RS1</sub>	1	1.2
R <sub>RS1b</sub>	0.9	--
R <sub>RO1</sub>	1	0.65

#### 4.3.3 Effects of temperature of the kinetics of BMFM hydrogenation

Initial rates of formation of **1a** (R<sub>RS1</sub>), **1b** (R<sub>RS1b</sub>), and **1c** and **1d** (R<sub>RO1</sub>) over Pd/C and Pt/C were measured at reaction temperatures from 413K to 453 K. Arrhenius plots for these reactions can be found in Figure S. 4.6. For these studies, the H<sub>2</sub> partial pressure was adjusted to account for differences in H<sub>2</sub> solubility and solvent vapor pressure with respect to temperature and a constant hydrogen concentration in solution was maintained in all studies. We compared the selectivity to products **1c** and **1d** as functions of reaction temperature for hydrogenation over Pd/C and Pt/C (Figure S. 4.7). 35% greater selectivity toward ring-opening was achieved during hydrogenation at 453K than at 413K (Table S. 4.2). We determined that for both Pt/C and Pd/C, the activation barrier for cleaving of the aromatic ring of furan is higher than for saturation of the aromatic ring. For both Pd/C and Pt/C, the apparent activation energy, E<sub>app</sub>, for ring saturation was ~20 kJ/mol and E<sub>app</sub> for ring opening was 37-43 kJ/mol (Table 4.5).

**Table 4.5.** Apparent activation energies determined from Arrhenius plots of the initial rates of hydrogenation over Pt/C and Pd/C.

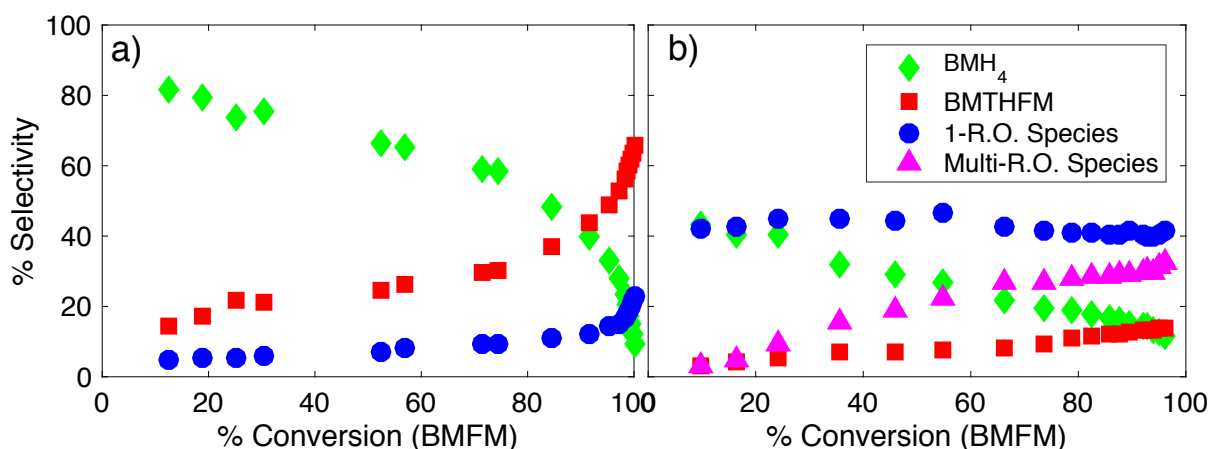
Reaction at 413 – 453 K, 1.1 MPa H<sub>2</sub>, 2.8mmol in octane.

	$E_{app}$ (kJ/mol)	
	Pd/C	Pt/C
$r_{BMH_4}$	20.6	18.0
$r_{BMTHFM}$	14.2	--
$r_{R.O.}$	37	43.0

## 4.4 Discussion

### 4.4.1 Identification of the network for BMFM hydrogenation over Pd/C and Pt/C

Differences in BMFM hydrogenation pathways for Pd/C and Pt/C were identified by monitoring the distribution of products (**1a-1d**) as a function of BMFM conversion. As seen in Figure 4.2, for Pd/C, ring saturation of BMFM to produce **1a** and **1b** occurs initially with high selectivity. Eventual consumption of intermediate **1a** leads to an increase in the selectivity to products **1b** and **1c**. High selectivity to products **1c** as well as **1a** was observed initially over Pt/C because ring opening and ring saturation of the furan ring occur in parallel and at comparable rates. Products **1b** and **1d** results from the consumption of intermediates **1a** and **1c**, respectively.



**Figure 4.2.** Selectivity to products described in Scheme 4.1 as a function of BMFM conversion.

a) Pd/C and b) Pt/C, 0.2 – 0.6 mol% metal loading, 433 K, 1.1 MPa H<sub>2</sub>, 2.8mmol in octane.

We were able to determine the degree of aromaticity in the reaction products (see Scheme 4.1) based on GC column retention times and mass fragmentation patterns. Products containing furan moieties elute earlier than those containing the respective saturated, tetrahydrofuran moieties. The MS fragmentation of aromatic products produce species with  $m/z = 81$ , characteristic of the 2-methylfuran functional group, whereas the fragmentation of products containing saturated rings produce species with  $m/z = 85$ , characteristic of the 2-methyltetrahydrofuran functional group. We have determined from previous studies [80], that Pd/C has a high activity toward ring saturation; therefore majority of the ring-opened species observed (group **1c**) contain fully saturated tetrahydrofuran rings and are secondary products resulting from C-O cleavage the half hydrogenated intermediate, **1a**, BMH<sub>4</sub>. However, in the

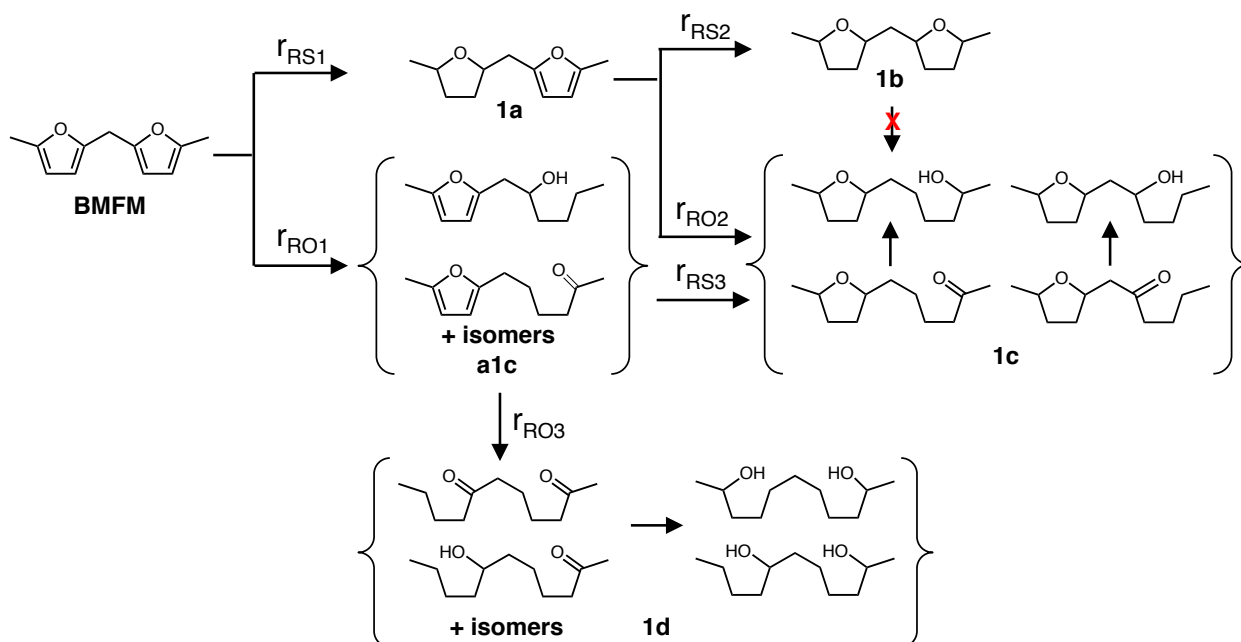


region below 30% conversion of BMFM, there were trace amounts of aromatic ring-opened species, indicating that direct ring opening of BMFM is a relevant pathway over Pd/C but the competitive reaction of ring saturation dominates and BMFM is hydrogenated before appreciable ring opening occurs. No multi-ring opened species were observed over Pd/C catalysts since we have determined that C-O hydrogenolysis only occurs at aromatic C-O bonds and not etheric C-O bonds, such as those in **1c**, under these reaction conditions.

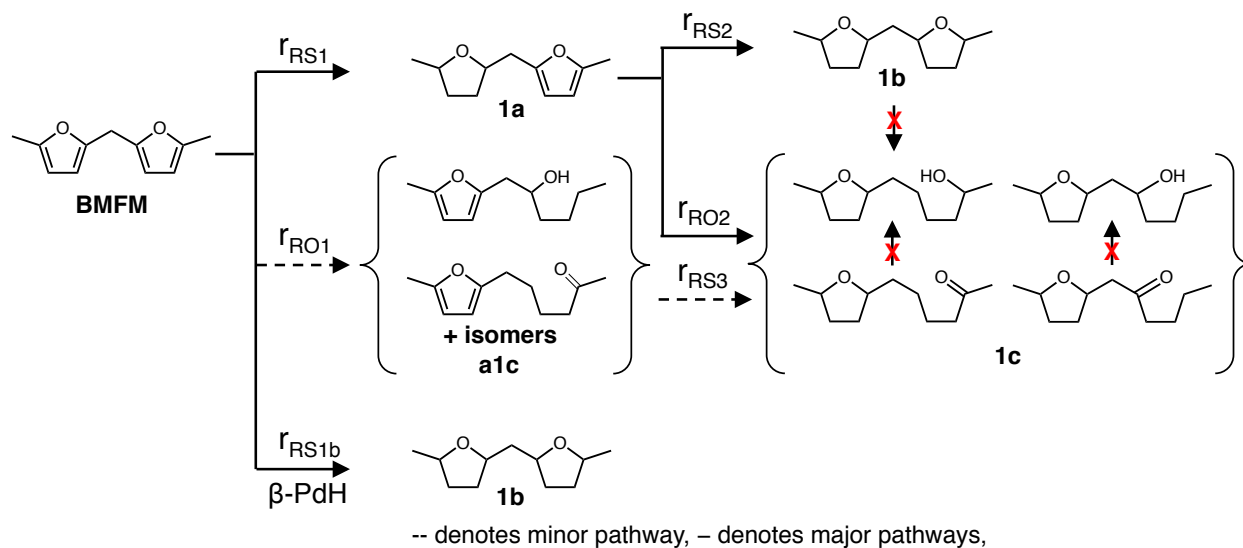
In the case for BMFM hydrogenation over Ru/C and Pt/C, C-O hydrogenolysis was as active as ring saturation, evidenced by significant quantities of aromatic ring opened products (**a1c**) observed during initial conversions. The formation of **1b** from **1a** occurred at a rate slower than the competing ring-opening reactions within the system, leading to less than 14% selectivity to **1b** compared to over 70% selectivity to ring opened products at 100% conversion of BMFM. This finding is similar what we reported previously in our studies DMF hydrogenation over Pt/C under mild conditions [80].

Based on the temporal evolution of products observed during BMFM hydrogenation, we propose the following reaction network for Pt/C and Ru/C (Scheme 4.2) and Pd/C (Scheme 4.3)

For all catalysts, ring saturation (RS) and ring opening (RO) can occur in parallel prior to or after C-O hydrogenolysis of the first aromatic ring, although this is a minor pathway over Pd/C. Furan containing intermediates (**1a** and **1c**) were observed as transient species during the time course studies and were eventually hydrogenated to fully saturated species. C=O containing species were slowly hydrogenated to alcohols or diols over Ru and Pt catalysts at extended reaction times. The formation and consumption of these species as a function of time are presented in detail in SI 4.6.3.



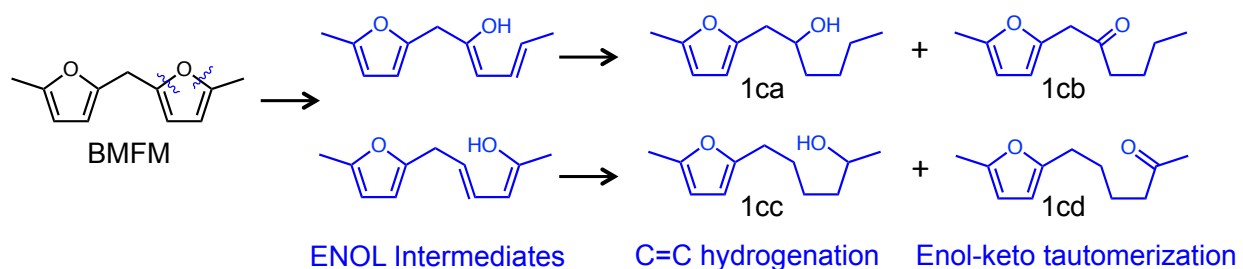
Scheme 4.2 Reaction network of BMFM hydrogenation and hydrogenolysis over Pt and Ru based catalysts.



**Scheme 4.3.** Reaction network of BMFM hydrogenation and hydrogenolysis over Pd based catalysts.

We also considered the sequence of reactions that must occur to form products **1c** and **1d** after initial cleavage of an aromatic ring. For BMFM and BMH<sub>4</sub>, cleavage of the interior or exterior aromatic C-O bond will lead to ring-opened species containing ketone or alcohol functional group at the C<sub>7</sub> (**1ca**, **1cb**) and C<sub>10</sub> (**1cc**, **1cd**) position, respectively (See Scheme 4.4). We propose that ring opening occurs through hydrogenation of the aromatic C-O bond, forming an enol intermediate, which can either undergo tautomerization followed by hydrogenation to form ketones or undergo hydrogenation of the C=C bonds to form alcohols. Evidence for this enol precursor is observed in the simultaneous production of both ketones and alcohol products in single ring-opened and multi-ring opened species (Figure S. 4.3).

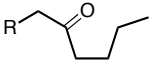
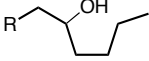
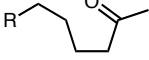
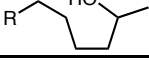
The existence of an enol intermediate is necessary to rationalize the production of **1cd** as the major ring opened product during hydrogenation over Pd/C. We have determined that the rate of C=O hydrogenation, using 2-undecanone as a substrate, is two orders of magnitude slower than the rate of formation of **1cd** from BMFM on Pd/C under identical reaction conditions, indicating that the -OH containing products, such as **1cd**, are not formed sequentially through hydrogenation of C=O.



**Scheme 4.4.** Cleavage of the internal vs. external aromatic C-O bond to form enol intermediates and ring opened species.

It is also noted that Pd/C also exhibits a high selectivity to alcohols after cleavage of the aromatic ring, whereas Pt/C results in greater selectivity to ketones. Of the products in **1c**, the percentage of alcohol species is 85% from ring opening over Pd/C compared to 38% from ring opening over Pt/C (Table 4.6). Within the context of our proposed mechanism after C-O hydrogenolysis, the observed distribution is a consequence of the relative rates of hydrogenation of the C=C and of tautomerization of the enol to the keto tautomer. Pd/C is known to have a higher activity for C=C bond saturation compared to Pt/C or Ru/C [85,86], resulting in a higher selectivity to -OH containing instead of C=O containing species. Tautomerization of enols to their keto analog is also favored with increasing temperature [80], and is reflected in higher ratios of ketones and di-ketones relative to their respective alcohol analogs as reaction temperature was increased from 413 K to 453 K.

**Table 4.6.** Distribution of single ring opened products resulting from hydrogenolysis of interior vs. exterior C-O bond to form either ketones or alcohols obtained at 30% conversion of BMFM.

Products of <b>1c</b> (Single ring opened species)		%Composition of 1-ring opened products (at 30% conversion of BMFM)		
		Pd/C	Ru/C	Pt/C
<b>1ca</b>		4.6	20.9	34.5
<b>1cb</b>		7.8	21.9	20.6
<b>1cc</b>		11.4	28.3	27.6
<b>1cd</b>		77.2	28.9	17.3

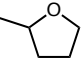
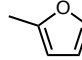
Where R =  or 

Table 4.6 shows that for ring opening over Pd/C, 90% of the products results from cleavage of the interior aromatic C-O bond (**1cc**, **1cd**). Ring opening over Pt/C and Ru/C appear to be unselective, with close to 50:50 distribution of products resulting from C-O hydrogenolysis of interior and exterior C-O bond. The calculated bond dissociation energies of the interior and exterior C-O bond are the same, 72-73 kcal/mol. The preference for cleavage of the interior C-O bond observed over Pd/C catalysts is thought result from differences in the adsorption of BMH<sub>4</sub> compared to BMFM over noble metal catalysts. The major products formed from BMH<sub>4</sub> over Pd/C are partially saturated species, **1c**, whereas these products are formed directly from BMFM over Pt/C and Ru/C. The mode of adsorption of aromatic furans and tetrahydrofurans on metal surfaces is known to be quite different; aromatic compounds adsorb in a flat configuration, whereas saturated species adsorb in an upright position via the oxygen atom [65,76]. Selective cleavage of the interior C-O bond of BMH<sub>4</sub> is observed for all catalysts at conversions of BMFM > 90%, beyond which no additional increases in yields of **1ca** and **1cb** occur but yields of **1cc** and **1cd** increase due to continuing increase in C-O bond cleavage of BMH<sub>4</sub>.

#### 4.4.2 Role of palladium hydride species

The temporal evolution of products (Figure 4.1) and the production distribution (Figure 4.2) observed during the hydrogenation of BMFM over Pd/C shows that the fully saturated species, **1b**, BMTHFM, is present in substantial quantities even at low conversions of BMFM (<30% conversion). In fact, the rate of formation of **1b** observed at low conversions (<30%) is significantly faster than its rate of formation from intermediate **1a**, determined at BMFM conversions > 90% (Table 4.7). In other words, the rate of **1b** formation from intermediate **1a** is inadequate to account for the initial rate of **1b** formation, especially since the concentration of **1a** is low during initial conversion. For BMFM conversions of < 3%, the selectivity to **1b** (BMTHFM) is 10%. Closer examination of the product distribution at low conversions (< 30%, Figure 4.1), suggests that products **1a** and **1b** appear to be formed in parallel.

**Table 4.7.** TOFs for ring saturation to form product **1b** (BMTHFM) at < 30% conversion and at over 90% conversion of BMFM.

	TOF (min <sup>-1</sup> )
R <sub>BMFM</sub> consumed (< 30 % conversion)	467
R <sub>BMTHFM</sub> produced (< 30% conversion)	101
R <sub>BMH4</sub> consumed (> 90% conversion)	6.8
R <sub>BMTHFM</sub> produced (> 90% conversion)	5.1

We propose that direct hydrogenation of BMFM to form **1b**, without desorption of intermediate **1a**, occurs over palladium hydrides (R<sub>RS1b</sub>, Scheme 4.3). In addition to dissociating H<sub>2</sub> on its surface atoms, palladium is known to be able to absorb hydrogen into its bulk, resulting in the formation of  $\beta$ -PdH<sub>x</sub> (palladium hydride), even for highly dispersed Pd particles [87,88]. The existence of such species in Pd/C was confirmed by H<sub>2</sub> TPR. After flushing a sample of Pd/C in Ar at room temperature, 10% H<sub>2</sub>/Ar was passed through sample while ramping the sample temperature at a rate of 5°C/min. A positive peak was observed at 52°C (Figure S. 4.8), indicating the release of hydrogen from the  $\beta$ -PdH<sub>x</sub> [88]. A similar peak was not observed for either Pt/C or Ru/C. As seen in Table 4.3, the TOF for Pd/C is significantly higher than that for Pt/C or Ru/C. Under our hydrogenation conditions, we expect a stable  $\beta$ -PdH phase on Pd/C that contributes to the direct conversion of BMFM to **1b** until complete conversion of BMFM [89]. This is reflected in the first-order rate dependence on hydrogen partial pressure for the formation of **1b** observed in initial-rate studies. No evidence for decomposition of the hydride phase was observed during reaction - no hydrogenated products were detected prior to the addition of H<sub>2</sub>, during of heating reaction mixture to operating temperature.

The role of  $\beta$ -PdH<sub>x</sub> has been investigated for acetylene hydrogenation to ethene and ethane over supported Pd. The hydrogen-rich  $\beta$ -PdH<sub>x</sub> has been observed to be more active than the hydrogen-poor  $\alpha$ -PdH phase for hydrogenation of acetylene, and more selective for complete hydrogenation to form ethane than ethene [87,90]. In fact, several studies have proposed the direct formation of ethane from acetylene on  $\beta$ -PdH<sub>x</sub> via hydrogenation of strongly adsorbed

surface intermediates that undergo full saturation before the desorption as ethene can occur [89]. Our kinetic studies indicate rapid conversion of BMFM to BMH<sub>4</sub> and BMTHFM occurring at low conversions, with hydrogenation rates ( $R_{RS1b}$ ) showing a first-order dependence on  $p_{H_2}$  and a zero-order dependence on aromatic substrates. These reaction orders are similar to those observed for acetylene hydrogenation over  $\beta$ -PdH-containing Pd/C [87,90,91].

#### 4.4.3 Development of a kinetic model for BMFM hydrogenation over Pd/C and Pt/C

Hydrogenation of BMFM over both Pt/C and Pd/C occurs via a complex network of reactions occurring in series and in parallel, as shown in Scheme 4.2 and Scheme 4.3. Given the large number of products observed during the hydrogenation of BMFM, it is impractical to describe the temporal evolution of each product and, therefore, only six species were selected for inclusion in the kinetic model; these are BMFM, BMH<sub>4</sub> (**1a**), BMTHFM (**1b**), and **a1c** (aromatic single ring opened species), **s1c** (saturated single ring opened species), and **1d** (multi-ring opened species). The sequence of elementary reactions of involved Scheme 4.2 and Scheme 4.3 are described in detail in SI 4.6.5. In short, the reactions are grouped into four categories, adsorption of reactants (BMFM, BMH<sub>4</sub>, and **a1c** and H<sub>2</sub>) and hydrogenation of BMFM, BMH<sub>4</sub>, and **a1c**. Each group of aromatic species can undergo competing ring opening (RO) or ring saturation (RS) reactions involving 4-6 additions of H atoms.

Ring opening and ring saturation reactions described are assumed to follow Langmuir-Hinshelwood kinetics with each atom of H being added sequentially on the catalyst surface. We consider the adsorption of organic species and H<sub>2</sub> species to occur non-competitively on metal surface sites. This assumption is motivated by the observation that mechanisms involving competitive adsorption of BMFM and H<sub>2</sub> on a single site do not lead to rate expressions consistent with the observed dependencies on  $p_{H_2}$  for ring opening and ring saturation and with the observed zero-order dependence on BMFM concentration for all reactions involved during initial rate studies. The independence of the initial rate of hydrogenation on the initial substrate concentration is attributed to substrate saturation of the catalyst, as has been discussed for hydrogenation of DMF over Pt/C [13].

The rate of ring saturation of BMFM has a roughly first-order dependence on H<sub>2</sub> partial pressure, for both Pt/C and Pd/C (Table 4.4) The rate of formation of BMTHFM over PdH<sub>x</sub> also shows a first-order dependence with respect to  $p_{H_2}$  during initial rate studies. This suggests that the first addition of a H atom is quasi-equilibrated and that the second addition of a H atom is rate-limiting. Under these constraints, the rate expression for ring-saturation of BMFM over both Pt and Pd is described by Eqns 1-2. We note that  $R_{RS1b}$  is not involved in BMFM hydrogenation over Pt catalysts since Pt does not form a hydride.

$$R_{RS1} = \frac{k_{RS1}C_{BMFM}(K_4H_{H_2}p_{H_2})}{(1+\sum K_jC_j)(1+\sqrt{K_4H_{H_2}p_{H_2}})} \quad (1)$$

$$R_{RS1b} = \frac{k_{RS1b}C_{BMFM}(K_4H_{H_2}p_{H_2})}{(1+\sum K_jC_j)(1+\sqrt{K_4H_{H_2}p_{H_2}})} \quad (2)$$

In the rate expressions above,  $k_{RS1}$  and  $k_{RS1b}$  are the rate coefficients associated with ring saturation of BMFM to form **1a** and **1b**, respectively.  $K_j$  ( $j = 1, 2, 3$ ) are the adsorption

equilibrium constants for the aromatic species BMFM, BMH<sub>4</sub>, and **a1c**;  $K_4$  is the equilibrium constant for dissociative adsorption of H<sub>2</sub>, and  $H_{H_2}$  is the Henry's constant relating the concentration of dissolved H<sub>2</sub> in the liquid phase to the partial pressure of H<sub>2</sub>,  $p_{H_2}$ . Predicted values for  $H_{H_2}$  in octane at 433K were determined from the studies by E. Brunner et al. [78].

Different  $p_{H_2}$  dependences of initial rates of BMFM ring-opening were observed for Pt/C and Pd/C (Table 4.4), which motivated us to consider different mechanisms of ring opening for Pt and Pd. An experimentally observed dependence on  $p_{H_2}$  of ~0.65 over Pt/C suggests that the rate-limiting step for ring opening is the irreversible addition of the first H atom to adsorbed BMFM. By contrast, the observed  $p_{H_2}$  dependence of ~1 for Pd/C suggests that the addition of the second H atom is responsible for ring opening of BMFM. The difference in ring opening mechanisms between Pt and Pd, is most likely a result of the difference in bonding configuration of adsorbed furanyl species on the two metals. In a DFT study estimating thermochemistry of furan derivatives on transition metal surfaces, Vorotnikov and Vlachos showed that the preferred adsorption mode of 2,5-dimethylfuran on Pt surfaces is via a di- $\sigma_{cc}$  complex, in which  $\alpha$  and  $\beta$  carbons are bound to two different metal atoms whereas the preferred adsorption via pi orbitals,  $\pi_{cc}$ , occurs on Pd surfaces [76]. Additional DFT studies by Vlachos and coworkers on furan hydrogenation over Pd metal centers suggest that the first H addition occurs at the  $\alpha$ -C<sub>1</sub> position, forming HF (adsorbed furan + 1H), a shared intermediate to both the ring-opening and ring-saturation pathways. The second H addition occurring at  $\beta$ -C<sub>2</sub> or at the O atom results in ring saturation or ring cleavage, respectively. The authors found that the formation of HF was critical to ring opening over Pd because ring cleavage of the resulting CH<sub>2</sub>-O bond was more facile than the CH-O bond (direct cleavage of the aromatic ring). Their energetic calculations are consistent with our observations in that during hydrogenation we see the same rate-order dependence on  $p_{H_2}$ , first order, for both ring opening and ring saturation over Pd, indicating that the second addition of an H atom is rate limiting. Based on these analyses, the rate expression for ring-opening of BMFM is described by Eq. 3.

$$R_{RO1} = \frac{k_{RO1}C_{BMFM}(K_4H_{H_2}p_{H_2})^\alpha}{(1+\sum K_jC_j)(1+\sqrt{K_4H_{H_2}p_{H_2}})} \quad (3)$$

where  $\alpha = 1$  for Pd catalysts;  $\alpha = 0.5$  for Pt/C, and  $k_{RO1}$  is the rate constants associated with ring opening of BMFM.

Ring saturation or C-O cleavage of the first, single furan ring of BMFM forms intermediates **1a** (BMH<sub>4</sub>) or **a1c**. These compounds were difficult to isolate and purify for use in separate initial rate studies, and, therefore, we assumed that secondary hydrogenation of the remaining aromatic ring occurs via a mechanism similar to that proposed for the initial hydrogenation. This assumption is valid for hydrogenation over Pd/C, where the selectivity ratio of RS product **1b** to RO product **1c** remains constant over the range of  $p_{H_2}$  studied (1.0-1.4 MPa) and converges to ~2.8 at 100% conversion of BMFM and BMH<sub>4</sub> (Figure S. 4.9). This finding suggests that the competing reactions of ring saturation and ring opening remain first-order with respect to  $p_{H_2}$  throughout the course of reaction.

Based on the discussion above, the rates of ring saturation ( $R_{RSi}$ ,  $R_{RS1b}$ ) and ring opening ( $R_{ROi}$ ) (see Scheme 4.2 and Scheme 4.3) can be represented by the following equations, where ( $i = 1, 2, 3$  associated with species BMFM, BMH<sub>4</sub>, and **a1c**):

$$R_{ROi} = \frac{k_{ROi}C_{BMFM}(K_4H_{H2}P_{H2})^\alpha}{(1+\sum K_jC_j)(1+\sqrt{K_4H_{H2}P_{H2}})} \quad (4)$$

$$R_{RSi} = \frac{k_{RSi}C_{BMFM}(K_4H_{H2}P_{H2})}{(1+\sum K_jC_j)(1+\sqrt{K_4H_{H2}P_{H2}})} \quad (5)$$

$$R_{RS1b} = \frac{k_{RS1b}C_{BMFM}(K_4H_{H2}P_{H2})}{(1+\sum K_jC_j)(1+\sqrt{K_4H_{H2}P_{H2}})} \quad (6)$$

The set of differential equations describing the temporal evolution of concentrations of species involved in Scheme 4.2 and Scheme 4.3  $C_{BMFM}$ ,  $C_{BMH_4}$ ,  $C_{BMTHFM}$ ,  $C_{a1c}$ ,  $C_{s1c}$ , and  $C_{1d}$ , can be written as:

$$\frac{V}{W} \frac{dC_{BMFM}}{dt} = -R_{RO1} - R_{RS1} - R_{RS1b} \quad (7)$$

$$\frac{V}{W} \frac{dC_{BMH_4}}{dt} = R_{RS1} - R_{RS2} - R_{RO2} \quad (8)$$

$$\frac{V}{W} \frac{dC_{a1c}}{dt} = R_{RO1} - R_{RS3} - R_{RO3} \quad (9)$$

$$\frac{V}{W} \frac{dC_{BMTHFM}}{dt} = R_{RS2} \quad (10)$$

$$\frac{V}{W} \frac{dC_{s1c}}{dt} = R_{RO2} + R_{RS3} \quad (11)$$

$$\frac{V}{W} \frac{dC_{1d}}{dt} = R_{RO3} \quad (12)$$

With the exception of  $C_{BMFM}$ , the initial concentrations of all species are set to zero. In eqns. 7 – 12,  $V$  is the solution volume in the reactor and  $W$  is the weight of catalyst.

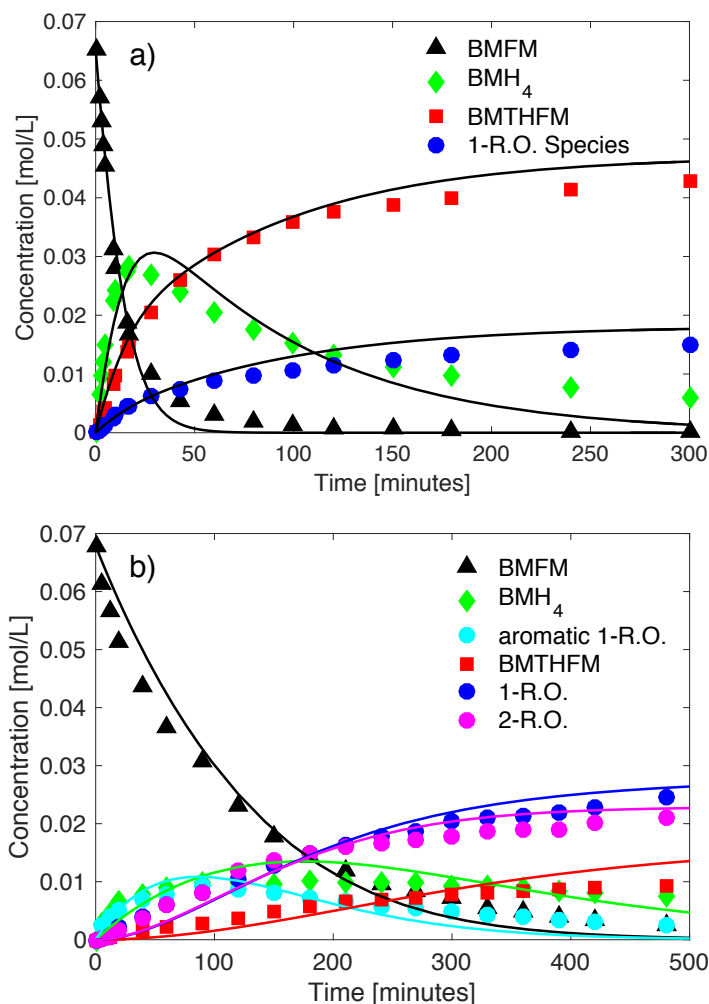
Since there was no evidence for direct hydrogenation of BMFM to BMTHFM over Pt/C, the value of  $R_{RS1b}$  was set to zero for this catalyst. Similarly, no multi-ring opened species (**1d**) were observed during hydrogenation of BMFM over Pd/C, and therefore  $R_{RO3}$  was set to zero for this catalyst. Aromatic products, **a1c**, were present in quantifiable concentrations during hydrogenation over Pt/C (Figure S. 4.3) and were gradually consumed (Eq. 9). Although direct ring opening of BMFM ( $R_{RO1}$ ) does occur for Pd/C, species **a1c** was difficult to quantify during reaction over Pd/C, thus our model for this catalyst assumes that species **a1c** behave as a reactive intermediate and is rapidly hydrogenated to the products **s1c**.

Values for the rate and equilibrium constants appearing in eqns. 1-3 were evaluated by solving the system of differential equations for an initial set of these parameters to determine concentrations of BMFM, BMH<sub>4</sub>, BMTHFM, and ring opened species (**a1c**, **s1c**, **1d**) as functions of time and then comparing these values to those obtained experimentally. An objective function

was minimized by a nonlinear, least-squares regression by varying the rate and equilibrium constants in order to obtain the best-fit values of these parameters. The ordinary differential equation solver, ODE15s, and the nonlinear optimization solver for the residual sum of squares, fmincon, available in Matlab were used for parameter estimation. The parameters evaluated at different temperatures (413K – 453K) were correlated using the Arrhenius equation to obtain activation energies and pre-exponential factors. The Arrhenius plots for all fitted parameters are shown in Figure S. 4.12 and **Figure S. 4.13**. Similarly, equilibrium constants evaluated at temperatures (413 K - 453 K) were correlated using the Van't Hoff equation to determine adsorption enthalpies for H<sub>2</sub> dissociation and aromatic species on metal surface (Figure S. 4.12 and **Figure S. 4.13**). Values of the kinetic parameters in eqns. 4-9 at 433K and their associated activation barriers and pre-exponential factors are summarized in Table 4.8 and Table 4.9, for reactions over Pd and Pt, respectively.

Figure 4.3 compares the concentration profiles for the aforementioned species as functions of time predicted by the model and those observed experimentally during hydrogenation of BMFM over a) Pd/C and b) Pt/C. Additional plots of observed and predicted concentration as a function of time for other reaction temperatures are given in Figure S. 4.10 and **Figure S. 4.11**. In all instances, the quality of the agreement between the predictions by the model and the experimental data is good. The model of the reaction kinetics captures the slower consumption of BMH<sub>4</sub> relative to BMFM and the parallel generation of secondary products. For BMFM hydrogenation over Pd/C, the model describes the three parallel primary reactions involving the substrate, and for hydrogenation over Pt/C, the model describes the competitive reactions of ring opening and ring saturation of BMFM to their respective aromatic intermediates, which are consumed in secondary reactions.





**Figure 4.3** Comparison of experimental and simulated concentration profiles reaction network of BMFM hydrogenation  
 For a) **Scheme 4.3** over Pd/C (0.2mol%) and b) **Scheme 4.2** over Pt/C (0.6mol%) at 433K, 1.1 MPa H<sub>2</sub>, 2.8mmol in octane. Model fit: solid lines. Measurement: symbols.

The thermodynamics of BMFM and BMH<sub>4</sub> adsorption deduced from the model show that for both catalysts BMH<sub>4</sub> has a lower heat of adsorption than that for the planar, more aromatic BMFM. This finding is consistent with previous studies which have shown that the THF ring interacts only weakly with the metal surface through the oxygen atom in a tilted configuration [65] and has a binding energy 0.6 eV lower than that of furan on Pd surfaces [75]. Our results also find that aromatic compounds, BMFM and BMH<sub>4</sub>, are more strongly adsorbed on Pd than on Pt (Table 4.8 and Table 4.9), consistent with DFT calculations of the enthalpies of adsorption of furanic derivatives on Pd and Pt [76]. The enthalpy for BMFM adsorption reported here, 11.2 kJ/mol, on Pt/C is comparable to that of DMF adsorption reported previously in our work, 12.3 kJ/mol [80].

Previous studies of the hydrogenation of furanic compounds [18, 38] have shown that the activation energy for C-O bond cleavage is higher than for C=C bond saturation. Table 4.8 and Table 4.9 show this to be the case, as well, for the present study, where the activation energy for

ring opening is always 20-30 kJ/mol higher than that for ring saturation, for all aromatic products (BMFM, BMH<sub>4</sub>, **a1c**) produced over both Pd/C and Pt/C. As a consequence, BMFM can be hydrogenated selectively to BMTHFM, at 373K, 2.1 MPa H<sub>2</sub> over Pd/C. The high activity of PdH<sub>x</sub> formed on Pd/C also contributes to the rapid and selective production of BMTHFM at low temperatures.

**Table 4.8.** Rate parameters obtained by non-linear, least squares fitting of experimental data to proposed kinetic model for BMFM hydrogenation over Pd/C.

Rate or Equilibrium Constant	Parameters at 433K		E <sub>a</sub> or ΔH <sub>ad</sub>		ln(A)	ΔS <sub>ad</sub> /R
<b>k<sub>RS1</sub></b>	2.1	mol/g-min	32.3	kJ/mol	9.7	--
<b>k<sub>RO1</sub></b>	0.2	mol/g-min	57.6	kJ/mol	14.6	--
<b>k<sub>RS2</sub></b>	0.9	mol/g-min	25.8	kJ/mol	7.1	--
<b>k<sub>RO2</sub></b>	0.5	mol/g-min	59.0	kJ/mol	15.7	--
<b>k<sub>RS1b</sub></b>	1.0	mol/g-min	31.0	kJ/mol	8.6	--
<b>K<sub>BMFM</sub></b>	10.9	L/mol	-16.1	kJ/mol	--	-2.1
<b>K<sub>BMH4</sub></b>	3.0	L/mol	-10.2	kJ/mol	--	-1.7
<b>K<sub>H2</sub></b>	0.4	L/mol	-9.5	kJ/mol	--	-3.4

**Table 4.9.** Rate parameters obtained by non-linear, least squares fitting of experimental data to proposed kinetic model for BMFM hydrogenation over Pt/C.

Rate or Equilibrium Constant	Parameters at 433K		E <sub>a</sub> or ΔH <sub>ad</sub>		ln(A)	ΔS <sub>ad</sub> /R
<b>k<sub>RS1</sub></b>	0.048	mol/g-min	32.3	kJ/mol	6.0	--
<b>k<sub>RO1</sub></b>	0.010	mol/g-min	53.5	kJ/mol	10.4	--
<b>k<sub>RS2</sub></b>	0.102	mol/g-min	41.2	kJ/mol	9.3	--
<b>k<sub>RO2</sub></b>	0.006	mol/g-min	62.9	kJ/mol	12.8	--
<b>k<sub>RS3</sub></b>	0.112	mol/g-min	44.8	kJ/mol	10.4	--
<b>k<sub>RO3</sub></b>	0.016	mol/g-min	52.6	kJ/mol	10.8	--
<b>K<sub>BMFM</sub></b>	10.0	L/mol	-11.2	kJ/mol	--	-0.9
<b>K<sub>BMH4</sub></b>	3.4	L/mol	-9.4	kJ/mol	--	-1.4
<b>K<sub>a1c</sub></b>	10.5	L/mol	-11.7	kJ/mol	--	-1.0
<b>K<sub>H2</sub></b>	0.3	L/mol	-8.4	kJ/mol	--	-3.4

Although different mechanisms were proposed for ring opening aromatic furans over Pd and Pt, the activation energies for ring opening of all aromatic reactants are similar for both Pd/C and Pt/C, ranging from 53-63 kJ/mol (Table 4.8 and Table 4.9). The comparable values in activation energies for Pt and Pd are attributed to similarities in the geometries of the C-O bond and degrees of hybridization of the α-C<sub>1</sub> prior to ring cleavage. For both proposed mechanisms prior to ring cleavage, the α-C<sub>1</sub> of the adsorbed furan is sp<sup>3</sup> hybridized, which weakens the aromatic C-O. In the case for Pd, furans adsorb via a π<sub>cc</sub> complex and ring cleavage occurs after hydrogenation of α-C<sub>1</sub> to form HF. Hydrogenation of the α-C<sub>1</sub> is not needed for Pt in order to weaken the aromatic C-O bond because furans adsorb onto Pt surfaces via di-σ<sub>cc</sub> complex instead, meaning that a sigma bond is formed between α-C<sub>1</sub> and a Pt atom. In both mechanisms, the C-O

bond to be cleaved is weakened in a similar fashion and the rate-limiting step for RO involves the addition of H to the O atom.

The selectivity between ring saturation and ring opening is dependent on the relative magnitudes of  $R_{RS}$  and  $R_{RO}$ , which are functions of the kinetic rate coefficients as for these reactions and the concentration of reacting species (BMFM,  $p_{H_2}$ ). In the case for Pd/C, the RS and RO pathways have the same dependence on  $p_{H_2}$  ( $\sim 1.0$ ) and the ratio of rate coefficients for RS to RO pathways of BMFM ( $k_{RS1}/k_{RO1} = 10.5$ ) is high, indicating that ring saturation is strongly preferred. This ratio decreases to  $k_{RS2}/k_{RO2} = 2.0$  for hydrogenation of  $BMH_4$ , consistent with our findings that the majority of the ring-opened products is formed from  $BMH_4$ . At complete hydrogenation of BMFM and  $BMH_4$  at 433K and 1.1 MPa  $H_2$ , 74% selectivity to BMTHFM was achieved over Pd/C. In the case for Pt/C, the ratio of rate coefficients for RS to RO of BMFM is similarly is about two-fold lower than that for Pd/C,  $k_{RS1}/k_{RO1} = 4.8$ . However,  $R_{RS}$  has a higher order dependence on the partial pressure of  $H_2$  ( $\sim 1.0$ ) compared to  $R_{RO}$  ( $\sim 0.6$ ). Since the concentration of  $H_2$  in the liquid phase is low under the reaction conditions employed, the overall rate of ring saturation occurs more slowly than the rate of ring-opening, resulting in less than 17% selectivity to BMTHFM at the end of reaction, at which point a majority of the products are present as single or multi-ring opened species.

It is interesting to compare and contrast the findings of the present study with our previous investigation of the liquid-phase hydrogenation of DMF. While DMF did not undergo ring-opening at 353 K, 0.55 MPa  $H_2$  over Pd/C, the aromatic C-O bond of furan rings in more complex furanyl substrates such as BMFM and TMFM [17] can be cleaved over Pd/C. The mechanism by which this occurs is described in our earlier study [80], and involves the hydrogenation of the aromatic C-O bond to form an enol intermediate. The high selectivity to alcohol products achieved over Pd/C and to ketone products over Pt/C are the result of the relative rates of C=C hydrogenation and enol-keto tautomerization for the two metals. Pd/C is known to have a higher activity for C=C bond saturation compared to Pt/C or Ru/C [85,86], resulting in a higher selectivity to -OH-containing compared to C=O-containing products.

## 4.5 Conclusions

The kinetics of liquid-phase hydrogenation of bis(5-methylfuran-2-yl)methane (BMFM) at moderate conditions (1.1 MPa, 433K) were investigated over carbon-supported Pt, Pd and Ru. In all cases, ring opening occurred solely at the aromatic ring and not after full ring saturation. It is proposed that an enol intermediate is formed after cleavage of the aromatic ring and then serves as the common intermediate for forming either ketones or alcohols. Models of the kinetics of BMFM hydrogenation over Pt/C and Pd/C based on the mechanisms proposed in Scheme 4.2 and Scheme 4.3 give good representations of the observed temporal evolution of products for both catalysts. The heat of adsorption for BMFM is greater than that for partially hydrogenated species by 2-6 kJ/mol. For both Pd and Pt, the activation energy for ring-opening is 20-30 kJ/mol than that higher for ring saturation. Ring opening involves the addition of H atom to the O atom of an adsorbed furan ring and ring saturation involves the addition of the second H atom to the  $\beta$ -C<sub>2</sub>. For all aromatic species, the rate coefficient associated with ring saturation ( $k_{RS}$ ) is larger than that for with ring opening ( $k_{RO}$ ), indicating that ring saturation is strongly preferred. This is observed during BMFM hydrogenation over Pd/C, resulting in 85% and 100% selectivity to

BMTHFM at 433 K and 373 K, respectively. Unlike Pd/C, the ring-opening pathway over Pt/C has a lower dependence on  $p_{H_2}$  than the competing ring saturation pathway; therefore, hydrogenation of BMFM over Pt/C under our reaction conditions (433 K, 2.0 MPa) results in over 75% selectivity to ring-opened species. The results of the present study elucidate the pathways by which complex furan condensates undergo hydrogenation over Pt/C and Pd/C and provide the information needed to achieve selective hydrogenation of such compounds to cyclic ethers or ring-opened compounds via hydrogenolysis of the C-O bond in the furan rings.

## 4.6 Supplemental Information

### 4.6.1 Catalysts properties

**Table S. 4.1** Density of supported metal and average particle size for metal nanoparticles. Average particle size determined by CO chemisorption.

Commercial catalysts (carbon supports) were used as received.

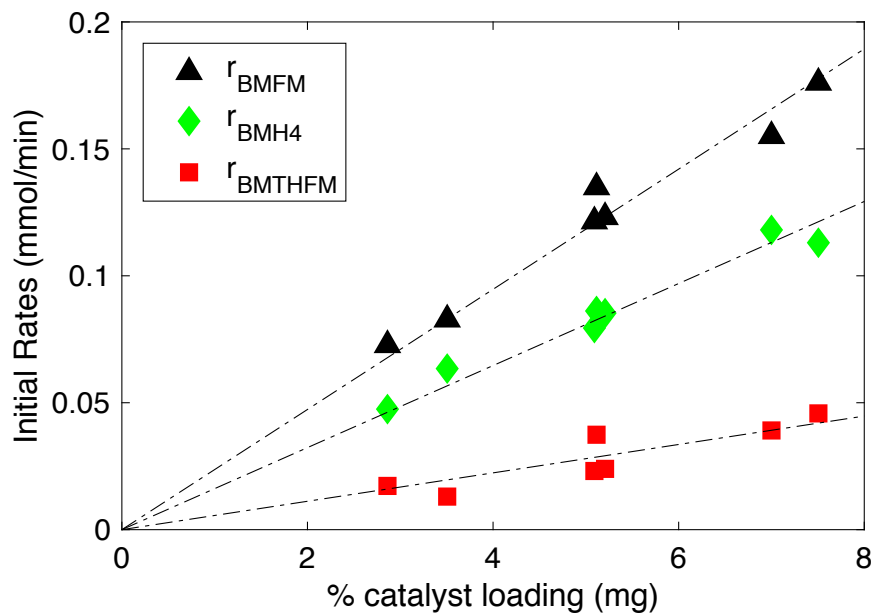
	<b>M/Support Density (mg M/m<sup>2</sup> support)</b>	<b>D<sub>p</sub>, Particle Size (nm)</b>
<b>1% Pd/C</b>	0.015	2.2
<b>5% Pd/C</b>	0.074	2.4
5% Pt/C	0.074	4.6
5% Rh/C	0.074	4.5
5% Ru/C	0.074	5.3

### 4.6.2 Elimination of mass transfer effects in semi-batch hydrogenation system

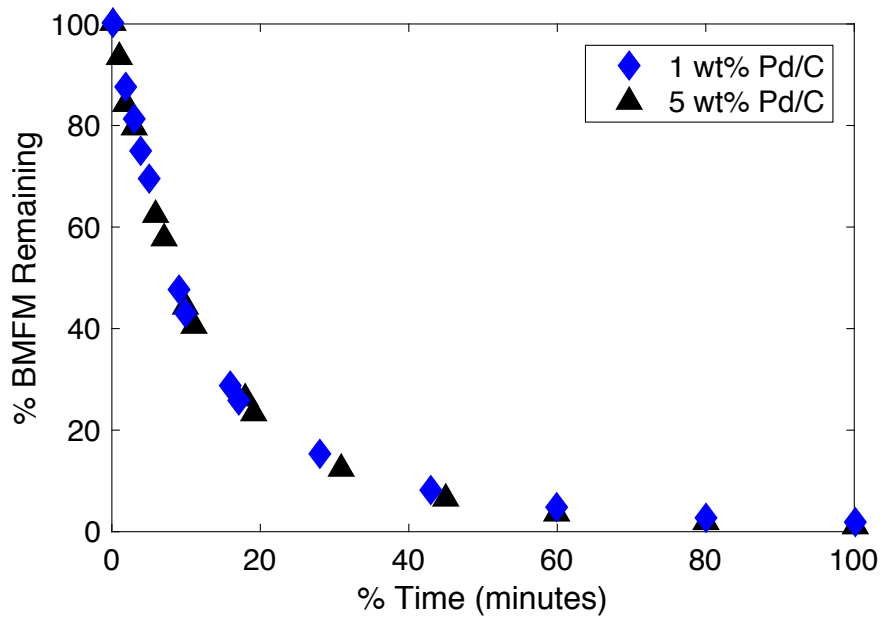
Since the reactions involved a 3-phase complex reactor system, a number of checks were made to assess whether or not mass-transfer from of H<sub>2</sub> from the gas phase to the liquid or from the liquid to the catalyst affected the measure rates of reaction. For up to 10mg of 1wt% Pd/C catalysts, the reaction rates for BMFM conversion increased proportionally with increase in catalyst loading (Figure S. 4.1). This indicates that the reaction rates were not limited by the transfer of reactant gas from the gas phase to the liquid solution.

Additionally, 1wt% Pd/C was sieved into the following particle sizes: (<25 $\mu$ m, 25 – 45  $\mu$ m, 45-65 $\mu$ m, and > 65 $\mu$ m). Additionally, the fraction of particles of <25 $\mu$ m were further grounded for 20 minutes using a mortar and pestle to achieve even more fine particles. No effect of particle size on the initial rates of DMF conversion was observed for particles smaller than <25 $\mu$ m. For all subsequent kinetic experiments, particles sizes of < 25 $\mu$ m were used.

Lastly, the Madon-Boudart test was also applied to verify the absence of internal and external transfer effects on our rates. Hydrogenation of BMFM using Pd/C catalyst of different surface concentrations but similar dispersion (1wt% and 5wt%) resulted in the same rate of consumption of our substrates (Figure S. 4.2), indicating that all sites of both catalyst were equally accessible.



**Figure S. 4.1** Initial BMFM hydrogenation rates over 1% Pd/C as a function of catalyst loading. Reactions at 433K, 1.1 MPa H<sub>2</sub>, 2.8mmol in octane



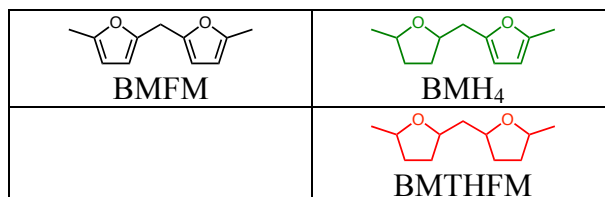
**Figure S. 4.2** Madon-Boudart test of 1 wt% and 5 wt% Pd/C catalyst. Reactions using 0.2mol% Pd/C at 433K, 1.1 MPa H<sub>2</sub>, 2.8mmol in octane

#### 4.6.3 Hydrogenation of BMFM over noble metals on carbon support

Approximately 18 different products were identified during the hydrogenation of BMFM over Pt/C catalysts (413K – 453K, 1.1MPa H<sub>2</sub>). The products are broken down into the 4 groups below and are identified by whether they contain aromatic or saturated rings, degree of ring cleavage, the position where ring cleavage occurred, and by their functional groups (hydroxyl vs. carbonyl).

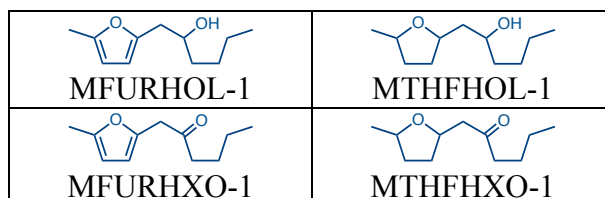
##### Group 1: Products 1a, 1b

Partially or fully ring saturated species



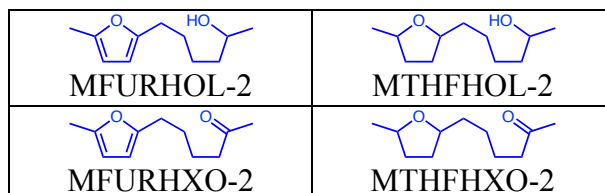
##### Group 2: Products 1c, cleavage at the external C-O bond

Single ring opened species that contain either a saturated or unsaturated furan ring. C-O bond cleavage at the external position results in either an alcohol or carbonyl group at the carbon atom adjacent to furan ring



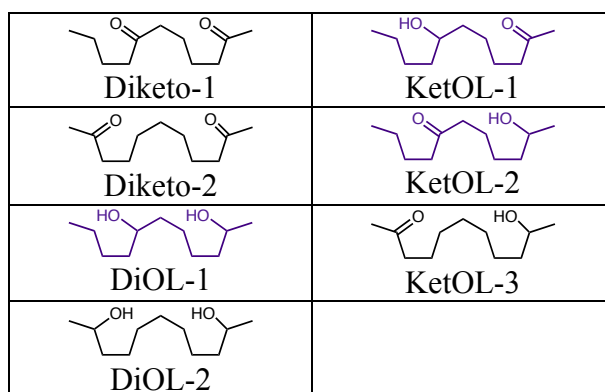
##### Group 3: Products 1c, cleavage at the internal C-O bond

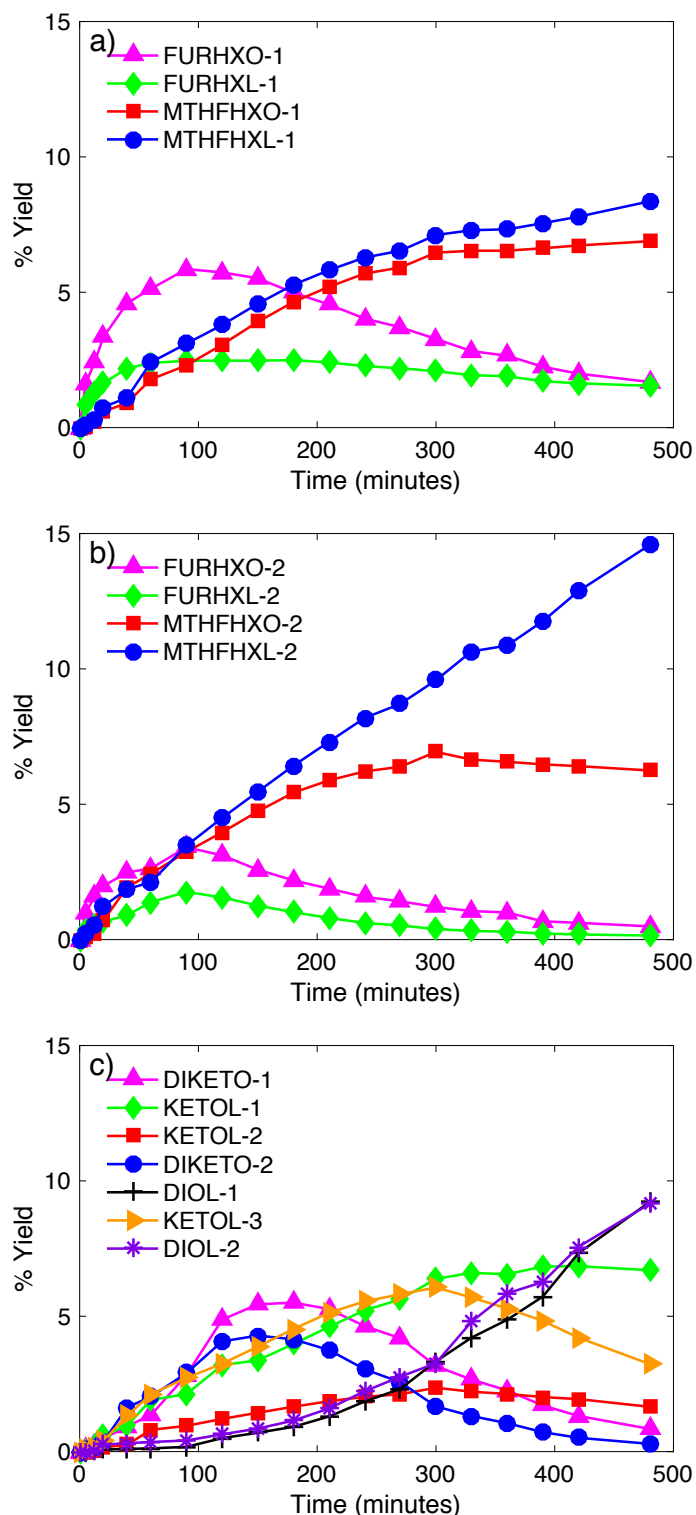
Single ring opened species that contain either a saturated or unsaturated furan ring. C-O bond cleavage at the internal position results in either an alcohol or carbonyl group 5 positions away from the furan ring.



##### Group 4: Products 1d, multi-ring opened species

Cleavage of both aromatic rings results in formation of diketones, diols, or ketols. Listed below are the isomers detected via GC/MS.

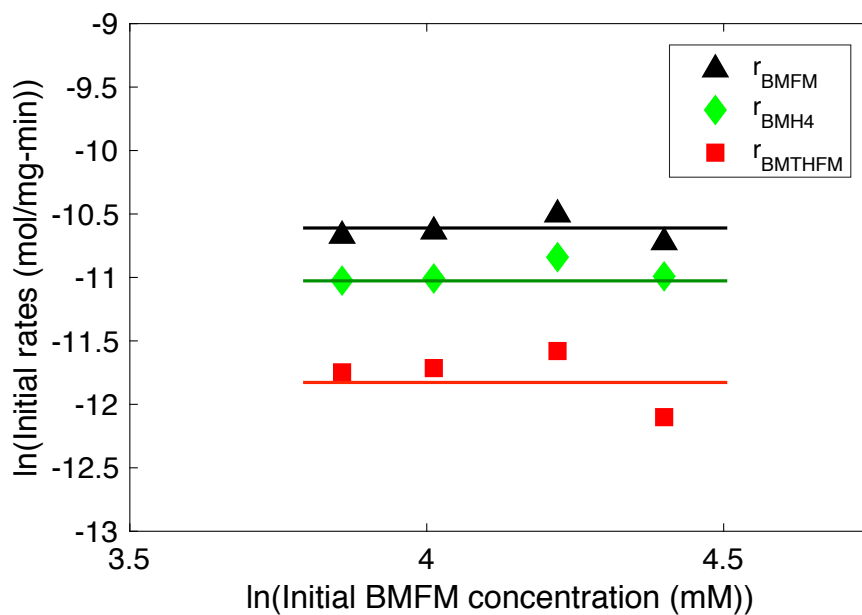




**Figure S. 4.3.** Detailed evolution of all product isomers within groups 1c and 1d during BFM hydrogenation over Pt/C at 0.6 mol% metal loading, 433 K, 1.1 MPa H<sub>2</sub>, 2.8mmol in octane.

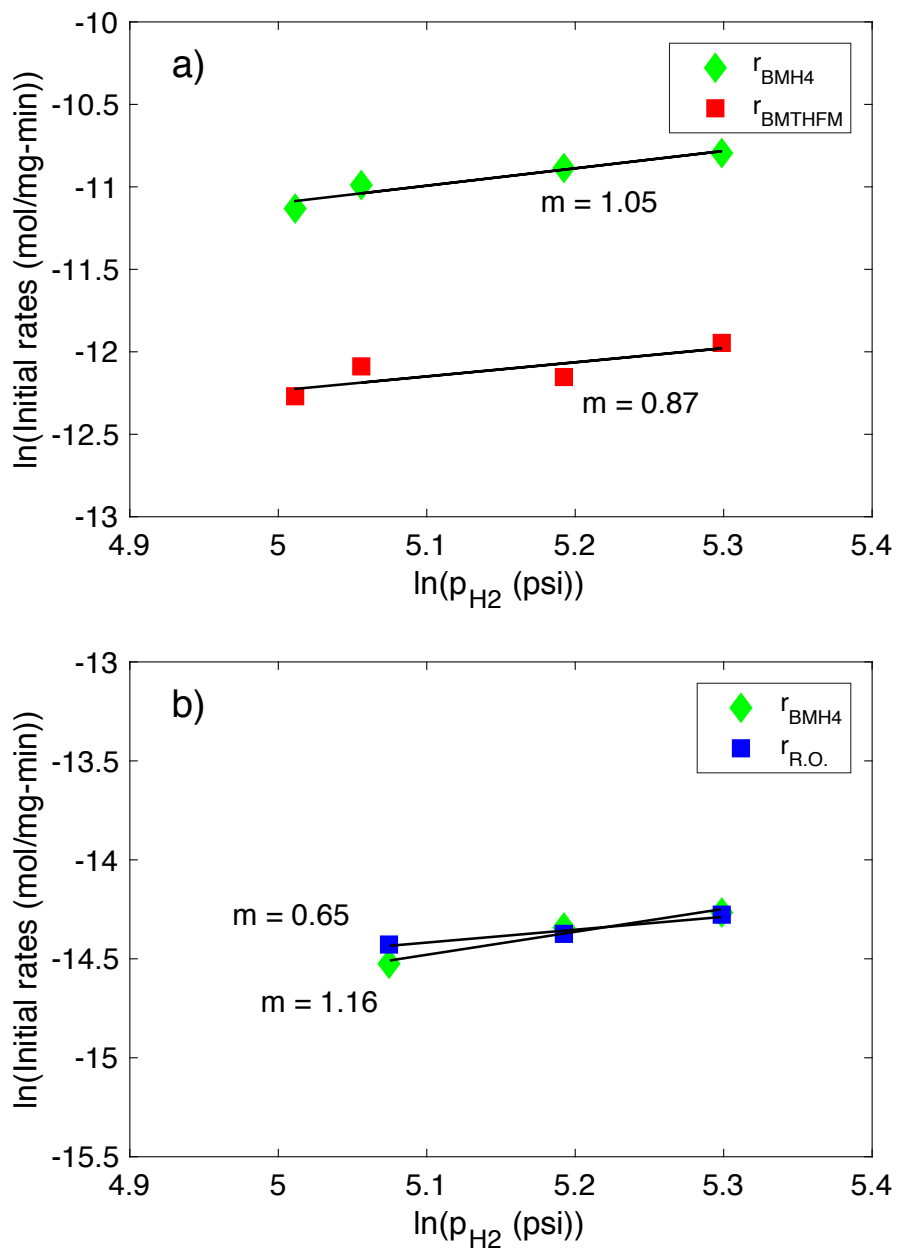
The ring opened hydrogenation products are grouped into a) Single ring-opened species through cleavage of the exterior C-O bond, b) Single ring-opened species through cleavage of the interior C-O bond, c) multi-ring-opened species containing alcohol and/or carbonyl groups.

4.6.4 BMFM hydrogenation kinetics over Pd/C and Pt/C catalysts

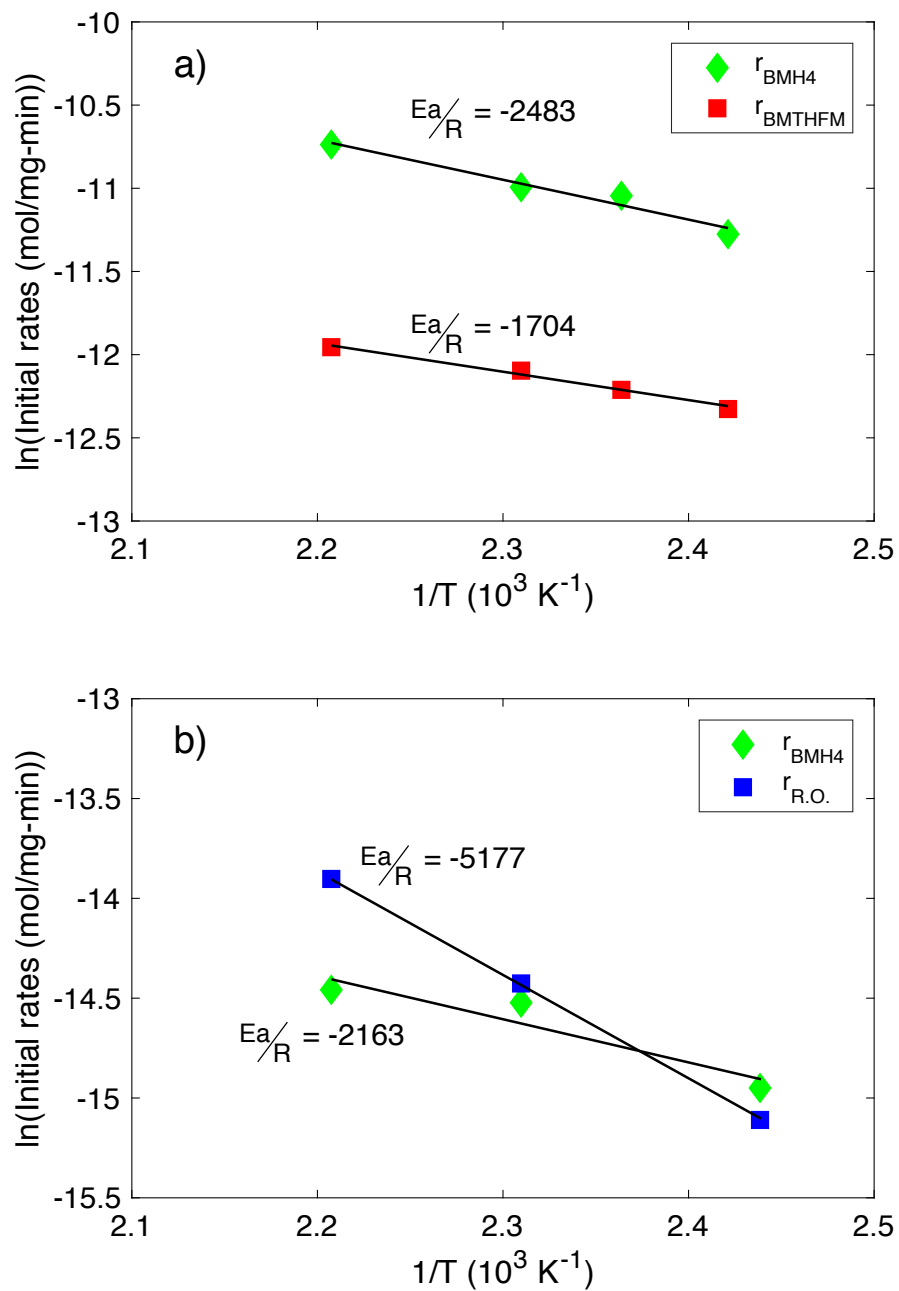


**Figure S. 4.4** Initial rates of hydrogenation of BMFM, initial rates of production of 1a and 1b, as a function of initial loading of BMFM  
0.2 mol% Pd/C loading, 433K, 1.1 MPa H<sub>2</sub>, 2.8mmol in octane.





**Figure S. 4.5** Initial rates of hydrogenation of BMFM, initial rates of production of 1a and 1b, and selectivity to ring opening (30% conv.) as a function of  $p_{H_2}$  433K, 1.1 MPa  $H_2$ , 2.8mmol in octane for a) 0.2 mol% Pd/C, b) 0.6mol% Pt/C.



**Figure S. 4.6.** Arrhenius plot of initial reaction rates for BMFM hydrogenation for reaction temperatures 413 K to 453 K, 1.0 – 1.2 MPa  $\text{H}_2$ , 2.8mmol in octane for a) 0.2 mol% Pd/C, b) 0.6mol% Pt/C.

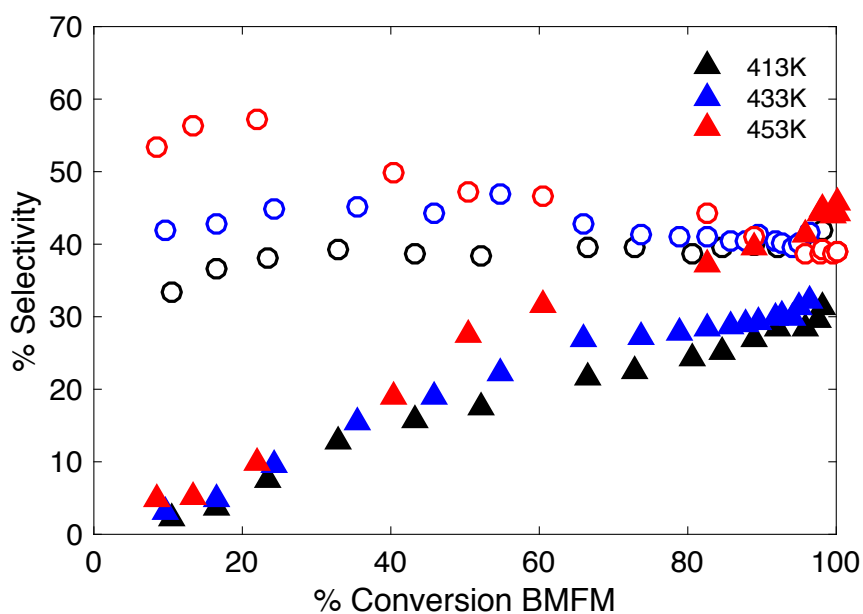
**Table S. 4.2** Selectivity toward ring opened products (1c and 1d) measured at 30% BMFM conversion as a function of reaction temperature for hydrogenation over Pd and Pt catalysts.

2 0.2 – 0.6 mol% metal loading, 433 K, 1.0-1.2 MPa H<sub>2</sub>, 2.8mmol in octane

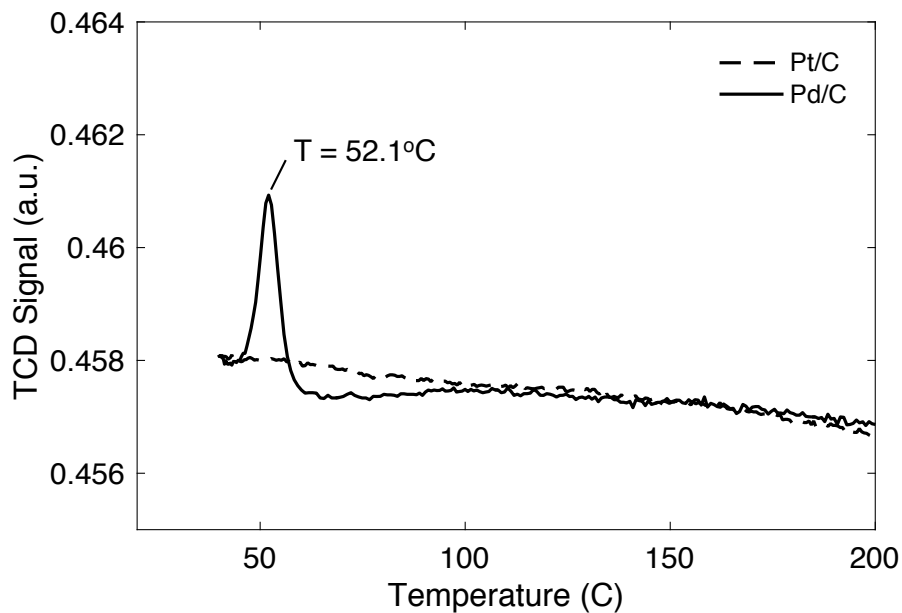
Reaction Temperature	Over Pd/C		Over Pt/C	
	(% 1c)	(% 1d)	(% 1c)	(% 1d)
413 K	4.6	11.2	38.9	11.2
433 K	5.3	12.5	44.9	12.5
453K	6.3	14.3	53.4	14.3

**Table S. 4.3** Selectivity toward ring opened species (1c and 1d) measured at 90% BMFM conversion as a function of reaction temperature for hydrogenation over Pd and Pt catalysts. 0.2 – 0.6 mol% metal loading, 433 K, 1.0-1.2 MPa H<sub>2</sub>, 2.8mmol in octane.

Reaction Temperature	Over Pd/C		Over Pt/C	
	(% 1c)	(% 1d)	(% 1c)	(% 1d)
413 K	7.5	27.0	39.7	27.0
433 K	10.6	29.3	41.4	29.3
453K	13.5	39.6	40.1	39.6

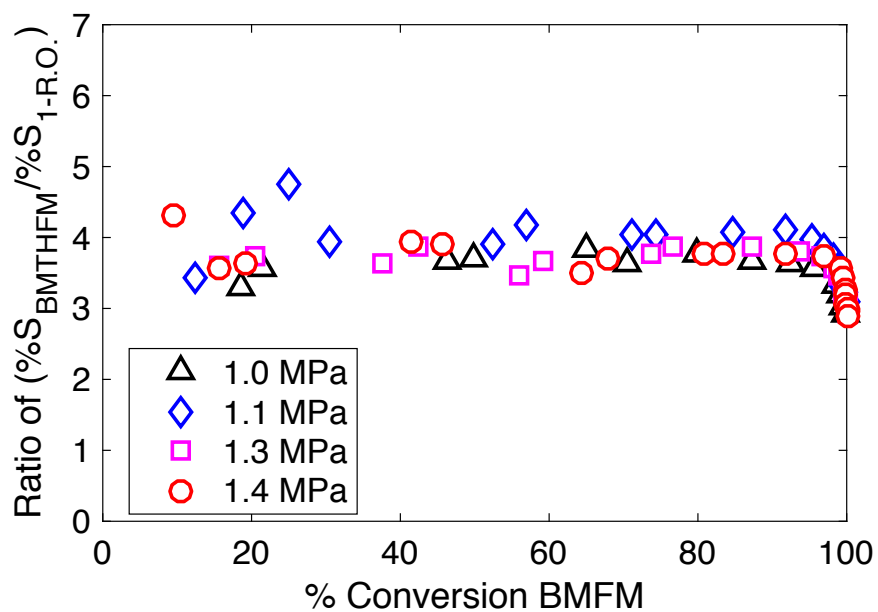


**Figure S. 4.7** Effect of temperature on selectivity to single ring-opened products, 1c, (●) and multi-ring-opened products, 1d, (Δ) as a function of conversion of BMFM over Pt  
0.6mol% Pt, 1.1 MPa H<sub>2</sub>, 2.8mmol in octane.



**Figure S. 4.8.** Temperature programmed reduction (TPR) profiles of reduced Pt/C and Pd/C catalysts for evidence of hydride species.

TPR performed under flowing 10% H<sub>2</sub>/Ar mixture at 50mL/min with a temperature ramp rate of 5°C /min.



**Figure S. 4.9.** Ratio of the selectivity of BMTHFM (1b) to the selectivity of ring opened products (1c) as a function of conversion of BMFM and  $p_{H_2}$  at 433K

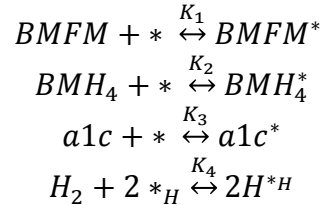
#### 4.6.5 Derivation of rate expressions in kinetic model

The kinetic model attempts to describe the following 6 species within the reaction network proposed in Scheme 4.2 and Scheme 4.3: BMFM, BMH<sub>4</sub>, BMTHFM, **a1c**, **s1c** and **1d**. The model is broken into 4 groups of reaction: adsorption of reacting species and the hydrogenation reactions involving the 3 aromatic furan containing species (BMFM, BMH<sub>4</sub>, and **a1c**).

The symbols \* and \*<sub>H</sub> represent vacant sites on the catalyst surface that can accommodate organic species and atomic hydrogen, respectively. Species I<sub>ia-ic</sub><sup>\*</sup> were mono-, di-, and tri-hydro intermediate species adsorbed to catalyst surface. Such intermediates were not detected as stable products during the reaction, suggesting that further hydrogenation of these intermediates to form tetrahydrofuran species are rapid. The rate-limiting step assumed for ring saturation reactions over Pt was the addition of 2<sup>nd</sup> H atom to the furan ring. The rate-limiting step assumed for ring opening over Pt was the addition of the 1<sup>st</sup> H atom to the furan ring.

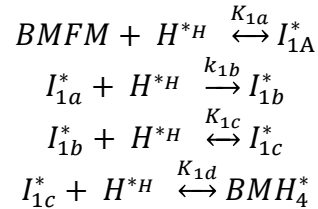
#### Sequence of elementary reactions in Scheme 4.2:

Group I: Adsorption of aromatic species (BMFM, BMH<sub>4</sub>, and **a1c**) and hydrogen

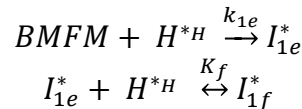


Group II: Hydrogenation reactions involving BMFM

Ring saturation (r<sub>RS1</sub>)



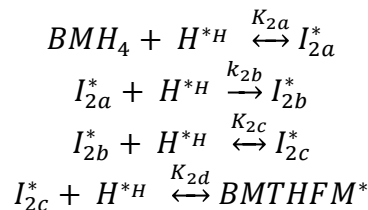
Ring opening (r<sub>RO1</sub>)

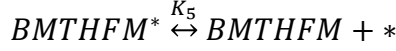


I<sub>1f</sub><sup>\*</sup> is the enol intermediate, precursor to all single ring opened products, **a1c**, containing carbonyls (after tautomerization) or alcohol groups (successive hydrogenation).

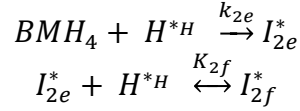
Group III: Hydrogenation reactions involving BMH<sub>4</sub>

Ring saturation (r<sub>RS2</sub>)

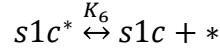




Ring opening ( $r_{RO2}$ )

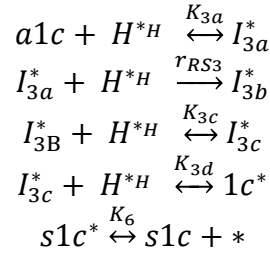


$I_{2f}^*$  is the enol intermediate, precursor to all saturated single ring opened products, **s1c**, containing carbonyls (after tautomerization) or alcohol groups (successive hydrogenation).

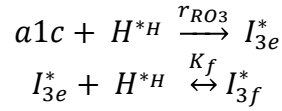


Group IV: Hydrogenation reactions involving **a1c**

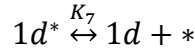
Ring saturation ( $r_{RS2}$ )



Ring opening ( $r_{RO3}$ )



$I_{3f}^*$  is the enol intermediate, precursor to all multi-ring opened products, **1d**, containing carbonyls (after tautomerization) or alcohol groups (successive hydrogenation).



The rates for ring opening ( $r_{ROi}$ ), ring saturation ( $r_{RSi}$ ), where  $i = 1, 2, 3$ , as functions of concentrations of BMFM, ( $C_{BMFM}$ ),  $BMH_4$  ( $C_{BMH4}$ ), **a1c** ( $C_{a1c}$ ) and  $H_2$  partial pressure ( $p_{H2}$ ) are derived as follows:

Surface coverage of species  $j$  ( $1 - 4$ ):

$$\theta_1 = \theta_{BMFM} = K_1 C_{BMFM} \theta^*$$

$$\theta_2 = \theta_{BMH4} = K_2 C_{BMH4} \theta^*$$

$$\theta_3 = \theta_{a1c} = K_3 C_{a1c} \theta^*$$

$$\theta_H = \sqrt{K_4 H_{H2} P_{H2}} \theta_H^*$$

Site balance for  $\theta^*$  and  $\theta_H^*$ :

$$\theta_{BMFM} + \theta_{BMH4} + \theta_{a1c} + \theta^* = 1$$

$$\theta_H + \theta_H^* = 1$$

$$\theta^* = \frac{1}{1 + K_1 C_{BMFM} + K_2 C_{BMH4} + K_3 C_{a1c}} = \frac{1}{(1 + \sum_{j=1}^3 K_j C_j)}$$

$$\theta_H^* = \frac{1}{1 + \sqrt{K_4 H_{H2} P_{H2}}}$$

For all reactions  $i$  ( $i = 1-3$ ) and species  $j$  ( $j=1-3$ )

Rate of ring saturation:

$$r_{RSi} = k_{ib} \theta_{ia} \theta_H$$

$$\theta_{ia} = \frac{K_{ia} \theta_j \theta_H}{\theta_H^*}$$

$$k_{RS} = k_{ib} K_{ia}$$

$$r_{RSi} = \frac{k_{RSi} K_j C_j (\sqrt{K_4 H_{H2} P_{H2}})^2}{(1 + \sum_{j=1}^3 K_j C_j) (1 + \sqrt{K_4 H_{H2} P_{H2}})}$$

Rate of ring opening:

$$r_{ROi} = k_{ie} \theta_j \theta_H$$

$$k_{ROi} = k_{ie}$$

$$r_{ROi} = \frac{k_{ROi} C_j (\sqrt{K_4 H_{H2} P_{H2}})}{(1 + \sum_{j=1}^3 K_j C_j) (1 + \sqrt{K_4 H_{H2} P_{H2}})}$$

The reaction network of BMFM hydrogenation over Pt catalysts can be described by the set of 6 differential equations here:

$$\frac{V}{W} \frac{dC_{BMFM}}{dt} = -r_{RS1} - r_{RO1}$$

$$\frac{V}{W} \frac{dC_{BMH4}}{dt} = r_{RS1} - r_{RS2} - r_{RO2}$$

$$\frac{V}{W} \frac{dC_{a1c}}{dt} = r_{RO1} - r_{RS3} - r_{RO3}$$

$$\frac{V}{W} \frac{dC_{BMTHFM}}{dt} = r_{RS2}$$

$$\frac{V}{W} \frac{dC_{s1c}}{dt} = r_{RO2} + r_{RS3}$$

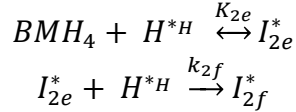
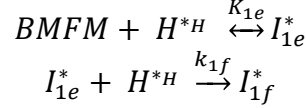
$$\frac{V}{W} \frac{dC_{1d}}{dt} = r_{RO3}$$

### Sequence of elementary reactions in Scheme 4.3:

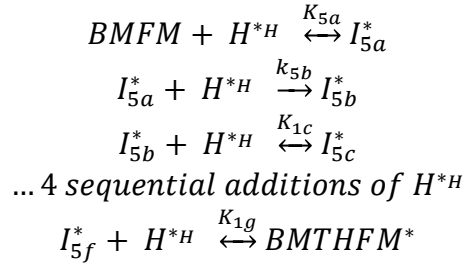
The kinetic model describing BMFM hydrogenation over Pd catalyst is similar to the model describing hydrogenation over Pt catalyst, discussed above. The same 4 groups of reactions described for the Pt system above still holds, except with the additional reaction of direct BMFM

hydrogenation to form BMTHFM over palladium hydride species and the rate limiting step for ring-opening is assumed to be the addition of the 2<sup>nd</sup> H atom instead of the 1<sup>st</sup> as assumed in the case for Pt.

Ring opening reactions over Pd ( $r_{ROi}$ ) :



Complete hydrogenation of BMFM over  $\beta$ -PdH ( $r_{RS1b}$ )



For hydrogenation over Pd, aromatic single ring opened products, species **a1c**, can be treated as reaction intermediates since they are quickly hydrogenated to the fully saturated species, **s1c** and no ring-opening ( $r_{RO3}$ ) occurs to form products **1d**.

$$\begin{aligned} \frac{d(\theta_{a1c})}{dt} &= 0 = r_{RO1} - r_{RS3} \\ r_{RS3} &= r_{RO1} \\ r_{RO3} &= 0 \end{aligned}$$

Therefore, we only have the following rate expressions relevant to the hydrogenation network over Pd catalyst: rates for ring opening ( $r_{ROi}$ ) and ring saturation ( $r_{RSi}$ ,  $r_{RS1b}$ ) where  $i = 1-2$ . These rate expressions are functions of concentrations of BMFM, ( $C_{\text{BMFM}}$ ), BMH<sub>4</sub> ( $C_{\text{BMH}_4}$ ), and H<sub>2</sub> partial pressure ( $p_{\text{H}_2}$ ) are derived as follows:

For all reactions  $i$  ( $i = 1-2$ ) and species  $j$  ( $j=1-2$ )

Rate of ring opening:

$$\begin{aligned} r_{ROi} &= k_{if} \theta_{ie} \theta_H \\ \theta_{ie} &= \frac{K_{ie} \theta_j \theta_H}{\theta_H^*} \\ k_{ROi} &= k_{if} K_{ie} \end{aligned}$$



$$r_{ROi} = \frac{k_{ROi} C_j (\sqrt{K_4 H_{H2} p_{H2}})^2}{(1 + \sum_{j=1}^2 K_j C_j) (1 + \sqrt{K_4 H_{H2} p_{H2}})}$$

Rate of ring saturation:

$$r_{RSi} = k_{ib} \theta_{ia} \theta_H$$

$$\theta_{ia} = \frac{K_{ia} \theta_j \theta_H}{\theta_H^*}$$

$$k_{RS} = k_{ib} K_{ia}$$

$$r_{RSi} = \frac{k_{RSi} K_j C_j (\sqrt{K_4 H_{H2} P_{H2}})^2}{(1 + \sum_{j=1}^2 K_j C_j) (1 + \sqrt{K_4 H_{H2} p_{H2}})}$$

$$r_{RS1b} = k_{5b} \theta_{5a} \theta_H$$

$$\theta_{5a} = \frac{K_{5a} \theta_{BMFM} \theta_H}{\theta_H^*}$$

$$k_{RS1b} = k_{5b} K_{5a}$$

$$r_{RS1b} = \frac{k_{RS1b} K_1 C_{BMFM} (\sqrt{K_4 H_{H2} P_{H2}})^2}{(1 + \sum_{j=1}^2 K_j C_j) (1 + \sqrt{K_4 H_{H2} p_{H2}})}$$

The reaction network of BMFM hydrogenation over Pd catalysts can be described by the set of 4 differential equations listed:

$$\frac{V}{W} \frac{dC_{BMFM}}{dt} = -r_{RO1} - r_{RS1} - r_{RS1b}$$

$$\frac{V}{W} \frac{dC_{BMH4}}{dt} = r_{RS1} - r_{RS2} - r_{RO2}$$

$$\frac{V}{W} \frac{dC_{BMTHFM}}{dt} = r_{RS2} + r_{RS1b}$$

$$\frac{V}{W} \frac{dC_{S1c}}{dt} = r_{RS2} + r_{RO1}$$

4.6.6 Results of kinetic model for BMFM hydrogenation Pd/C and Pt/C catalysts

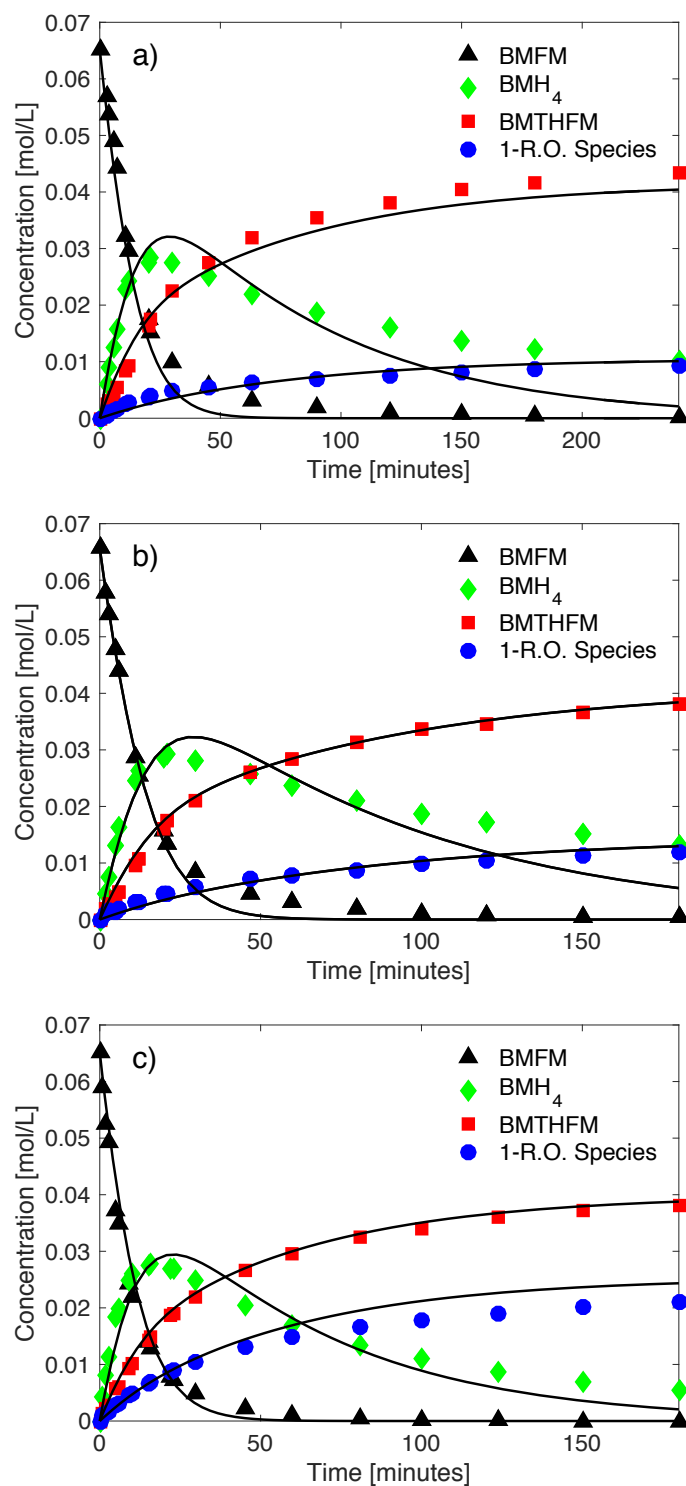
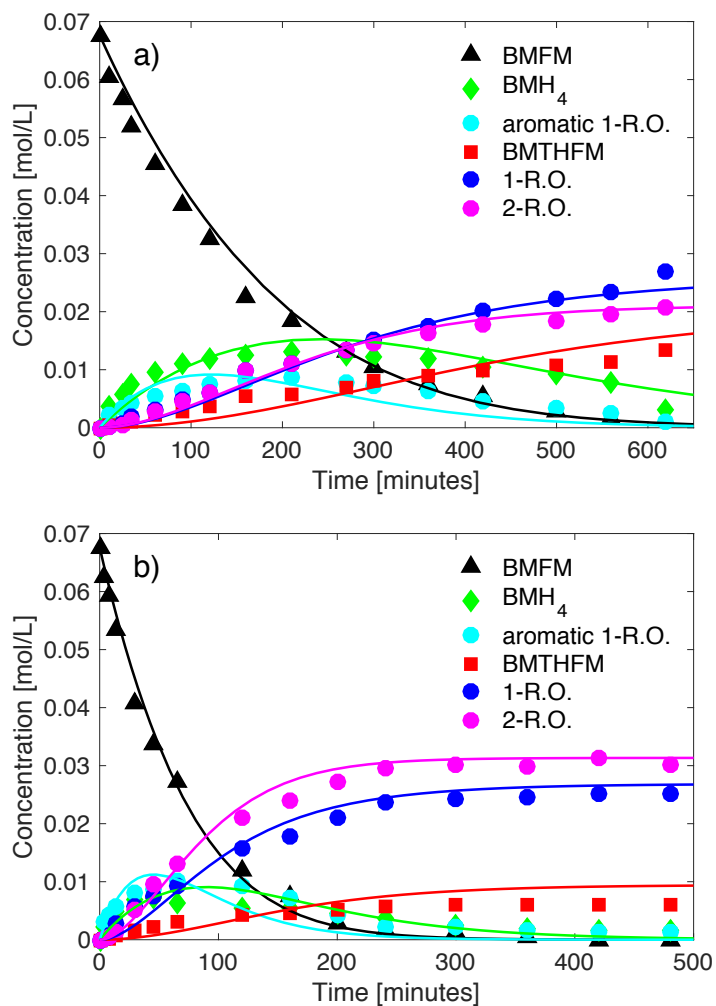
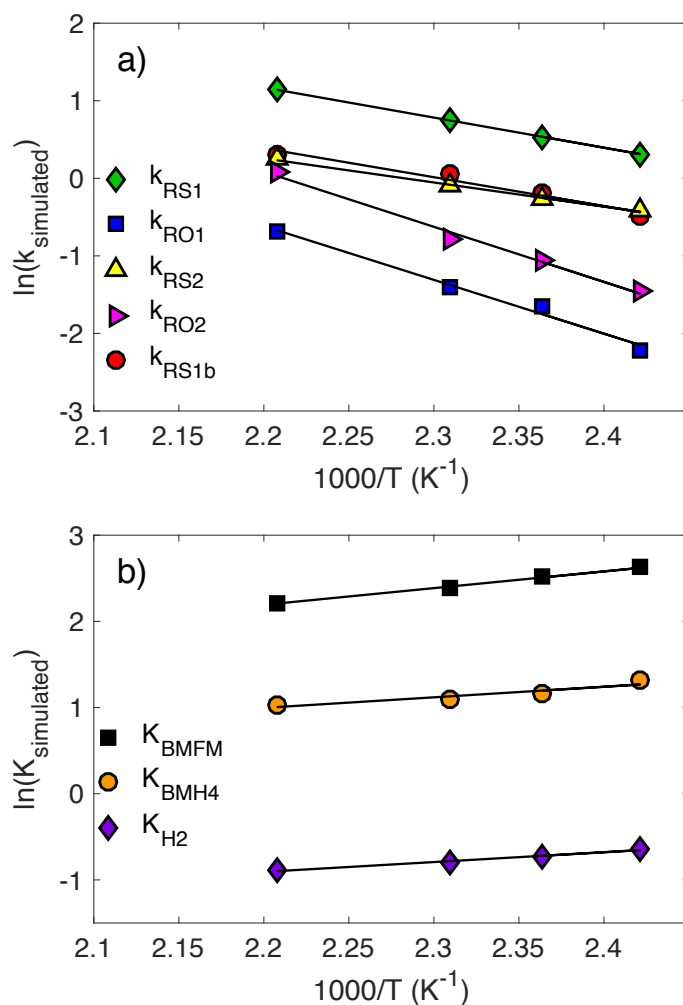


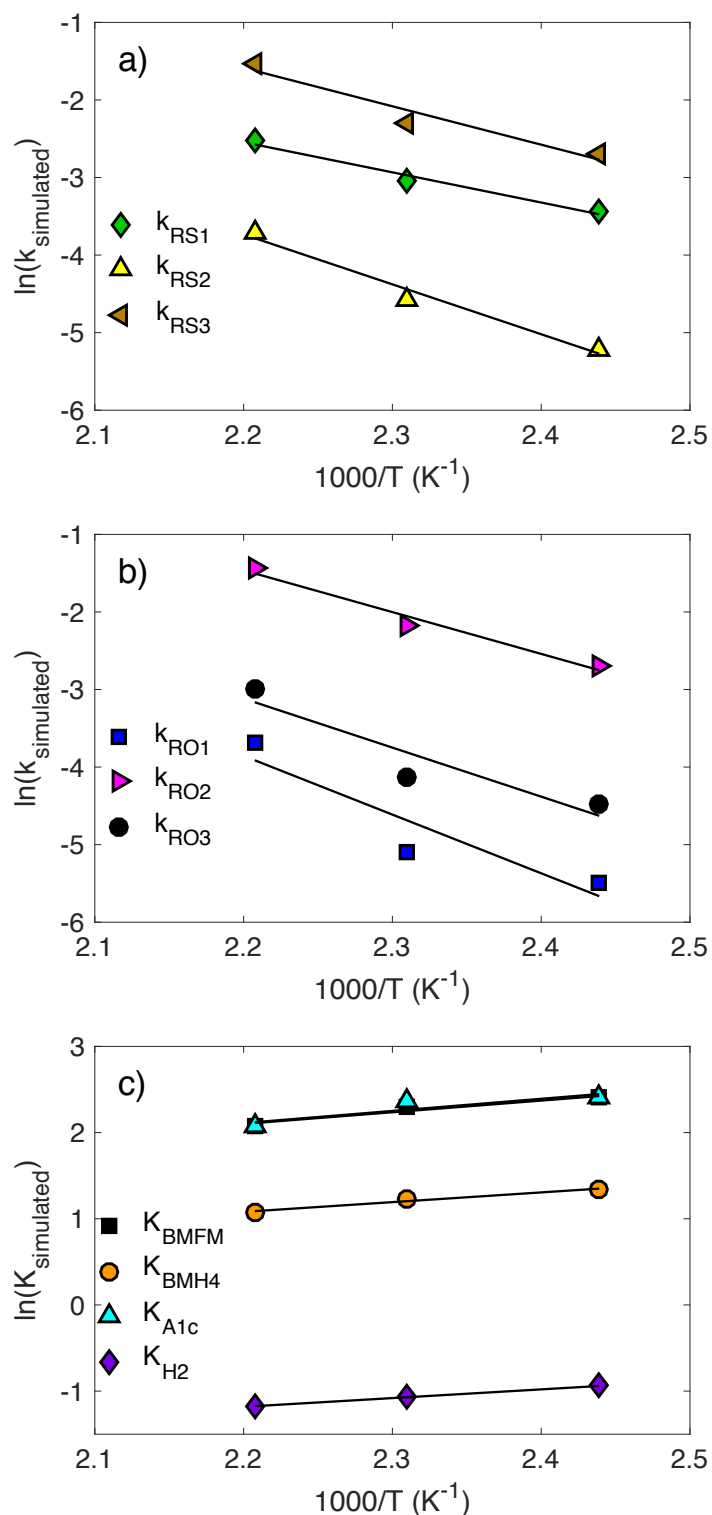
Figure S. 4.10 Comparison of experimental and fitted concentration profiles for all products in Scheme 4.3 during BMFM hydrogenation over 1% Pd/C at temperatures a) 413K , b) 423K and c) 453K. Reactions performed at 1.0 – 1.2 MPa H<sub>2</sub>, 2.8mmol in octane. Model fit: solid lines. Measurement: symbols.



**Figure S. 4.11. Comparison of experimental and fitted concentration profiles for all products in Scheme 4.2 during BMFM hydrogenation over 5% Pt/C at temperatures a) 413K and b) 453K.**  
 Reactions performed at 1.0 – 1.2 MPa H<sub>2</sub>, 2.8mmol in octane. Model fit: solid lines. Measurement: symbols.



**Figure S. 4.12. Arrhenius plots of estimated rate parameters fitted through the proposed kinetic model for Scheme 4.3 of BMFM hydrogenation over Pd/C at temperatures (413K – 453K).**  
 a) Rate coefficients of all kinetically relevant reactions in the network. b) Equilibrium constants for the adsorption of BMFM, BMH<sub>4</sub>, and dissociative adsorption of H<sub>2</sub>.



**Figure S. 4.13. Arrhenius plots of estimated rate parameters fitted through the proposed kinetic model for Scheme 4.2 of BMFM hydrogenation over Pt/C at temperatures (413K – 453K).**  
 a) Rate coefficients of ring saturation (RS) pathways in the network, b) Rate coefficients of ring opening (RO) pathways in the network. c) Equilibrium constants for the adsorption of BMFM, BMH<sub>4</sub>, aromatic 1-R.O. products, and dissociative adsorption of H<sub>2</sub>.

## 5 Selective Hydrogenation of Nucleophilic Condensation Products

### 5.1 Introduction

The conversion of lignocellulosic biomass to liquid fuels poses environmental advantages by reducing CO<sub>2</sub> greenhouse gas emissions from the transportation sector. Biomass-derived fuels can be considered CO<sub>2</sub>-neutral since CO<sub>2</sub> generated from combustion of these fuels is consumed within the cycle to generate additional biomass for fuels [2]. Lignocellulosic biomass is rich in carbohydrate sugars, cellulose and hemicellulose (70-75%), which can be converted into C<sub>6</sub> and C<sub>5</sub> furan compounds, hydroxymethylfurfural (HMF) and furfural (FUR) via dehydration in acid-catalyzed treatments. The carbon chain length of these furanic products is too short for jet or diesel fuel applications, which require C<sub>8</sub> – C<sub>16</sub> and C<sub>9</sub> – C<sub>21</sub>, respectively. Therefore, HMF and FUR are often upgraded to larger organic molecules via condensation of these platform compounds and other biomass-derived compounds, such as 2-methylfuran or methylketones in acid catalyzed hydroalkylation reactions [10–12] and base catalyzed aldol condensation reactions [8,9], respectively.

In order to produce candidate fuel with appropriate combustion properties (e.g., octane or cetane number), these furanyl condensates must undergo hydro-treatment in order to saturate any double bonds and to remove all or some the oxygen content. The reaction network and kinetics of hydrogenation for simple aromatic furans, such as 2,5-dimethylfuran (DMF), and for complex condensates from acid-catalyzed hydroalkylation reactions, such as bis(5-methylfuran-2-yl)methane (BMFM), over Pt and Pd metals have been discussed in earlier chapters. In this chapter, the hydrogenation of 5-(2-(5-methylfuran-2-yl)vinyl)furan-2-aldehyde (MFVFAL), a dimer product from the base-catalyzed condensation reactions of 5-MF, over Pt/C and Pd/C is investigated. MFVFAL contains two incongruent aromatic furan rings and other functional group moieties common in based catalyzed condensation reactions such as conjugated furanyl and C=C systems, and furanyl aldehydes.

The aim of the present study is to understand the hydrogenation of the different functionalities in MFVFAL over Pt- and Pd-based catalysts. We would also like to identify catalysts and reaction conditions that promote selective hydrodeoxygenation (HDO) of the C=O bond in the aldehyde groups of MFVFAL and subsequent selective saturation of the aromatic ring to form cyclic ethers. These cyclic ethers have derived cetane numbers (DCN) that are comparable to those of alkanes but require a lower hydrogen input for their production (See Table 1.1). The conversion of MFVFAL into cyclic ether product requires a HDO catalyst that can selectively cleave the C-O bond and remove the oxygen atom of the aldehyde functional group while keeping the C-O bond inside the furan ring intact.

The reaction network for hydrogenation and HDO of substrates as complex as MFVFAL has not been explored. Selective HDO of simpler furanyl aldehydes such as HMF and FUR into DMF and 2-MF, respectively, has been attempted in alcohol solvents using noble metal based catalysts such as Pd/C [92,93], Ru/C [94,95], Pt/C [96]. These reactions provided moderate yields of deoxygenated product (50-75%) due to undesired side reactions occurring before and after hydrodeoxygenation, such as etherification, decarbonylation, and ring hydrogenolysis. One of the approaches to improving the yields of 2-MF and DMF during hydrodeoxygenation of FUR and HMF, respectively, is to employ bimetallic catalysts that can improve the selectivity for

hydrodeoxygenation of the furanyl aldehyde [97,98]. The incorporation of an additional metal influences geometric, electronic, and adsorption properties of its monometallic analog. Prior work has shown that addition of non-noble metals, such as Au, Co, Cu, Ni, and Fe, to hydrogenation noble metal catalysts discussed earlier has resulted in greater selectivity for C=O reduction to C-OH and for hydrodeoxygenation [25,96,99–101]. Employment of these non-noble metals alone in the conversion of HMF to DMF resulted in poor catalytic activity and deactivation [102].

In addition to Pd/C and Pt/C catalysts, we have synthesized Pd alloy catalysts containing Cu, Ni, or Fe metal in order to understand the influence of bimetallic materials on the hydrogenation network of MFVFAL. Catalysts containing Cu or Fe metal along with Pd resulted in greater selectivity to HDO products than catalysts containing Pd or Cu only. The HDO of a similar but simpler substrate to MFVFAL, 5-methylfurfural (5-MF) was performed in order to determine optimal operating conditions for selectively removing the C=O group of furan aldehydes. The optimal conditions were determined to be 5.2 MPa H<sub>2</sub>, 453 K and were applied during selective HDO studies of MFVFAL over noble metal and Pd alloy catalysts.

## 5.2 Experimental

### 5.2.1 Chemicals and catalysts

5-methylfurfural (5-MF), furfural (FUR), benzaldehyde were purchased from Sigma-Aldrich. Ethanol solvent (200 proof) was purchased from Koptec. Molecular sieves (Grade 564, Type 3A) were obtained from Fisher Chemicals. Potassium phosphate, K<sub>3</sub>PO<sub>4</sub>, was purchased from Arcos Chemicals, was prepared by calcining the oxide material at 873 K in static air in a muffle furnace. The furnace was heated to the desired temperature at a ramp rate of 2 K/min, held for 2 h, and then cooled to 423 K before catalysts was removed from the oven and stored.

Pd/Carbon (1wt%), Pt/Carbon (5wt%), and Ru/Carbon (5wt%) were purchased from Sigma-Aldrich. All catalysts were sieved to < 25 μm prior to use. Carbon supported Pd alloys were synthesized using 1% Pd/C catalyst with the following metal nitrate precursors: Cu(NO<sub>3</sub>)<sub>2</sub>·2.5H<sub>2</sub>O, Ni(NO<sub>3</sub>)<sub>2</sub>·6H<sub>2</sub>O, and Fe(NO<sub>3</sub>)<sub>3</sub>·9H<sub>2</sub>O via the incipient wetness procedure adapted from Wang et al [96]. In short, the metal nitrate was dissolved in ethanol and added to carbon support containing 1wt% Pd via incipient wetness impregnation for a total metal loading of 2 wt%. 15% Cu/SiO<sub>2</sub> was prepared by the same procedure using Cu(NO<sub>3</sub>)<sub>2</sub>·2.5H<sub>2</sub>O and silica gel (pore size 60 Å, 230-400 mesh, Sigma-Aldrich). All prepared catalysts were dried at room temperature overnight, hydrogenated in 10% H<sub>2</sub>/Ar at 673K for 2 h at 2 K/min and then at 773 for 2h at 1 K/min. All commercial catalysts were hydrotreated in the same way prior to experiments.

The number of active metal sites available on commercial noble metal catalysts and on the synthesized materials were quantified by CO chemisorption at 313K using a Micromeritics AutoChem 2920 Pulse Chemisorption System. Prior to CO exposure, the catalyst was pretreated in flowing H<sub>2</sub> (10% in He) at 50mL/min for 1 h at 523K. The number of moles of CO titrated per mass of catalyst was the metric used to normalize catalyst loading for reactions.

### 5.2.2 Synthesis of substrates via nucleophilic addition

The synthesis procedure of MFVFAL, discussed in Chapter 2, was scaled up in order to produce enough starting material for hydrogenation studies. For the synthesis of MFVFAL, 48.6g of 5-MF dissolved in 420 mL of ethanol, 16.3 g K<sub>3</sub>PO<sub>4</sub>, and 16.3 g of grounded molecular

sieves were added into a 1L round bottom flask and heated to 338 K under N<sub>2</sub>. Reaction was carried out at 338 K, under N<sub>2</sub> atmosphere, for 6 h before cooling to room temperature. The resulting viscous red-brown product solution was diluted with 200 mL of ethyl acetate and filtered to remove all solid materials. The product filtrate was transferred to a 1 L round bottom flask and solvents, ethanol and ethyl acetate, were removed by rotary evaporation at 40 mbar and 313 K. Excess 5-MF in the mixture was first removed by vacuum distillation at 3 mbar, 343 K. The dimer product, MFVFAL, in the product mixture was isolated using flash-column chromatography on silica gel and 1:6 ethyl acetate:hexane solution as eluent. Fractions containing MFVFAL were collected and MFVFAL was purified via crystallization. MFVFAL was isolated as yellow-orange crystals and characterized by NMR spectroscopy, FTIR spectroscopy, and mass spectrometry.

### 5.2.3 Catalytic Hydrogenation

Semi-batch hydrodeoxygenation of 5-methylfurfural (5-MF) to 2,5-dimethylfuran (DMF) was conducted in a HEL ChemScan high-pressure parallel reaction system equipped with eight 16 mL, independently controlled Hastelloy autoclave reactors. Reactors were loaded with a solution containing 0.25 mol% catalyst to 5-MF, 200 mg 5-MF, 1.8 g ethanol solvent, and 50 mg dodecane as an internal standard. The reactors were purged three times with N<sub>2</sub> and twice with H<sub>2</sub> prior to loading 3.0 MPa H<sub>2</sub> and heated to reaction temperature. Reactors were operated at pressures ranging from 3.0 MPa to 5.5 MPa H<sub>2</sub>, and temperatures ranging from 333 K to 393 K for 4h. After reaction, the reactors were removed from the heating unit and cooled to room temperature, after which the reactors were vented and their contents collected. Solid catalyst was separated from the reaction mixture by centrifugation and the resulting liquid was diluted with acetone to reach a concentration suitable for quantification by GC/MS.

Semi-batch hydrogenations of MFVFAL and other substrates were conducted in a 100 mL Parr Series 4590 Bench Top Micro Reactor equipped with a sampling dip tube, thermocouple, and an external gas burette containing H<sub>2</sub> (99.99% Praxair). A regulator located at the base of the gas burette maintained the pressure within the reactor at the value set. For each reaction, the reactor was initially loaded with 0.16 mol% metal catalyst to substrate, MFVFAL (200 mg) dissolved in ethanol (35 mL), and dodecane (30 mg) as internal standard. Reactors were purged three times with N<sub>2</sub> and twice with H<sub>2</sub> before loading 4.2 MPa of H<sub>2</sub> and heating to 453 K over 25 min. Each reactor was maintained a total pressure of 5.5 MPa for the duration of reaction. On-line sampling of the reacting solution was achieved through the dip-tube, and product sampling was driven by the pressure difference between the reactor contents and atmosphere. Each sample passed through a condenser and was collected in an Eppendorf tube (0.4 mL). The catalyst contained in the sample was separated from the reaction mixture by centrifugation, and the residual liquid was collected for quantification by GC/MS. Carbon balances for all experimental measurements were within 89-99%.



## 5.3 Results and Discussion

### 5.3.1 Characterization of catalysts

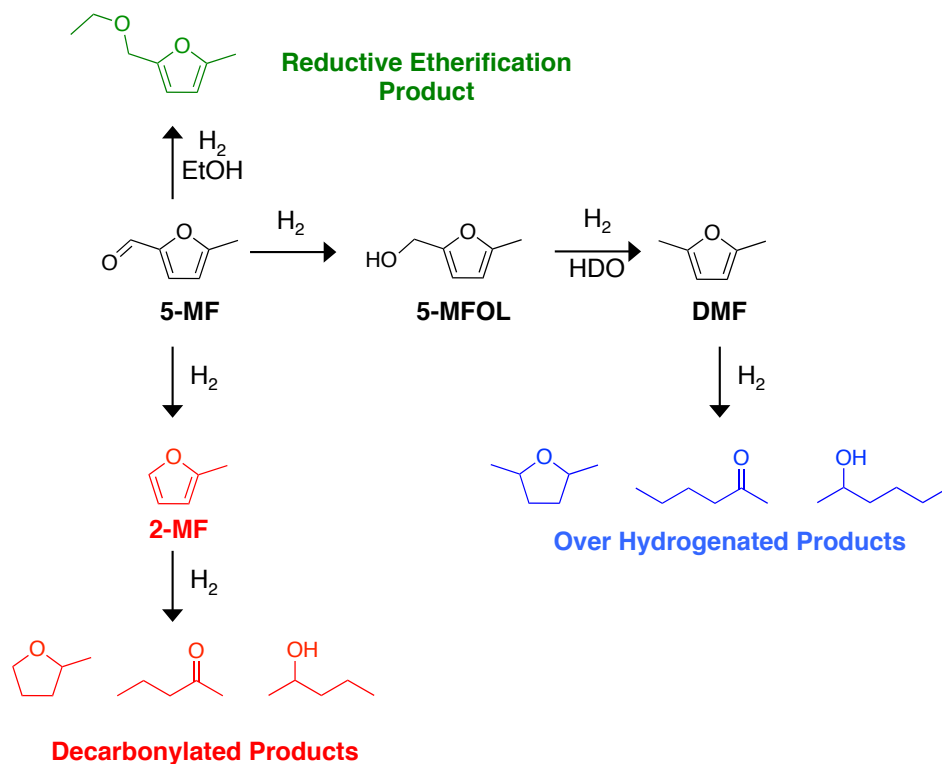
**Table 5.1** CO chemisorption at 310 K to titrate and quantify metal sites.

	(mol CO/g cat) x10 <sup>5</sup>
<b>5% Pt/C</b>	6.3
<b>5% Ru/C</b>	9.9
<b>1% Pd/C</b>	2.4
<b>2% PdCu/C</b>	2.2
<b>2% PdNi/C</b>	2.3
<b>2% PdFe/C</b>	0.96
<b>15% Cu/SiO<sub>2</sub></b>	0.65

The method chosen for synthesis of PdCu, PdNi, and PdFe bimetallics involved incipient wetness impregnation preparation of commercial Pd/C [96]. All catalysts were subjected to identical hydrogenation reduction at 673-773K. After reduction, the metal dispersion of the commercial catalysts: Pd/C, Pt/C, and Ru/C decreased by only 5-7% and the particle size of the dispersed metal remained < 5 nm, indicating that the H<sub>2</sub> treatment post-impregnation of Cu, Ni, and Fe on 1% Pd/C did not affect the size of the original Pd nanoparticles. CO titration via chemisorption analysis was used to determine the number of active metal sites (Table 5.1).

### 5.3.2 Selective HDO of 5-MF over noble metal catalysts

Prior to investigating the hydrodeoxygenation of MFVFAL over noble metal catalysts, we investigated the conversion of a simpler furanyl aldehyde, 5-methylfurfural (5-MF) to 2,5-dimethylfuran (DMF). 5-MF contains 2 functional groups, aromatic furan and aldehyde, also present in MFVFAL. 5-MF was dissolved in ethanol and hydrogenated at 453 K and 2.75 MPa H<sub>2</sub> over the series of catalysts listed in Table 5.1. The main product for all reactions was the deoxygenated product of 5-MF, DMF. 5-methylfurfuryl alcohol (MFOL) was observed in low yields (2-10%) and is likely to be the intermediate product prior to hydrodeoxygenation to DMF [37,99,102]. Over hydrogenated products such as 2,5-dimethyltetrahydrofuran, 2-hexanone, and 2-hexanol were also observed. These products resulted from hydrogenation and hydrogenolysis of the aromatic ring of DMF, as described in our earlier studies using Pd/C and Pt/C [80]. Other by-products observed during HDO of 5-MF include C<sub>5</sub> species, such as 2-methylfuran, produced from decarbonylation reaction of the aldehyde functionality, and 2-(ethoxymethyl)-5-methylfuran, produced by reductive etherification reaction between 5-MF and ethanol solvent. These products and the rest of the hydrodeoxygenation network of 5-MF are shown in Scheme 5.1.



**Scheme 5.1** Hydrogenation/hydrodeoxygenation network of 5-methylfurfural (5-MF) over noble metals

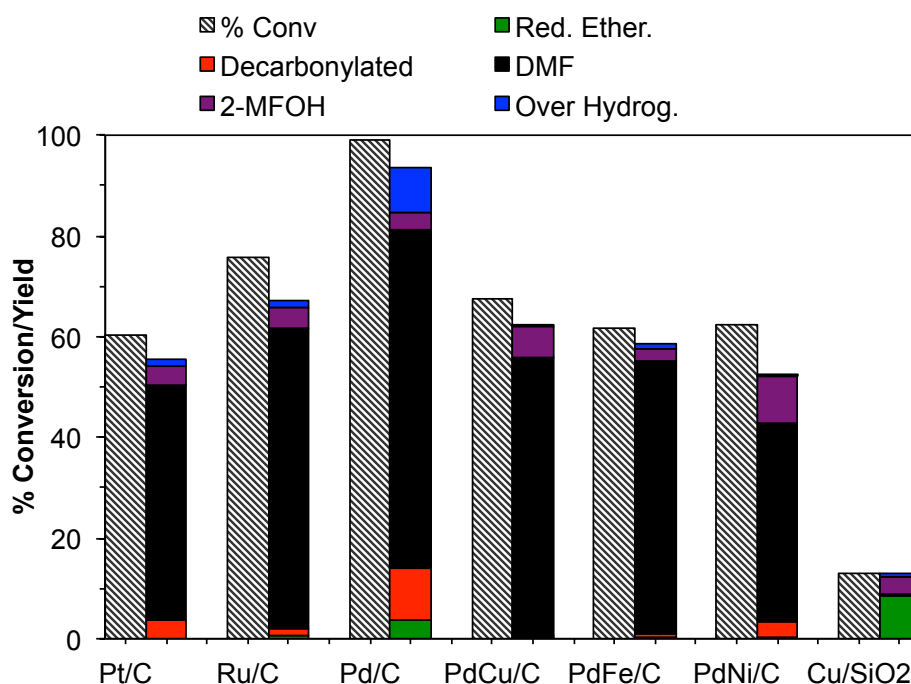
The conversion of 5-MF and yields of products after 4h of reaction for the hydrogenation metal catalysts are shown in Figure 5.1. Among the catalysts studied, Pd/C was the most active - achieving over 98% conversion of 5-MF in 4 h. Less active Pd-based alloys resulted in 60-67% conversion of 5-MF under the same reaction conditions. It is likely that formation of alloys between Pd and metals resulted in a decrease of available Pd sites. PdCu alloys, and Cu and Ni metals have been found to be inherently less active than Pd metals for the hydrodeoxygenation of FUR into 2-MF [64,101] and for conversion of HMF into DMF [102].

Although Pd/C was the most active catalyst for hydrogenation of 5-MF, its selectivity to DMF was lower than that of the remaining alloys and noble metals catalysts (See Table 5.2). Decarbonylation and reductive etherification of 5-MF, and ring saturation reactions of DMF into 2,5-dimethyltetrahydrofuran are significant over Pd/C and resulted in undesired byproducts. Pd/C has been reported to be highly active for saturation of aromatic furans [64,80] and for reductive etherification of aldehydes with primary alcohols [13]. Decarbonylation of 5-MF occurred over Pd/C, resulting in 10% selectivity to 2-MF and other C<sub>5</sub> species. This is significantly lower than the 75% selectivity to decarbonylation observed in vapor phase studies of furfural over Pd/C at 483 K [64]. Hydrogenation in liquid phase systems, at lower temperatures, and at higher hydrogen partial pressure has been found to reduce decarbonylation of aromatic aldehydes over noble metal catalysts [37].

With the exception of Cu/SiO<sub>2</sub>, all metal hydrogenation catalysts were active for the HDO of 5-MF to DMF (Figure 5.1), Cu/SiO<sub>2</sub> was not very active – resulting in <13% conversion for a 100% higher catalyst loading than that used for reactions with other catalysts (Figure 5.1). The main products formed during hydrogenation over Cu/SiO<sub>2</sub> were furanyl ethers and MFOL, at 66% and 27% selectivity, respectively. DMF was produced at <2% selectivity (Entry 7, Table

5.2). Cu/SiO<sub>2</sub> has been reported to deactivate quickly during the conversion of HMF to DMF [102], and was also observed in our system based on the color change of the catalyst after 4 h.

Higher selectivities to DMF (81-87%) were achieved over Pd alloys, PdFe and PdCu (Table 5.2) than over Pd/C or Cu/SiO<sub>2</sub>. 5-MF hydrogenation over bimetallic PdCu and PdFe nanoparticles resulted in lower yields of decarbonylation products, reductive etherification products, and over hydrogenation products compared to Pd/C. As reported in literature, incorporation of Cu and Fe into the hydrogenation catalysts significantly improved the selectivity for deoxygenation but lowered the hydrogenation activity [100,101]. For example, increasing the Cu content in PdCu/SiO<sub>2</sub> resulted in less decarbonylation and etherification, and greater activity toward C=O reduction of FUR to furfuryl alcohol, an intermediate to the HDO product, 2-MF [101].



**Figure 5.1** Conversion and product distribution of hydrogenation of 5-MF over noble metal catalysts. Reaction conditions: 0.25 mol% M/C to 5-MF, 200mg 5-MF, 2 mL EtOH, and 30mg dodecane, 453K, 2.8 MPa H<sub>2</sub>, 4h

**Table 5.2.** Conversion of 5-MF and selectivity to DMF and to decarbonylation.

Reaction conditions: 0.25 mol% M/C to 5-MF, 200mg 5-MF, 2 mL EtOH, and 30mg dodecane, 453K, 2.8 MPa H<sub>2</sub>, 4h

Entry	Catalysts	Pressure (MPa)	Temp. (K)	% Conv.	(%S) DMF	(%S) Decarbonyl.
1	Pt/C	2.8	453	60.2	77.4	6.3
2	Ru/C	2.8	453	75.7	78.6	2.1
3	Pd/C	2.8	453	98.9	67.7	10.3
4	PdCu/C	2.8	453	67.5	81.7	0.6
5	PdNi/C	2.8	453	62.2	63.5	4.6
6	PdFe/C	2.8	453	61.6	87.7	1.1
7	Cu/SiO <sub>2</sub>	2.8	453	12.9	1.7	0

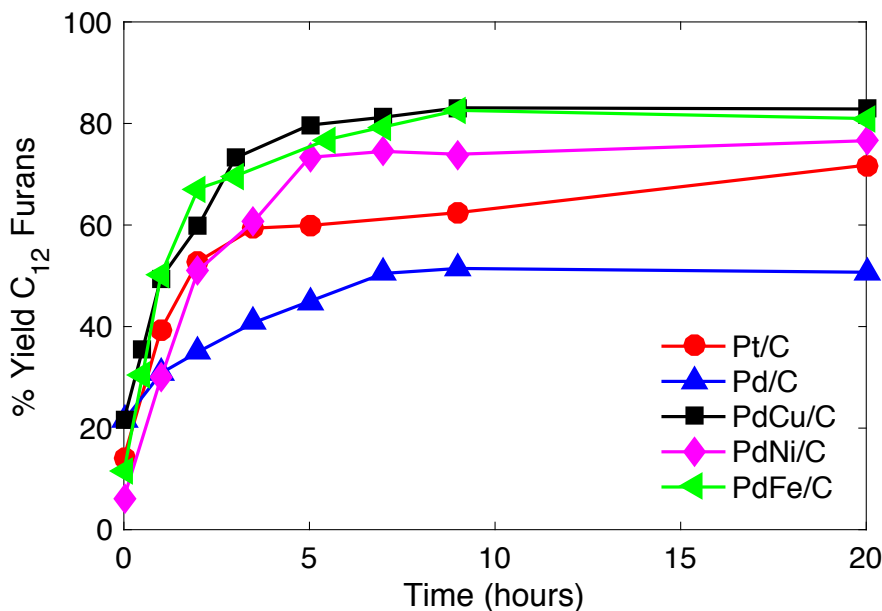
<b>8</b>	PdCu/C	3.4	453	85.6	85.2	0.2
<b>9</b>	PdCu/C	5.2	433	98.0	72.7	0.2
<b>10</b>	PdCu/C	5.2	453	99.7	91.5	0.8
<b>11</b>	PdCu/C	5.2	473	100	78.2	1.0

Reactions conditions explored to improve the selectivity and yields of production of DMF from 5-MF were temperatures 433K – 473 K and 2.75 – 5.2 MPa (Entries 8-10, Table 5.2) over PdCu/C. Rates of reaction increased with  $p_{H_2}$  and we were able to achieve 100% conversion of 5-MF at 5.2 MPa  $H_2$  in 4h. 5-MF hydrogenation rates also increased as a function of temperature and maximum selectivity for DMF (> 91%) was achieved at 453K. Decarbonylation over PdCu/C was still insignificant (<1% selectivity) at 473 K. The lower selectivity to DMF observed at 473 K in comparison to at 453 K was due a greater degree of over hydrogenated products, 2,5-dimethyltetrahydrofuran, 2-hexanone, and 2-hexanol. Since high conversion and selectivity to HDO product was achieved at 453 K and 5.2MPa, these reaction conditions were applied for the hydrogenation studies of MFVFAL.

### 5.3.3 Selective HDO of MFVFAL over noble metal catalysts

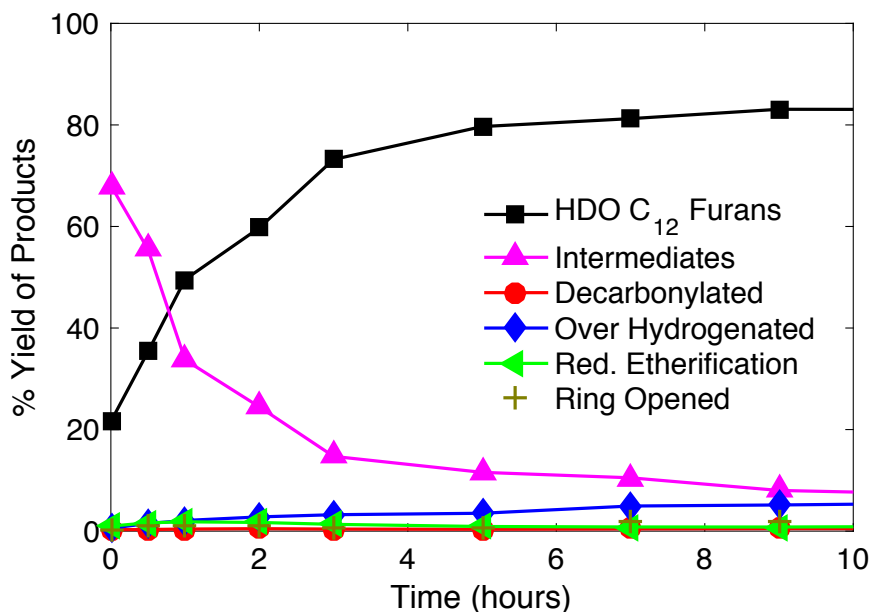
The hydrogenation of MFVFAL over noble metal and Pd metal alloys was monitored over a period of 20 h (453 K, 5.2 MPa) by periodically sampling the contents of the autoclave. The reactor was initially loaded with 4.1 MPa  $H_2$  and the first sample ( $t = 0$ ) was collected after 25 min during which time the autoclave was heated from room temperature to 453 K. All catalysts, with the exception of Pt/C and Cu/SiO<sub>2</sub>, readily hydrogenated the C=C bond of MFVFAL during heat up and little starting material (<3%) remained in the first sample collected ( $t = 0$ ). In contrast to Pt/C, 35% of the MFVFAL remained in solution after heat up. As discussed in earlier chapters, Pt catalysts have a lower activity for C=C hydrogenation compared to Pd but have a higher activity for C=O hydrogenation [85,86]. During hydrogenation over Pt/C, we observed products where the C=O was reduced prior to hydrogenation of the interior C=C bond of MFVFAL. Such products were not detected over Pd/C, Ru/C, or Pd alloys since C=C hydrogenation occurred more readily than C=O reduction.

The desired products in our hydrogenation studies are **(3)** (Scheme 5.2) and C<sub>12</sub>, dual furan ring-containing oxygenates, formed by selectively removing the O atom of the C=O of MFVFAL while maintaining the C-O bond inside the furan ring intact for subsequent ring saturation into cyclic ethers. The production of HDO product **(3)**, at various degrees of ring saturation, as a function of reaction time over different hydrogenation metal catalysts is shown in Figure 5.2. All catalysts were active in the HDO of the aldehyde group of MFVFAL. 5-20% yield of deoxygenated C<sub>12</sub> furans **(3)** were observed in the first sample ( $t = 0$ ) collected after heating reactor contents from room temperature to 453 K in 25 min. Final yields of **(3)** after 20h of reaction over Pd/C and Pt/C catalysts (50-72% yield) were much lower than those obtained over Pd alloys (76-82% yield).



**Figure 5.2.** Production of selective HDO products over time during hydrogenation of MFVFAL over noble metal and Pd alloy catalysts.

Reaction conditions: 0.16 mol% metal catalyst to MFVFAL, MFVFAL (200 mg) dissolved in ethanol (35 mL), dodecane (30 mg), 453 K, 5.2 MPa, 20h



**Figure 5.3.** Product distribution as a function of time for MFVFAL hydrogenation over PdCu/C catalysts.

Reaction conditions: 0.16 mol% metal catalyst to MFVFAL, MFVFAL (200 mg) dissolved in ethanol (35 mL), dodecane (30 mg), 453 K, 5.2 MPa, 10h

The transformation of MFVFAL over PdCu/C into various product groups shown in Scheme 5.2 for the first 10h of reaction is shown in Figure 5.3. The key intermediates to selective HDO of the C=O group of MFVFAL were identified as species **(2a)** and **(2b)**, products resulting from hydrogenation of C=C bond and subsequent reduction of the C=O bond,

respectively. At  $t = 0$ , these species accounted for over 40% yield of the intermediates and steadily declined over the course of reaction. Based on the initial formation and disappearance of the furanyl alcohol species (**2b**), we suspect that (**2b**) is the intermediate that leads to selective hydrodeoxygenation and formation of C<sub>12</sub> furanyl oxygenates, (**3**). Furfuryl alcohol and 2,5-bishydroxymethylfuran have often been proposed to be the intermediates in the hydrodeoxygenation of FUR to 2-MF and HMF to DMF, respectively [64,99,102,103].

Unlike 5-MF, MFVFAL contains two incongruent aromatic rings - one adjacent to an electron donating methyl group and the other adjacent to an electron withdrawing aldehyde group. We observed intermediates (**2c**), for which the furan ring adjacent to the methyl group was hydrogenated first before selective HDO of the C=O group occurred. Electron-donating substituents attached to aromatic groups promote hydrogenation more than electron-withdrawing substituents due to the  $\pi$  electron delocalization [104]. Selective HDO of the C-OH group adjacent to the remaining aromatic ring of (**2c**) converts (**2c**) to half-hydrogenated C<sub>12</sub> oxygenate (**3b**).

The products resulting from hydrogenation of the furan ring adjacent to an electron withdrawing group, C=O or C-OH, are classed as over-hydrogenated products (**6**) and not as intermediates to (**3**). The yield of (**6**) increases over the course of reaction because the HDO of (**6**) is more difficult the ring is hydrogenation and aromaticity is lost. The importance of the aromatic furan ring for HDO of its adjacent aldehyde group is demonstrated by comparing the yields of HDO products obtained when furfural (FUR) and tetrahydrofurfuryl alcohol (THFOL) were used as substrates. Under the same set of reaction conditions, only 5% of THFOL was converted to 2-methyltetrahydrofuran whereas 42% of HDO products (2-methylfuran and 2-methyltetrahydrofuran) were achieved through the HDO of furfural (Table 5.3). The low yield of HDO products obtained when THFOL was used as substrate indicates that the saturated species is not an intermediate to HDO and the aromaticity of the ring adjacent to the aldehyde allows for selective HDO of the C=O group. Other groups have observed that activity for HDO of benzaldehyde species over Pd or Cu catalysts was significantly reduced when the distance between the aldehyde and the aromatic ring [105,106]. Therefore, in order to maintain high yields and selectivity to HDO products (**3**), we aim to minimize the formation of over hydrogenated species (**6**).

**Table 5.3.** Hydrodeoxygenation of furfural and tetrahydrofurfuryl alcohol over PdCu/C catalysts.

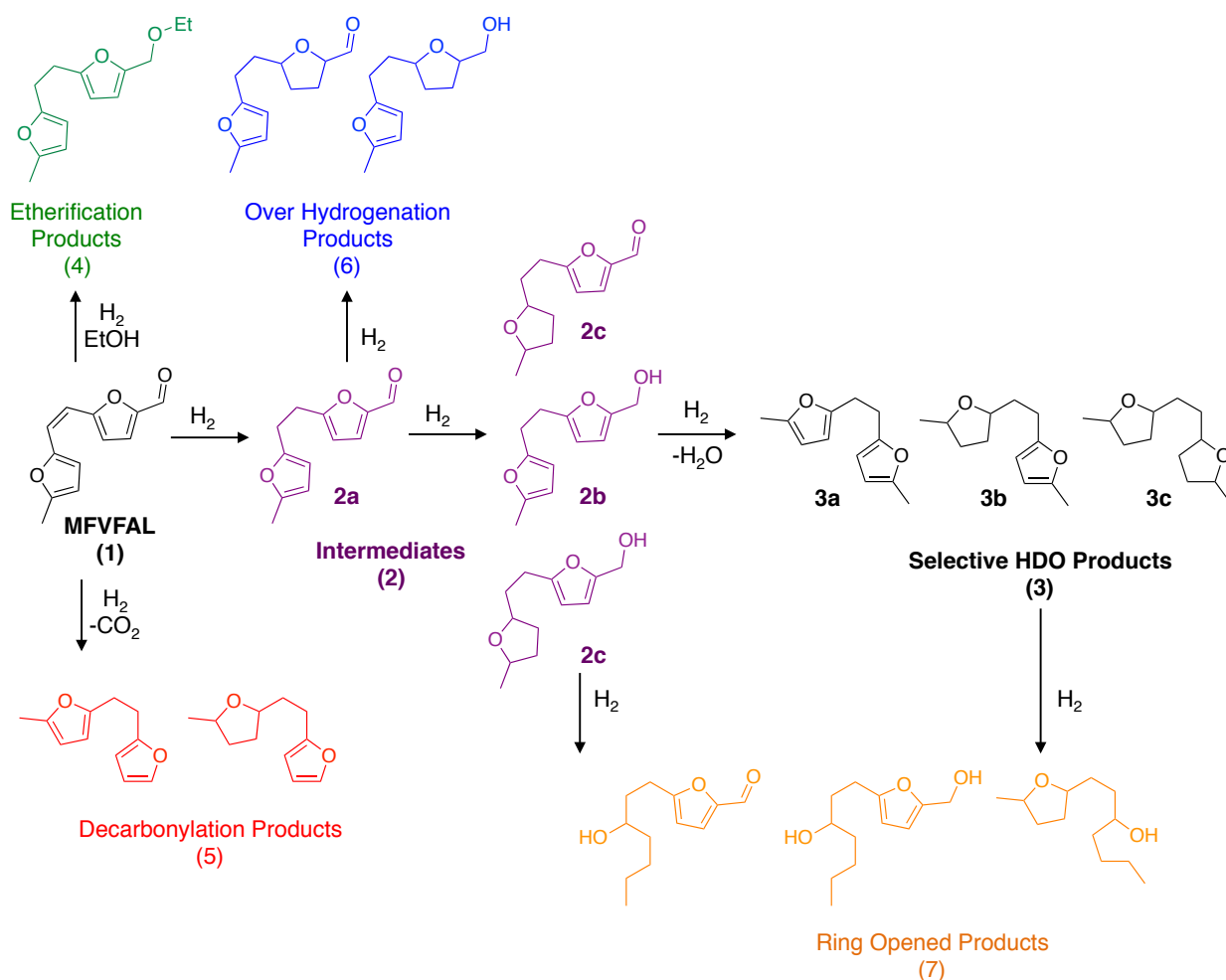
Substrate	% Conversion	% HDO products <sup>a</sup>	% Others <sup>b</sup>
Furfural	60	42	18
Tetrahydrofuryl alcohol	5	5	0

<sup>a</sup> - HDO products include 2-methylfuran and 2-methyltetrahydrofuran

<sup>b</sup> - Others include tetrahydrofurfuryl alcohol, furfuryl alcohol, 2-ethoxymethylfuran

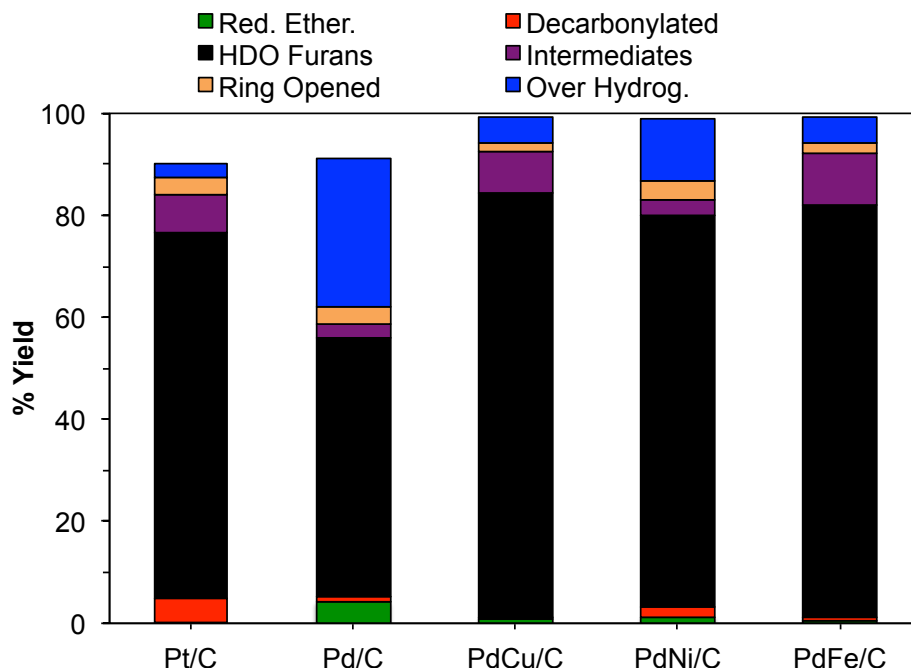
In addition to over hydrogenation of the furanyl aldehyde, other undesired side reactions were identified within the reaction network. These include reductive etherification of the C=O group and ethanol, the solvent, to form ethers (**4**), decarbonylation of the C=O group to form CO, which results in C<sub>11</sub> oxygenates (**5**), such as 2-(2-(furan-2-yl)ethyl)-5-methylfuran, and ring-opening hydrogenolysis of intermediates (**2**) or deoxygenated products (**3**) forms species (**7**). We learned from our earlier studies of DMF and BMFM hydrogenation that aromatic furans could be cleaved to form ketone or alcohol functionalities over Pd and Pt. Since alcohol products have lower cetane values than their analogous cyclic ethers [17], ring cleavage is highly undesirable.

We aim to maximize C-O hydrogenolysis of the aldehyde group while avoiding C-O hydrogenolysis of the aromatic ring.



**Scheme 5.2.** Reaction network for MFVFAL Hydrogenation/hydrodeoxygenation in ethanol over noble metal catalysts

The proposed reaction network for MFVFAL hydrodeoxygenation into 7 product categories is shown in Scheme 5.2. The yields of products (2-7) after 20 h of reaction over hydrogenation metal catalysts are shown in Figure 5.3. The highest yields of selective HDO products (3) were achieved over PdCu/C and PdFe/C. The low selectivity to (3) achieved over Pd/C was due to over hydrogenation of the furan ring, forming (6) and reductive etherification, forming (4). Pd is known to be more active in ring saturation and in etherification than Pt [13,80].

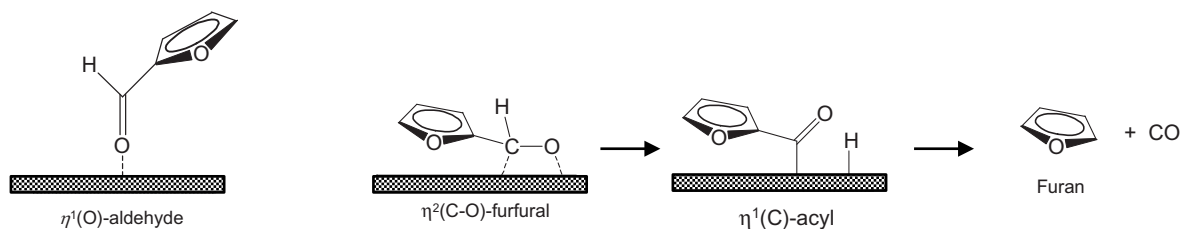


**Figure 3.** Production distribution of MFVFAL hydrogenation after 20h over noble metal and Pd alloy catalysts. Reaction conditions: 0.16 mol% metal catalyst to MFVFAL, MFVFAL (200 mg) dissolved in ethanol (35 mL), dodecane (30 mg), 453 K, 5.2 MPa, 10h

The types of adsorption and interaction between the various functional groups of MFVFAL and the hydrogenation metal surfaces influence the product distribution obtained over these metal catalysts. For instance, Pt, Pd, and PdNi have greater activity for decarbonylation because the carbonyl group adsorbs parallel to the metal surface in a  $\eta^2$ -(C-O) configuration (Scheme 5.3), in which both C and O atoms of the carbonyl group interact with the metal surface. Spectroscopic results and DFT calculations have shown that this is the preferred configuration of aldehydes on Group VIII metals [100,107]. The  $\eta^2$ -(C-O) configuration tends to transform into a more stable  $\eta^2$ (C)-acyl intermediate, where the C atom of the carbonyl is strongly bound to the surface, which is the precursor to decarbonylation of the C=O into CO [64,101,108].

Hydrogenation of MFVFAL over this group of catalysts (Pt, Pd, and PdNi) gave the highest yield of over-hydrogenated products (**6**) or ring-opened products (**7**). Ring opening and hydrogenation of aromatic furans have been previously observed over such metals [37,64,102]. Group VIII metals, such as Pd, Pt, and Ni, interact strongly with furanyl rings due to the overlap between the  $\pi$ -bonds of the aromatic ring with the d-orbitals of the metals [100,107]. These interactions between the furanyl rings and the metal surface need to be reduced in order to minimize C-O cleavage of the ring and improve selectivity to HDO of C=O group.

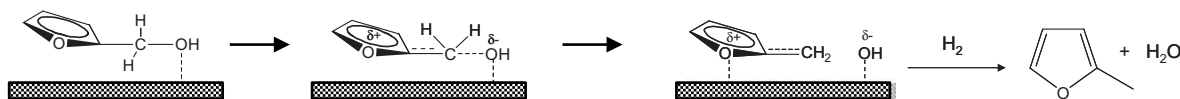




**Scheme 5.3.** Adsorption modes of furfural over hydrogenation metal surfaces as described by Sitthisa et al. [64,101,108]

During hydrogenation over PdCu/C and PdFe/C catalysts, we observed lower yields of products resulting from etherification, decarbonylation, over hydrogenation, and ring opening compared to hydrogenation over Pd/C. The addition of these metals to Pd significantly improved selectivity to **(3)** from 51% over Pd/C to 81-83%. The greater selectivity to HDO products obtained over PdCu bimetallics can be explained by comparing molecular interactions of the various functional groups of MFVFAL with metal surfaces of Pd and Cu. Less ring cleavage and over hydrogenation of the furan rings occur for PdCu catalysts because aromatic furans experience repulsive forces on Cu surfaces in contrast to strong molecular interactions with noble metal surfaces such as Pd [64,101]. Decarbonylation reactions are reduced and C=O reduction reactions to C-OH are promoted over PdCu because the  $\eta^1$ -(O) aldehyde configuration is preferred over the  $\eta^2$ -(C-O) configuration, preventing the formation of the acyl intermediate (Scheme 5.3) [108]. The adsorption of the C=O via  $\eta^1$ -(O) aldehyde configuration was observed to promote the reduction of FUR to furfuryl alcohol [101].

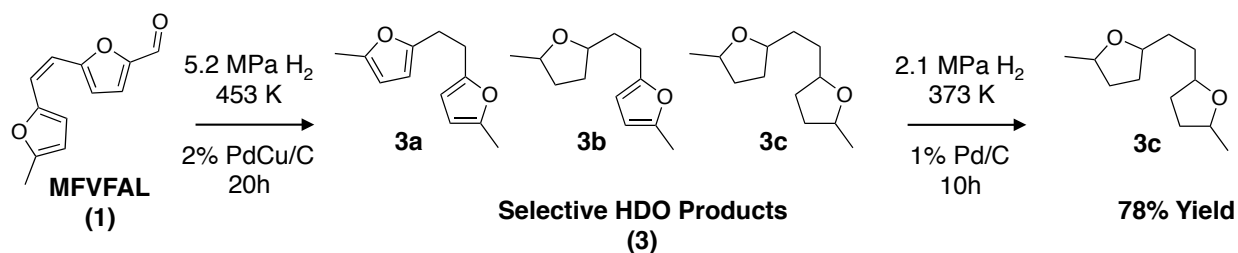
Similarly, the incorporation of Fe into Pd/C promoted both C=O hydrogenation and C-O hydrogenolysis, and suppressed decarbonylation, leading to improved selectivity to HDO products **(3)** as compared to Pd/C. Theoretical calculations for FUR HDO over NiFe catalysts suggest that the oxophilic Fe atoms promoted a stronger interaction between the C=O group and metal surface and increased the stability of the surface  $\eta^2$ -(C-O) species, thereby hindering the formation of acyl surface species, which would lead to decarbonylation of C=O [100]. The oxophilicity of Fe metal has been attributed to be responsible for increased activity for C-O hydrogenolysis reactions [25,100].



**Scheme 5.4.** Possible species on the surface of hydrogenation metal catalysts during conversion of furfuryl alcohol to 2-MF proposed by Sitthisa et al.

We have identified **(2b)**, resulting from the reduction of C=O of MFVFAL, as the intermediate to selective HDO into products **(3)**. Similarly, furfuryl alcohol and 5-methylfurfuryl alcohol have been proposed as intermediates to form 2-MF, and DMF, respectively, in HDO reactions [101,102]. We have also identified that the aromaticity in the ring alpha to the C=O or C-OH group is necessarily for HDO. However, the mechanism by which C-O hydrogenolysis of furanyl alcohol occurs to form a methyl group remains unclear. Sitthisa et al. have suggested the surface intermediates, shown in Scheme 5.4, that may be present during conversion of furfuryl

alcohol to 2-MF but theoretical calculations and spectroscopic evidence to support this intermediate were not presented [100]. The HDO mechanism of furanyl alcohols over reducible metal oxides such as RuO<sub>2</sub> [94] and Co<sub>3</sub>O<sub>x</sub> [36,103] has been proposed to be radical in nature – where C-O scission of the –OH occurs on the surface oxides and forms a radical species and a surface –OH group. However, the HDO mechanism over hydrogenation metals, such as Pt and Pd, has not been addressed. More work remains to understand the deoxygenation of furanyl alcohols over hydrogenation metal surfaces.



**Scheme 5.5.** Two-step selective hydrodeoxygenation/hydrogenation over PdCu/C and Pd/C catalysts for the production of cyclic ethers.

In order to maximize production of the saturated cyclic ether, 1,2-bis(5-methyltetrahydrofuran-2-yl)ethane (BMTHFE, **3c**), from MFVFAL, we propose a two-step selective hydrodeoxygenation/hydrogenation process shown in Scheme 5.5. The first step involves selective HDO of MFVFAL into C<sub>12</sub> furans (**3**) over PdCu/C at 453 K. The second step is the selective ring saturation of aromatic products **3a** and **3b** into BMTHFE over Pd/C at mild hydrogenation conditions (373K, 2.1 MPa H<sub>2</sub>). PdCu/C is required in the first step to minimize over hydrogenation of the rings into (**6**) and to prevent undesired reactions of involving the C=O group of MFVFAL. A second step requiring Pd/C is needed in order to fully saturate the aromatic rings to form BMTHFE because the weak interactions between furans and Cu surface make PdCu a less efficient catalyst for ring hydrogenation than Pd. With our two-step hydro-treatment of MFVFAL, we were able to achieve 78% yield of BMTHFE, a C<sub>12</sub> oxygenate with a high DCN value (See Table 1.1) and potential to be a diesel additive.

#### 5.4 Conclusions

The conversion of 5-(2-(5-methylfuran-2-yl)vinyl)furan-2-aldehyde (MFVFAL) into a high cetane value diesel fuel candidate, 1,2-bis(5-methyltetrahydrofuran-2-yl)ethane (BMTHFE), requires selective deoxygenation of the C=O group, hydrogenation of C=C bonds and aromatic furans. The incorporation of Cu into Pd/C significantly improves selectivity to HDO of MFVFAL by 30% over monometallic Pd/C or Cu/C. The presence of Cu reduces over hydrogenation and ring opening hydrogenolysis of the aromatic rings as well as reducing the decarbonylation and etherification reactions of the C=O group of MFVFAL. We have been able to achieve the selective conversion of MFVFAL to BMTHFE (78% yield) via a two-step hydrogenation process involving both PdCu/C and Pd/C.

## References

- [1] EPA, Sources of Greenhouse Gas Emissions, EPA United States Environ. Prot. Agency. (2015). <https://www.epa.gov/ghgemissions/sources-greenhouse-gas-emissions>.
- [2] Center for Climate and Energy Solutions, Reducing greenhouse gas emission from US transportation, 2011.
- [3] F.H. Isikgor, C.R. Becer, Lignocellulosic biomass: a sustainable platform for the production of bio-based chemicals and polymers, *Polym. Chem.* 6 (2015) 4497–4559.
- [4] D.M. Alonso, J.Q. Bond, J.A. Dumesic, Catalytic conversion of biomass to biofuels, *Green Chem.* 12 (2010) 1493–1513.
- [5] M.E. Dry, The Fischer-Tropsch process: 1950-2000, *Catal. Today.* 71 (2002) 227–241.
- [6] X.W. Zhong He, Hydrodeoxygenation of model compounds and catalytic systems for pyrolysis bio-oils upgrading, *Catal. Sustain. Energy.* (2012) 28–52.
- [7] S. Altun, C. Öner, F. Yaşar, H. Adin, Effect of n-Butanol Blending with a Blend of Diesel and Biodiesel on Performance and Exhaust Emissions of a Diesel Engine, *Ind. Eng. Chem. Res.* 50 (2011) 9425–9430.
- [8] R.M. West, Z.Y. Liu, M. Peter, J.A. Dumesic, Liquid alkanes with targeted molecular weights from biomass-derived carbohydrates, *ChemSusChem.* 1 (2008) 417–424.
- [9] G.W. Huber, J.N. Chheda, C.J. Barrett, J.A. Dumesic, Production of Liquid Alkanes by Aqueous-Phase Processing of Biomass-Derived Carbohydrates, *Science* (80-. ). 308 (2005) 1446–1450.
- [10] A. Corma, O. de la Torre, M. Renz, Production of high quality diesel from cellulose and hemicellulose by the Sylvan process: catalysts and process variables, *Energy Environ. Sci.* 5 (2012) 6328.
- [11] G. Li, N. Li, Z. Wang, C. Li, A. Wang, X. Wang, Y. Cong, T. Zhang, Synthesis of High-Quality Diesel with Furfural and 2-Methylfuran from Hemicellulose, *ChemSusChem.* 5 (2012).
- [12] M. Balakrishnan, E.R. Sacia, A.T. Bell, Syntheses of Biodiesel Precursors: Sulfonic Acid Catalysts for Condensation of Biomass-Derived Platform Molecules, *ChemSusChem.* 7 (2014) 1078–1085.
- [13] M. Balakrishnan, E.R. Sacia, A.T. Bell, Etherification and reductive etherification of 5-(hydroxymethyl)furfural: 5-(alkoxymethyl)furfurals and 2,5-bis(alkoxymethyl)furans as potential bio-diesel candidates, *Green Chem.* 14 (2012) 1626–1634.
- [14] E.R. Sacia, M. Balakrishnan, A.T. Bell, Biomass conversion to diesel via the etherification of furanyl alcohols catalyzed by Amberlyst-15, *J. Catal.* 313 (2014) 70–79.
- [15] ASTM, ASTM D975 - 15c Standard Specification for Diesel Fuel Oils, (2015) 27.
- [16] European Committee for Standardization, European Standard EN 590. Automotive fuels - Diesel - Requirements and test methods, (2009) 1–12.
- [17] M. Balakrishnan, E.R. Sacia, A.T. Bell, Selective Hydrogenation of Furan-Containing Condensation Products as a Source of Biomass-Derived Diesel Additives, *ChemSusChem.* 7 (2014) 2796–2800.
- [18] C.J. Kliewer, C. Aliaga, M. Bieri, W. Huang, C.-K. Tsung, J.B. Wood, K. Komvopoulos, G.A. Somorjai, Furan Hydrogenation over Pt(111) and Pt(100) Single-Crystal Surfaces and Pt Nanoparticles from 1 to 7 nm: A Kinetic and Sum Frequency Generation Vibrational Spectroscopy Study, *J. Am. Chem. Soc.* 132 (2010) 13088–13095.
- [19] R.C. Runnebaum, T. Nimmanwudipong, J. Doan, D.E. Block, B.C. Gates, Catalytic

- Conversion of Furan to Gasoline-Range Aliphatic Hydrocarbons via Ring Opening and Decarbonylation Reactions Catalyzed by Pt/ $\gamma$ -Al<sub>2</sub>O<sub>3</sub>, *Catal. Letters*. 142 (2012) 664–666.
- [20] J. Kang, A. Vonderheide, V. V Gulians, Deuterium-Labeling Study of the Hydrogenation of 2-Methylfuran and 2,5-Dimethylfuran over Carbon-Supported Noble Metal Catalysts, *ChemSusChem*. 8 (2015) 3044–3047.
- [21] I.F. Bel'skii, N.I. Shuikin, CATALYTIC HYDROGENATION AND HYDROGENOLYSIS OF FURAN COMPOUNDS, *Russ. Chem. Rev.* 32 (1963) 307.
- [22] E. Furimsky, The mechanism of catalytic hydrodeoxygenation of furan, *Appl. Catal.* 6 (1983) 159–164.
- [23] H.A. Smith, J.F. Fuzek, Catalytic Hydrogenation of Furan and Substituted Furans on Platinum, *J. Am. Chem. Soc.* 71 (1949) 415–419.
- [24] J. Yang, N. Li, G. Li, W. Wang, A. Wang, X. Wang, Y. Cong, T. Zhang, Solvent-Free Synthesis of C10 and C11 Branched Alkanes from Furfural and Methyl Isobutyl Ketone, *ChemSusChem*. 6 (2013) 1149–1152.
- [25] J. Yang, S. Li, L. Zhang, X. Liu, J. Wang, X. Pan, N. Li, A. Wang, Y. Cong, X. Wang, T. Zhang, Hydrodeoxygenation of furans over Pd-FeOx/SiO<sub>2</sub> catalyst under atmospheric pressure, *Appl. Catal. B Environ.* 201 (2017) 266–277.
- [26] A.D. Sutton, F.D. Waldie, R. Wu, M. Schlaf, L.A. “Pete” Silks, J.C. Gordon, The hydrodeoxygenation of bioderived furans into alkanes, *Nat. Chem.* 5 (2013) 428–432.
- [27] C.R. Waidmann, A.W. Pierpont, E.R. Batista, J.C. Gordon, R.L. Martin, L.A. “Pete” Silks, R.M. West, R. Wu, Functional group dependence of the acid catalyzed ring opening of biomass derived furan rings: an experimental and theoretical study, *Catal. Sci. Technol.* (2012).
- [28] T. Kessler, E.R. Sacia, A.T. Bell, J.H. Mack, Artificial Neural Network Based Predictions of Cetane Number for Furanic Biofuels, 2017.
- [29] J. Yanowitz, M.J. Murphy, J.D. Taylor, R.L. McCormick, Compendium of Experimental Cetane Numbers, Technical Report NREL/TP-5400-61693, 2014.
- [30] B.C. Windom, M.L. Huber, T.J. Bruno, A.L. Lown, C.T. Lira, Measurements and Modeling Study on a High-Aromatic Diesel Fuel, (2012).
- [31] J.P. Lange, E. van der Heide, J. van Buijtenen, R. Price, Furfural--a promising platform for lignocellulosic biofuels, *ChemSusChem*. 5 (2012) 150–166.
- [32] J.Q. Bond, D.M. Alonso, D. Wang, R.M. West, J.A. Dumesic, Integrated catalytic conversion of gamma-valerolactone to liquid alkenes for transportation fuels, *Science* (80-. ). 327 (2010) 1110–1114.
- [33] Y. Roman-Leshkov, Phase Modifiers Promote Efficient Production of Hydroxymethylfurfural from Fructose, *Science* (80-. ). 312 (2006) 1933–1937.
- [34] R.S. Rao, R. Terry, K. Baker, M. Albert Vannice, Furfural hydrogenation over carbon-supported copper, *Catal. Letters*. 60 (1999) 51–57.
- [35] Y. Roman-Leshkov, C.J. Barrett, Z.Y. Liu, J.A. Dumesic, Production of dimethylfuran for liquid fuels from biomass-derived carbohydrates, *Nature*. 447 (2007) 982–985.
- [36] J. Luo, H. Yun, A. V. Mironenko, K. Goulas, J.D. Lee, M. Monai, C. Wang, V. Vorotnikov, C.B. Murray, D.G. Vlachos, P. Fornasiero, R.J. Gorte, Mechanisms for High Selectivity in the Hydrodeoxygenation of 5-Hydroxymethylfurfural over PtCo Nanocrystals, *ACS Catal.* 6 (2016) 4095–4104.
- [37] J. Luo, M. Monai, H. Yun, L. Arroyo-Ramírez, C. Wang, C.B. Murray, P. Fornasiero, R.J. Gorte, The H<sub>2</sub> Pressure Dependence of Hydrodeoxygenation Selectivities for Furfural

- Over Pt/C Catalysts, *Catal. Letters*. 146 (2016) 711–717.
- [38] Y.-B. Huang, Z. Yang, J.-J. Dai, Q.-X. Guo, Y. Fu, Production of high quality fuels from lignocellulose-derived chemicals: a convenient C–C bond formation of furfural, 5-methylfurfural and aromatic aldehyde, *RSC Adv.* 2 (2012) 11211.
- [39] S. Sreekumar, M. Balakrishnan, K. Goulas, G. Gunbas, A.A. Gokhale, L. Louie, A. Grippo, C.D. Scown, A.T. Bell, F.D. Toste, Upgrading Lignocellulosic Products to Drop-In Biofuels via Dehydrogenative Cross-Coupling and Hydrodeoxygenation Sequence, *ChemSusChem*. 8 (2015) 2609–2614.
- [40] R. Xing, A. V Subrahmanyam, H. Olcay, W. Qi, G.P. van Walsum, H. Pendse, G.W. Huber, Production of jet and diesel fuel range alkanes from waste hemicellulose-derived aqueous solutions, *Green Chem.* 12 (2010) 1933.
- [41] G. Li, N. Li, X. Wang, X. Sheng, S. Li, A. Wang, Y. Cong, X. Wang, T. Zhang, Synthesis of Diesel or Jet Fuel Range Cycloalkanes with 2-Methylfuran and Cyclopentanone from Lignocellulose, *Energy & Fuels*. 28 (2014) 5112–5118.
- [42] W. Wang, N. Li, S. Li, G. Li, F. Chen, X. Sheng, A. Wang, X. Wang, Y. Cong, T. Zhang, Synthesis of renewable diesel with 2-methylfuran and angelica lactone derived from carbohydrates, *Green Chem.* 18 (2016) 1218–1223.
- [43] S. Li, N. Li, G. Li, A. Wang, Y. Cong, X. Wang, T. Zhang, Synthesis of diesel range alkanes with 2-methylfuran and mesityl oxide from lignocellulose, *Catal. Today*. 234 (2014) 91–99.
- [44] G. Li, N. Li, J. Yang, A. Wang, X. Wang, Y. Cong, T. Zhang, Synthesis of renewable diesel with the 2-methylfuran, butanal and acetone derived from lignocellulose, *Bioresour. Technol.* 134 (2013) 66–72.
- [45] C. Coutterez, A. Gandini, Synthesis and characterization of oligo(heteroarylene vinylene)s incorporating furan and thiophene moieties, *Polymer (Guildf)*. 39 (1998) 7009–7014.
- [46] P. Froimowicz, M.N. Belgacem, A. Gandini, M.C. Strumia, Design, synthesis and photo-cross-linking of a new photosensitive macromonomer from tetra-branched poly(ethylene oxide)s, *Eur. Polym. J.* 44 (2008) 4092–4097.
- [47] C. Meales, Z. Hui, A. Gandini, Conjugated Polymers Bearing Furan Rings .1. Synthesis and Characterization of Oligo(2,5-Furylene Vinylene) and Its Thiophene Homolog, *Polymer (Guildf)*. 37 (1996) 2273–2279.
- [48] F.G. Bordwell, R.J. McCallum, W.N. Olmstead, Acidities and Hydrogen Bonding of Phenols in Dimethyl Sulfoxide, *J. Org. Chem.* 49 (1984) 1424–1427.
- [49] W.N. Olmstead, Z. Margolin, F.G. Bordwell, Acidities of water and simple alcohols in dimethyl sulfoxide solution, *J. Org. Chem.* 45 (1980) 3295–3299.
- [50] H.A. Chiong, Potassium Phosphate, in: *Encycl. Reagents Org. Synth.*, John Wiley & Sons, Ltd, 2001.
- [51] E.M. Valentin, I. Montes, W. Adam, Counterion effects in the nucleophilic substitution reaction of the acetate ion with alkyl bromides in the synthesis of esters, *J. Chem. Educ.* 86 (2009) 1315–1318.
- [52] R. Appel, R. Loos, H. Mayr, Nucleophilicity parameters for phosphoryl-stabilized carbanions and phosphorus ylides: Implications for Wittig and related olefination reactions, *J. Am. Chem. Soc.* 131 (2009) 704–714.
- [53] A. Bohre, B. Saha, M.M. Abu-Omar, Catalytic Upgrading of 5-Hydroxymethylfurfural to Drop-in Biofuels by Solid Base and Bifunctional Metal–Acid Catalysts, *ChemSusChem*. 8 (2015) 4022–4029.

- [54] K.K. Rao, M. Gravelle, J.S. Valente, F. Figueras, Activation of Mg–Al Hydrotalcite Catalysts for Aldol Condensation Reactions, *J. Catal.* 173 (1998) 115–121.
- [55] R. Radhakrishnan, D.M. Do, S. Jaenicke, Y. Sasson, G.K. Chuah, Potassium phosphate as a solid base catalyst for the catalytic transfer hydrogenation of aldehydes and ketones, *ACS Catal.* 1 (2011) 1631–1636.
- [56] G. Guan, K. Kusakabe, S. Yamasaki, Tri-potassium phosphate as a solid catalyst for biodiesel production from waste cooking oil, *Fuel Process. Technol.* 90 (2009) 520–524.
- [57] S. Murov, *Properties of Organic Solvents*, (2016). <http://murov.info/orgsolvents.htm>.
- [58] V.I. Voronin, Y.S. Ponosov, I.F. Berger, N. V. Proskurnina, V.G. Zubkov, A.P. Tyutyunnik, S.N. Bushmeleva, A.M. Balagurov, D. V. Sheptyakov, E.I. Burmakin, G.S. Shekhtman, E.G. Vovkotrub, Crystal structure of the low-temperature form of K<sub>3</sub>PO<sub>4</sub>, *Inorg. Mater.* 42 (2006) 908–913.
- [59] N. Qafisheh, S. Mukhopadhyay, A. V. Joshi, Y. Sasson, G.K. Chuah, S. Jaenicke, Potassium phosphate as a high-performance solid base in phase-transfer-catalyzed alkylation reactions, *Ind. Eng. Chem. Res.* 46 (2007) 3016–3023.
- [60] D.M. Alonso, J.Q. Bond, J.C. Serrano-Ruiz, J.A. Dumesic, Production of liquid hydrocarbon transportation fuels by oligomerization of biomass-derived C<sub>9</sub> alkenes, *Green Chem.* 12 (2010) 992–999.
- [61] G. Li, N. Li, Z. Wang, C. Li, A. Wang, X. Wang, Y. Cong, T. Zhang, Synthesis of high-quality diesel with furfural and 2-methylfuran from hemicellulose, *ChemSusChem.* 5 (2012) 1958–1966.
- [62] E.R. Sacia, M. Balakrishnan, M.H. Deaner, K.A. Goulas, F.D. Toste, A.T. Bell, Highly Selective Condensation of Biomass-Derived Methyl Ketones as a Source of Aviation Fuel, *ChemSusChem.* 8 (2015) 1726–1736.
- [63] P. Biswas, J.-H. Lin, J. Kang, V. V Gulians, Vapor phase hydrogenation of 2-methylfuran over noble and base metal catalysts, *Appl. Catal. A Gen.* 475 (2014) 379–385.
- [64] S. Sitthisa, D.E. Resasco, Hydrodeoxygenation of Furfural Over Supported Metal Catalysts: A Comparative Study of Cu, Pd and Ni, *Catal. Letters.* 141 (2011) 784–791.
- [65] C. Aliaga, C.-K. Tsung, S. Alayoglu, K. Komvopoulos, P. Yang, G.A. Somorjai, Sum Frequency Generation Vibrational Spectroscopy and Kinetic Study of 2-Methylfuran and 2,5-Dimethylfuran Hydrogenation over 7 nm Platinum Cubic Nanoparticles, *J. Phys. Chem. C.* 115 (2011) 8104–8109.
- [66] C.L. Wilson, Reactions of Furan Compounds. X. Catalytic Reduction of Methylfuran to 2-Pentanone, *J. Am. Chem. Soc.* 70 (1948) 1313–1315.
- [67] A. V Mironenko, M.J. Gilkey, P. Panagiotopoulou, G. Facas, D.G. Vlachos, B. Xu, Ring Activation of Furanic Compounds on Ruthenium-Based Catalysts, *J. Phys. Chem. C.* 119 (2015) 6075–6085.
- [68] J. Miller, A fundamental study of platinum tetraammine impregnation of silica<sub>2</sub>. The effect of method of preparation, loading, and calcination temperature on (reduced) particle size, *J. Catal.* 225 (2004) 203–212.
- [69] H.-Y. Zheng, Y.-L. Zhu, B.-T. Teng, Z.-Q. Bai, C.-H. Zhang, H.-W. Xiang, Y.-W. Li, Towards understanding the reaction pathway in vapour phase hydrogenation of furfural to 2-methylfuran, *J. Mol. Catal. A Chem.* 246 (2006) 18–23.
- [70] S.D. Lin, M.A. Vannice, Hydrogenation of Aromatic Hydrocarbons over Supported Pt Catalysts .I. Benzene Hydrogenation, *J. Catal.* 143 (1993) 539–553.
- [71] B. Sen, M.A. Vannice, Metal-support effects on acetone hydrogenation over platinum

- catalysts, *J. Catal.* 113 (1988) 52–71.
- [72] Y. Román-Leshkov, M.E. Davis, Activation of Carbonyl-Containing Molecules with Solid Lewis Acids in Aqueous Media, *ACS Catal.* 1 (2011) 1566–1580.
- [73] L.R. Baker, G. Kennedy, M. Van Spronsen, A. Hervier, X. Cai, S. Chen, L.W. Wang, G.A. Somorjai, Furfuraldehyde hydrogenation on titanium oxide-supported platinum nanoparticles studied by sum frequency generation vibrational spectroscopy: acid-base catalysis explains the molecular origin of strong metal-support interactions, *J. Am. Chem. Soc.* 134 (2012) 14208–14216.
- [74] F.L. Pilar, J.R. Morris, Choice of Parameters for the Hückel  $\pi$ -Electronic Structure of Furan: Tentative Extension to Pyrrole and Thiophene, *J. Chem. Phys.* 34 (1961) 389–392.
- [75] S. Wang, V. Vorotnikov, D.G. Vlachos, A DFT study of furan hydrogenation and ring opening on Pd(111), *Green Chem.* 16 (2014) 736–747.
- [76] V. Vorotnikov, D.G. Vlachos, Group Additivity and Modified Linear Scaling Relations for Estimating Surface Thermochemistry on Transition Metal Surfaces: Application to Furanics, *J. Phys. Chem. C.* 119 (2015) 10417–10426.
- [77] L. Faba, E. Díaz, S. Ordóñez, Hydrodeoxygenation of acetone–furfural condensation adducts over alumina-supported noble metal catalysts, *Appl. Catal. B Environ.* 160–161 (2014) 436–444.
- [78] E. Brunner, Solubility of hydrogen in 10 organic solvents at 298.15, 323.15, and 373.15 K, *J. Chem. Eng. Data.* 30 (1985) 269–273.
- [79] J.N. Chheda, Y. Roman-Leshkov, J. a. Dumesic, Production of 5-hydroxymethylfurfural and furfural by dehydration of biomass-derived mono- and poly-saccharides, *Green Chem.* 9 (2007) 342.
- [80] Y.L. Louie, J. Tang, A.M.L. Hell, A.T. Bell, Kinetics of hydrogenation and hydrogenolysis of 2,5-dimethylfuran over noble metals catalysts under mild conditions, *Appl. Catal. B Environ.* 202 (2017) 557–568.
- [81] R. Ramos, Z. Tišler, O. Kikhtyanin, D. Kubička, Towards understanding the hydrodeoxygenation pathways of furfural–acetone aldol condensation products over supported Pt catalysts, *Catal. Sci. Technol.* (2016) 1829–1841.
- [82] H. Li, S. Saravanamurugan, S. Yang, A. Riisager, Catalytic Alkylation of 2-Methylfuran with Formalin Using Supported Acidic Ionic Liquids, *ACS Sustain. Chem. Eng.* 3 (2015) 3274–3280.
- [83] P. Canton, G. Fagherazzi, M. Battagliarin, F. Menegazzo, F. Pinna, N. Pernicone, Pd/CO average chemisorption stoichiometry in highly dispersed supported Pd/ $\gamma$ -Al<sub>2</sub>O<sub>3</sub> catalysts, *Langmuir.* 18 (2002) 6530–6535.
- [84] R.J. Madon, M. Boudart, Experimental criterion for the absence of artifacts in the measurement of rates of heterogeneous catalytic reactions, *Ind. Eng. Chem. Fundam.* 21 (1982) 438–447.
- [85] S. Schimpf, J. Gaube, P. Claus, Selective hydrogenation of multiple unsaturated compounds, *75* (2004) 85–123.
- [86] A.K. Aboul-Gheit, S.M. Aboul-Fotouh, N.A.K. Aboul-Gheit, Hydroconversion of cyclohexene using catalysts containing Pt, Pd, Ir and Re supported on H-ZSM-5 zeolite, *Appl. Catal. A Gen.* 283 (2005) 157–161.
- [87] D. Teschner, J. Borsodi, Z. Kis, L. Szentmiklósi, Z. Révay, A. Knop-Gericke, R. Schlögl, D. Torres, P. Sautet, Role of Hydrogen Species in Palladium-Catalyzed Alkyne Hydrogenation, *J. Phys. Chem. C.* 114 (2010) 2293–2299.

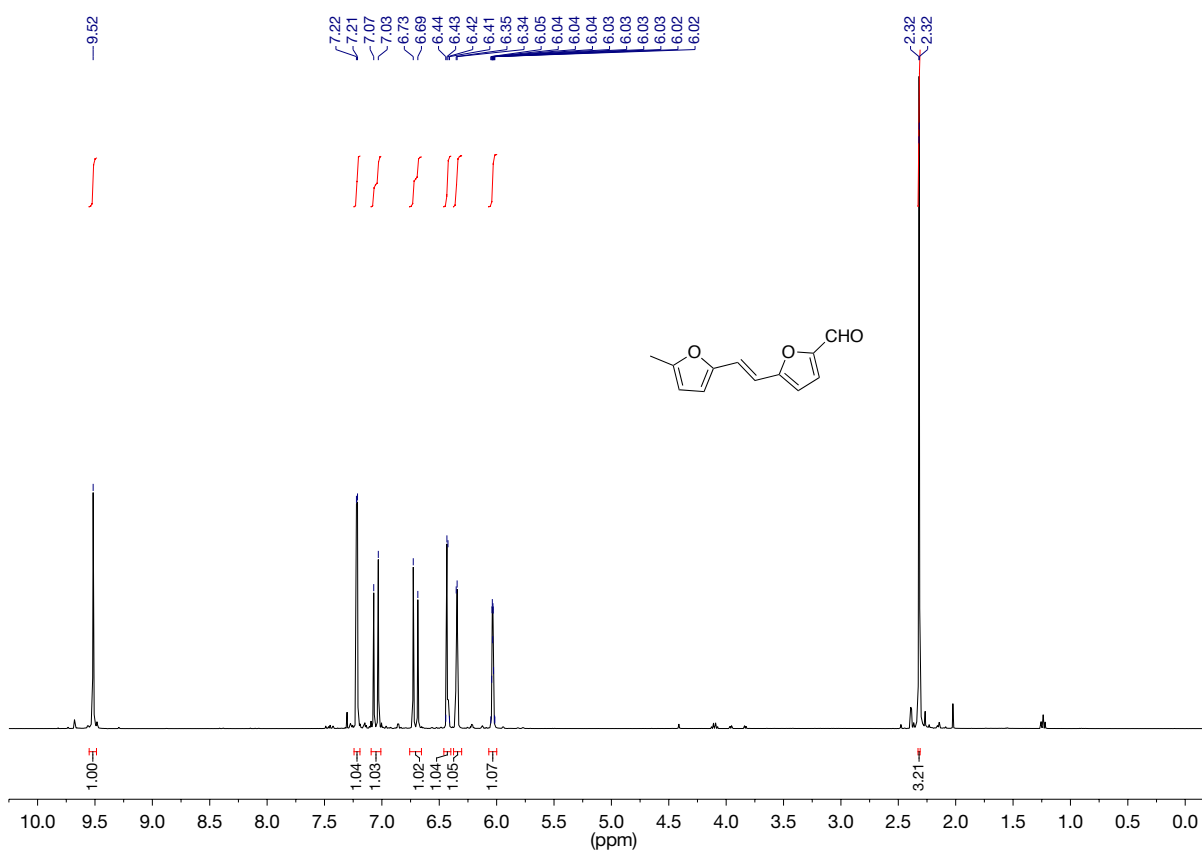
- [88] N.K. Nag, A Study on the Formation of Palladium Hydride in a Carbon-Supported Palladium Catalyst, *J. Phys. Chem. B.* 105 (2001) 5945–5949.
- [89] A. Borodziński, G.C. Bond, Selective Hydrogenation of Ethyne in Ethene-Rich Streams on Palladium Catalysts, Part 2: Steady-State Kinetics and Effects of Palladium Particle Size, Carbon Monoxide, and Promoters, *Catal. Rev.* 50 (2008) 379–469.
- [90] A.N.R. Bos, K.R. Westerterp, Mechanism and kinetics of the selective hydrogenation of ethyne and ethene, *Chem. Eng. Process. Process Intensif.* 32 (1993) 1–7.
- [91] W.T. McGown, C. Kembal, D.A. Whan, M.S. Scurrrell, Hydrogenation of acetylene in excess ethylene on an alumina supported palladium catalyst in a static system, *J. Chem. Soc. Faraday Trans. 1 Phys. Chem. Condens. Phases.* 73 (1977) 632–647.
- [92] D. Scholz, C. Aellig, I. Hermans, Catalytic transfer hydrogenation/hydrogenolysis for reductive upgrading of furfural and 5-(hydroxymethyl)furfural, *ChemSusChem.* 7 (2014) 268–275.
- [93] T. Thananathanachon, T.B. Rauchfuss, Efficient production of the liquid fuel 2,5-dimethylfuran from fructose using formic acid as a reagent, *Angew. Chemie - Int. Ed.* 49 (2010) 6616–6618.
- [94] J. Jae, W. Zheng, A.M. Karim, W. Guo, R.F. Lobo, D.G. Vlachos, The role of Ru and RuO<sub>2</sub> in the catalytic transfer hydrogenation of 5-hydroxymethylfurfural for the production of 2,5-dimethylfuran, *ChemCatChem.* 6 (2014) 848–856.
- [95] J. Jae, W. Zheng, R.F. Lobo, D.G. Vlachos, Production of dimethylfuran from hydroxymethylfurfural through catalytic transfer hydrogenation with ruthenium supported on carbon, *ChemSusChem.* 6 (2013) 1158–1162.
- [96] G.-H. Wang, J. Hilgert, F.H. Richter, F. Wang, H. Bongard, B. Spliethoff, C. Weidenthaler, F. Schüth, Platinum-cobalt bimetallic nanoparticles in hollow carbon nanospheres for hydrogenolysis of 5-hydroxymethylfurfural., *Nat. Mater.* 13 (2014) 293–300.
- [97] R. Luque, *Nanomaterials for Sustainable Energy*, 1213 (2015).
- [98] K. Xiong, W. Wan, J.G. Chen, Reaction pathways of furfural, furfuryl alcohol and 2-methylfuran on Cu(111) and NiCu bimetallic surfaces, *Surf. Sci.* 652 (2016) 91–97.
- [99] S. Nishimura, N. Ikeda, K. Ebitani, Selective hydrogenation of biomass-derived 5-hydroxymethylfurfural (HMF) to 2,5-dimethylfuran (DMF) under atmospheric hydrogen pressure over carbon supported PdAu bimetallic catalyst, *Catal. Today.* 232 (2014) 89–98.
- [100] S. Sitthisa, W. An, D.E. Resasco, Selective conversion of furfural to methylfuran over silica-supported NiFe bimetallic catalysts, *J. Catal.* 284 (2011) 90–101.
- [101] S. Sitthisa, T. Pham, T. Prasomsri, T. Sooknoi, R.G. Mallinson, D.E. Resasco, Conversion of furfural and 2-methylpentanal on Pd/SiO<sub>2</sub> and Pd–Cu/SiO<sub>2</sub> catalysts, *J. Catal.* 280 (2011) 17–27.
- [102] J. Luo, L. Arroyo-Ramírez, J. Wei, H. Yun, C.B. Murray, R.J. Gorte, Comparison of HMF hydrodeoxygenation over different metal catalysts in a continuous flow reactor, *Appl. Catal. A Gen.* 508 (2015) 86–93.
- [103] P. Yang, Q. Cui, Y. Zu, X. Liu, G. Lu, Y. Wang, Catalytic production of 2,5-dimethylfuran from 5-hydroxymethylfurfural over Ni/Co<sub>3</sub>O<sub>4</sub> catalyst, *Catal. Commun.* 66 (2015) 55–59.
- [104] A. Stanislaus, B.H. Cooper, Aromatic Hydrogenation Catalysis: A Review, *Catal. Rev.* 36 (1994) 75–123.
- [105] F. Zaccheria, N. Ravasio, M. Ercoli, P. Allegrini, Heterogeneous Cu-catalysts for the



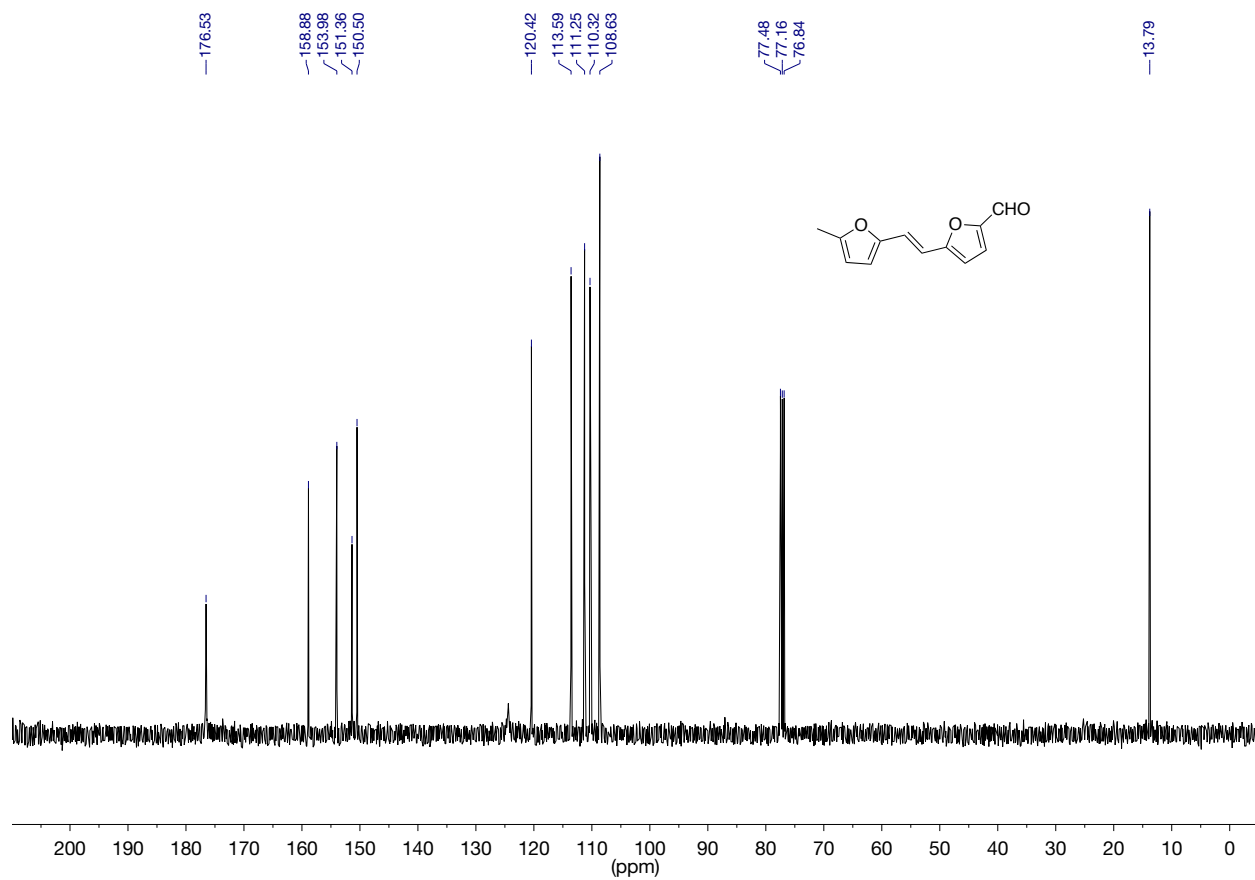
- reductive deoxygenation of aromatic ketones without additives, *Tetrahedron Lett.* 46 (2005) 7743–7745.
- [106] D. Procházková, P. Zámotný, M. Bejblová, L. Červený, J. Čejka, Hydrodeoxygenation of aldehydes catalyzed by supported palladium catalysts, *Appl. Catal. A Gen.* 332 (2007) 56–64.
- [107] M. Mavrikakis, M.A. Barteau, Oxygenate reaction pathways on transition metal surfaces, *J. Mol. Catal. A Chem.* 131 (1998) 135–147.
- [108] S. Sitthisa, T. Sooknoi, Y. Ma, P.B. Balbuena, D.E. Resasco, Kinetics and mechanism of hydrogenation of furfural on Cu/SiO<sub>2</sub> catalysts, *J. Catal.* 277 (2011) 1–13.

## Appendix A1 – Chemical Characterization

### A1.1 NMR 5-MF Dimer (MFVFAL)

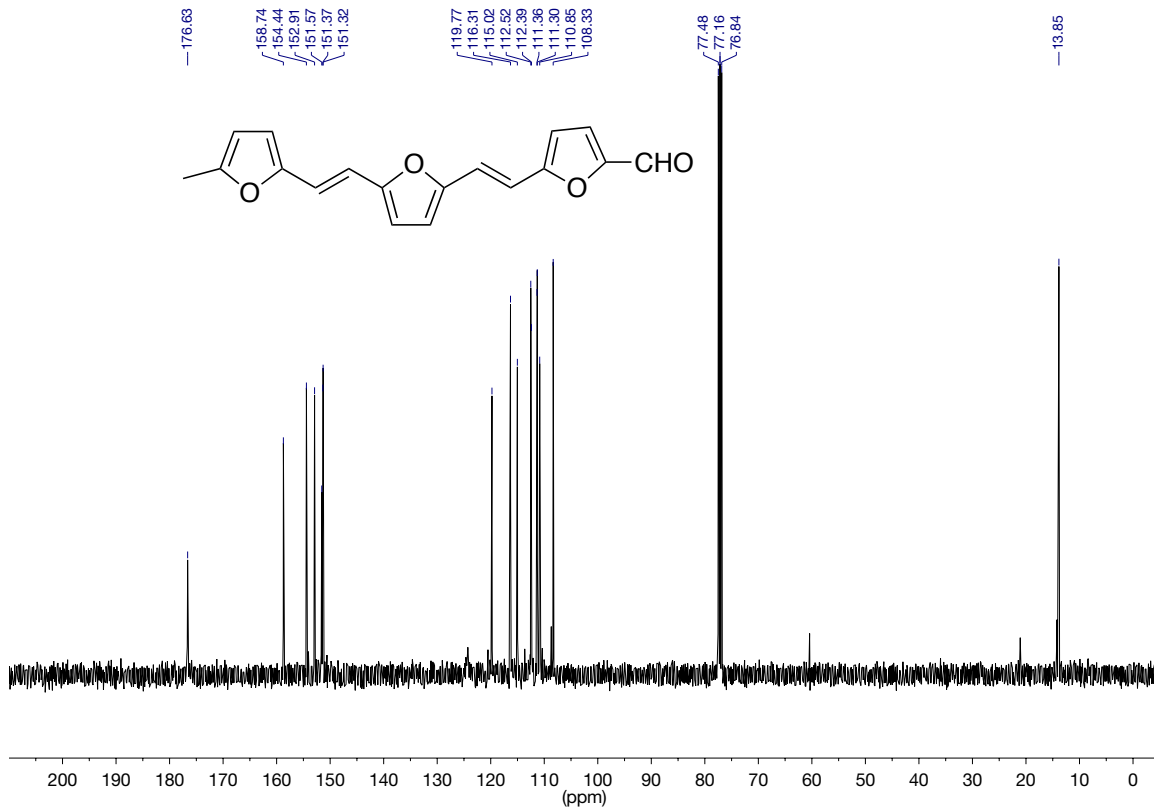
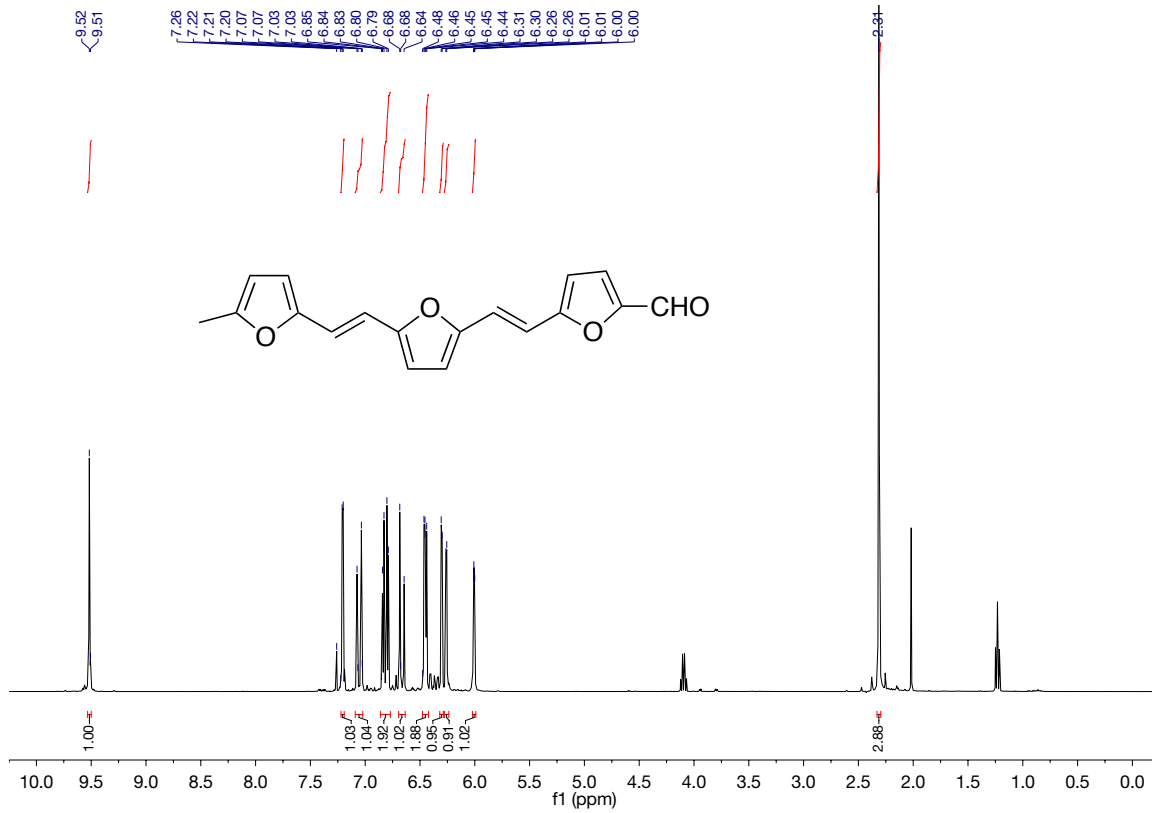


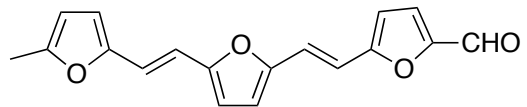
<sup>1</sup>H NMR (400 MHz, CDCl<sub>3</sub>) δ 9.52 (s, 1H), 7.22 (d, *J* = 3.7 Hz, 1H), 7.05 (d, *J* = 16.0 Hz, 1H), 6.71 (d, *J* = 15.9 Hz, 1H), 6.43 (d, *J* = 3.7 Hz, 1H), 6.35 (d, *J* = 3.2 Hz, 1H), 6.03 (dq, *J* = 3.1, 1.0 Hz, 1H), 2.32 (s, 3H).



$^{13}\text{C}$  NMR (101 MHz,  $\text{CDCl}_3$ )  $\delta$  176.5, 158.9, 153.9, 151.3, 150.5, 120.4, 113.6, 111.2, 110.3, 108.6, 13.8.

# A1.2 NMR Data 5-MF Trimer

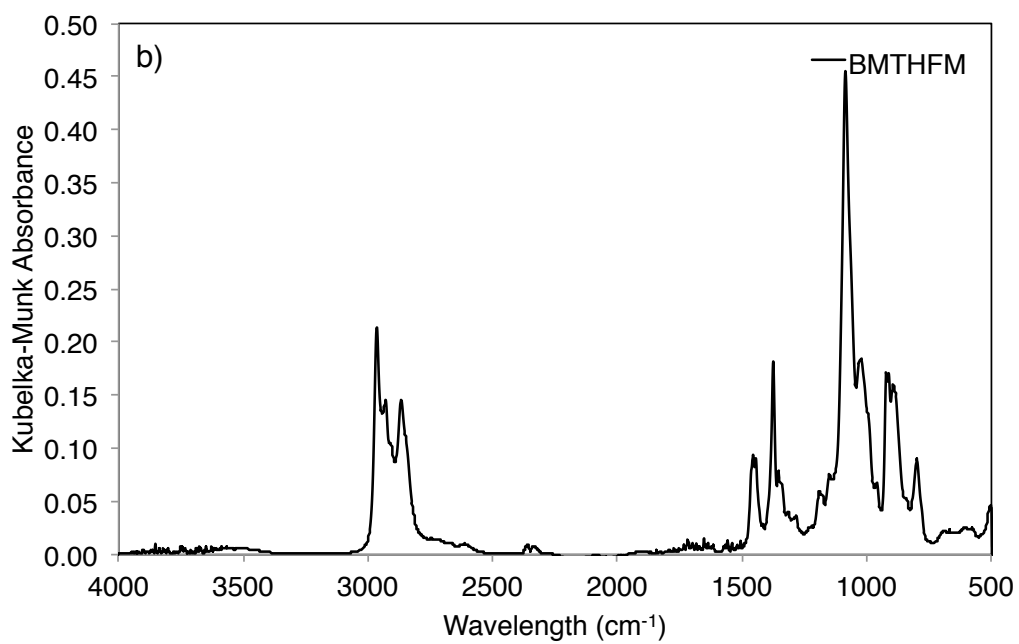
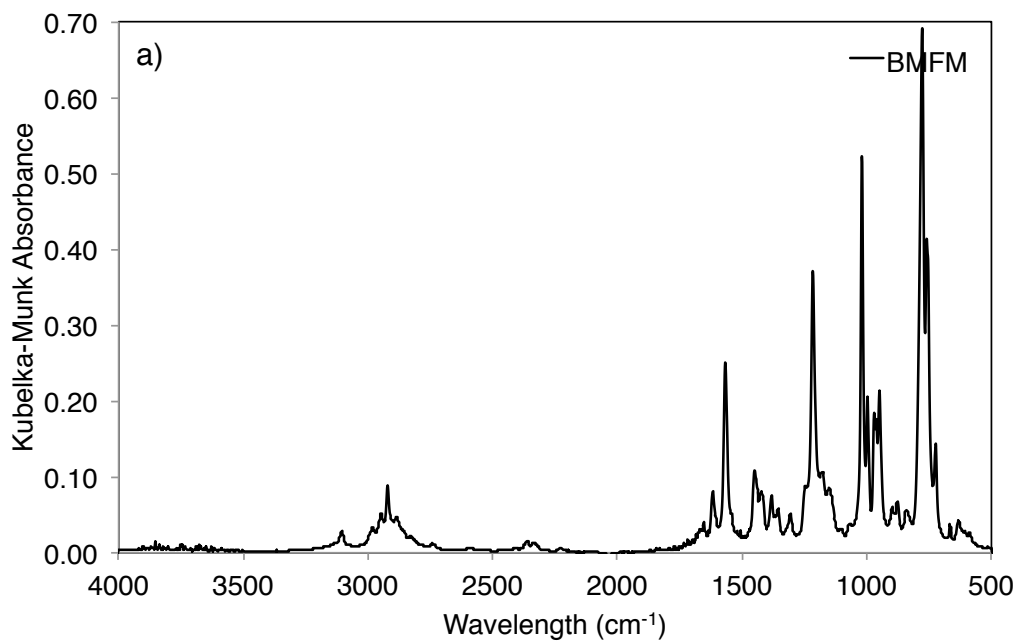


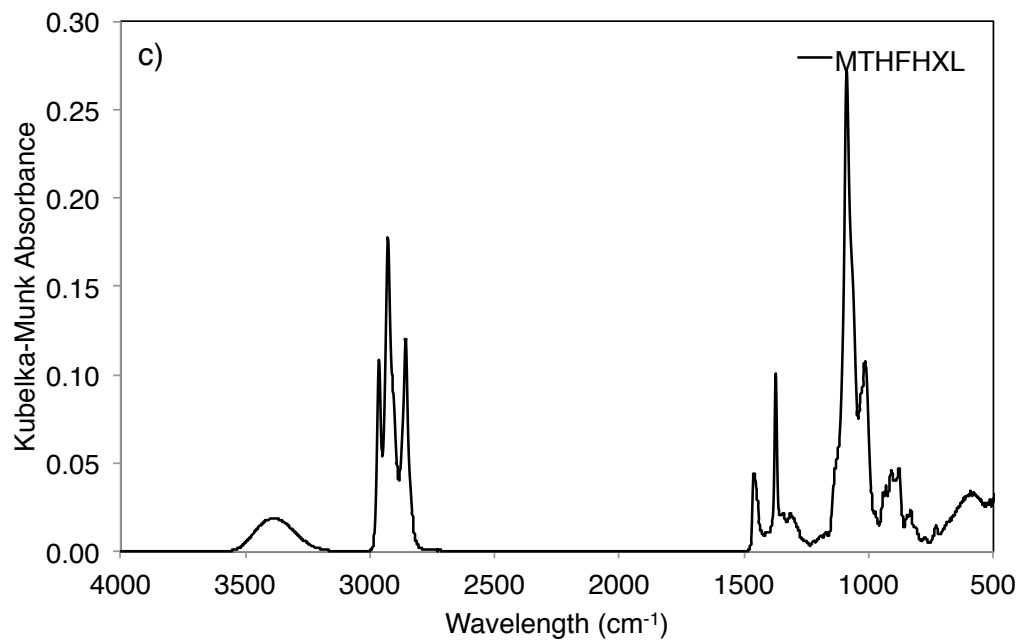


$^1\text{H}$  NMR (400 MHz, Chloroform-*d*)  $\delta$  9.52 (s, 1H), 7.21 (d,  $J = 3.8$  Hz, 1H), 7.05 (d,  $J = 15.9$  Hz, 1H), 6.85 – 6.79 (m, 2H), 6.66 (d,  $J = 15.9$  Hz, 1H), 6.45 (dd,  $J = 6.4, 3.6$  Hz, 2H), 6.30 (d,  $J = 3.5$  Hz, 1H), 6.26 (d,  $J = 3.2$  Hz, 1H), 6.01 (dd,  $J = 3.2, 1.2$  Hz, 1H), 2.31 (s, 3H).

$^{13}\text{C}$  NMR (101 MHz,  $\text{CDCl}_3$ )  $\delta$  176.6, 158.7, 154.4, 152.9, 151.5, 151.4, 151.3, 119.8, 116.3, 115.0, 112.5, 112.4, 111.4, 111.3, 110.9, 108.3, 13.8.

### A1.3 FT-IR spectra of C11 oxygenates





FT-IR spectra of a) BMFM, b) BMTHFM purified by vacuum distillation and c) MTHFHXL purified by column chromatography. All spectra were recorded in ATR mode and corrected by the Kubelka-Munk algorithm.